Features of muscle-specific tyrosine kinase autoantibodies and B cells derived from myasthenia gravis patients

Please check the document version of this publication:

• A submitted manuscript is the version of the article upon submission and before peer-review. There can be important differences between the submitted version and the official published version of record. People interested in the research are advised to contact the author for the final version of the publication, or visit the DOI to the publisher's website.
• The final author version and the galley proof are versions of the publication after peer review.
• The final published version features the final layout of the paper including the volume, issue and page numbers.

Link to publication

Download date: 07 Feb. 2024

Features of muscle-specific tyrosine kinase autoantibodies and B cells derived from myasthenia gravis patients

DISSERTATION

to obtain the degree of Doctor at
Maastricht University on the authority of the Rector Magnificus
Prof. Dr. Pamela Habibovic
in accordance with the decision of the Board of Deans,
to be defended in public on

Tuesday, 24th of October 2023 at 16.00 hrs.

by

Miriam Franziska Laura Fichtner

Supervisors:

Prof. Dr. Pilar Martinez

Prof. Dr. Kevin C. O'Connor (Yale University, USA)

Co-supervisor:

Dr. Mario Losen

Assessment Committee:

Prof. Dr. G.M.J. Bos (Chair)

Prof. Dr. E.A.L Biessen

Prof. Dr. A. Evoli (Catholic University Rome, Italy)

Dr. J.G.J. Hoeijmakers

Prof. Dr. A. Punga (Uppsala University, Sweden)

CONTENT

LIST OF ABBREVIATIONS

AAV	ANCA-associated vasculitis
Ab	antibody
AChR	acetylcholine receptor
AIRR-Seq	adaptive immune receptor repertoire sequencing
APC	allophycocyanin
APRIL	a proliferation-inducing ligand
ASC	antibody-secreting cell
BAFF	B cell activating factor
BAFF-R	B cell activating factor receptor
BCDT	B cell depletion therapy
BCMA	B cell maturation antigen
BCR	B cell receptor
BRCA1	breast cancer 1 gene
Bregs	regulatory B cells
BTK	Bruton's tyrosine kinase
CAAR T cells	chimeric autoantibody receptor T cells
CAR T cells	chimeric antigen receptor T cells
CBA	cell-based assay
CD20	cluster of differentiation 20
CD24	cluster of differentiation 24
cDNA	complementary deoxyribonucleic acid
CHRNA1	cholinergic receptor nicotinic alpha 1 subunit
CHRNB1	cholinergic receptor nicotinic beta 1 subunit
CIDP	chronic inflammatory demyelinating polyneuropathy
CPM	counts per minute
CSR	complete stable remission
CTLA4	cytotoxic T-lymphocyte-associated Protein 4
DNA	deoxyribonucleic acid
DOK7	downstream of tyrosine kinase 7
ELISA	enzyme-linked immunosorbent assay
EOMG	early-onset myasthenia gravis
f	female
Fab	fragment antigen-binding
Fc	fragment crystallizable
Fz domain	frizzled domain
HC	healthy control
HD	healthy donor
HEK cell line	human embryonic kidney cell line

hGH	human growth hormone
HLA	human leukocyte antigen
Ig	immunoglobulin
IgA	immunoglobulin A
IgD	immunoglobulin D
IgG	immunoglobulin G
IGH	immunoglobulin heavy chain
IGHD	immunoglobulin heavy constant delta
IGHV	immunoglobulin Heavy chain variable region
IGK	immunoglobulin light chain, kappa
IGL	immunoglobulin light chain, lambda
IgM	immunoglobulin M
IL-10	interleukin 10
IL4R	interleukin-4 receptor
ITGA4	integrin Subunit Alpha 4
LLPC	long-lived plasma cells
LOMG	late-onset myasthenia gravis
LRP4	low density lipoprotein receptor-related protein 4
m	male
mAb	monoclonal antibody/monoclonal autoantibody
MG	myasthenia gravis
MGFA	Myasthenia Gravis Foundation of America
MM	minimal manifestation
mo	month
MOG	myelin oligodendrocyte glycoprotein
mRNA	messenger ribonucleic acid
MS	multiple sclerosis
MuSK	muscle-specific tyrosine kinase
MYC	myelocytomatose
NA	not available
ND	not determined
NMJ	neuromuscular junction
NMOSD	neuromyelitis optica spectrum disorder
PC	positive control
PCR	polymerase chain reaction
PFA	paraformaldehyde
PLEX	plasma exchange
PRDM1	PR domain zinc finger protein 1
Pred	prednisone
PTPN22	protein tyrosine phosphatase non-receptor type 22
PV	pemphigus vulgaris

RA	rheumatoid arthritis
RIA	radioimmunoassay
RIPA	radioimmunoprecipitation assays
RNA	ribonucleic acid
RTX	rituximab
scPCR	single-cell polymerase chain reaction
scRNA-seq	single-cell ribonucleic acid sequencing
SD	standard deviation
SHM	somatic hypermutation
SIPR1	sphingosine-1-phosphate receptor 1
SLE	systemic lupus erythematosus
SMRT sequencing	single-molecule real-time sequencing
SNMG	seronegative myasthenia gravis
STAIR	single-cell Tracing of Adaptive Immune Receptor
TACI	transmembrane activator and CAML interactor
TCL1A	T-cell leukemia/lymphoma protein 1A
Tfh	T-follicular helper cells
Tfr	T-follicular regulatory cells
Th cells	T helper cells
Th1	subset of T helper cells
Th17	subset of T helper cells
Th$_{CD103}$	subset of T helper cells
Th$_{GM}$	subset of T helper cells
TNIP1	TNFAIP3-interacting protein 1
TOC	time of collection
TP53	tumor protein P53
Tregs	regulatory T cells
UCA	unmutated common ancestor
UMI	unique molecular identifier
V(D)J recombination	variable (diversity) joining recombination
VLA-4	integrin α4β1 (very late antigen-4)
XBP1	X-box binding protein 1

Kenmerken van spier-specifieke tyrosinekinase auto-antistoffen en B-cellen afkomstig van myasthenia gravis patiënten

SAMENVATTING

Myasthenia gravis (MG) is een auto-immuunziekte waarin het immuunsysteem, door de productie van autoantistoffen die gericht zijn tegen de neuromusculaire overgang, interfereert met de synaptische transmissie in de skeletspier. Antistoffen tegen de acetylcholine receptor (AChR) van de neuromusculaire overgang komen het meest voor in MG-patiënten, en, in mindere mate, komen antistoffen voor tegen spier-specifieke tyrosine kinase (MuSK) en 'low-density lipoprotein receptor-related protein' (LRP4) en agrin. De immunopathologie van MuSK MG is het onderwerp van dit proefschrift.

Het extracellulaire domein van MuSK bestaat uit drie Ig-achtige domeinen (Ig1-3) en een 'krul' ('frizzled') domein. MuSK autoantistoffen ontstaan uit plasmablasten, zijn hoofdzakelijk van de IgG4 klasse en herkennen meestal het Ig-achtige domein 1 van MuSK. MuSK-MG patiënten reageren gunstig op therapie gebaseerd op anti-CD20–gemedieerde B cell depletie (BCDT) en komen daarmee in een stabiele remissie. Een relapse komt echter vaak voor. Het immunomechanisme hierachter en hoe individuele autoantistoffen bijdragen tot de pathologie van de ziekte, wordt nog niet goed begrepen. Humane monoclonale autoantistoffen (mAbs), werden gebruikt om dit te onderzoeken.

Zes MuSK-specifieke mAbs werden gegenereerd. Twee mAbs herkenden het Ig-achtige domein 1 (2E6 en 6C6), drie mAbs herkenden het Ig-achtige domein 2 (MuSK1A, MuSK1B en MuSK3-28), en één het krul domein (MuSK3B). Vier van de zes mAbs hadden hun origine in plasmablasten. De vijf mAbs die het Ig-achtige domein 1 en Ig-achtige domein 2 konden detecteren, vertoonden binding met MuSK over een wijde range van concentraties en hadden pathogeniciteit in een in vitro AChR clustering assay. Voor het eerst werden hiermee de pathogene eigenschappen van MuSK mAbs aangetoond om het Ig-achtige domein 2 te detecteren. Het is niet bekend of de autoantistoffen van MuSK-MG patiënten,die in een relapse zijn na anti-CD20-gemedieerde BCDT, gegenereerd worden uit nieuwe auto-reactieve B cel klonen dan wel uit reeds bestaande B cel klonen die de BCDT-behandeling hebben 'overleefd'. Om deze reden werden bloedmonsters van drie MuSK MG-patiënten bestudeerd, pre- en post-anti-CD20-gemedieerde BCDT, met behulp van single-cel transcriptional en B cel receptor profilering. Een sub set van B cel-klonen bleek te persisteren na anti-CD20-gemedieerde BCDT en hiervan waren er B cellen die MuSK konden herkennen. De pathogene mAbs MuSK1A, MuSK1B en MuSK3-28 werden geïsoleerd tijdens een relapse in twee van deze patiënten. Varianten van deze pathogene klonen werden echter niet gedetecteerd in monsters van pre-anti-CD20-gemedieerde BCDT. De MuSK mAbs 2E6 en 6C6 werden specifiek gegenereerd om na te gaan of we een pathogene kloon en de varianten daarvan kunnen volgen via anti-CD20-gemedieerde BCDT. Door het vervolgen van het B cel repertoire in longitudinale bloedmonsters werd duidelijk dat klonale varianten van 2E6 aanwezig waren op meerdere tijdspunten gedurende

5

een periode van bijna zes jaar. Deze klonale varianten waren aanwezig in de circulatie voor een klinische relapse waarbij de titers van MuSK antistoffen waren toegenomen.

Het onderzoek van dit proefschrift geeft een nieuw inzicht van de immunopathologie van MuSK-MG en van het mechanisme van de relapse na anti-CD20-gemedieerde BCDT. De karakterisering van de nieuw-ontwikkelde mAbs geven een nieuw inzicht in de pathogene effecten van de autoantistoffen die het Ig-achtige domein 2 van de MuSK receptor detecteren. Daarbij vinden we dat anti-CD20-gemedieerde BCDT niet geheel effectief is in het verwijderen van antistof producerende B cellen. Een reservoir van zeldzame, pathogene MuSK autoantistof producerende B cel klonen overleeft anti-CD20-gemedieerde BCDT en komt opnieuw in circulatie voorafgaande aan tekenen van een klinisch detecteerbare relapse. Hiermee worden deze klonen en varianten hiervan een waardevolle kandidaat als bio-marker om een relapse te kunnen voorspellen.

ABSTRACT

Myasthenia gravis (MG) is an autoimmune disease in which the immune system causes impairment of neuromuscular function by producing autoantibodies that interrupt signaling from nerves to muscles. Most patients harbor autoantibodies against the acetylcholine receptor (AChR), followed by antibodies against muscle-specific tyrosine kinase (MuSK), low density lipoprotein receptor-related protein 4 (LRP4) and agrin. The work of this thesis focuses solely on the immunopathology of MuSK MG. The extracellular domain of MuSK is comprised of three immunoglobulin(Ig)-like domains (Ig1-3) and a frizzled domain. MuSK autoantibodies are predominantly IgG4, most often recognize the Ig-like domain 1 of MuSK and originate from plasmablasts. MuSK MG patients respond well to anti-CD20-mediated B cell depletion therapy (BCDT) and go into stable remission. However, relapse often occurs. The immunomechanism of relapse and how individual autoantibodies contribute to disease pathology is currently not well understood. Human monoclonal autoantibodies (mAbs) were created to investigate both.

Six unique MuSK-specific mAbs were generated. Two mAbs recognized the Ig-like domain 1 (2E6 and 6C6), three the Ig-like domain 2 (MuSK1A, MuSK1B and MuSK3-28), and one the frizzled domain (MuSK3B). Four out of six mAbs originated from plasmablasts. The five mAbs that detected the Ig-like domain 1 or Ig-like domain 2 bound to MuSK over a wide range of concentrations and showed pathogenic capacity in an *in vitro* AChR clustering assay. This was the first time

that pathogenic capacity was shown for MuSK mAbs detecting the Ig-like domain 2. It is not known whether the autoantibodies of MuSK MG patients in relapse after anti-CD20-mediated BCDT are generated from new autoreactive B cell clones or pre-existing B cell clones that persist through treatment. Therefore, samples of three MuSK MG patients were studied pre- and post-anti-CD20-mediated BCDT using single-cell transcriptional and B cell receptor profiling. A subset of B cell clones was found to persist through anti-CD20-mediated BCDT and among these were B cells that recognized MuSK. The pathogenic mAbs MuSK1A, MuSK1B and MuSK3-28 were isolated at the time of relapse in two of these patients. Clonal variants of these pathogenic clones were, however, not detected in samples pre-anti-CD20-mediated BCDT. Therefore, the MuSK mAbs 2E6 and 6C6 were specifically generated to investigate whether we can follow a pathogenic clone and its clonal variants through anti-CD20-mediated BCDT. B cell receptor repertoire tracing of longitudinal samples showed that clonal variants of 2E6 were detected at multiple timepoints over the course of almost six years. We found that these clonal variants are present in the circulation before clinically detectable relapse together with rising MuSK autoantibody titers.

Overall, the studies described in this thesis provide both novel insights into the immunopathology of MuSK MG and a mechanistic understanding of relapse after anti-CD20-mediated BCDT. The characterization of newly generated MuSK mAbs gave new insights into the pathogenic effects of autoantibodies detecting the Ig-like domain 2 on the MuSK receptor. Furthermore, we found that anti-CD20-mediated BCDT is not fully effective at eliminating autoantibody-producing B cells. A reservoir

of rare pathogenic MuSK autoantibody-expressing B cell clones survive anti-CD20-mediated BCDT and reemerge into circulation prior to manifestation of clinically detectable relapse making these clones and clonal variants novel valuable candidate biomarkers for relapse prediction.

Keywords

1. GENERAL INTRODUCTION

1.1. EPIDEMIOLOGY OF MYASTHENIA GRAVIS

Autoimmune myasthenia gravis (MG) is a rare disorder of the neuromuscular transmission [1, 2]. The prevalence of MG worldwide ranges from 2.19 to 36.71 cases per 100.000 population [3] and it has risen consistently over the last 50 years with the total number of MG patients doubling over the last 20 years [3, 4]. The number of MG patients in Europe is estimated at 56.000 to 123.000 [5] and at around 60.000 in the United States [4]. The incidence of MG ranges worldwide from 0.15-61.33 per million person-years [3]. The reason behind the divergent incidence rates in MG is multifactorial. MG subtype, ethnicity, sex, age as well as study design have been implicated as contributing factors [3, 6, 7]. Autoimmune MG subgroups are categorized by autoantibody status. Approximately 80-85% of MG patients have autoantibodies against the nicotinic acetylcholine receptor (AChR) [8], followed by around 5-14% with autoantibodies against muscle-specific tyrosine kinase (MuSK) [9, 10], and the much rarer entities of autoantibodies against Low Density Lipoprotein Receptor-Related Protein 4 (LRP4) [11-13] and agrin which is the ligand of LRP4 [12]. The age of onset in AChR MG is bimodally distributed [14]. Early-onset MG (EOMG) has a peak of incidence between 20-40 years with females being predominantly affected [14, 15]. In contrast, primarily men are diagnosed with late onset MG (LOMG) which peaks around the age of 60-80 years [14, 15]. The age of onset in MG with autoantibodies against MuSK peaks below the age of 40 years with mainly women being affected [16-19]. MG is a chronic

disease impacting patients and their families life-long. Disease related mortality in MG is at 5-9% [20]. Around 20% of patients experience at least one MG crisis in their lifetime and require hospitalization and endotracheal intubation [21]; around 3% of these patients die [22].

1.2. PATHOGENESIS AND IMMUNOPATHOGENESIS OF MYASTHENIA GRAVIS

The pathogenesis of MG seems to be the result of a combination of defects in the immune system together with environmental and genetic factors similar to the observed pathogenesis of other autoimmune disorders including multiple sclerosis (MS), systemic lupus erythematosus (SLE), and type 1 diabetes [23-27]. Genetic susceptibility contributes to the underlying pathology in MG [28-30]. Most genetic studies are currently based on AChR MG. The genes are mostly associated with target structures at the neuromuscular junction or the immune system in general. Two risk genes were related with the AChR receptor, specifically the cholinergic receptor nicotinic alpha 1 subunit (CHRNA1) and cholinergic receptor nicotinic beta 1 subunit (CHRNB1) genes [28]. Cytotoxic T-lymphocyte-associated protein 4 (CTLA4) is another gene that was identified as a risk gene in MG [30]. CTLA4 is a receptor expressed on T regulatory cells (Tregs) and a negative regulator of the immune system [31, 32]. The human leukocyte antigen (HLA), class II, alpha chain 1 region (allele HLA-DQA1) is important for peptide presentation in the immune system [33]. The HLA-DQA1 allele locus is associated with both EOMG and LOMG [30], although usage of distinct polymorphisms within HLA-DQA1 allele indicate

11

differences between EOMG and LOMG [30]. Further genetic differences between EOMG and LOMG have been found in other genes. The protein tyrosine phosphatase non-receptor type 22 (PTPN22) and TNFAIP3 interacting protein 1 (TNIP1) and HLA class region 1 (allele HLA-B*08) are loci implicated in autoimmune diseases [34-36] and linked to EOMG [29], whereas changes located in the gene receptor activator of nuclear factor κ B (RANK; TNFRSF11A) gene were found in LOMG [30]. The relevance of genetic susceptibility in MG has been further validated by studying monozygotic and dizygotic twins [37]. The concordance in monozygotic twins was at approximately 36%, while dizygotic were at 4-5% [37].

MG is a prototypical autoantibody-mediated autoimmune disease. The significance of B cells in disease pathogenesis is apparent in the subcategorization of MG according to the different antigens recognized by the autoantibodies. These autoantibodies interfere with the interaction of the ligand acetylcholine with the AChR at the neuromuscular junction (NMJ) by either targeting the AChR directly or structures within the MuSK/LRP4 pathway, which is necessary for the correct clustering and functionality of the AChR **(Figure 1)** [38]. This results in disruption of the signaling from the nerves to the muscle. Generally, patients suffer from muscle weakness and increased fatiguability [1, 2].
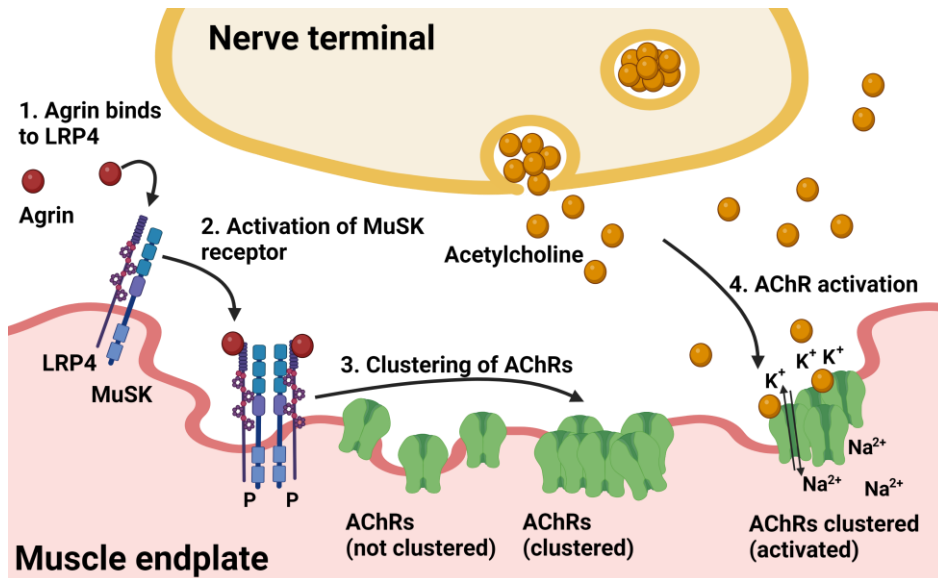
Figure 1. AChR clustering and activation at the neuromuscular junction. Several receptors and ligands are involved in the process of AChR clustering and activation at the neuromuscular junction. The LRP4 receptor forms a hetero-dimer with the MuSK receptor at the NMJ. The binding of the ligand agrin to its receptor LRP4 (1) increases the binding strength between MuSK and LRP4 and results in the formation of a hetero-tetramer between two agrin and two LRP4 molecules [39]. This results in the activation of the MuSK receptor (2) which leads to the dense clustering of AChR receptors (3). The clustered AChRs get activated upon binding of acetylcholine which is released from the nerve terminal (4). The AChR is an ionotropic receptor; activation results in the opening of an ion channel which is permeable for K^+ and Na^{2+}. The flow of the ions triggers depolarization and muscle contraction. LRP4 = Low Density Lipoprotein Receptor-Related Protein 4; MuSK = muscle-specific tyrosine kinase; AChR = nicotinic acetylcholine receptor. This Figure was created with Biorender.com.

Autoantibodies cannot yet be detected in all patients with clinically diagnosed MG. The subgroup of patients without an identifiable target antigen is termed seronegative MG (SNMG). Recent studies indicate that autoantibodies may be involved in the immunopathogenesis of SNMG [40]. Nevertheless, it is not clear whether these findings in SNMG are caused by low affinity autoantibodies to known antigens that cannot be detected by commercially available tests or autoantibodies recognizing novel antigens. More sensitive detection methods using cell-based assays were able to identify autoantibodies against known MG targets in a

13

subcohort of patients previously characterized as SNMG [41-43]. Thus, a broader usage of these assays would be beneficial in the diagnostic process. The study of B cells further revealed that B regulatory cells (Bregs) and Breg subsets secreting the anti-inflammatory interleukin 10 (IL-10) are decreased in MG potentially resulting in a more severe course of disease [44]. Additionally, the survival of autoreactive B cells might be facilitated by the increased expression of a protein associated with the inhibition of apoptosis (survivin) [45].

The immune system has several control mechanisms to prevent self-reactive B and T cells from being effective [46, 47]. For B cells, the first checkpoint of tolerance is during early B cell maturation in the bone marrow (central checkpoint) **(Figure 2)** [46, 48]. Antibodies are the soluble equivalent to the B cell receptor (BCR) on the B cell surface. The composition of the variable region of the heavy and light chains of the early BCR is the result of V(D)J recombination, where variable (V), joining (J) and diversity (D; only for heavy chains) genes are randomly combined [49, 50]. Although a broad diversity of BCR is desired for subsequent protection against an extensive array of foreign pathogens, self-reactive B cells are a possible byproduct of V(D)J recombination. Therefore, the first checkpoint to prevent self-reactive B cells from further development is at the stage of initial surface expression of the BCR (pre-B cell) [48]. Central tolerance halts Pre-B cells that interact too strongly with self-antigens through either receptor-editing or clonal deletion. Receptor-editing seems to be the main mechanism of central tolerance [46, 51] and it results in the rearrangement of the variable region of the BCR [51, 52], whereas self-reactive B cell clones that undergo clonal deletion get permanently eliminated

14

through apoptosis [53, 54]. After passing the central tolerance checkpoint pre-B cells develop further into transitional B cells and leave the bone marrow to enter the naïve B cell repertoire **(Figure 2)**. B cells in the periphery can become self-reactive during the process of affinity maturation while gaining somatic mutations in germinal centers [55]. Additionally, self-reactive B cells might be the consequence of failed central tolerance [56]. Anergy, clonal deletion, inhibition by Tregs, inhibition by Fc receptor (Fc receptor IIB) and clonal ignorance are known mechanisms of peripheral tolerance **(Figure 2)** [46]. Central and peripheral tolerance were shown to be defective in numerous autoimmune diseases including SLE, Sjogren's Syndrome, rheumatoid arthritis (RA), neuromyelitis optica [47, 57-60]. Interestingly, in most autoimmune disorders both central and peripheral are simultaneously affected, whereas solitary loss of peripheral tolerance seems to be prevalent in some patients with MS [47, 61]. In AChR and MuSK MG both central and peripheral tolerance are compromised resulting in a higher proportion of self-reactive B cells within the naïve and mature B cell repertoire [62]. A possible mechanism for the loss of peripheral tolerance in AChR MG could be the decreased expression of the Fc receptor IIB which was detected in EOMG [63] and for MuSK MG reduced receptor editing of the light chain might contribute to the loss of central tolerance [64].
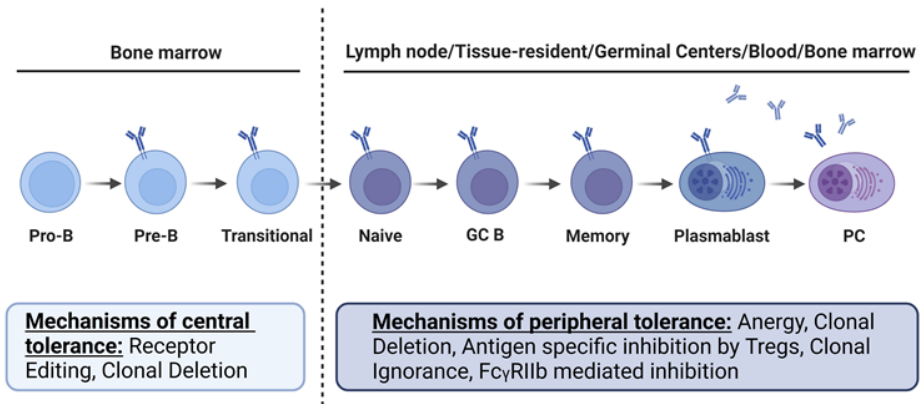
Figure 2. Mechanisms of central and peripheral B cell tolerance checkpoints. (On the left) Receptor editing and clonal deletion are the main mechanisms of central tolerance. (On the right) Anergy, clonal deletion, antigen specific inhibition by Tregs, clonal ignorance and FcγRIIb mediated inhibition are mechanisms of peripheral tolerance. Pro-B = Pro-B cell; Pre-B = Pre-B cell; Transitional = Transitional B cell; Naïve = Naïve B cell; GC B = Germinal center B cell; Memory = Memory B cell; PC = Plasma cell. This figure was adapted after [46] and created on biorender.com by modifying a pre-existing template.

It is undeniable that B cells play a crucial role in the immunopathogenesis of MG. Nevertheless, T cells and especially T helper cells (Th cells; CD4$^+$) promote the immunopathology in MG by creating a pro-inflammatory and B cell development nurturing environment [25, 65-68]. In that regard, the pro-inflammatory Th1 and Th17 cells were shown to contribute to immunopathology in MG [69-71]. Tregs are capable to dampen immune responses and help to maintain tolerance [72] and it was found that Tregs show reduced regulatory functionality in MG patients [73, 74]. T-follicular helper cells (Tfh) and T-follicular regulatory (Tfr) in germinal centers exhibit impaired pro-inflammatory and regulatory functions. Tfh cells interact with B cells in germinal centers supporting the development and maturation of B cells [75, 76], whereas Tfr cells inhibit the B cell/Tfh cell interaction [77-79]. Elevated levels of Tfh cells and decreased levels of Tfr are associated with MG [80-82]. The pro-inflammatory Th cell subsets Th$_{CD103}$ and Th$_{GM}$ cells have recently been identified

in MG patients and shown to be reduced in the circulation of patients with active disease [83]. These Th cell subsets mainly reside in the thymus and could be detected in the circulation after thymectomy [83]. It was found that impaired Tregs, activated Th cells and disease-relevant B cells reside in the inflamed thymus of AChR MG patients indicating the important role of the thymus in the immunopathology of AChR MG [84-88].

The thymus of approximately 60% of AChR MG patients is hyperplastic; especially women with EOMG have abnormalities in the morphology of the thymus [89]. The term thymic hyperplasia can be used for both true thymic hyperplasia caused by elevated numbers of epithelial cells in the thymus and lymphofollicular hyperplasia which is a consequence of hyperplastic lymph follicles [90]. In MG the hyperplasia if lymphofollicular [90, 91]. The epithelial cells in the thymus were found to express the AChR and its subunits on the cell surface making the antigen available to be presented to immune cells [92, 93]. Half of the patients presenting with thymoma develop MG over time [94] and these tumors were shown to express the AChR [95]. Thymectomy is an effective therapy for AChR MG with beneficial long-term effects including stable remission (40-50%) [96-98]. However, B cell clones originating from the thymus reemerge in the circulation after thymectomy [99]. Thymectomy did not achieve similar results in MuSK MG indicating a lesser relevant role of the thymus in the immunopathogenesis [100, 101], while a small cohort of LRP4 MG patients showed promising results after thymectomy [102, 103]. Nevertheless, the morphology of the thymus in LRP4 MG did not show structural changes and immune infiltrates [103].

1.3. PROPERTIES OF AUTOANTIBODIES IN DIFFERENT SUBTYPES OF MYASTHENIA GRAVIS

AChR MG autoantibodies are mainly produced by plasma cells [25, 104, 105]. Properties of autoantibodies in AChR MG have been studied using both serum-derived polyclonal and recombinant monoclonal AChR-specific autoantibodies. As described in more in detail in 1.2., the thymus plays a crucial part in the immunopathology of AChR MG patients [89]. Pathogenic B cells are present in the thymus which made it possible that the first AChR-specific monoclonals were isolated from the thymus [85, 106, 107]. Newer studies isolated and produced autoantibodies from the circulation [108, 109]. AChR antibodies were shown to be pathogenic *in vivo* [110-113]. The autoantibodies are mainly of the IgG1 and IgG3 subclasses which are capable of activating the complement cascade [114]. Thus, activation of the complement cascade as well as the formation of the membrane attack complex and complement-mediated damage at the NMJ were shown to be present in AChR MG patients [114-118]. Recent findings indicate that complement activation can be enhanced due to the interaction of several polyclonal autoantibodies by cross-linking the AChR at the muscle endplate [109]. The relevance of complement to the immunopathology is further evident in the success of complement targeting drugs in MG [119-121]. AChR autoantibodies can additionally block the binding site of acetylcholine at the AChR directly and thus inhibit the signaling from the nerve to the muscle [122-124]. Another pathogenic mechanism of AChR-specific autoantibodies is termed modulation. Modulating autoantibodies cross-link the AChR, which results in the internalization of the AChR

and subsequent reduced numbers of available receptors at the NMJ [125, 126]. Not all autoantibodies that recognize the AChR seem to have pathogenic properties as the titer in AChR MG was found to not correlate well with clinical disease severity suggesting the presence of non-pathogenic autoantibodies in the circulation [127-132]. Although AChR titers do not correlate well with disease severity at certain timepoints, it was found that changes of the AChR titer of individual patients correlate well with clinical disease outcome [133, 134].

Recently, monoclonal autoantibodies (mAbs) against MuSK were isolated and characterized improving our understanding of MuSK-MG [135, 136]. The ectodomain of the MuSK receptor contains three Ig-like (Ig1-3) and a frizzled domain [137, 138]. It was previously found that most MuSK autoantibodies recognize the Ig-like domain 1 on the MuSK receptor using human polyclonal sera [139]. These polyclonal autoantibodies were shown to be pathogenic [140-142] and to directly inhibit the interaction of MuSK with LRP4 [139]. Plasmablasts are a source of MuSK mAbs [143], and these mAbs are mainly, but not exclusively of the IgG4 subclass [144-146]. Antibodies of the IgG4 subclass can become functionally monovalent antibodies through the process of antigen-binding fragment (Fab)-arm exchange [147] . The effect of valency on the pathogenicity of MuSK mAbs was first shown in sera-based experiments [148] and could be replicated with human MuSK mAbs [136, 149, 150]. It was also shown that affinity maturation is important for the pathogenic development of MuSK mAbs and that antibodies reverted back to their corresponding germline-encoded unmutated common ancestor (UCA) sequence still recognize the autoantigen MuSK [149]. Much less is known about

the pathogenic properties of LRP4 and agrin autoantibodies and SNMG. Passive transfer of serum-derived IgG containing both LRP4 and agrin simultaneously into mouse showed that these antibodies are pathogenic and that they interfere with the MuSK/LRP4 pathway [12].

1.4. ANTI-CD20-MEDIATED B-CELL DEPLETION THERAPY IN MYASTHENIA GRAVIS

Cluster of differentiation 20 (CD20) is expressed at almost all steps of B cell differentiation, except for B cells at the plasma cell stage, Pro-B-cell, and Pre-B-I [151]. B cell depletion therapy (BCDT) using anti-CD20 therapies was first established for the treatment of B cell malignancies [152-154]. Anti-CD20-mediated BCDT showed beneficial effects in several autoimmune diseases including multiple sclerosis, pemphigus vulgaris, rheumatoid arthritis, chronic inflammatory demyelinating polyneuropathy (CIDP) and MuSK MG [155-159], whereas no effect of anti-CD20-mediated BCDT therapy could be observed on the titer and clinical outcome in the majority of AChR MG patients [158, 160]. Positive effects of anti-CD20-mediated BCDT have been described for severe refractory AChR MG [161, 162] and the response seems better at early stages of AChR MG [163]. MG is a very heterogeneous disease [164-167]. The heterogeneity of MG is not only defined by autoantibody status or age of disease onset, but remarkable differences can also be observed in the underlying immunopathology within patients of the same age and autoantibody specificity as evident in the heterogeneous distribution of complement fixing antibodies in cohort of AChR MG patients [165]. Therefore, this

difference in treatment response is most likely the consequence of the divergent immunopathologies of AChR and MuSK MG and particularly the difference of B cell subsets that produce pathogenic autoantibodies [164]. Furthermore, anti-CD20-mediated BCDT has a remarkable good efficacy in IgG4 autoantibody diseases, which was observed for CIDP and pemphigus in addition to MuSK MG [157, 158, 168]. Most MuSK MG patients go into stable remission for several years following anti-CD20-mediated BCDT with almost non-detectable or reduced MuSK autoantibody titers [158, 169, 170], but some patients experience relapse over time [16, 170-172]. The MuSK autoantibody titer can increase months before MuSK MG patients experience clinical-detectable relapse and often before they receive prophylactic cycles of anti-CD20-mediated BCDT [169, 173]. During relapse plasmablast and memory B cell frequencies are increased [143, 174, 175]; among these cell populations disease-related autoantibody expressing B cells were identified [135, 143]. Therefore, MuSK MG patients receiving anti-CD20-mediated BCDT undergo several cycles of remission followed by phases of clinical relapse. Nevertheless, not all MuSK MG patients respond to anti-CD20-mediated BCDT showing that MuSK MG is a heterogenous disease [162, 169]. The efficacy of anti-CD20-mediated BCDT has not been evaluated for MG with autoantibodies targeting LRP4 and agrin yet, while initial promising results showed a beneficial effect of anti-CD20-mediated BCDT in the case of a patient with juvenile seronegative MG [176]. It is, however, not known whether this patient had antibodies to AChR, MuSK, LRP4 or agrin below the level of detection or autoantibodies to unknown antigens.

2.   OBJECTIVE AND STRATEGY

How individual autoantibody-producing B cell clones and the IgG they produce contribute to pathology in MG and the immunomechanisms underlying relapse after anti-CD20-mediated BCDT is currently not well understood. This gap in our knowledge impedes the development of new therapies and personalized tailoring of existing therapies. Investigative opportunities are limited by the availability of patient-derived serum IgG and the heterogeneity of serum between patients. The isolation of individual autoantibody-producing B cells is essential to generate reliable disease models. Therefore, the objectives of this thesis were to (i) study the properties and pathogenic capacity of autoantibodies in MuSK MG (Publication I and III (Chapter 3 section 3.1 (I) and 3.3 (III)), and (ii) to elucidate the mechanisms of relapse after anti-CD20-mediated BCDT in MuSK MG patients **(Publication II and III** (Chapter 3 section 3.2 (II) and 3.3 (III)**; Figure 3)**. Human mAbs are used as a valuable tool to investigate both. First, bait antigens - a MuSK tetramer and a monomer- were developed to enrich for MuSK-specific B cells. The monomeric bait antigen was validated using a novel B cell line that was engineered to express a MuSK-specific BCR on the cell surface. MuSK-specific B cells were found to be rare in the circulation of MuSK MG patients. Next, single-cell sorted MuSK-specific B cells were either cultured, expanded and screened for positive clones or directly subjected to cloning of the heavy and light chains of their respective antibodies. These antibodies were expressed and validated for binding specificity using a live cell-based assay, radioimmunoassay and mouse muscle staining. Pathogenic capacities were evaluated using an *in vitro* AChR clustering assay. Single-cell

transcriptional and B cell receptor profiling was used to evaluate the B cell repertoire and phenotype of B cells, and B cell repertoire tracing was used to identify clonal variants in longitudinal samples. Publication I focus on the generation, validation, and characterization of MuSK mAbs using a tetrameric MuSK antigen. Publication II describes the investigation of the B cell repertoire of MuSK MG patients pre- and post-anti-CD20-mediated BCDT, while Publication III introduces two new MuSK monoclonals and traces their presence in longitudinal samples through anti-CD20-mediated BCDT.
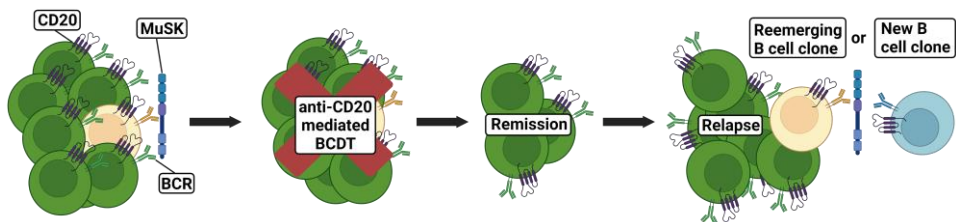
Figure 3. Diagram showing an illustration of the main objective of the thesis: Investigating the immunomechanism of relapse after anti-CD20-mediated BCDT in MuSK MG. B cells that express cluster of differentiation molecule (CD20) get targeted by anti-CD20-mediated B cell depletion therapy (BCDT). Some of these B cells express B cell receptor (BCRs) specific for muscle-specific tyrosine kinase (MuSK). The levels of B cells are diminished at the timepoint of remission. At relapse B cell numbers are replenished and MuSK-specific B cells are present. It is not known if these antigen-specific B cells persist and reemerge or whether the develop de novo. MuSK-specific B cell are presented in yellow or blue and non-diseases related B cells in green. The red x indicates anti-CD20 mediated B cell depletion therapy. The figure is adapted after the graphical abstract featured in [177]. This Figure was created with Biorender.com.

3. PUBLICATIONS

PUBLICATION I: Characterization of pathogenic monoclonal autoantibodies derived from muscle-specific kinase myasthenia gravis patients

PUBLICATION II: Single-cell repertoire tracing identifies rituximab-resistant B cells during myasthenia gravis relapses

PUBLICATION III: Reemergence of pathogenic, autoantibody-producing B cell clones in myasthenia gravis following B cell depletion therapy

3.1.   PUBLICATION I: CHARACTERIZATION OF PATHOGENIC
MONOCLONAL AUTOANTIBODIES DERIVED FROM MUSCLE-
SPECIFIC KINASE MYASTHENIA GRAVIS PATIENTS

Characterization of pathogenic monoclonal autoantibodies derived from muscle-specific kinase myasthenia gravis patients

Kazushiro Takata,[1,2] Panos Stathopoulos,[1,2] Michelangelo Cao,[3] Marina Mané-Damas,[4] **Miriam L. Fichtner,[1,2]** Erik S. Benotti,[1,2] Leslie Jacobson,[5] Patrick Waters,[5] Sarosh R. Irani,[5] Pilar Martinez-Martinez,[4] David Beeson,[3] Mario Losen,[4] Angela Vincent,[3] Richard J. Nowak[1], and Kevin C. O'Connor[1,2]

[1]Department of Neurology and [2]Department of Immunobiology, Yale School of Medicine, Yale University, New Haven, Connecticut, USA. [3]Neurosciences Group, Weatherall Institute of Molecular Medicine and Nuffield Department of Clinical Neurosciences, Oxford, England. [4]Department of Psychiatry and Neuropsychology, School for Mental Health and Neuroscience, Maastricht University, Maastricht, Netherlands. [5]Oxford Autoimmune Neurology Group, Nuffield Department of Clinical Neurosciences, John Radcliffe Hospital, University of Oxford, Oxford, England.

Authorship note: KT and PS contributed equally to this work.

Address correspondence to: Kevin C. O'Connor, Yale School of Medicine, Departments of Neurology and Immunobiology, Room 353J, 300 George St., New Haven, Connecticut 06511. Phone: 203.737.3321; Email: kevin.oconnor@yale.edu.

Direct contributions of the PhD candidate Miriam Fichtner (MLF) to the work of this study: MLF designed and performed additional cell-based antibody assay experiments and contributed to the execution and analysis of the C2C12 assays that PS established and performed. KT, with assistance from MLF and ESB, built and tested the MuSK domain deletion constructs.

Abstract

Myasthenia gravis (MG) is a chronic autoimmune disorder characterized by muscle weakness and caused by pathogenic autoantibodies that bind to membrane proteins at the neuromuscular junction. Most patients have autoantibodies against the acetylcholine receptor (AChR), but a subset of patients have autoantibodies against muscle-specific tyrosine kinase (MuSK) instead. MuSK is an essential component of the pathway responsible for synaptic differentiation, which is activated by nerve-released agrin. Through binding MuSK, serum-derived autoantibodies inhibit agrin-induced MuSK autophosphorylation, impair clustering of AChRs, and block neuromuscular transmission. We sought to establish individual MuSK autoantibody clones so that the autoimmune mechanisms could be better understood. We isolated MuSK autoantibody-expressing B cells from 6 MuSK MG patients using a fluorescently tagged MuSK antigen multimer, then generated a panel of human monoclonal autoantibodies (mAbs) from these cells. Here we focused on 3 highly specific mAbs that bound quantitatively to MuSK in solution, to MuSK-expressing HEK cells, and at mouse neuromuscular junctions, where they colocalized with AChRs. These 3 IgG isotype mAbs (2 IgG4 and 1 IgG3 subclass) recognized the Ig-like domain 2 of MuSK. The mAbs inhibited AChR clustering, but intriguingly, they enhanced rather than inhibited MuSK phosphorylation, which suggests an alternative mechanism for inhibiting AChR clustering.

Introduction

Patients with myasthenia gravis (MG) experience skeletal muscle weakness, worsened by activity. Typically, they present with ocular muscle weakness, which then generalizes to involve limb muscles and bulbar and respiratory muscles in particular (1, 2). The molecular immunopathology of MG is directly attributed to the presence of circulating autoantibodies specifically targeting extracellular domains of postsynaptic membrane proteins at the neuromuscular junction (NMJ; refs. 1, 3). The disease has multiple subtypes, defined by different autoantibody targets (4–7). Autoantibodies against the acetylcholine receptor (AChR), which are present in around 85% of patients, are mainly IgG1 and cause loss of AChRs via divalent binding, which leads to internalization of AChRs and complement-mediated damage to the NMJ (1, 8). Some of the 15% of patients without AChR autoantibodies have, instead, autoantibodies against muscle-specific tyrosine kinase (MuSK) (7) or, less commonly, low-density lipoprotein receptor–related protein 4 (LRP4; refs. 9, 10). The MuSK autoantibody form of MG can be severe because it usually involves mainly bulbar muscles (11), which affects speaking, chewing, swallowing, and breathing, and can cause permanent muscle atrophy over time (12, 13). MuSK autoantibodies are particularly interesting because they are predominantly (14) of the non-complement-activating IgG4 subclass; the subclass can be functionally monovalent for antigen binding and hence does not cross-link its antigen (15). Yet MuSK autoantibodies are demonstrably pathogenic, which can be established by passive transfer of the human disease phenotype to mice by injection of patients' IgG or active immunization with MuSK (16–18).

MuSK is an essential component of the agrin/LRP4/MuSK/downstream of tyrosine kinase 7 (DOK7) pathway that is responsible for clustering of AChRs at the NMJ, both during development and in mature muscle (19). Serum-derived MuSK autoantibodies mainly recognize the N-terminal Ig-like domain 1 of MuSK and prevent the binding of LRP4 to MuSK (20–22). As a result, autophosphorylation of MuSK is inhibited and DOK7 is not recruited to complete the pathway. These effects can be demonstrated in the mouse myotube-forming C2C12 cell line, where MuSK autoantibodies prevent agrin/LRP4-induced clustering of AChRs. In this model, isolated antigen-binding fragments (Fabs) from MuSK-specific antibodies are sufficient to inhibit AChR clustering (23). In contrast, AChR autoantibodies require divalent binding to cause loss of AChRs (8, 24, 25). Although some of the mechanisms underlying MuSK autoantibody-associated MG appear well understood, patients' autoantibodies are heterogeneous. For instance, IgG1, IgG2, and IgG3 MuSK autoantibodies exist in most patients, and their pathogenic mechanisms have not been well studied. Moreover, it is unclear whether autoantibodies against domains other than the first Ig-like domain in MuSK may contribute to disease. We sought to establish individual MuSK IgG clones so that the mechanisms in this disease could be better analyzed both *in vitro* and *in vivo*.

All forms of MG improve with immunotherapies, but B cell depletion with a therapeutic monoclonal autoantibody (mAb; rituximab) against the B cell marker CD20 leads to substantial reductions in MuSK autoantibodies and relatively quick clinical improvement (11, 26, 27). The success of anti-CD20 therapy suggests that the autoantibodies are derived from circulating MuSK-specific B cells rather than

bone marrow-resident long-lived plasma cells (LLPCs). LLPCs, which produce the majority of circulating antibodies, express negligible levels of CD20 and thus are not targets of rituximab treatment (28). This is confirmed by commonly unchanged serum Ig levels and sustained vaccine-specific titers after treatment (26, 29, 30). Accordingly, we proposed a speculative model in which an autoreactive fraction of memory B cells and circulating short-lived plasmablasts are responsible for much of the MuSK autoantibody production (3, 31) and recently demonstrated that circulating plasmablasts do indeed contribute to MuSK MG autoantibody production (32).

Given the accessibility of circulating autoantibody-producing cells, we adapted a previously reported approach (33) to produce a high-avidity, fluorescently tagged MuSK tetramer that could identify and assist with sorting rare autoantibody-expressing B cells from patient-derived blood samples. The specificity of the isolation was validated by single-cell sorting of antigen-labeled B cells and by reconstruction of recombinant human mAbs, which were then tested for binding to MuSK.

Results

Study subjects. Patients (n = 6, all female; mean age 44 ± 12 years, range 37–63; consistent with reported demographics of MuSK MG in refs. 34–36) with laboratory and clinically confirmed MuSK autoantibody-positive MG were selected for study. Their clinical severity and serum autoantibody status at the time of sampling are summarized in **Table 1**. The controls included 2 healthy individuals, 1 male aged

37 years and 1 female aged 30 years **(Table 1)**. Both had no history of autoimmune disease and no recent inflammatory events and were negative for serum MuSK autoantibodies.

Table 1. Study subject clinical, laboratory and demographic data

Patient	Sex	Age	Diagnosis	Ab status	MGFA Class at TOC	Rituximab	Other therapy	Serum MuSK Ab titer
MuSK1	F	37	Generalized MuSK MG	MuSK	IIIB	1 cycle[A] 19 mo before TOC	None	5.7[B]
MuSK2a	F	45	Generalized MuSK MG[D]	MuSK	I[C]	4 cycles 78 mo before TOC	None	11.6[B]
MuSK3	F	53	Generalized MuSK MG	MuSK	IIA	2 cycles 21 mo before TOC	Prednisone 10mg/d PLEX	0.9[B]
MuSK4	F	35	Generalized MuSK MG	MuSK	IIB	None	Mycophenolate 1500mg	1:1280[D]
MuSK5	F	31	Generalized MuSK MG	MuSK	IIB	None	PLEX	1:640[D]
MuSK6	F	63	Generalized MuSK MG	MuSK	IIB	5 cycles 20 mo before TOC	None	1:5120[D]
HD1	M	37	-	-	-	-	-	-
HD2	F	30	-	-	-	-	-	-

All data were acquired at the time of study specimen collection, unless otherwise noted. Additional specimens from 3 of the patients (MuSK1, MuSK2a, and MuSK3) had been studied in our previous investigation and are named as indicated in that report (32). [A] A cycle of rituximab consisted of 1 infusion per week for 4 weeks; dose per infusion: 375 mg/m2. [B] Determined by radioimmunoassay; levels in nmol/l. [C] This patient (MuSK2a) was diagnosed with generalized MG based on prior clinical assessments but had only ocular signs and symptoms at the time of sample collection. [D] Determined by radioimmunoassay; levels reported as serum titer. F, female; M, male; MGFA, MG Foundation of America clinical classification; mo, month; MuSK, muscle-specific tyrosine kinase; NA, not available; PLEX, plasma exchange; TOC, time of collection.

Generation of a multimeric, fluorescent MuSK antigen. We expressed the extracellular domain of MuSK, which was tagged, at the C-terminus, with a BirA site that allows for posttranslational biotinylation. The addition of allophycocyanin-conjugated (APC-conjugated) streptavidin was then used to generate a fluorescent antigen tetramer/multimer **(Supplemental Figure 1A)**. To validate that MuSK-specific antibodies were able to recognize the tetramer, antibody binding was tested in a flow cytometry-based assay. Flow cytometry beads, coated with anti-mouse Ig antibodies, were incubated with either the hybridoma-derived murine mAb, 4A3, that recognizes human MuSK or a control mAb, 8-18C5, that recognizes human myelin oligodendrocyte glycoprotein (MOG). Antibody-coated beads were incubated with fluorescent MuSK multimers and then analyzed by flow cytometry. The MuSK multimer was bound by beads that were coated with the MuSK-specific mAb but not those coated with the MOG mAb **(Supplemental Figure 1B)**. These data established that the multimerized, labeled MuSK retained properties required for antibody recognition and was suitable for identifying B cells expressing MuSK-specific B cell receptors. Thus, the reagent was applied for the identification and isolation of human MuSK-specific B cells. Antibody-secreting cells (plasmablast-like phenotype) and antigen-experienced B cells (memory-like phenotype) that bound the fluorescent MuSK multimer **(Supplemental Figure 2)** were isolated.

Screening of recombinant human mAbs. We cloned and expressed human recombinant mAbs from single sorted memory B cells or plasmablasts, which were positive for staining with the fluorescent MuSK multimer. We cloned 77 mAbs from the 6 MuSK MG patients and another 29 from the 2 healthy controls **(Supplemental**

Table 1). For initial screening of MuSK-binding capacity, all the variable heavy chain domains were cloned into a human IgG1 subclass expression vector, irrespective of their native isotype or IgG subclass usage, which was not determined at this step. The variable light chain domains were cloned into either a κ or λ expression vector based on their native usage. We first screened the mAbs for MuSK binding at 10 μg/mL using a live cell-based assay (CBA). At this mAb concentration, many of the mAbs, including those from the healthy controls, showed binding (not shown). However, using a concentration of 1 μg/ mL, 3 mAbs (MuSK1A, MuSK1B, and MuSK3B) from 2 patients (MuSK1 and MuSK3), unlike the mAbs from the 2 healthy donors (HDs), demonstrated robust binding to MuSK **(Figure 1 and Table 2)**. Most other mAbs from the MuSK patients (MuSK2a, MuSK4, MuSK5, and MuSK6) did not bind at this concentration **(Figure 1)**. Consequently, we focused on the 3 robustly binding mAbs (MuSK1A, MuSK1B, and MuSK3B). We also included an additional MuSK mAb that we had previously isolated (MuSK3-28; ref. 32), without the use of the labeled MuSK multimeric antigen, from subject MuSK3. Although production of this MuSK mAb was reported previously, the native IgG subclass, binding properties, MuSK domain specificity, and pathogenic capacity had not been characterized.
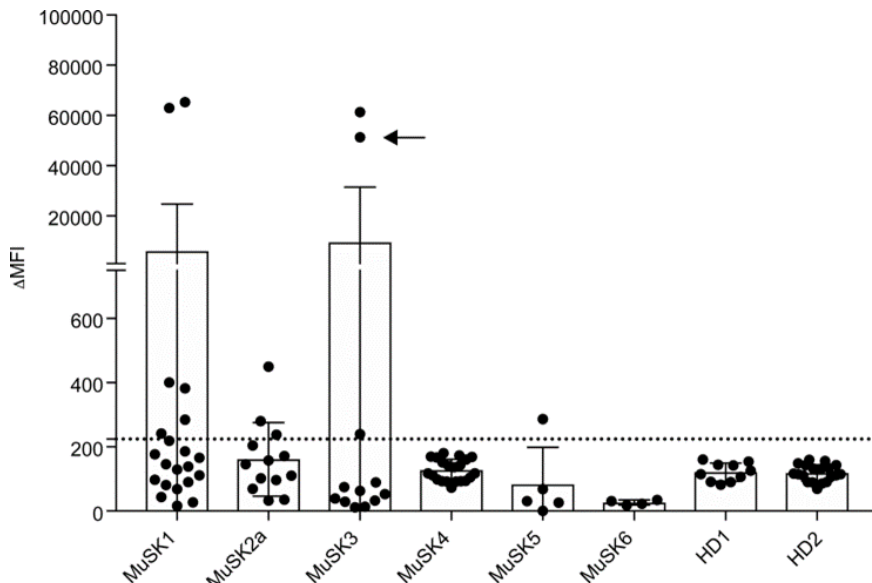
Figure 1. Screening of human recombinant mAbs. Recombinant mAbs were produced from single MuSK multimer-sorted B cells. Binding of these clones to MuSK-expressing cells was determined using a flow cytometry–based antibody-binding assay. Each data point represents the mean ΔMFI of each mAb tested at 1 μg/mL in triplicate. Bars represent the mean of means and error bars the SDs. The mAbs were derived from patients with MuSK MG and healthy donors (HDs): MuSK1 (n = 22), MuSK2a (n = 5), MuSK3 (n = 12), MuSK4 (n = 13), MuSK5 (n = 21), MuSK6 (n = 6), HD1 (n = 10), and HD2 (n = 19). A human recombinant MuSK mAb that we previously produced from single-cell–sorted plasmablasts (indicated with an arrow) was included with those tested from patient MuSK3. Values greater than the mean plus 4 SDs of the HD-derived mAbs (indicated by the horizontal dotted line) were considered positive.

Cellular origins and binding properties of MuSK-specific recombinant mAbs. During the MuSK-specific B cell sort, the FACS analyzer marked each cell in the scatter plot and its corresponding position in the 96-well plate (index sorting). After the mAbs were expressed and their MuSK specificity validated on the CBA, the exact position of the cell on the scatter plot was determined and consequently its phenotype was assessed. With this approach, we determined **(Table 2)** that mAbs MuSK1A and MuSK3B were derived from B cells displaying a memory-like phenotype (CD19$^+$CD27$^+$CD38$^-$) and MuSK1B was derived from a B cell displaying

a $CD38^+$ plasmablast-like phenotype ($CD19^+CD27^+CD38^{hi}$). The mAb MuSK3-28 had been isolated from a single-cell-sorted total plasmablast population (32).

Table 2. Molecular characteristics of MuSK-binding human recombinant monoclonal autoantibodies

Clone	B cell subset phenotype (by index sorting)	Source sort method		Isotype and IgG subclass	Variable region family	Joining region family	Diversity region family	Amino acid replacements in variable region gene segment[A]	Amino acid replacements in CDR3[a]
MuSK1A	B cell CD27+	Tetramer	H	IgG4	IGHV1	IGHJ4	IGHD5-12	8	2
			L	λ	IGLV3	IGLJ2		9	1
MuSK1B	Plasma-blast	Tetramer	H	IgG3	IGHV4	IGHJ4	IGHD6-19	14	3
			L	λ	IGLV3	IGLJ3		7	2
MuSK3-28[B]	Plasma-blast	Plasma-blast	H	IgG4	IGHV3	IGHJ3	IGHD3-10	10	1
			L	κ	IGKV1	IGKJ1		4	1
MuSK3B	B cell CD27+	Tetramer	H	IgM	IGHV4	IGHJ6	IGHD6-6	0	0
			L	κ	IGKV1	IGKJ4		0	0

[A] Variable region gene segment replacement mutations were counted from the beginning of framework 1 through the invariable cysteine at position 104. CDR3 mutations were counted between cysteine 104 and the invariable tryptophan (W) or phenylalanine (F) at position 118 in the heavy chain and the light chain, respectively. No FR4 mutations were observed. [B] This mAb had been produced and studied in our previous investigation (32).

Isotype, IgG subclass usage, and molecular properties of MuSK-specific recombinant mAbs. The native isotype and IgG subclass were determined using an additional PCR and sequencing step. The mAb MuSK1A was natively expressed as IgG4, mAb MuSK1B as IgG3, and mAb MuSK3B as IgM **(Table 2)**. The mAb MuSK3-28 was natively expressed using IgG4. B cell receptor sequence analysis of the 4 MuSK mAbs revealed that these autoantibodies are represented by diverse clones that use different variable region gene segments **(Table 2)**. A number of somatic mutations, a hallmark of affinity maturation, had accumulated in the variable heavy and variable light CDR regions of the 3 IgG isotype mAbs, strongly suggesting that antigenic selection had occurred. The fourth mAb, which used IgM, did not include any somatic hypermutations. These Ig sequencing data show that MuSK autoantibodies are mostly class switched and suggest that the development of MuSK autoantibodies often requires the processes of clonal selection, affinity maturation, and class switching.

Binding properties of MuSK-specific recombinant mAbs. We next sought to examine the binding properties of the IgG mAbs. The IgM isotype-derived mAb, MuSK3B, was not further investigated in this study because this isotype has not been implicated in MuSK MG pathology. Given the importance of IgG4 autoantibodies in MuSK MG and to discount any influence of the subclass constant region on the IgG4 mAbs, we subcloned the variable region of the IgG4 subclass autoantibodies (MuSK1A and MuSK3-28) into human IgG4 expression vectors, thus, matching the native subclass and ensuring they were expressed as divalent,

monospecific recombinant mAbs. Unless otherwise noted, the IgG4 subclass versions of mAbs MuSK1A and MuSK3-28 were used.

Binding of the mAbs was tested over a range of concentrations using a live CBA. These tests demonstrated that binding could be detected with only 20 ng/mL for the IgG mAbs MuSK1A, MuSK1B, and MuSK3- 28 **(Figure 2, A and B)**. An independent RIPA, commonly used for clinical diagnosis of MuSK MG, showed that as little as 0.3 ng of mAbs MuSK1A, MuSK1B, and MuSK3-28 could bind 30% to 50% of ^{125}I-MuSK **(approximately 1 fmol/assay; Figure 2C)**. To explore their specificity and potential pathogenicity, we also tested these mAbs in CBAs using GFP-transfected HEK cells or cells transfected with AChR or MOG **(Figure 2D)**. MOG was chosen because its structure (37), a classical Ig (Ig variable domain) fold, is highly similar to that of MuSK (38). The mAbs MuSK1A, MuSK1B, and MuSK3-28 did not show any detectable binding to GFP-transfected HEK cells or HEK cells expressing AChR or MOG on their surface **(Figure 2D)**. Finally, we tested the mAbs on sections of mouse muscle tissue to determine whether they could recognize mouse MuSK. The mAbs that were highly positive in the CBA, using human MuSK, also bound to mouse NMJs where the mAbs closely colocalized with AChRs **(Figure 2E)**. These data also demonstrated that the mAbs can recognize MuSK when presented in its native biological environment, an important requisite for future pathogenicity experiments in mouse-derived cells and disease models.
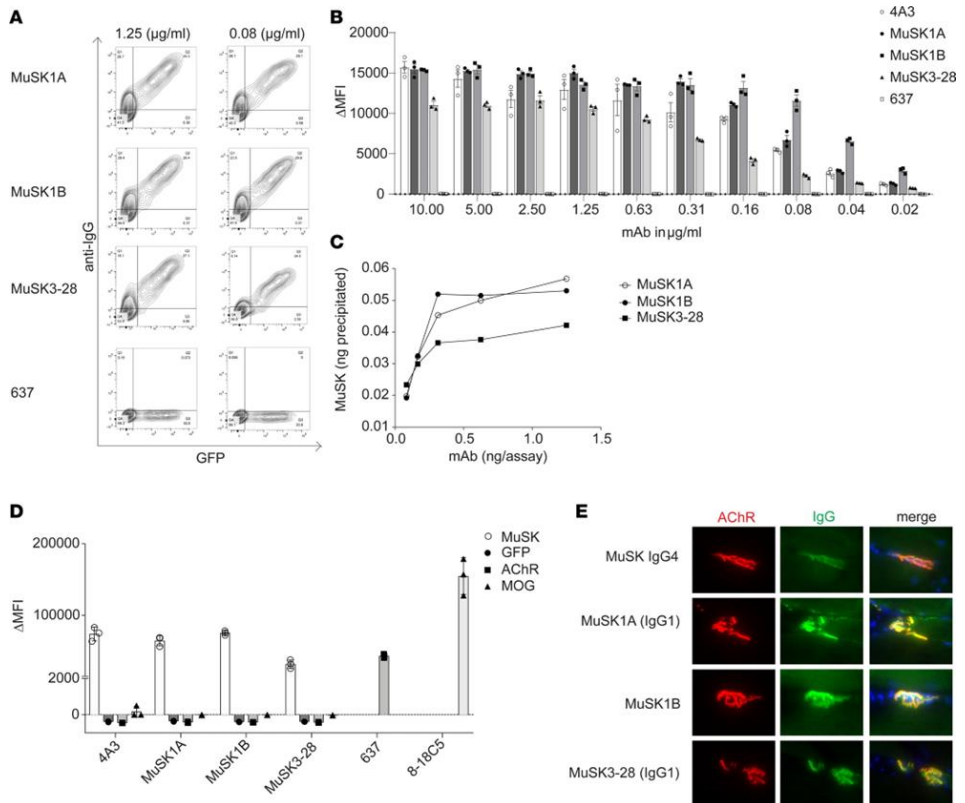
Figure 2. Characterization of human MuSK mAb-binding properties. Binding properties of mAbs MuSK1A, MuSK1B, and MuSK3-28 were tested in several *in vitro* antibody-binding assays. **(A)** Representative cell-based assay (CBA) flow cytometry plots are shown for 3 MuSK mAbs and a negative control (AChR-specific mAb 637). Binding was tested at both 1.25 and 0.08 μg/mL. The x axis represents GFP fluorescence intensity and, consequently, the fraction of transfected HEK cells. The y axis represents Alexa Fluor 647 fluorescence intensity, which corresponds to secondary anti-human IgG antibody binding and, consequently, primary antibody binding to MuSK. Hence, transfected cells are located in the right quadrants and transfected cells with MuSK autoantibody binding in the upper right quadrant. **(B)** Binding to MuSK was tested over a wide range of mAb concentrations in the CBA. Controls included the MuSK-specific humanized mAb 4A3 and AChR-specific mAb 637 tested with MuSK mAbs MuSK1A, MuSK1B, and MuSK3-28. Each data point represents a separate replicate within the same experiment. Bars represent means and error bars SDs. **(C)** A solution phase radioimmunoassay was used to measure MuSK binding over a range of mAb concentrations. Each data point represents a value within the same experiment. **(D)** Specificity of the mAbs was evaluated using CBAs that tested binding to HEK cells transfected with MuSK, GFP alone, AChR, or MOG. Positive controls included MuSK-specific humanized mAb 4A3, AChR-specific mAb 637, and MOG-specific 8-18C5. Each data point represents a separate replicate within the same experiment. Bars represent means and error bars SDs. **(E)** Immunofluorescent staining of mouse NMJs. Tibialis anterior muscles were cut longitudinally in cryosections and fixed with PFA. AChRs were stained with Alexa Fluor 648 α-bungarotoxin (shown in red) and DNA with Hoechst (shown in blue in the merged panels). The first row shows staining with polyclonal IgG4 from a patient with MuSK MG. Binding of mAbs (MuSK1A, MuSK1B, MuSK3-28) against MuSK (1.6 μg/mL for 1 hour) was detected with goat anti–human IgG Alexa Fluor 488 (IgG, shown in green). In A–E the IgG4 subclass mAbs MuSK1A and MuSK3-28 were tested in their native IgG subclass unless indicated otherwise.

MuSK autoantibody epitope mapping. To map the targets of the mAbs, we engineered a series of plasmid constructs **(Figure 3A and Supplemental Figure 3)** to express either individual subdomains of MuSK or MuSK with deletions of individual subdomains and tested binding of the mAbs using a CBA. The mAbs MuSK1A, MuSK1B, and MuSK3-28 bound to HEK cells expressing full-length MuSK, MuSK ΔIg1, MuSK Δfrizzled (ΔFz), and MuSK Ig2 only **(ΔIg1, Ig3, and Fz; Figure 3B)** but did not bind to MuSK in which the Ig-like domain 2 was deleted (ΔIg2) or when the Ig-like domain 1/Fz-like domain were expressed alone **(Figure 3B)**. Thus, mAbs MuSK1A, MuSK1B, and MuSK3-28 recognize epitope(s) in Ig-like domain 2. The control humanized mAb 4A3, previously produced (32), recognized the Fz-like domain **(Figure 3B)**. We also tested sera from MuSK MG patients MuSK1 and MuSK3 for binding to the different MuSK domain constructs. MuSK1 serum contained autoantibodies that recognized full-length MuSK, as well as each of the domain deletion constructs and the isolated domain constructs. These findings indicate that MuSK1 serum contains a heterogeneous collection of autoantibody specificities, which collectively recognize epitopes present in all the tested MuSK domains **(Figure 3C)**. MuSK3 serum displayed lower reactivity compared with MuSK1 serum when testing binding to full-length MuSK. In addition, MuSK3 serum contained autoantibodies that preferentially recognized isolated MuSK domains that included the Ig-like domain 2, indicating that the epitope(s) could be more restricted in this patient **(Figure 3C)**. These results using MuSK1 and MuSK3 serum provide further evidence for surface expression of the constructs tested. Moreover, the results concerning MuSK3 serum binding showed that the

39

specificity of the mAb MuSK3-28 for the MuSK Ig-like domain 2 reflected the specificity of the circulating autoantibody repertoire.
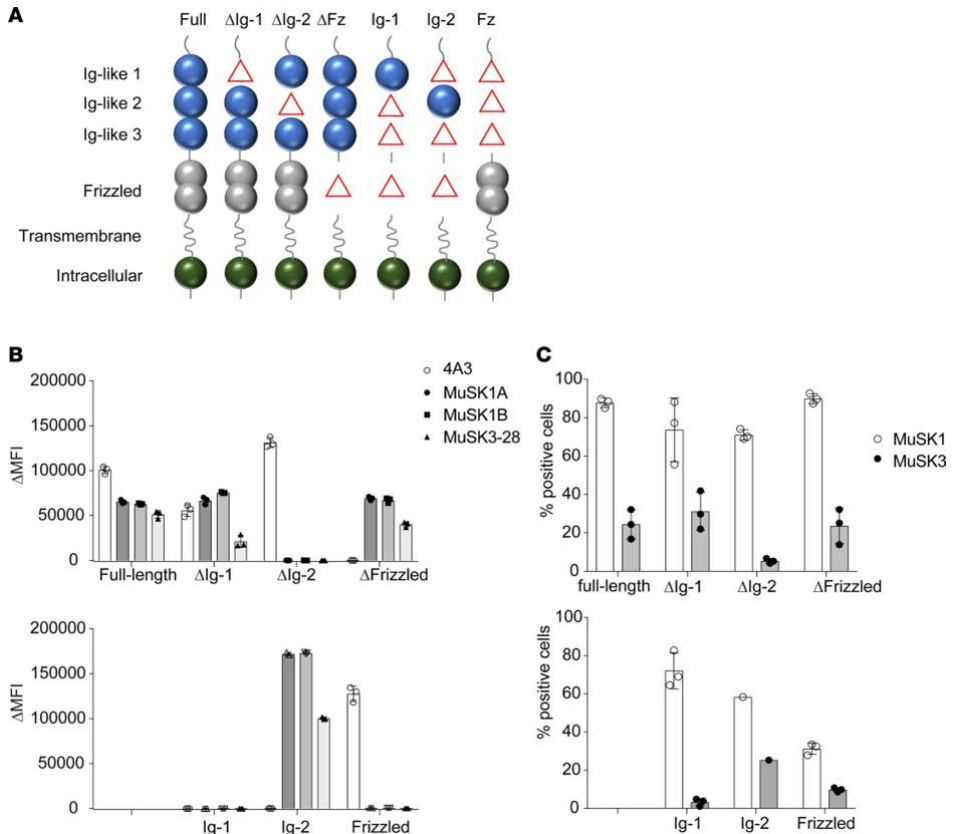

Figure 3. MuSK domain-binding results. To map the human MuSK mAb epitopes, MuSK constructs that had particular domains deleted and full-length MuSK were each expressed in HEK cells and tested with the CBA. **(A)** The schematic illustrates the mutant forms of MuSK. For example, "ΔIg-1" includes only the Ig-like domains 2 and 3 and the frizzled-like (Fz-like) domain because the Ig-like domain 1 was deleted (shown as "Δ" in the schematic). Similarly, "Ig-1" includes only the Ig-like domain 1 because the Ig-like domains 2 and 3 and Fz-like domain were deleted (shown as "Δ" in the schematic). Binding of mAbs (MuSK1A, MuSK1B, MuSK3-28, and the positive control humanized MuSK mAb 4A3) to these mutant forms of MuSK was tested in our standardized flow cytometry CBA. Results for each **(B)** mAb or **(C)** serum specimen are shown. Serum was obtained from the same patients from whom the mAbs were derived. Each data point represents a separate replicate within the same experiment. Bars represent means and error bars SDs.

Pathogenic capacity - MuSK mAbs interfere with agrin-induced AChR clustering.
To evaluate the pathogenicity of the MuSK-specific recombinant mAbs, we used
the well-established *in vitro* C2C12 AChR-clustering assay. The C2C12 mouse
myotubes express all the components that are required for agrin to stimulate AChR
clustering (39). Serum-derived MuSK autoantibodies have been demonstrated to
interrupt this interaction and consequentially inhibit AChR clustering (7, 18, 23).
The C2C12 myotubes were incubated with each of the 3 MuSK mAbs and controls;
then AChR clusters were visualized **(Figure 4, A–D)** and the mean number of
clusters recorded. All 3 mAbs reduced agrin-induced AChR clustering, whereas
mAb 4A3, which recognized the Fz-like domain, had no effect **(Figure 4E)**. These
findings indicate that mAbs MuSK1A, MuSK1B, and MuSK3-28 are pathogenic in
this model. The ability of the mAbs to induce AChR clustering in the absence of
agrin was also evaluated. When added to C2C12 cultures, each of the 3 MuSK
mAbs induced a modest, although not significant, increase in AChR clustering
(Supplemental Figure 4) compared with 3 non-MuSK-binding mAbs and the
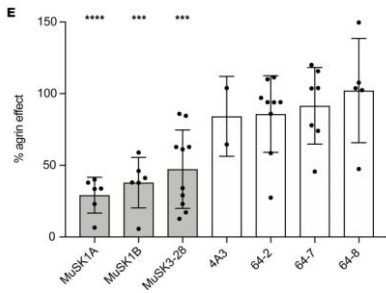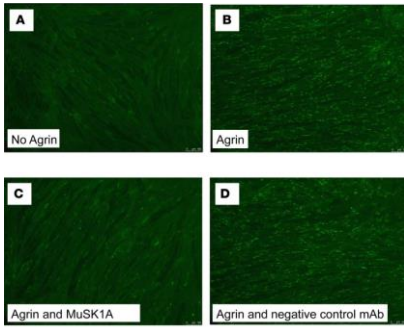MuSK Fz-like domain-specific 4A3 mAb.

Figure 4. AChR-clustering assay in C2C12 mouse myotubes demonstrates pathogenic capacity of MuSK mAbs. The presence of agrin in C2C12 myotube cultures leads to dense clustering of AChRs that can be readily visualized with fluorescent α-bungarotoxin and quantified. Pathogenic MuSK autoantibodies disrupt this clustering. Three different human MuSK-specific mAbs, the humanized murine control MuSK mAb 4A3, and 3 human non-MuSK-specific mAbs derived from AChR MG patient plasmablasts (plasmablasts 64-2, 64-7, and 64-8) were tested for their ability to disrupt the AChR clustering. Each mAb was added to the cultures at 1 μg/mL. **(A-D)** Representative images (original magnification, ×100) from the clustering experiments are shown. **(A)** Cultured myotubes do not show AChR clustering until **(B)** agrin is added (bright spots reveal AChR clusters). **(C)** The mAb MuSK1A added at 1 μg/mL inhibits clustering **(D)**, whereas a control mAb does not inhibit the formation of AChR clusters. **(E)** Clustering of AChR was quantified relative to the measured effect of agrin. Quantitative results are normalized to clustering induced by only agrin. Each data point represents the mean value from an independent experiment. Bars represent the mean of means and error bars the SDs. Multiple-comparisons ANOVA (against the pooled results for the 3 human non-MuSK-specific mAbs), Dunnett's test; *$P < 0.05$, **$P < 0.01$, ***$P < 0.001$, and ****$P < 0.0001$, shown only when significant.

Pathogenic capacity - MuSK mAbs modify agrin-induced MuSK phosphorylation.
One of the crucial steps in the agrin/LRP4/MuSK/DOK7 pathway is MuSK phosphorylation. Serum IgG or IgG4 antibodies from patients with MuSK MG inhibit agrin-induced MuSK tyrosine phosphorylation (20). MuSK MG serum-derived IgG or recombinant human mAbs were added to cultured C2C12 myotubes, with agrin. MuSK tyrosine phosphorylation was then detected using immunoblotting with a phosphotyrosine-specific antibody **(Figure 5A)**. Agrin-induced phosphorylation was blocked by the patient-derived serum IgG whereas the 3 non-MuSK-binding mAbs and the control mAb 4A3, which recognizes an epitope in the Fz-like domain, did not alter the agrin-induced MuSK phosphorylation **(Figure 5B)**. By contrast, and intriguingly, the 3 MG patient-derived MuSK-specific mAbs, MuSK1A, MuSK1B, and MuSK3-28, all modestly amplified the agrin-induced phosphorylation **(Figure 5B)**. Thus, these mAbs increased agrin-induced MuSK phosphorylation while inhibiting agrin-induced AChR clustering. The mAbs MuSK1A and MuSK3-28 were tested both as their native IgG4 subclass and as IgG1. Similar amplification of agrin-induced phosphorylation was observed with both subclasses **(Figure 5B)**. These results suggest that divalent (and monospecific) MuSK autoantibodies that bind Ig-like domain 2 can activate MuSK phosphorylation, irrespective of their subclass.
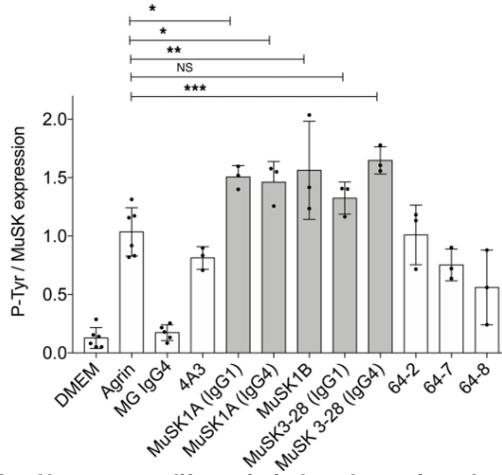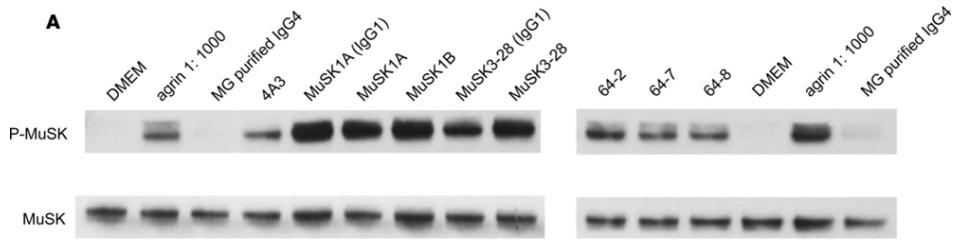
Figure 5. MuSK mAbs can amplify agrin-induced tyrosine phosphorylation. (A) Immunoblots showing phosphotyrosine bands and related MuSK expression in C2C12 murine myotubes that were incubated with agrin in the presence of MuSK MG serum-derived IgG4 or recombinant MuSK/control mAbs. 4A3 is a humanized murine MuSK mAb; MuSK1A, MuSK1B, and MuSK3-28 are human MuSK mAbs from patients with MuSK MG; and 64-2, 64-7, and 64-8 are non-MuSK-binding human mAbs derived from AChR MG patient plasmablasts. IgG4 subclass mAbs MuSK1A and MuSK3-28 were expressed in vectors reflecting the native subclass and as IgG1 (as indicated). **(B)** Normalized densitometry analysis results from the MuSK phosphorylation immunoblots are plotted. Each data point represents an independent experiment. Bars represent means and error bars SDs. Phosphorylation of MuSK was determined by normalizing to MuSK expression, detected by a commercial anti-MuSK antibody after stripping the blot, and the ratio of phosphotyrosine MuSK/MuSK is plotted. Multiple-comparisons ANOVA (versus agrin), Dunnett's test; ns $P > 0.05$, *$P < 0.05$, **$P < 0.01$, and ***$P < 0.001$, shown for MuSK mAbs versus agrin comparisons.

44

Discussion

There is much interest in production of human mAbs from patients with antigen-specific autoimmune diseases, but identification and isolation of autoantibody-producing cells is challenging because many reside in the lymphatics, bone marrow, or other tissue compartments and are scarce in the circulation (33, 40).

Moreover, even if circulating antigen-specific B cells can be detected (41, 42), screening approaches, such as Epstein-Barr virus transformation of circulating B cells or bulk isolation of antigen-experienced B cells, may provide only low yields of the relevant antibodies (43–45). Here, we used a multimerized, fluorescent MuSK construct to identify, capture, and characterize mAbs. Three mAbs from 2 patients with MG bound at sub-nanomolar concentrations to MuSK. These autoantibodies, when expressed as divalent IgG1 or IgG4 subclasses, bound to MuSK at the NMJ, colocalizing with AChRs, and demonstrated the pathogenic mechanism of inhibition of agrin-induced AChR clustering, typical of the patients' serum autoantibodies. Surprisingly, MuSK phosphorylation, which is typically inhibited by patients' serum or native monovalent IgG4 autoantibodies, was moderately increased rather than reduced by the mAbs. This interesting finding is likely due to the divalence of the expressed MuSK mAbs.

A large number of MuSK autoantibodies were identified on the first screens when testing the mAbs at 10 μg/mL, but many showed considerably lower or absent binding capacity at 1 μg/mL. Many of these mAbs were derived from IgM B cells of HDs and patients, had low or absent somatic mutational loads, and are, therefore,

45

unlikely to have been antigen driven and thus may be of inconsequential biological significance in MG. It is possible that these IgM-expressing B cells are part of a normal repertoire that can bind multivalently but nonspecifically to the tetrameric MuSK protein. Indeed, sensitive and specific detection of MuSK autoantibodies using CBAs on clinical samples requires the use of IgG-Fc-specific antisera because of the risk of detecting nonspecific IgM binding to MuSK (46). A similar problem is seen with testing autoantibodies against MOG and may reflect interactions between IgM molecules and the extracellular Ig-like domains of these proteins (47).

A set of mAbs, which did demonstrate high binding capacity to MuSK, were studied further. The extracellular domain of MuSK is composed of 3 Ig-like domains (Ig1, -2, and -3) and a cysteine-rich Fz-like domain, which occupies the region between the Ig-like domains and the extracellular juxtamembrane region (38, 48). The majority of patient serum–derived MuSK autoantibodies are reported to recognize the N-terminal Ig-like domains Ig1 and Ig2 (7, 14); Ig1 interacts with LRP4 and is thought to form the most pathophysiologically relevant epitope because of inhibition of LRP4 binding (20, 49). It was surprising, therefore, that all 3 IgG mAbs recognized the Ig2 domain of MuSK. Two of the 3 were isolated with the tetrameric antigen, and it is possible that this conformation preferentially selects for Ig-like 2 domain autoantibodies. However, because the biotinylation site was in the C-terminal of the extracellular domain, this seems less likely, and the Ig-like 2 domain specificity may simply represent a stochastic or patient-specific event. The humanized murine control MuSK mAb 4A3, by contrast, recognized the Fz-like

domain. This domain in mammalian MuSK appears to be dispensable for AChR clustering (50, 51), and mAb 4A3 provided a useful control for the experimental studies discussed below.

In patients, the majority of MuSK autoantibodies are IgG4, while a variable minority are IgG1, -2, or -3 (14, 52). IgG4 antibodies have very weak inter-heavy chain S-S bonds and are able to exchange Fab arms with other IgG4s; thus, IgG4 antibodies become functionally monovalent (24). MG patient serum antibodies have been shown to be largely Fab-arm exchanged, and serum MuSK autoantibodies reduce AChR clustering in the C2C12 model (23), as do polyclonal Fabs against MuSK (21). However, because our IgG4 mAbs were expressed as individual clones, they were not able to Fab-arm exchange with other IgG4s and were thus divalent. Both MuSK1A and MuSK3-28 are of the IgG4 subclass, while MuSK1B is IgG3 subclass. However, irrespective of their native subclass or the Ig-like domain targeted by the mAbs, all 3 IgG mAbs inhibited the formation of agrin-induced AChR clusters in the C2C12 myotube model, which suggests that they are likely to have full pathogenic potential and questions the pathogenic dominance of monovalent IgG4 autoantibodies against the Ig-like 1 domain in MuSK MG. Indeed, a previous study (21) demonstrated that IgG1, -2, and -3 MuSK autoantibodies purified from 2 patients with MuSK MG, which did not inhibit LRP4 binding to MuSK, inhibited AChR clustering even more effectively than IgG4 MuSK autoantibodies from those patients. Overall, the results of these highly selected MuSK mAbs support that the patients' autoantibodies, of all IgG subclasses, are capable of inhibiting MuSK function and do not per se require one to invoke other mechanisms. Nevertheless,

in contrast with native IgG4, both the native IgG1 and IgG3 subclasses are effective at initiating complement activation. Consequently, the presence of IgG3 MuSK mAbs in 1 patient, along with several recently reported IgG1 MuSK mAbs (53), suggests that the immunopathology of MuSK MG may include inflammatory, potentially damaging, mechanisms as well as inhibitory mechanisms. As previously proposed, IgG-mediated damage may be most important in isolated muscles, such as facial and bulbar muscles that are susceptible to atrophy (21).

When agrin binds to LRP4, which then forms a complex with MuSK, it leads to MuSK autophosphorylation, recruitment of DOK7, and eventually rapsyn and AChR clustering, as usually studied in the C2C12 myotubes used here. Until recently, inhibition of phosphorylation was considered in determining the pathogenicity of MuSK autoantibodies. However, the results here question this assumption. All 3 human MuSK mAbs inhibited AChR clustering in the C2C12 cells, but these divalent autoantibodies led to modest but significant increases in phosphorylation rather than reduced phosphorylation. The explanation probably lies in their divalence, which may have been associated with the cross-linking of MuSK as found in murine models (19, 51, 54). The native monovalent IgG4 mAbs would not cross-link MuSK or increase phosphorylation, as recently shown in cloned IgG4 mAbs (53). Patient MuSK IgG1, -2, and -3 autoantibodies act in a similar manner, inhibiting AChR clustering while not inhibiting MuSK phosphorylation (MC, DB, and AV, unpublished observations). The mAbs described here will be essential for understanding how the divalent IgG1, -2, or -3 MuSK autoantibodies cause

inhibition of AChR clustering and alter MuSK phosphorylation and studying more fully their contribution to the disease.

The mAb MuSK1B was derived from a cell with a plasmablast-like phenotype, expressing both CD27 and high levels of CD38. This plasmablast, along with that which produced mAb MuSK3-28 (32), supports the notion that this circulating, short-lived cell type contributes to MuSK MG immunopathology (31). The isolated cell that yielded mAb MuSK1A displayed a memory B cell-like phenotype. The appearance of this cellular subtype among MuSK autoantibody-expressing cells suggests that immunological memory might have been established and that these cells can provide a reservoir from which autoantibody-secreting plasmablasts originate. Given that memory B cells express CD20, their direct elimination by CD20-targeted therapy (rituximab) may be the mechanism by which this treatment induces remarkable serum autoantibody decline and excellent clinical response in patients. That memory B cells do not secrete antibodies leaves open the possibility that such cells play an antibody-independent role in the immunopathology. Antigen presentation by B cells contributes to autoimmunity (55–57) and is necessary for models of neurological autoimmunity (58, 59). Indeed, the autoimmune mechanism in neuromyelitis optica, although principally attributed to aquaporin-4 autoantibodies, is accompanied by B cell–mediated antigen presentation to T cells and cytokine production of both the proinflammatory and antiinflammatory varieties associated with a more complex neuroinflammation (60).

Three mAbs that bound to MuSK robustly were successfully isolated from 2 patients, while 3 additional patient samples did not yield any strong MuSK-binding mAbs. These results suggest that such cells may be rare in the circulation of MG patients, even though such patients were experiencing active disease and had conspicuous serum autoantibody titers at the time of specimen collection. Furthermore, the clinical status of the patients may be important for isolation of the disease-specific cells. The patients in this study, from whom the strong-binding mAbs were sourced, were experiencing a disease exacerbation after having achieved remission through B cell depletion therapy. Remission often affords the withdrawal of treatment, including immunomodulatory treatments, that may suppress activated B cells and plasmablasts. Indeed, elevated plasmablasts have been associated with autoimmune disease activity (61). Thus, these data support the concept that breakthrough relapses after withdrawal of aggressive immunomodulatory treatments that previously had successfully suppressed the immune response could be the optimal time at which to study the otherwise sequestered pathogenic B cells and plasmablasts.

The collective data in this report highlight the importance of demonstrating the full spectrum of autoantibody characteristics and pathological potential. We anticipate that these human MuSK mAbs and the approach to their isolation will be recognized as highly valuable tools in future studies. First, these mAbs can be used to dissect the molecular mechanisms of MuSK autoantibody pathology, particularly for understanding how MuSK phosphorylation can be associated with inhibition of clustering, using both *in vitro* and *in vivo* models. Second, once the relevance of

the different IgGs and epitope specificities are established, the development of preclinical models that do not rely on the limited human MG-derived serum autoantibodies will aid in the investigation of MuSK immunopathology and help explain why facial and bulbar muscle groups are the principal target in patients. Third, the identification and isolation of rare MuSK mAb-producing cells, using the fluorescent MuSK antigen, will allow further investigation into their roles in initiation and perpetuation of the disease and whether their frequency in the circulation may represent a valuable biomarker for predicting relapse and therapeutic response. Finally, these cells should be viable targets for antigen-targeted therapies (62) that would seek to eliminate only those cells that directly contribute to autoimmunity, which would replace current nonselective immune-modulating treatments.

Methods

Isolation of serum and PBMCs from patients with MuSK MG. Peripheral blood samples were obtained from 2 healthy donors (HD1 and HD2) and 6 patients (MuSK1-6) with autoantibody and clinically confirmed MuSK MG. Patients showed typical clinical and serological features of MuSK MG **(Table 1)**. PBMCs were isolated by Ficoll's separation and stored in liquid nitrogen until use, using a described protocol (63). Time locked serum specimens were also obtained.

MuSK multimer generation. The extracellular domain of human MuSK was subcloned into the pMT/ Bip/His-A vector. The C-terminal region contained a short, flexible linker followed by a BirA site (amino acids: GLNDIFEAQKIEWHE), downstream of which was a thrombin-cleavable (amino acids: LVPRGS) 6× histidine tag. Protein expression was induced in S2 Drosophila cells (Thermo Fisher Scientific). Culture supernatant was collected and MuSK protein was purified using cobalt resin beads (Thermo Fisher Scientific) according to the manufacturer's instructions. For tetramer formation, MuSK protein was biotinylated by incubation with BirA enzyme at a 1:100 molar ratio overnight at 4°C in a buffer containing 50 mM Tris, 50 mM bicine at pH 8.3, 10 mM magnesium acetate, 10 mM adenosine-5'-triphosphate, and 50 µM biotin. Excess biotin was removed using a 10-kDa MWCO Slide-A-Lyzer dialysis cassette (Thermo Fisher Scientific). Fluorescent multimers were formed using stepwise addition of APC-conjugated streptavidin (Invitrogen) to biotinylated MuSK until a 1:4 molar ratio was reached.

Flow cytometry and cell sorting. For sorting MuSK multimer-reactive B cells, B cells were enriched from cryopreserved PBMCs using negative selection beads

(Stemcell Technologies). They were incubated with live/dead stain, then stained with 20 μg/ml MuSK multimer on ice for 30 minutes. Cells were then co-stained (using manufacturer's recommended dilutions) with fluorescently labeled antibodies against CD3 (Invitrogen, Pacific orange; UCTH1), CD14 (Invitrogen, Pacific orange; TUK4), CD19 (BD Biosciences, PE Cy7; SJ25C1), CD27 (BD Biosciences, PE; M-T271), and CD38 (BD Biosciences, V450; HB7) before sorting on an FACSAria (BD Biosciences) instrument. For general B cell immunophenotyping, B cells were defined as live CD3$^-$CD14$^-$CD19$^+$ cells, memory B cells as live CD3$^-$CD14$^-$CD19$^+$CD27$^+$CD38$^-$ cells, and antibody-secreting cells (plasmablast phenotype) as CD3$^-$CD14$^-$CD19$^+$CD27$^+$CD38^{hi}.

MuSK, AChR, and MOG mAbs. A set of mAbs for binding to MuSK, AChR, and MOG were used as controls. Cell culture supernatant from either an established murine MuSK mAb (4A3; ref. 32) or a murine MOG mAb (8-18C5; ref. 64) hybridoma was applied to a Protein G/Sepharose column (GE Healthcare) to isolate the IgG. We also engineered the MuSK mAb (4A3) and the MOG mAb (8-18C5) as chimeric mouse-human recombinant mAbs. They were produced to contain the murine mAb heavy and light chain variable regions fused to the respective human constant regions using an approach we described (65). These chimeric recombinant mAbs served as positive controls in the human antibody-binding assays and did not require a substitute (murine-specific) secondary antibody because the constant regions were identical to those of human mAbs. The AChR mAb (clone 637) was derived from a human MG thymus (24, 25, 66). The variable regions were synthesized as gBlock gene fragments (Integrated DNA

Technologies), then subcloned into expression vectors, expressed, and purified using approaches we described (67).

Recombinant human mAb production, IgG subclass determination, and subcloning. Detailed methods describing the recombinant human mAb production are available in Supplemental Methods. Briefly, reverse transcription of fresh or frozen single-cell-sorted, antigen-labeled B cell RNA; nested PCR reactions; subcloning into IgG expression vectors; antibody expression; and purification were all performed as described (63). To determine the isotype and IgG subclass, a specialized single-cell PCR using leftover cDNA from the same single cells used to make individual mAbs was performed. This PCR used a primer in a downstream region of the IgG such that the PCR product included a region of the IgG1, -2, -3, and -4 that is unique to each subclass (68, 69). Thus, identification of IgG subclass required sequence alignment of this region to each of the 4 human IgG subclasses. Following the determination of the endogenous IgG subclass for each human mAb, the variable heavy chain region was subcloned into the respective subclass-containing expression vectors.

Cell-based antibody assays. Antibody binding was tested using live HEK293T cells (ATCC, CRL-11268) transiently transfected with DNA encoding MuSK, AChR with rapsyn, or MOG (all coding human proteins), using an assay protocol we described (32). The following plasmid constructs were used for expression: full-length human MuSK (21) subcloned into a pIRES2-EGFP vector, which delivered translation of MuSK and GFP separately; human AChR α-, β-, δ-, or ε-subunits subcloned into pcDNA3.1-hygro plasmid vectors (70) and rapsyn (70), which was subcloned into

a p-EGFP-N plasmid (Clontech Laboratories); full-length human MOG (47) was also subcloned, like rapsyn, into the pEGFP-N plasmid, which produced rapsyn or MOG as fusion proteins with C-terminal GFP. CBA results were calculated as ΔMFI and percentage of transfected cells that bound secondary antibody (termed "% positive") as follows: (a) ΔMFI = Alexa Fluor 647 MFI in MuSK GFP-transfected cells minus Alexa Fluor 647 MFI in untransfected cells of the same tube; (b) % positive cells = % cells in upper right quadrant divided by % cells in upper right and lower right quadrants.

MuSK protein mutagenesis. Human MuSK deletional mutants were generated by modifying the full- length MuSK expression construct **(Supplemental Figure 3)**. Regions coding for specific domains were deleted using the Q5 Site-Directed Mutagenesis Kit (BioLabs) according to the manufacturer's instructions. Primer sequences were generated using the NEBaseChanger tool. All construct modifications were confirmed through Sanger-based DNA sequencing.

Ig sequence analysis. The heavy- and light-chain variable region germline gene segments were identified with the IMGT/V-QUEST program (71) version 3.4.14 (10 September 2018) - IMGT/V-QUEST reference directory release: 201839-3 (September 26, 2018). Somatic mutations resulting in replacement amino acids were evaluated through the alignment to germline genes provided by the IMGT/V-QUEST program. Ig isotype and IgG subclasses were determined by aligning acquired sequences to those present in the ImMunoGeneTics repertoire reference set (72).

Immunofluorescence mouse muscle sections. The binding of the different human mAbs was analyzed by immunofluorescence using cryosections of mouse tibialis anterior muscles (obtained from the Central Animal Testing Facilities of Maastricht University). Muscles were cut longitudinally at 10 μm thickness on a Leica CM3050 S cryostat; sections were mounted on gelatin-coated glass slides and stored at -80°C. After thawing, cryosections were fixed with 4% paraformaldehyde (PFA, Sigma-Aldrich) for 10 minutes at room temperature and then blocked for 30 minutes with 2% bovine serum albumin (GE Healthcare). Sections were incubated for 1 hour at room temperature with 1 of the different human mAbs (1.5 μg/mL each) combined with Alexa Fluor 647–conjugated α-bungarotoxin (1:300, B35450, Thermo Fischer Scientific). As controls, protein G-purified IgG from a patient with MuSK MG (final concentration 5 μg/mL) was used instead of the mAbs. After washing, slides were incubated with human Fcγ-specific Alexa Fluor 488-conjugated goat F(ab′)2 (3 μg/mL, 109-546-170, Jackson ImmunoResearch), combined with Alexa Fluor 594-conjugated streptavidin (1:20,000, S11227, Invitrogen) and Hoechst 33342 (2 μg/mL, B2261, MilliporeSigma) for 1 hour at room temperature in the dark. Sections were washed and mounted with 80% glycerol. All washing steps consisted of 3 incubations of the slides (5 minutes at room temperature) in 0.05% Triton X-100. Endplates were identified using the red immunofluorescence of the α-bungarotoxin staining. Triple-fluorescent photomicrographs of the endplate regions were acquired using μManager software ver2.0 (73) on an Olympus BX51WI spinning-disk confocal fluorescence microscope with a Hamamatsu EM-CCD C9100 digital camera. Endplates were

analyzed using ImageJ software (NIH) as described (73, 74). All staining procedures and fluorescent analysis were performed on coded samples by 2 independent, blinded investigators.

AChR-clustering assay. The AChR-clustering assay was performed as described (7). Briefly, C2C12 mouse myoblasts (ATCC) were grown in DMEM supplemented with 20% fetal bovine serum (FBS) and 1% penicillin/streptomycin (Gibco). C2C12 cells were plated in 24-well plates and differentiated with DMEM supplemented with 2% FBS, 0.5% penicillin/streptomycin, and 1 µM insulin (MilliporeSigma). As soon as fusion was evident (36–48 hours), AChR clustering was induced for 14 hours with 10 ng/mL (0.1 nM) agrin (R&D Systems). mAbs were applied at 1 µg/mL with agrin or alone. After the induction of AChR clustering, AChRs were visualized through the application of 1 µg/mL Alexa Fluor 647-labeled α-bungarotoxin (Invitrogen) for 1 hour at 37°C. Following staining, cells were washed twice with medium (5 minutes at 37°C) and fixed with 3% PFA for 20 minutes at room temperature. Microscopy was performed at a ×100 magnification on a Leica DMi8 fluorescence microscope. For each well, 4 visual fields of 100% myotube confluence were selected on phase contrast and captured on fluorescence; AChR clusters were counted using ImageJ software. For each condition, duplicate wells were used, and the mean of the clusters per visual field per condition was calculated. Experiments were performed at a minimum of 3 repetitions and were normalized for the effect of agrin. Reported results are from experiments in which a minimum 3-fold effect of agrin-induced clustering over the baseline was observed.

MuSK tyrosine phosphorylation assays. Myotubes (C2C12) were stimulated with 0.4 nM neural agrin or agrin with purified serum IgG4 (0.5 nM) from MuSK MG patients or mAbs (1 µg/mL) for 30 minutes at 37°C. To detect and quantify MuSK phosphorylation levels, myotubes were extracted in cold lysis buffer (10 mM Tris-HCl, 1 mM EDTA, 100 mM NaCl, 1% Triton X-100, 1× protease inhibitor cocktail, 1× phosphatase inhibitor cocktail) followed by centrifugation (16,000 g). To precipitate endogenous MuSK, the whole-cell lysate was incubated with an anti-MuSK polyclonal antibody (AF562, R&D Systems) at 4°C overnight. Bound antibody was captured with Dynabeads protein G (Invitrogen). Bead-precipitated proteins were eluted into SDS sample buffer, subjected to SDS-PAGE, and incubated with monoclonal mouse anti-phosphotyrosine antibody (4G10, Upstate Biotechnology), which was detected using a goat anti-mouse HRP antibody (P 0447; Dako, Denmark) at 1:1000 dilution. The membrane was then harshly stripped (in 62.5 mM Tris buffer at pH 6.8, containing 2.0% SDS and 0.8% β-mercaptoethanol) and reprobed for MuSK by incubating with a goat anti-MuSK polyclonal antibody (AF562, R&D), which was detected using a polyclonal rabbit anti-goat HRP antibody (P 0449; Dako, Denmark) at 1:1000 dilution. Densitometry of bands was analyzed using ImageJ software and the level of MuSK phosphorylation normalized to levels of immunoprecipitated MuSK.

Statistics. AChR clustering on the C2C12 cells and MuSK tyrosine phosphorylation were analyzed using a 1-way ANOVA with Dunnett's correction. P values below 0.05 were considered significant. Statistics were performed on GraphPad Prism (version 7.0a) software.

Study approval. This study was approved by the Human Investigation Committee at the Yale School of Medicine. Informed consent was obtained from all subjects. Tibialis muscles were obtained from mice that had been sacrificed for an experiment unrelated to this study. Animal care and use for this experiment were approved by the Animal Welfare Committee of Maastricht University and followed the laws, rules, and guidelines of the Netherlands.

Author contributions

This study was originally conceived, then initiated and directed by KCO. RJN provided all characterized subject specimens and directed the clinical aspects of the study. KT produced the tetramer. KT and PS performed the single-cell isolation, mAb expression, mAb sequencing, and cell-based antibody assays and interpreted those data. MLF designed and performed additional cell-based antibody assay experiments and contributed to the execution and analysis of the C2C12 assays that PS established and performed. KT, with assistance from MLF and ESB, built and tested the MuSK domain deletion constructs. MC, DB, and AV designed, performed, and interpreted the phosphorylation assays. MMD, PMM, and ML designed and performed the murine muscle staining and interpreted those data. PW, SRI, and LJ initially confirmed mAb specificity, in a blinded manner, by providing independent data from multiple assays. AV and LJ performed and analyzed the radioimmunoassay titration experiments. The manuscript was initially drafted by KCO and AV with substantial input from PS and ML. Key contributions in editing and revising were further provided by PS and ML.

Acknowledgments

Conflict of interest

Supplemental material

Contents:

Figure S1. Multimerized, labeled MuSK retains properties required for antibody recognition and detection by flow cytometry. Schematic diagram **(A)** showing MuSK expression construct and posttranslational tetramer assembly. FACS plots **(B)** showing feasibility of MuSK tetramer-mediated isolation. Flow cytometry beads coated with murine monoclonal antibodies that recognize MuSK (4A3) or myelin oligodendrocyte glycoprotein MOG (8-18C5) were stained with APC-conjugated MuSK multimer. Detection of binding to the beads was analyzed by flow cytometry. Data shown is one of two representative experiments.
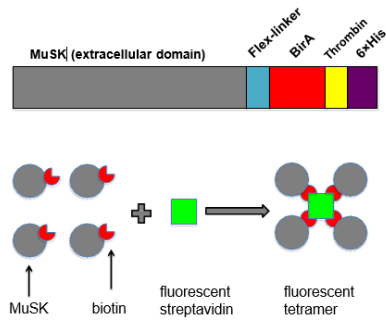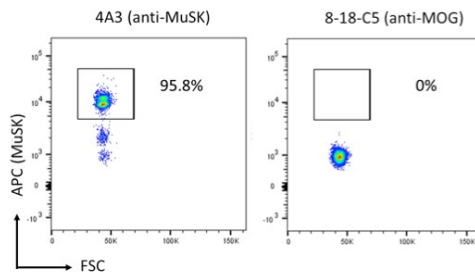
Figure S2. MuSK multimer FACS gating strategy. A representative example of the MuSK multimer positive population sorting strategy is shown. B cells that were enriched through bead-based negative selection, were initially gated in the SSC/FSC graph. After doublets and dead cells were excluded, $CD19^+CD3^-CD14^-$ cells were gated. MuSK multimer positive cells were subsequently gated from the B cell gate ($CD19^+CD3^-CD14^-$) using $CD27^+$ MuSK multimer$^+$ cells. Plasmablasts were defined as $CD27^{hi}CD38^{hi}$ cells for purposes of back-gating and index-sorting (not shown).
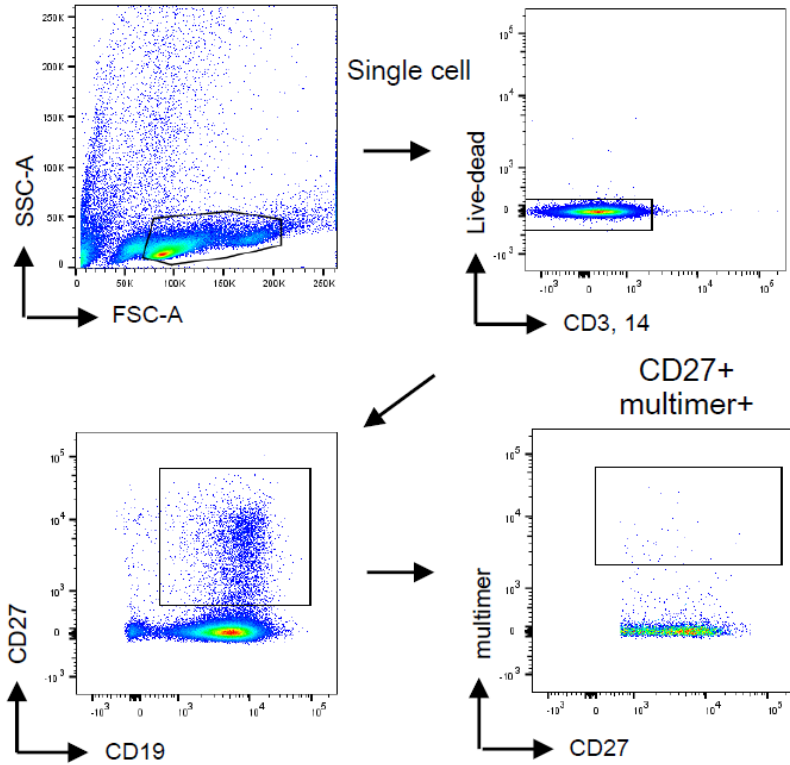
Figure S3. Protein sequences (amino acid) of different MuSK domain expression constructs. Bold letters indicate particular domains. Dots represent deleted regions.

```
Full length MuSK sequence:
                                            |----------------------------· Ig-like domain-1                          |
                                                                                   ----------------------------·
MRELVNIPLV HILTLVAFSG TEKLPKAPVI TTPLETVDAL VEEVATFMCA VESYPQPEIS WTRNKILIKL FDTRYSIREN GQLLTILSVE DSDDGIYCCT ANNGVGGAVE SCGALQVKMK
              |----------------------· Ig-like domain-2 -------------------------------|        |----------------------------·
PKITRPPINV KIIEGLKAVL PCTTMGNPKP SVSWIKGDSP LRENSRIAVL ESGSLRIHNV QKEDAGQYRC VAKNSLGTAY SKVVKLEVEV FARILRAPES HNVTFGSFVT LHCTATGIPV
Ig-like domain-3 ---------------------------------------------|          |----------------------------· Frizzled domain ----
PTITWIENGN AVSSGSIQES VKDRVIDSRL QLFITKPGLY TCIATNKHGE KFSTAKAAAT ISIAEWSKPQ KDNKGYCAQY RGEVCNAVLA KDALVFLNTS YADPEEAQEL LVHTAWNELK
----------------------------------------------------------------------------------------- |
VVSPVCRPAA EALLCNHIFQ ECSPGVVPTP IPICREYCLA VKELFCAKEW LVMEEKTHRG LYRSEMHLLS VPECSKLPSM HWDPTACARL PHLAFPPMTS SKPSVDIPNL PSSSSSSFSV


Ig-like domain 1 deletion:
                                            |---------------------------· Ig-like domain-1 ----------------------------·
MRELVNIPLV HILTLVAFSG TEKLPKAPVI TTPLETVDA ................................................................................................ALQVKMK
              |----------------------· Ig-like domain-2 -------------------------------|        |----------------------------·
PKITRPPINV KIIEGLKAVL PCTTMGNPKP SVSWIKGDSP LRENSRIAVL ESGSLRIHNV QKEDAGQYRC VAKNSLGTAY SKVVKLEVEV FARILRAPES HNVTFGSFVT LHCTATGIPV
Ig-like domain-3 ---------------------------------------------|          |----------------------------· Frizzled domain ----
PTITWIENGN AVSSGSIQES VKDRVIDSRL QLFITKPGLY TCIATNKHGE KFSTAKAAAT ISIAEWSKPQ KDNKGYCAQY RGEVCNAVLA KDALVFLNTS YADPEEAQEL LVHTAWNELK
----------------------------------------------------------------------------------------- |
VVSPVCRPAA EALLCNHIFQ ECSPGVVPTP IPICREYCLA VKELFCAKEW LVMEEKTHRG LYRSEMHLLS VPECSKLPSM HWDPTACARL PHLAFPPMTS SKPSVDIPNL PSSSSSSFSV


Ig-like domain 2 deletion:
                                            |---------------------------· Ig-like domain-1 ----------------------------·
MRELVNIPLV HILTLVAFSG TEKLPKAPVI TTPLETVDAL VEEVATFMCA VESYPQPEIS WTRNKILIKL FDTRYSIREN GQLLTILSVE DSDDGIYCCT ANNGVGGAVE SCGALQVKMK
              |----------------------· Ig-like domain-2 -------------------------------|        |----------------------------·
PKITRPPINV KI........ .......... .......... .......... .......... .......... .......... ....KLEVEV FARILRAPES HNVTFGSFVT LHCTATGIPV
Ig-like domain-3 ---------------------------------------------|          |----------------------------· Frizzled domain ----
PTITWIENGN AVSSGSIQES VKDRVIDSRL QLFITKPGLY TCIATNKHGE KFSTAKAAAT ISIAEWSKPQ KDNKGYCAQY RGEVCNAVLA KDALVFLNTS YADPEEAQEL LVHTAWNELK
----------------------------------------------------------------------------------------- |
VVSPVCRPAA EALLCNHIFQ ECSPGVVPTP IPICREYCLA VKELFCAKEW LVMEEKTHRG LYRSEMHLLS VPECSKLPSM HWDPTACARL PHLAFPPMTS SKPSVDIPNL PSSSSSSFSV


Frizzled-like domain deletion:
                                            |---------------------------· Ig-like domain-1 ----------------------------·
MRELVNIPLV HILTLVAFSG TEKLPKAPVI TTPLETVDAL VEEVATFMCA VESYPQPEIS WTRNKILIKL FDTRYSIREN GQLLTILSVE DSDDGIYCCT ANNGVGGAVE SCGALQVKMK
              |----------------------· Ig-like domain-2 -------------------------------|        |----------------------------·
PKITRPPINV KIIEGLKAVL PCTTMGNPKP SVSWIKGDSP LRENSRIAVL ESGSLRIHNV QKEDAGQYRC VAKNSLGTAY SKVVKLEVEV FARILRAPES HNVTFGSFVT LHCTATGIPV
Ig-like domain-3 ---------------------------------------------|          |----------------------------· Frizzled domain ----
PTITWIENGN AVSSGSIQES VKDRVIDSRL QLFITKPGLY TCIATNKHGE KFSTAKAAAT ISIAEWSKPQ KD........ .......... .......... .......... ..........
----------------------------------------------------------------------------------------- |
.......... .......... .......... ........ .......... .......... .......... .......... PHLAFPPMTS SKPSVDIPNL PSSSSSSFSV


Ig-like domain 1 only:
                                            |---------------------------· Ig-like domain-1 ----------------------------·
MRELVNIPLV HILTLVAFSG TEKLPKAPVI TTPLETVDAL VEEVATFMCA VESYPQPEIS WTRNKILIKL FDTRYSIREN GQLLTILSVE DSDDGIYCCT ANNGVGGAVE SCGALQVKMK
              |----------------------· Ig-like domain-2 -------------------------------|        |----------------------------·
.......... .......... .......... .......... .......... .......... .......... .......... .......... .......... .......... ..........
Ig-like domain-3 ---------------------------------------------|          |----------------------------· Frizzled domain ----
.......... .......... .......... .......... .......... .......... .......... .......... .......... .......... .......... ..........
----------------------------------------------------------------------------------------- |
.......... .......... .......... ........ .......... .......... .......... .......... PHLAFPPMTS SKPSVDIPNL PSSSSSSFSV


Ig-like domain 2 only:
                                            |---------------------------· Ig-like domain-1 ----------------------------·
MRELVNIPLV HILTLVAFSG TEKLPKAPVI TTPLETVDA .................................................................................... ALQVKMK
              |----------------------· Ig-like domain-2 -------------------------------|        |----------------------------·
PKITRPPINV KIIEGLKAVL PCTTMGNPKP SVSWIKGDSP LRENSRIAVL ESGSLRIHNV QKEDAGQYRC VAKNSLGTAY SKVVKLEVEV F........ .......... ..........
Ig-like domain-3 ---------------------------------------------|          |----------------------------· Frizzled domain ----
.......... .......... .......... .......... .......... .......... .......... .......... .......... .......... .......... ..........
----------------------------------------------------------------------------------------- |
.......... .......... .......... ........ .......... .......... .......... .......... PHLAFPPMTS SKPSVDIPNL PSSSSSSFSV
```

65

Frizzled-like domain only:

```
                                  |-------------------------- Ig-like domain-1 --------------------------|
MRELVNIPLV HILTLVAFSG TEK....... .......... .......... .......... .......... .......... .......... ..........

          |---------------------- Ig-like domain-2 --------------------------|    |--------------------------
.......... .......... .......... .......... .......... .......... .......... .......... .......... ..........

Ig-like domain-3 ----------------------------------------------|        |-------------------------- Frizzled domain ----
.......... .......... .......... ......... .......... .......SKPQ KDNKGYCAQY RGEVCNAVLA KDALVFLNTS YADPEEAQEL LVHTAWNELK
--------------------------------------------------------------------------------------- |
VVSPVCRPAA EALLCNHIFQ ECSPGVVPTP IPICREYCLA VKELFCAKEW LVMEEKTHRG LYRSEMHLLS VPECSKLPSM HWDPTACARL PHLAFPPMTS SKPSVDIPNL PSSSSSSFSV
```

66

Figure S4. Antibody-induced AChR clustering in C2C12 mouse myotubes. The presence of agrin in C2C12 myotube cultures leads to dense clustering of AChRs that can be readily visualized with fluorescent α-bungarotoxin and quantified. Pathogenic MuSK autoantibodies can disrupt this clustering (see main text and figures). Three different human MuSK-specific mAbs (MuSK1A, MuSK1B, and MuSK3-28), the humanized murine control MuSK mAb 4A3 and three human non-MuSK-specific mAbs (64-2, 64-7, 64-8) were tested for their ability to induce the AChR clustering in the absence of agrin. Clustering of AChR was quantified relative to the measured effect of agrin. Quantitative results are normalized to agrin-only induced clustering. Each mAb was added to the cultures at 1 µg/mL. Each data point represents the mean value from an independent experiment. Bars represent the mean of means and error bars SDs. Multiple comparisons ANOVA (against agrin), Dunnet's test; * $p<0.05$, ** $p<0.01$, *** $p<0.001$, **** $p<0.0001$, only shown when significant).
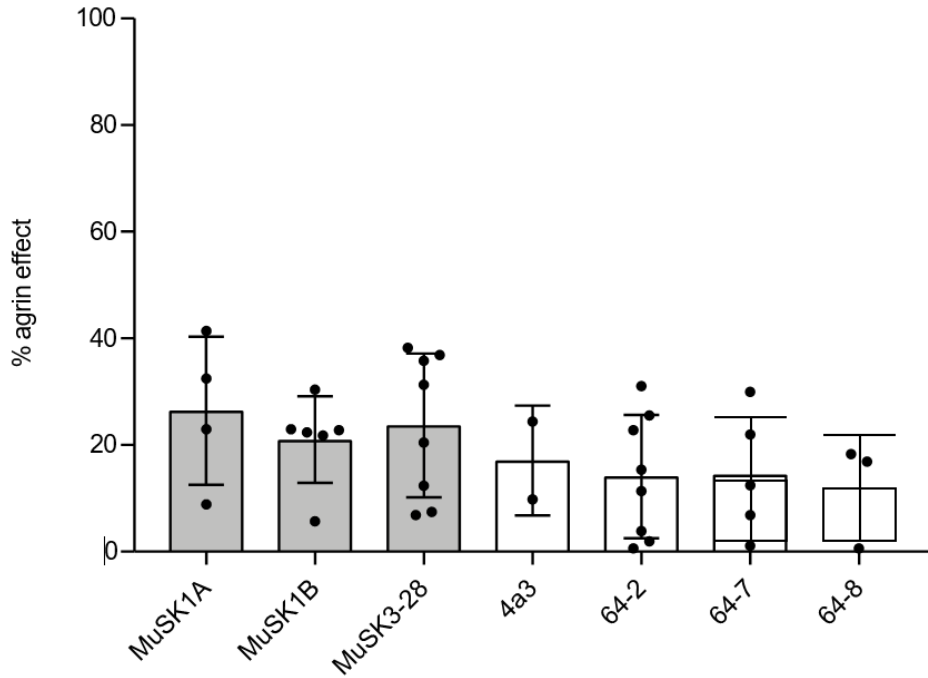
Supplemental methods. Recombinant IgG cloning and expression.

Single cell RT-PCR and Ig gene amplification

Single human B cells were isolated as described in the Methods section of the main text. Variable region domains from all cells were amplified using an established RT-PCR approach (Tiller et al., 2008). Total RNA from single cells was reverse transcribed in nuclease-free water using 150 ng random hexamer primer (pd(N)6, GE Healthcare), 0.5 µl of 10 mM each nucleotide dNTP-Mix (Invitrogen), 1 µl 0.1 M DTT (Invitrogen), 0.5% v/v Igepal CA-630 (Sigma), 4 U RNAsin® (Promega), 6 U Prime RNAse Inhibitor™ (Eppendorf) and 50 U Superscript® III reverse transcriptase (Invitrogen). Reverse transcription (RT) reaction was performed at 42 °C for 10 min, 25 °C for 10 min, 50 °C for 60 min and 94 °C for 5 min. Synthesis of cDNA was carried out in a total volume of 14 µl/well in the original 96-well sorting plate. cDNA was stored at -20 °C. IgH, Igλ and Igκ V gene transcripts were amplified independently by a nested PCR starting from 3.5 µl of cDNA as template. All PCR reactions were performed in 96-well plates in a total volume of 42 µl per well containing 20 nM each primer or primer mix (oligonucleotide primer sequences as previously described (Tiller et al., 2008), 10 uM each dNTP (Invitrogen) and 1.2 U HotStar® Taq DNA polymerase (Qiagen). All nested PCR reactions with gene-specific primers or primer mixes were performed with 4 µl of unpurified first PCR product. Each round of PCR was performed for 50 cycles at 94 °C for 30 s, 59 °C (IgH/Igκ) or 60 °C (Igλ) for 30 s, 72 °C for 55 s (1st PCR) or 45 s (2nd PCR).

Immunoglobulin gene sequence analysis

Aliquots of the VH, Vκ and Vλ chain nested PCR products were purified with QIAquick PCR Purification Kit (Qiagen) according to the manufacturer's instructions. These products were then sequenced with the respective reverse primer (Tiller et al., 2008). Sequences were analyzed by IMGT/HighV-QUEST. The heavy- and light-chain variable region germline gene segments were assigned with IMGT/HighV-QUEST (http://imgt.org) (Alamyar et al., 2012) using the July 7, 2015, version of the IMGT gene database. Somatic mutations resulting in replacement amino acids were evaluated through the alignment to germline genes provided by the IMGT V-base algorithm. The PCR sequencing step was verified by sequencing of the plasmids containing the subcloned variable heavy and light chain domains (Tiller et al., 2008).

Immunoglobulin gene IgG subclass by constant region sequencing

To determine the immunoglobulin IgG subclass, two strategies were used. First, the product of the first heavy chain PCR was used in a second PCR with the IgG internal reverse primer (5'- GTTCGGGGAAGTAGTCCTTGAC-3') (Tiller et al., 2008). Second, a nested PCR was performed as described above starting with cDNA and using the same forward primers (Tiller et al., 2008) and a different reverse primer (5'-GGGGAAGTAGTCCTTGACCAG-3', (Maillette de Buy Wenniger et al., 2013)). The PCR product was purified and send to sequencing.

Expression vector cloning IgG1, kappa and lambda

All single-cell PCR products were purified using the QIAquick PCR Purification Kit (Qiagen) prior to subcloning. Volumes obtained after elution were 30 µl. Digestions

were carried out with the respective restriction enzymes AgeI, BsiWI, SalI and XhoI (all from NEB) in a total volume of 35-40 µl (Tiller et al., 2008). Digested PCR products were purified as described above (Qiagen) before ligation into human Igγ1, Igκ and Igλ expression vectors containing a murine Ig gene signal peptide sequence (GenBank accession no. DQ407610) and a multiple cloning site upstream of the human Igγ1 (IGHG1), Igκ (IGKC) or Igλ (IGLC2) constant regions. Transcription is under the influence of the human cytomegalovirus (hCMV) promotor and clones can be selected based on resistance to ampicillin. Ligation was performed in a total volume of 10 µl with 1 U T4 DNA-Ligase (Invitrogen), 7.5 µl of digested and purified PCR product and 25 ng linearized vector. Competent E. coli DH10B bacteria (Clontech) were transformed at 42 °C with 4.5 µl of the ligation product. Colonies were screened by PCR using 5′Absense as forward primer and 3′IgGinternal, 3′Cκ494 or 3′Cλ as reverse primer, respectively (Tiller et al., 2008). PCR products of the expected size (650 bp for Igγ1, 700 bp for Igκ and 590 bp for Igλ) were sequenced to confirm identity with the original PCR products. Plasmid DNA was isolated from 4 ml bacteria cultures grown for 16 h at 37 °C in Terrific Broth (Difco Laboratories) containing 75 µg/ml ampicillin (Sigma) using QIAprep Spin columns (Qiagen). All plasmids were sequenced to validate that the correct variable regions were subcloned and that open reading frames (from the signal peptide through to the Ig constant domain) were present.

Expression vector cloning IgG4

For initial antigen specificity screening, all of the variable heavy chain domains were cloned into the human IgG1 subclass expression vector (described above),

irrespective of their native isotype or IgG subclass usage. Variable heavy chain domains that were derived from cells expressing IgG4 were cloned, in addition to the IgG1 vector, into a human IgG4 subclass expression vector. PCR-amplified variable heavy chain domains were directionally sub-cloned downstream of the CMV promoter into a pcDNA3.3-based vector (selected based on resistance to kanamycin or ampicillin) generated in our laboratory to harbor the human immunoglobulin constant domain for IgG4. The variable heavy chain domains were cloned into a cassette downstream of a signal peptide for prolactin (UniProtKB - P01239 (PRL_BOVIN)), MDSKGSSQKGSRLLLLLVVSNLLLCQGVVS, followed by an Afe I site (at the 5' end of the VH domain) and Apa I present at the 5' end of the IgG4 constant domain. Digests were carried out with the respective restriction enzymes and digested PCR products were subcloned and validated as described above.

Recombinant human monoclonal antibody production

Human embryonic kidney (HEK) 293A (ThermoFisher R70507) cells were cultured in 100 mm plates (Falcon, Becton Dickinson) under standard conditions in Dulbecco's Modified Eagle's Medium (DMEM; 12030 Gibco) supplemented with 10% certified fetal calf serum (FCS) (Gibco 16000), 1% non-essential amino acids (Gibco), 1% P/S (Penicillin-Streptomycin (10,000 U/mL) (Gibco), 2mM L-Glutamine (Gibco). Transient transfections of exponentially growing 293A cells were performed by using linear polyethylenimine (Polysciences Cat# 23966) for 16 h at approximately 80-90% cell confluency. Equal amounts (3µg each) of IgH and corresponding IgL chain expression vector DNA were added to 800µL of DMEM

containing PEI. This solution was vortexed, then allowed to incubate at room temperature for 15 minutes, before being evenly distributed in the culture dish. 24 h later the transfection media was removed and the cells were cultured for 6 days in 8 ml Basal media (DMEM (Gibco, 12430) 50%, RPMI (Gibco, 11875) 50%, A/A 0.75% (ThermoFisher, 15240062), L-glutamine 0.2 mM (Gibco, 25030081), Sodium-Pyruvat 1% (ThermoFisher, 11360070) supplemented with 1% Nutridoma-SP (Roche,11363743001)). Cells and cell debris was then removed by centrifugation at 800 ×g for 10 min and culture supernatants were stored at 4°C with prior to Ig purification (below).

Recombinant human monoclonal antibody purification

Recombinant antibodies were purified with Protein G Sepharose 4 Fast Flow beads (GE Healthcare, 17061801). In brief, approximately 25 ml cell culture supernatants were incubated with 200 µl Protein G beads for at least 48 h overnight at 4 °C under rotation. Supernatants were removed after centrifugation at 1500 rpm for 10 min and the beads were transferred to a chromatography spin column (BioRad) equilibrated with PBS. After two rounds of washing with 1 ml PBS, antibodies were eluted in 3-4 fractions (200 µl each) with 0.1 M glycine (pH 3.0). Eluates were collected in tubes containing 20 µl 1 M Tris (pH 8.0) and 20 µl of 10xPBS (pH 7.4). The pH was confirmed to be near neutral (pH 7.4) using narrow range (pH 5.0 - 10) indicator strips. Purified recombinant human monoclonal antibody concentrations were determined by measuring absorption at 280 nm with a microvolume UV-Vis spectrophotometer (NanoDrop 2000, ThermoFisher). As an additional means to validate expression, only purified recombinant immunoglobulins that were both

above 50 µg/mL and generated an expected UV spectral curve shape (250-300 nm) for purified proteins were used for subsequent experiments.

References of Supplemental Material

Alamyar E, Duroux P, Lefranc MP, Giudicelli V. IMGT((R)) tools for the nucleotide analysis of immunoglobulin (IG) and T cell receptor (TR) V-(D)-J repertoires, polymorphisms, and IG mutations: IMGT/V-QUEST and IMGT/HighV-QUEST for NGS. Methods Mol Biol 2012; 882: 569-604.

Maillette de Buy Wenniger LJ, Doorenspleet ME, Klarenbeek PL, Verheij J, Baas F, Elferink RP, et al. Immunoglobulin G4+ clones identified by next-generation sequencing dominate the B cell receptor repertoire in immunoglobulin G4 associated cholangitis. Hepatology 2013; 57(6): 2390-8.

Tiller T, Meffre E, Yurasov S, Tsuiji M, Nussenzweig MC, Wardemann H. Efficient generation of monoclonal antibodies from single human B cells by single cell RT-PCR and expression vector cloning. J Immunol Methods 2008; 329(1-2): 112-24.

Table S1. Molecular characteristics of human recombinant monoclonal autoantibodies. Variable region gene segment replacement mutations were counted from the beginning of framework 1 through the invariable cysteine at position 104. CDR3 mutations were counted between cysteine 104 and the invariable tryptophan (W) or phenylalanine (F) at position 118 in the heavy chain and the light chain respectively. FR4 mutations were not considered. ND, not determined.

Clone		Isotype and IgG subclass	Variable region family	Joining region family	Diversity region family	Amino acid replacements in variable region gene segment	Amino acid replacements in CDR3
MuSK1A	H	IgG4	IGHV1	IGHJ4	IGHD5	8	2
	L	λ	IGLV3	IGLJ2		1	0
MuSK1B	H	IgG3	IGHV4	IGHJ4	IGHD6	15	3
	L	λ	IGLV3	IGLJ3		8	2
MuSK3-28	H	IgG4	IGHV3	IGHJ3	IGHD3	10	0
	L	κ	IGKV1	IGKJ1		4	1
MuSK3B	H	M	IGHV4	IGHJ6	IGHD6	0	0
	L	κ	IGKV1	IGKJ4		0	0
MuSK1-2	H	M	IGHV3	IGHJ6	IGHD3	0	0
	L	λ	IGLV3	IGLJ2		1	0
MuSK1-3	H	M	IGHV3	IGHJ6	IGHD2	1	2
	L	κ	IGKV4	IGKJ3		1	0
MuSK1-4	H	M	IGHV3	IGHJ4	IGHD5	2	0
	L	λ	IGLV4	IGLJ3		0	0
MuSK1-6	H	M	IGHV3	IGHJ3	IGHD3	2	0
	L	λ	IGLV2	IGLJ1		0	0
MuSK1-7	H	ND	IGHV3	IGHJ6	IGHD2	0	0
	L	κ	IGKV1	IGKJ2		0	0
MuSK1-8	H	A	IGHV1	IGHJ4	IGHD1	0	0
	L	λ	IGLV2	IGLJ3		0	0
MuSK1-9	H	M	IGHV3	IGHJ3	IGHD3	1	1
	L	κ	IGKV1	IGKJ1		0	0
MuSK1-12	H	M	IGHV3	IGHJ4	IGHD3	2	1

	L	κ	IGKV2	IGKJ1		ND	1
MuSK1-17	H	M	IGHV4	IGHJ4	IGHD5	0	0
	L	λ	IGLV9	IGLJ3		0	0
MuSK1-18	H	M	IGHV1	IGHJ6	IGHD3	0	0
	L	κ	IGKV2	IGKJ5		0	0
MuSK1-20	H	ND	IGHV1	IGHJ6	IGHD3	0	0
	L	λ	IGLV2	IGLJ2 or IGLJ3		0	0
MuSK1-22	H	ND	IGHV1	IGHJ6	IGHD4	0	0
	L	λ	IGLV3	IGLJ2 or IGLJ3		0	0
MuSK1-29	H	M	IGHV4	IGHJ4	IGHD6	0	0
	L	κ	IGKV1	IGKJ4		0	0
MuSK1-30	H	M	IGHV4	IGHJ6	IGHD3	0	1
	L	λ	IGLV3	IGLJ2 or IGLJ3		0	0
MuSK1-33	H	ND	IGHV5	IGHJ4	IGHD6	1	0
	L	κ	IGKV2	IGKJ1		0	0
MuSK1-36	H	ND	IGHV3	IGHJ6	IGHD3	0	0
	L	λ	IGLV1	IGLJ1		0	0
MuSK1-41	H	IgG1	IGHV3	IGHJ5	IGHD2	0	1
	L	κ	IGKV3	IGKJ4		2	0
MuSK1-42	H	M	IGHV3	IGHJ6	IGHD2	0	0
	L	κ	IGKV1	IGKJ1		0	0
MuSK1-44	H	M	IGHV3	IGHJ4	IGHD3	0	0
	L	κ	IGKV1	IGKJ4		0	0
MuSK1-46	H	ND	IGHV4	IGHJ4	IGHD3	0	1
	L	κ	IGKV3	IGKJ4		0	0
MuSK2a-2	H	ND	IGHV4	IGHJ4	IGHD1	0	0
	L	κ	IGKV3	IGKJ1		0	0
MuSK2a-7	H	ND	IGHV4	IGHJ4	IGHD4	1	0
	L	ND	ND	ND		ND	ND

MuSK2a-10	H	ND	IGHV4	ND	ND	9	ND
	L	ND	ND	ND		ND	ND
MuSK2a-16	H	ND	IGHV3	IGHJ4	IGHD5	3	0
	L	λ	IGLV2	IGLJ3		0	1
MuSK2a-17	H	ND	IGHV3	IGHJ4	IGHD5	10	5
	L	λ	IGLV2	IGLJ3		5	0
MuSK5-1	H	M	IGHV3	IGHJ4	IGHD4	5	2
	L	κ	IGKV3	IGLJ2		9	0
MuSK5-2	H	ND	IGHV4	IGHJ2	IGHD4	2	2
	L	κ	IGKV1	IGKJ1		4	0
MuSK5-5	H	IgG2	IGHV3	IGHJ4	IGHD6	6	2
	L	λ	IGLV2	IGLJ3		0	3
MuSK5-6	H	ND	IGHV1	IGHJ5	IGHD4	12	2
	L	κ	IGKV1	IGKJ3		6	1
MuSK5-7	H	ND	IGHV3	IGHJ6	IGHD2	4	3
	L	κ	IGKV1	IGKJ3		3	1
MuSK5-8	H	ND	IGHV1	IGHJ5	IGHD3	0	2
	L	λ	IGLV1	IGLJ3		0	0
MuSK5-9	H	ND	IGHV4	IGHJ5	IGHD3	8	1
	L	κ	IGKV1	IGKJ2		9	2
MuSK5-11	H	ND	IGHV3	IGHJ4	IGHD3	9	3
	L	κ	IGKV1	IGKJ5		4	2
MuSK5-13	H	ND	IGHV4	IGHJ6	IGHD6	2	2
	L	κ	IGKV1	IGKJ2		2	0
MuSK5-15	H	ND	IGHV4	IGHJ4	IGHD3	7	3
	L	κ	IGKV2	IGKJ2		3	0
MuSK5-17	H	ND	IGHV3	IGHJ6	IGHD3	12	1
	L	κ	IGKV3	IGKJ1		6	2
MuSK5-18	H	IgG1	IGHV4	IGHJ6	IGHD3	ND	2
	L	κ	IGKV3	IGKJ2		7	2
MuSK5-21	H	ND	IGHV4	IGHJ6	IGHD2	5	3
	L	κ	IGKV2	IGKJ5		3	1

MuSK5-22	H	ND	IGHV4	IGHJ4	IGHD3	2	2
	L	κ	IGKV1	IGKJ1		0	0
MuSK5-23	H	ND	IGHV4	IGHJ6	IGHD5	2	1
	L	κ	IGKV1	IGKJ1		0	0
MuSK5-26	H	ND	IGHV3	IGHJ4	IGHD2	6	0
	L	κ	IGKV1	IGKJ2		8	1
MuSK5-28	H	ND	IGHV3	IGHJ2	IGHD1	9	3
	L	κ	IGKV1	IGKJ2		8	0
MuSK5-30	H	ND	IGHV3	IGHJ4	IGHD2	5	3
	L	κ	IGKV1	IGKJ4		7	1
MuSK5-31	H	ND	IGHV4	IGHJ4	IGHD3	7	4
	L	κ	IGKV4	IGKJ1		3	0
MuSK5-34	H	ND	IGHV3	IGHJ4	IGHD3	7	2
	L	κ	IGKV2	IGKJ2		5	1
MuSK5-35	H	ND	IGHV3	IGHJ2	IGHD6	19	2
	L	κ	IGKV2	IGKJ1		5	0
MuSK4-1	H	ND	IGHV3	IGHJ2	IGHD2	0	0
	L	κ	IGKV3	IGKJ1		0	0
MuSK4-3	H	ND	IGHV3	IGHJ4	IGHD1	0	0
	L	κ	IGKV3	IGKJ1		0	0
MuSK4-4	H	ND	IGHV4	IGHJ6	IGHD6	0	0
	L	λ	IGLV1	IGLJ3		0	0
MuSK4-8	H	ND	IGHV3	IGHJ3	IGHD6	5	1
	L	κ	IGKV3	IGKJ2		2	0
MuSK4-11	H	ND	IGHV4	IGHJ5	IGHD3	3	2
	L	κ	IGKV4	IGKJ1		2	2
MuSK4-12	H	ND	IGHV1	IGHJ4	IGHD3	1	1
	L	λ	IGLV2	IGLJ2 or IGLJ3		0	0
MuSK4-14	H	ND	IGHV3	IGHJ4	IGHD3	0	0
	L	κ	IGKV1	IGKJ1		0	0
MuSK4-18	H	ND	IGHV3	IGHJ4	IGHD6	9	1

	L	κ	IGKV1	IGKJ1		2	0
MuSK4-19	H	ND	IGHV4	IGHJ4	IGHD3	11	0
	L	λ	IGLV2	IGLJ2 or IGLJ3		4	2
MuSK4-22	H	ND	IGHV3	IGHJ3	IGHD6	1	1
	L	λ	IGLV1	IGLJ2 or IGLJ3		1	2
MuSK4-23	H	ND	IGHV1	IGHJ5	IGHD5	0	0
	L	λ	IGLV2	IGKJ1		0	0
MuSK4-26	H	ND	IGHV1	IGHJ6	IGHD2	0	0
	L	λ	IGLV2	IGLJ2 or IGLJ3		0	0
MuSK4-31	H	M	IGHV3	IGHJ3	IGHD5	0	1
	L	κ	IGKV1	IGKJ1		2	0
MuSK3-1	H	ND	IGHV4	IGHJ5	IGHD5	1	0
	L	κ	IGKV3	IGKJ1		0	0
MuSK3-6	H	ND	IGHV1	IGHJ1	IGHD6	1	0
	L	κ	IGKV1	IGKJ1		0	0
MuSK3-13	H	IgG1	IGHV3	IGHJ3	IGHD5	5	1
	L	λ	IGLV3	IGLJ2 or IGLJ3		2	1
MuSK3-16	H	IgG1	IGHV1	IGHJ1	IGHD2	15	3
	L	κ	IGKV1	IGKJ2		13	2
MuSK3-19	H	ND	IGHV3	IGHJ6	IGHD6	1	0
	L	κ	IGKV2	IGKJ4		0	0
MuSK3-20	H	ND	IGHV3	IGHJ4	IGHD2	0	1
	L	κ	IGKV1	IGKJ1		1	0
MuSK3-22	H	ND	IGHV4	IGHJ4	IGHD1	6	0
	L	λ	IGLV1	IGLJ2 or IGLJ3		3	0
MuSK3-23	H	ND	IGHV4	IGHJ2	IGHD3	0	0
	L	κ	IGKV1	IGKJ2		0	0

MuSK3-24	H	ND	IGHV3	IGHJ4	IGHD3	0	1
	L	κ	IGKV3	IGKJ1		0	0
MuSK3-25	H	ND	IGHV4	IGHJ5	IGHD3	0	0
	L	κ	IGKV1	IGKJ1		1	0
MuSK6-2	H	M	IGHV1	IGHJ4	IGHD6	0	1
	L	κ	IGKV1	IGKJ3		0	0
MuSK6-5	H	M	IGHV4	IGHJ4	IGHD3	0	0
	L	λ	IGLV2	IGLJ2 or IGLJ3		1	0
MuSK6-12	H	M	IGHV3	IGHJ4	IGHD2	2	0
	L	λ	IGLV2	IGLJ3		1	0
MuSK6-13	H	IgG1	IGHV4	IGHJ6	IGHD1	8	1
	L	λ	IGLV2	IGLJ2 or IGLJ3		3	1
HD1-4	H	M	IGHV3	IGHJ4	IGHD1	7	2
	L	λ	IGLV1	IGLJ2 or IGLJ3		3	2
HD1-6	H	M	IGHV3	IGHJ4	IGHD3	0	2
	L	κ	IGKV3	IGKJ4		3	0
HD1-9	H	ND	IGHV1	IGHJ6	IGHD5	2	1
	L	λ	IGLV2	IGLJ3		3	1
HD1-10	H	M	IGHV1	IGHJ6	IGHD3	0	0
	L	λ	IGLV2	IGLJ2 or IGLJ3		3	0
HD1-11	H	M	IGHV3	IGHJ4	IGHD2	5	2
	L	κ	IGKV1	IGKJ4		2	0
HD1-20	H	M	IGHV3	IGHJ5	IGHD6	0	0
	L	κ	IGKV1	IGKJ4		0	0
HD1-21	H	M	IGHV3	IGHJ6	IGHD4	4	0
	L	κ	IGKV1	IGKJ1		1	0
HD1-28	H	ND	IGHV3	IGHJ4	IGHD5	1	1
	L	λ	IGLV2	IGLJ1		4	1

HD1-29	H	MND	IGHV3	IGHJ4	IGHD3	5	2
	L	κ	IGKV1	IGKJ3		0	0
HD1-30	H	M	IGHV3	IGHJ3	IGHD1	10	3
	L	κ	IGKV4	IGKJ1		1	0
HD2-3	H	ND	IGHV3	IGHJ4	IGHD3	14	4
	L	κ	IGKV3	IGKJ4		7	1
HD2-4	H	ND	IGHV1	IGHJ5	IGHD3	12	1
	L	κ	IGKV3	IGKJ4		4	0
HD2-6	H	ND	IGHV4	IGHJ3	IGHD1	3	0
	L	κ	IGKV3	IGKJ1		3	0
HD2-7	H	M	IGHV3	IGHJ4	IGHD5	0	0
	L	κ	IGKV3	IGKJ4		0	0
HD2-8	H	M	IGHV3	IGHJ4	IGHD4	7	1
	L	κ	IGKV3	IGKJ4		1	0
HD2-15	H	ND	IGHV3	IGHJ4	IGHD1	7	0
	L	λ	IGLV2	IGLJ2 or IGLJ3		3	0
HD2-16	H	ND	IGHV3	IGHJ4	IGHD4	4	0
	L	κ	IGKV1	IGKJ4		5	0
HD2-18	H	ND	IGHV3	IGHJ4	IGHD5	7	2
	L	κ	IGKV1	IGKJ4		6	1
HD2-19	H	ND	IGHV3	IGHJ4	IGHD1	5	1
	L	κ	IGKV1	IGKJ3		8	2
HD2-20	H	M	IGHV3	IGHJ4	IGHD2	5	2
	L	λ	IGLV2	IGLJ1		3	0
HD2-26	H	ND	IGHV4	IGHJ4	IGHD5	6	1
	L	λ	IGLV2	IGLJ1		3	1
HD2-27	H	ND	IGHV3	IGHJ4	IGHD4	4	0
	L	κ	IGKV3	IGKJ4		1	1
HD2-28	H	M	IGHV3	IGHJ4	IGHD6	6	1
	L	λ	IGLV7	IGLJ3		2	0
HD2-31	H	ND	IGHV3	IGHJ4	IGHD3	0	0

	L	κ	IGKV1	IGKJ2		0	0
HD2-32	H	ND	IGHV3	IGHJ5	IGHD6	5	3
	L	λ	IGLV2	IGLJ3		2	2
HD2-33	H	ND	IGHV3	IGHJ4	IGHD4	3	0
	L	λ	IGLV2	IGLJ3		6	0
HD2-34	H	ND	IGHV3	IGHJ4	IGHD3	1	1
	L	λ	IGLV2	IGLJ2 or IGLJ3		2	0
HD2-35	H	M	IGHV1	IGHJ4	IGHD3	6	1
	L	λ	IGLV2	IGLJ1		4	0
HD2-37	H	M	IGHV4	IGHJ6	IGHD2	1	1
	L	κ	IGKV1	IGKJ1		0	0

[a]Variable region gene segment replacement mutations were counted from the beginning of framework 1 through the invariable cysteine at position 104. CDR3 mutations were counted between cysteine 104 and the invariable tryptophan (W) or phenylalanine at position 118 in the heavy chain and the light chain respectively. No FR4 mutations were observed.

References

1. Vincent A. Unravelling the pathogenesis of myasthenia gravis. Nat Rev Immunol. 2002;2(10):797–804.

2. Gilhus NE. Myasthenia gravis. N Engl J Med. 2016;375(26):2570–2581.

3. Yi JS, Guptill JT, Stathopoulos P, Nowak RJ, O'Connor KC. B cells in the pathophysiology of myasthenia gravis. Muscle Nerve. 2018;57(2):172–184.

4. Vincent A, Beeson D, Lang B. Molecular targets for autoimmune and genetic disorders of neuromuscular transmission. Eur J Biochem. 2000;267(23):6717–6728.

5. Lindstrom JM, Engel AG, Seybold ME, Lennon VA, Lambert EH. Pathological mechanisms in experimental autoimmune myasthenia gravis. II. Passive transfer of experimental autoimmune myasthenia gravis in rats with anti-acetylcholine receptor antibodies. J Exp Med. 1976;144(3):739–753.

6. Shen C, et al. Antibodies against low-density lipoprotein receptor-related protein 4 induce myasthenia gravis. J Clin Invest. 2013;123(12):5190–5202.

7. Hoch W, McConville J, Helms S, Newsom-Davis J, Melms A, Vincent A. Autoantibodies to the receptor tyrosine kinase MuSK in patients with myasthenia gravis without acetylcholine receptor antibodies. Nat Med. 2001;7(3):365–368.

8. Drachman DB, Angus CW, Adams RN, Michelson JD, Hoffman GJ. Myasthenic antibodies cross-link acetylcholine receptors to accelerate degradation. N Engl J Med. 1978;298(20):1116–1122.

9. Zisimopoulou P, et al. A comprehensive analysis of the epidemiology and clinical characteristics of anti-LRP4 in myasthenia gravis. J Autoimmun. 2014;52:139–145.

10. Higuchi O, Hamuro J, Motomura M, Yamanashi Y. Autoantibodies to low-density lipoprotein receptor-related protein 4 in myasthenia gravis. Ann Neurol. 2011;69(2):418–422.

11. Keung B, et al. Long-term benefit of rituximab in MuSK autoantibody myasthenia gravis patients. J Neurol Neurosurg Psychiatry. 2013;84(12):1407–1409.

12. Huijbers MG, et al. Myasthenia gravis with muscle specific kinase antibodies mimicking amyotrophic lateral sclerosis. Neuromuscul Disord. 2016;26(6):350–353.

13. Nikolić AV, et al. Myopathy, muscle atrophy and tongue lipid composition in MuSK myasthenia gravis. Acta Neurol Belg. 2015;115(3):361–365.

14. McConville J, et al. Detection and characterization of MuSK antibodies in seronegative myasthenia gravis. Ann Neurol. 2004;55(4):580–584.

15. Aalberse RC, Stapel SO, Schuurman J, Rispens T. Immunoglobulin G4: an odd antibody. Clin Exp Allergy. 2009;39(4):469–477.

16. Klooster R, et al. Muscle-specific kinase myasthenia gravis IgG4 autoantibodies cause severe neuromuscular junction dysfunction in mice. Brain. 2012;135(pt 4):1081–1101.

17. Viegas S, et al. Passive and active immunization models of MuSK-Ab positive myasthenia: electrophysiological evidence for pre and postsynaptic defects. Exp Neurol. 2012;234(2):506–512.

18. Shigemoto K, et al. Induction of myasthenia by immunization against muscle-specific kinase. J Clin Invest. 2006;116(4):1016–1024.

19. Hopf C, Hoch W. Dimerization of the muscle-specific kinase induces tyrosine phosphorylation of acetylcholine receptors and their aggregation on the surface of myotubes. J Biol Chem. 1998;273(11):6467–6473.

20. Huijbers MG, et al. MuSK IgG4 autoantibodies cause myasthenia gravis by inhibiting binding between MuSK and Lrp4. Proc Natl Acad Sci U S A. 2013;110(51):20783–20788.

21. Koneczny I, Cossins J, Waters P, Beeson D, Vincent A. MuSK myasthenia gravis IgG4 disrupts the interaction of LRP4 with MuSK but both IgG4 and IgG1-3 can disperse preformed agrin-independent AChR clusters. PLoS One. 2013;8(11):e80695.

22. Otsuka K, et al. Collagen Q and anti-MuSK autoantibody competitively suppress agrin/LRP4/MuSK signaling. Sci Rep. 2015;5:13928.

23. Koneczny I, et al. IgG4 autoantibodies against muscle-specific kinase undergo Fab-arm exchange in myasthenia gravis patients. J Autoimmun. 2017;77:104–115.

24. van der Neut Kolfschoten M, et al. Anti-inflammatory activity of human IgG4 antibodies by dynamic Fab arm exchange. Science. 2007;317(5844):1554–1557.

25. Losen M, et al. Hinge-deleted IgG4 blocker therapy for acetylcholine receptor myasthenia gravis in rhesus monkeys. Sci Rep. 2017;7(1):992.

26. Díaz-Manera J, et al. Long-lasting treatment effect of rituximab in MuSK myasthenia. Neurology. 2012;78(3):189–193.

27. Nowak RJ, Dicapua DB, Zebardast N, Goldstein JM. Response of patients with refractory myasthenia gravis to rituximab: a retrospective study. Ther Adv Neurol Disord. 2011;4(5):259–266.

28. Mei HE, et al. A unique population of IgG-expressing plasma cells lacking CD19 is enriched in human bone marrow. Blood. 2015;125(11):1739–1748.

29. Cambridge G, et al. Serologic changes following B lymphocyte depletion therapy for rheumatoid arthritis. Arthritis Rheum. 2003;48(8):2146–2154.

30. Hall RP, et al. Association of serum B-cell activating factor level and proportion of memory and transitional B cells with clinical response after rituximab treatment of bullous pemphigoid patients. J Invest Dermatol. 2013;133(12):2786–2788.

31. Stathopoulos P, Kumar A, Heiden JAV, Pascual-Goñi E, Nowak RJ, O'Connor KC. Mechanisms underlying B cell immune dysregulation and autoantibody production in MuSK myasthenia gravis. Ann N Y Acad Sci. 2018;1412(1):154–165.

32. Stathopoulos P, Kumar A, Nowak RJ, O'Connor KC. Autoantibody-producing plasmablasts after B cell depletion identified in muscle-specific kinase myasthenia gravis. JCI Insight. 2017;2(17):94263.

33. Franz B, May KF, Dranoff G, Wucherpfennig K. Ex vivo characterization and isolation of rare memory B cells with antigen tetramers. Blood. 2011;118(2):348–357.

34. Evoli A, et al. Clinical correlates with anti-MuSK antibodies in generalized seronegative myasthenia gravis. Brain. 2003;126(pt 10):2304–2311.

35. Deymeer F, et al. Clinical comparison of anti-MuSK- vs anti-AChR-positive and seronegative myasthenia gravis. Neurology. 2007;68(8):609–611.

36. Sanders DB, El-Salem K, Massey JM, McConville J, Vincent A. Clinical aspects of MuSK antibody positive seronegative MG. Neurology. 2003;60(12):1978–1980.

37. Clements CS, et al. The crystal structure of myelin oligodendrocyte glycoprotein, a key autoantigen in multiple sclerosis. Proc Natl Acad Sci U S A. 2003;100(19):11059–11064.

38. Stiegler AL, Burden SJ, Hubbard SR. Crystal structure of the agrin-responsive immunoglobulin-like domains 1 and 2 of the receptor tyrosine kinase MuSK. J Mol Biol. 2006;364(3):424–433.

39. Kim N, et al. Lrp4 is a receptor for Agrin and forms a complex with MuSK. Cell. 2008;135(2):334–342.

40. Colliou N, et al. Long-term remissions of severe pemphigus after rituximab therapy are associated with prolonged failure of desmoglein B cell response. Sci Transl Med. 2013;5(175):175ra30.

41. Wilson R, et al. Condition-dependent generation of aquaporin-4 antibodies from circulating B cells in neuromyelitis optica. Brain. 2018;141(4):1063–1074.

42. Makuch M, et al. N-methyl-D-aspartate receptor antibody production from germinal center reactions: Therapeutic implications. Ann Neurol. 2018;83(3):553–561.

43. Di Zenzo G, et al. Pemphigus autoantibodies generated through somatic mutations target the desmoglein-3 cis-interface. J Clin Invest. 2012;122(10):3781–3790.

44. Cho MJ, et al. Shared VH1-46 gene usage by pemphigus vulgaris autoantibodies indicates common humoral immune responses among patients. Nat Commun. 2014;5:4167.

45. Makino T, et al. Analysis of peripheral B cells and autoantibodies against the anti-nicotinic acetylcholine receptor derived from patients with myasthenia gravis using single-cell manipulation tools. PLoS One. 2017;12(10):e0185976.

46. Huda S, et al. IgG-specific cell-based assay detects potentially pathogenic MuSK-Abs in seronegative MG. Neurol Neuroimmunol Neuroinflamm. 2017;4(4):e357.

47. Waters P, et al. MOG cell-based assay detects non-MS patients with inflammatory neurologic disease. Neurol Neuroimmunol Neuroinflamm. 2015;2(3):e89.

48. Stiegler AL, Burden SJ, Hubbard SR. Crystal structure of the frizzled-like cysteine-rich domain of the receptor tyrosine kinase MuSK. J Mol Biol. 2009;393(1):1–9.

49. Huijbers MG, et al. Longitudinal epitope mapping in MuSK myasthenia gravis: implications for disease severity. J Neuroimmunol. 2016;291:82–88.

50. Remédio L, et al. Diverging roles for Lrp4 and Wnt signaling in neuromuscular synapse development during evolution. Genes Dev. 2016;30(9):1058–1069.

51. Cantor S, Zhang W, Delestrée N, Remédio L, Mentis GZ, Burden SJ. Preserving neuromuscular synapses in ALS by stimulating MuSK with a therapeutic agonist antibody. Elife. 2018;7.

52. Niks EH, et al. Clinical fluctuations in MuSK myasthenia gravis are related to antigen-specific IgG4 instead of IgG1. J Neuroimmunol. 2008;195(1–2):151–156.

53. Huijbers MG, et al. MuSK myasthenia gravis monoclonal antibodies: Valency dictates pathogenicity. Neurol Neuroimmunol Neuroinflamm. 2019;6(3):e547.

54. Mori S, et al. Divalent and monovalent autoantibodies cause dysfunction of MuSK by distinct mechanisms in a rabbit model of myasthenia gravis. J Neuroimmunol. 2012;244(1–2):1–7.

55. Noorchashm H, et al. I-Ag7-mediated antigen presentation by B lymphocytes is critical in overcoming a checkpoint in T cell tolerance to islet beta cells of nonobese diabetic mice. J Immunol. 1999;163(2):743–750.

56. Serreze DV, Fleming SA, Chapman HD, Richard SD, Leiter EH, Tisch RM. B lymphocytes are critical antigen-presenting cells for the initiation of T cell-mediated autoimmune diabetes in nonobese diabetic mice. J Immunol. 1998;161(8):3912–3918.

57. Shlomchik MJ, Craft JE, Mamula MJ. From T to B and back again: positive feedback in systemic autoimmune disease. Nat Rev Immunol. 2001;1(2):147–153.

58. Molnarfi N, et al. MHC class II-dependent B cell APC function is required for induction of CNS autoimmunity independent of myelin-specific antibodies. J Exp Med. 2013;210(13):2921–2937.

59. Parker Harp CR, et al. B cell antigen presentation is sufficient to drive neuroinflammation in an animal model of multiple sclerosis. J Immunol. 2015;194(11):5077–5084.

60. Krumbholz M, Meinl E. B cells in MS and NMO: pathogenesis and therapy. Semin Immunopathol. 2014;36(3):339–350.

61. Jacobi AM, et al. HLA-DRhigh/CD27high plasmablasts indicate active disease in patients with systemic lupus erythematosus. Ann Rheum Dis. 2010;69(1):305–308.

62. Ellebrecht CT, et al. Reengineering chimeric antigen receptor T cells for targeted therapy of autoimmune disease. Science. 2016;353(6295):179–184.

63. Lee JY, et al. Compromised fidelity of B-cell tolerance checkpoints in AChR and MuSK myasthenia gravis. Ann Clin Transl Neurol. 2016;3(6):443–454.

64. Linnington C, Webb M, Woodhams PL. A novel myelin-associated glycoprotein defined by a mouse monoclonal antibody. J Neuroimmunol. 1984;6(6):387–396.

65. Owens GP, et al. Antibodies produced by clonally expanded plasma cells in multiple sclerosis cerebrospinal fluid. Ann Neurol. 2009;65(6):639–649.

66. Graus YF, et al. Human anti-nicotinic acetylcholine receptor recombinant Fab fragments isolated from thymus-derived phage display libraries from myasthenia gravis patients reflect predominant specificities in serum and block the action of pathogenic serum antibodies. J Immunol. 1997;158(4):1919–1929.

67. Cotzomi E, et al. Early B cell tolerance defects in neuromyelitis optica favour anti-AQP4 autoantibody production. Brain. 2019;142(6):1598–1615.

68. Maillette de Buy Wenniger LJ, et al. Immunoglobulin G4+ clones identified by next-generation sequencing dominate the B cell receptor repertoire in immunoglobulin G4 associated cholangitis. Hepatology. 2013;57(6):2390–2398.

69. Schanz M, et al. High-throughput sequencing of human immunoglobulin variable regions with subtype identification. PLoS One. 2014;9(11):e111726.

70. Leite MI, et al. IgG1 antibodies to acetylcholine receptors in 'seronegative' myasthenia gravis. Brain. 2008;131(Pt 7):1940–1952.

71. Brochet X, Lefranc MP, Giudicelli V. IMGT/V-QUEST: the highly customized and integrated system for IG and TR standardized V-J and V-D-J sequence analysis. Nucleic Acids Res. 2008;36(Web Server issue):W503–W508.

72. Lefranc MP. IMGT, the international ImMunoGeneTics database. Nucleic Acids Res. 2001;29(1):207–209.

73. Tse N, et al. The neuromuscular junction: measuring synapse size, fragmentation and changes in synaptic protein density using confocal fluorescence microscopy. J Vis Exp. 2014;(94):52220.

74. Gomez AM, et al. Silencing of Dok-7 in adult rat muscle increases susceptibility to passive transfer myasthenia gravis. Am J Pathol. 2016;186(10):2559–2568.

3.2.   PUBLICATION II: SINGLE-CELL REPERTOIRE TRACING IDENTIFIES RITUXIMAB-RESISTANT B CELLS DURING MYASTHENIA GRAVIS RELAPSES

![JCI Insight logo]

Single-cell repertoire tracing identifies rituximab-resistant B cells during myasthenia gravis relapses

Ruoyi Jiang,[1] **Miriam L. Fichtner,[1,2]** Kenneth B. Hoehn,[4] Minh C. Pham,[1] Panos Stathopoulos,[1,2] Richard J. Nowak,[2] Steven H. Kleinstein,[1,3,4] and Kevin C. O'Connor[1,2]

[1]Department of Immunobiology and [2]Department of Neurology, Yale School of Medicine, New Haven, Connecticut, USA. [3]Interdepartmental Program in Computational Biology & Bioinformatics, Yale University, New Haven, Connecticut, USA. [4]Department of Pathology, Yale School of Medicine, New Haven, Connecticut, USA.

Authorship note: SHK and KCO are co–senior authors.

Address correspondence to: Steven H. Kleinstein or Kevin C. O'Connor, Yale University School of Medicine, 300 George Street, New Haven, Connecticut 06511, USA. Phone: 203.785.6685; Email: steven. kleinstein@yale.edu (SHK). Phone: 203.737.3321; Email: kevin.oconnor@yale.edu (KCO).

Abstract

Rituximab, a B cell-depleting therapy, is indicated for treating a growing number of autoantibody- mediated autoimmune disorders. However, relapses can occur after treatment, and autoantibody- producing B cell subsets may be found during relapses. It is not understood whether these autoantibody-producing B cell subsets emerge from the failed depletion of preexisting B cells or are generated de novo. To further define the mechanisms that cause postrituximab relapse, we studied patients with autoantibody-mediated muscle-specific kinase (MuSK) myasthenia gravis (MG) who relapsed after treatment. We carried out single-cell transcriptional and B cell receptor profiling on longitudinal B cell samples. We identified clones present before therapy that persisted during relapse. Persistent B cell clones included both antibody-secreting cells and memory B cells characterized by gene expression signatures associated with B cell survival. A subset of persistent antibody-secreting cells and memory B cells were specific for the MuSK autoantigen. These results demonstrate that rituximab is not fully effective at eliminating autoantibody-producing B cells and provide a mechanistic understanding of postrituximab relapse in MuSK MG.

Introduction

Acquired myasthenia gravis (MG) is an autoimmune disorder caused by pathogenic autoantibodies that bind to membrane proteins at the neuromuscular junction, leading to muscle weakness (1). While the majority of MG patients have serum autoantibodies against the acetylcholine receptor (AChR), a subset of patients have autoantibodies against muscle-specific tyrosine kinase (MuSK) (2, 3). MuSK is essential for AChR clustering and synaptic differentiation (4). Through binding MuSK, serum-derived autoantibodies impair clustering of AChRs, and neuromuscular transmission, thereby causing disease (5).

Anti-CD20-mediated B cell depletion therapy (BCDT) is indicated for the treatment of multiple autoimmune disorders (6–8). The conspicuous clinical benefit of BCDT in patients with MuSK MG was recently demonstrated (9–11). However, a fraction of patients treated with the anti-CD20 BCDT agent rituximab (RTX) experienced postrituximab (post-RTX) relapses despite initial symptomatic responses and a fall in MuSK autoantibody titer (9, 12–14). Post-RTX relapse in MuSK MG is associated with the presence of circulating plasmablast expansions, which include those that secrete MuSK-specific autoantibodies (15, 16). Previous studies have shown that antigen-experienced plasma cells or plasmablasts are resistant to BCDT owing to their low CD20 expression (17–20). Moreover, memory B cells, which express CD20, can also be abundant after BCDT, and their increased frequency is associated with post-RTX relapses (21, 22). Whether or not plasmablasts, plasma cells, or memory B cells emerge from inadequately depleted circulating B cells (versus emerging entirely de novo) is not known. The

characteristics of antigen-experienced B cells that resist depletion also remain unclear.

Understanding the mechanisms underlying post-RTX relapse is important for the development of new modalities for monitoring depletion and more effective therapy combinations for treating MG and other autoimmune disorders. Accordingly, we sought to further understand whether post-RTX relapse in MuSK MG is associated with the failed depletion of preexisting B cells, including autoantibody-producing B cell subsets. In addition, we investigated the phenotype of the B cells that persist throughout the course of treatment and relapse. To this end, we integrated data from multiple profiling methods on the same patients, including (a) adaptive immune receptor repertoire sequencing (AIRR-Seq) to generate high-depth B cell receptor (BCR) libraries from unselected PBMCs collected at pre-RTX treatment time points and during episodes of post-RTX relapse; (b) previously published sequences of human monoclonal autoantibodies, with known specificity for the MuSK autoantigen, that emerged during post-RTX relapses; and (c) single-cell gene expression analysis with paired BCR repertoire sequencing, to trace B cell populations temporally and to identify the phenotype of B cells that emerge during post-RTX relapse. In comparison with the examination of clonal overlap between bulk BCR repertoires alone, this approach, which we refer to as Single-cell Tracing of Adaptive Immune Receptor (STAIR) repertoires, allows for the unbiased characterization of the gene expression profile of persistent, disease-relevant B cells (including those specific for the autoantigen) at single-cell resolution. By using this approach, we offer new insights into the mechanism of post-RTX relapse in

93

patients with MuSK MG and potential avenues for improving the treatment of MG and other autoantibody-driven autoimmune diseases.

Results

Experimental design. We used the following experimental approach **(Figure 1A)** to identify and characterize B cell clones that resist RTX depletion in 3 patients with MuSK MG who experienced relapses. We first tested whether B cell clones persisted across pre- and post-RTX repertoires by sequencing the BCR repertoire of unselected PBMCs at high-depth using a bulk approach to capture a large number of sequences for identifying persistent clones. Second, we tested whether MuSK autoantibody-producing B cells were among these persistent clones. In previous studies of these same patients, we produced MuSK-specific recombinant human monoclonal antibodies (15, 16) from single B cells isolated during post-RTX relapses. Here, though, we sought to determine whether those specific BCR clones were present in pre-RTX repertoires. Third, we identified the phenotype of both persistent and nonpersistent B cell clones. This was achieved through paired transcriptional profiling and BCR sequencing of single cells. These BCR sequences were traced to high-depth bulk sequencing repertoires derived from pre-RTX time points. The transcriptional profiles of persistent and nonpersistent B cell clones were then compared.

A subset of B cell clones are refractory to depletion. We first sought to identify clones that escape RTX depletion and contribute to relapses when the B cell compartment repopulates after treatment. To that end, we sequenced the B cell repertoire, using our high-depth bulk approach, from 3 patients with MG before and

after treatment **(Figure 1B, Supplemental Table 1, and Supplemental Table 2)**.

The number of V(D)J sequences isolated for patient 1 was 639,715; 82,720 from

patient 2; and 107,504 from patient 3. Grouping the sequences into clones - those

with a common ancestor based on their V, J gene usage and junction sequences

(23) - generated 187,195; 34,719; and 14,579 clones for patients 1, 2, and 3,

respectively **(Supplemental Figure 1)**. A total of 2462 clones were found with

members that were present in both the pre-RTX and post-RTX relapse repertoire

(termed persistent clones) in patient 1 (or 1.6% of pre-RTX clones); 902 (4.9%) and

345 (7.6%) were found in patients 2 and 3, respectively **(Figure 2A)**. Given that

clonal relationships are inferred computationally, we next sought to substantiate

that these persistent clones were not the result of sequence similarity that

happened by chance. To estimate the frequency at which clones are spuriously

observed to be shared between the post-RTX and pre-RTX repertoires, the

average background sharing between the post-RTX circulation and the pre-RTX

circulation of unrelated individuals was calculated (e.g., post-RTX patient 1 was

compared with pre-RTX patient 2). This rate was used as a null hypothesis to

establish the significance of the observed clonal sharing between post-RTX and

pre-RTX repertoires in the same patient. Patient 1 shared an average of 0.4%

clones in comparison with other patients, patient 2 shared an average of 1.4%, and

patient 3 shared an average of 0.9%. Quantification using a clonal overlap metric

demonstrated that the observed overlaps between pre-RTX and post-RTX

repertoires were significantly higher relative to the background (t test $P = 0.037$)

(Figure 2B). These collective data demonstrate that circulating B cell clones persist

despite RTX-mediated depletion of the repertoire.
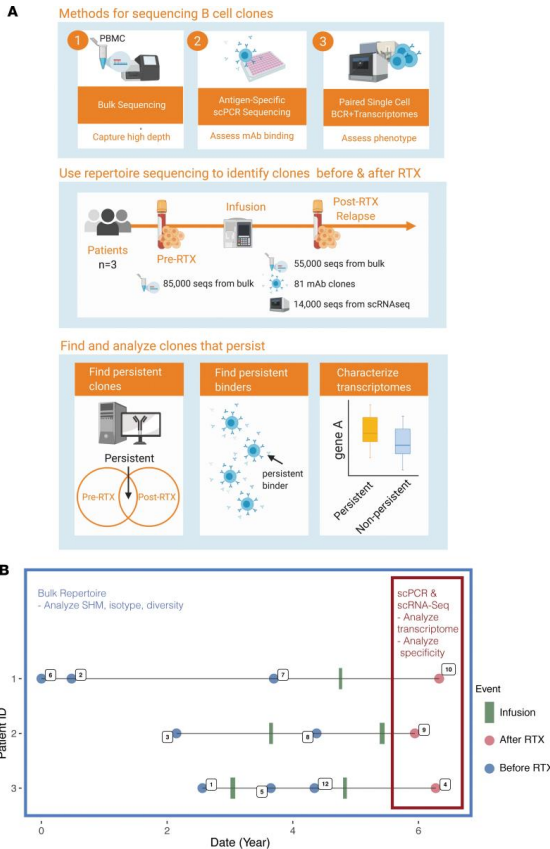
Figure 1. Schematic diagram showing overall workflow from clinical data elements and sample collection to computational analysis of BCR repertoires along with a timeline of sample collection dates. **(A)** Three approaches were used for sequencing. First, bulk repertoires using next-generation sequencing by isolating unpaired IGH V(D)J sequences directly from RNA were generated. Second, paired heavy and light chain V(D)J sequences from circulating B cells expressed as recombinant antibodies and tested for antigen specificity were traced to pre-RTX repertoires. Finally, paired transcriptome and heavy and light chain V(D)J sequence repertoires from high-throughput emulsion-based single-cell sequencing was performed. These 3 types of repertoires were analyzed together in our analysis workflow for each patient across the sampled time points. **(B)** Timeline of clinical events, specimen collection, and B cell analysis for 3 patients with MG who experienced post-RTX relapses. Infusion describes a time point associated with a recorded infusion of RTX. Post- RTX describes an event associated with a disease exacerbation during which B cells were observed to secrete MuSK-specific autoantibodies. Pre-RTX describes any collection time point preceding post- RTX by an intervening infusion event. Dates of events are approximations.
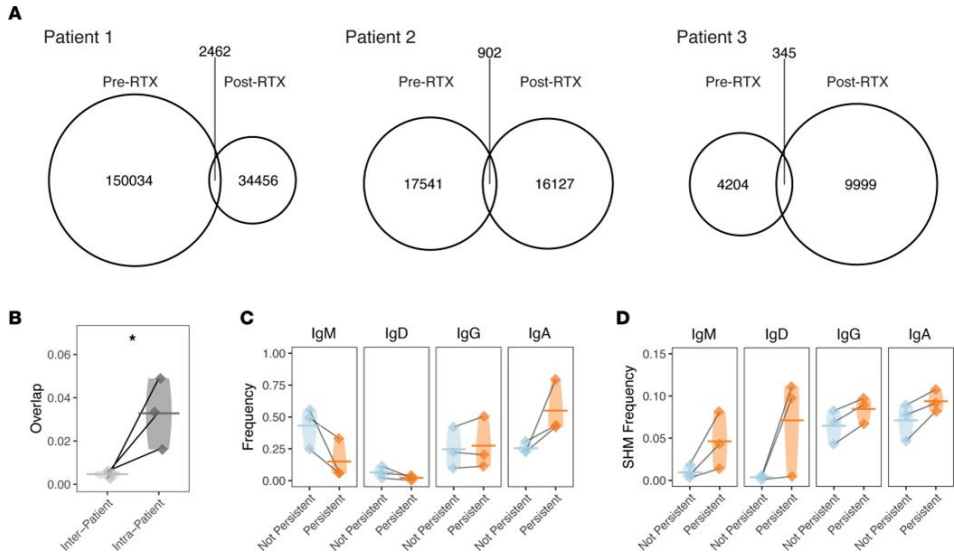
Figure 2. B cell clones that overlap pre-RTX and post-RTX bulk IGH repertoires (i.e., persistent clones) are associated with switched isotypes and increased somatic hypermutation frequency. (A) Venn diagrams show counts of clones present at pre-RTX and post-RTX time points and those that overlap both time points for all study subjects (the relative area of each circle corresponds to the proportion of clones found at different time points for each patient). **(B)** Shared B cell clones between pre-RTX and post-RTX time points quantified as Bray-Curtis overlap for the same patient (intrapatient) or across different patients (interpatient). Horizontal bars show the mean overlap of each comparison. A 1-tailed t test was used to assess the significance of the null hypothesis that intrapatient overlap was not higher than interpatient overlap. Overall distribution of frequencies of different isotypes **(C)** and average somatic hypermutation frequencies **(D)** among the set of sequences belonging to persistent and nonpersistent clones during post-RTX relapse for study subjects. Two-way ANOVA was performed to assess significance for an overall somatic hypermutation frequency difference and isotype usage frequency difference between nonpersistent compared with persistent clones across isotypes; specifically, the effect of isotype, persistence, and interaction between the 2 was assessed for significance. Post hoc 2-tailed t tests were also performed, although no significant differences were observed in C and D. Data for the same n = 3 patients are shown for all panels. Violin plots are used in place of error bars to show the full range of values. Statistical differences are shown only when significant (***$P < 0.001$; **$P < 0.01$; *$P < 0.05$).

Persistent clones are antigen experienced. Next, we compared the V(D)J properties of nonpersistent clones with persistent clones that emerge post-RTX to investigate whether the latter have distinct characteristics that might contribute to their persistence **(Figure 2, C and D)**. Given the possible role of persistent B cells in recognizing antigen, we characterized features of the repertoire associated with antigen experience, namely isotype switching and elevated somatic hypermutation

97

(SHM) frequency. High-depth bulk repertoires were first examined to quantify the difference in isotype frequency among V(D)J sequences from persistent and nonpersistent post-RTX clones. Only B cells displaying an antigen-experienced phenotype were found to be persistent; when the approach shown in **Figure 2B** was applied to only B cells displaying a naive phenotype (unmutated IgM and IgD B cells), no clonal sharing was observed (1-tailed t test P = 0.317, data not shown). Furthermore, nonpersistent sequences were 43.2% IgM, 6.4% IgD, 24.7% IgG, and 25.5% IgA of the repertoire on average **(Figure 2C)**, and persistent ones were disproportionately switched (15.0% IgM, 2.2% IgD, 27.4% IgG, and 55.0% IgA) (ANOVA P = 0.027). In addition, the overall SHM frequency of persistent clones was significantly elevated **(Figure 2D)** (ANOVA P = 0.014), and this difference in SHM frequency did not depend on the isotype of the sequence (ANOVA P = 0.287). Therefore, persistent clones are preferentially isotype switched with elevated SHM, reflecting a more antigen-experienced phenotype.

Persistent clones do not consistently expand or gain SHM. We next sought to determine whether antigen experience (in terms of clonal expansion and SHM) was gained by persistent clones during reconstitution of the B cell compartment after RTX. To that end, the high-depth bulk repertoire was first examined to test whether persistent clones expanded between pre-RTX and post-RTX time points. Clonal expansion was assessed by computing the change in size of persistent clones between pre-RTX and post-RTX time points. Average decreases of -11% (95% CI -93% to +1313%), -85% (95% CI -98% to +439%), and -7% (95% CI -99% to +40.5%) in clonal size were observed across patients 1, 2, and 3, respectively (1-

sample t test P = 0.37) **(Supplemental Figure 2, A-C)**. Thus, decreases in clonal size were observed but these decreases were not significant. Given that persistent clones have elevated frequencies of SHM, we tested whether individual clones acquire additional SHM by quantifying the average change in SHM frequency of persistent clones between pre-RTX and post-RTX time points. The median change in SHM frequency was -0.2% (95% CI -89% to +1132%), -2.4% (95% CI -74% to +187%), and +4.5% (95% CI -41% to +67%) for patients 1, 2, and 3, respectively **(Supplemental Figure 2, D-F)**; no consistent change in the SHM frequency of persistent clones between pre-RTX and post-RTX samples was detected (1-sample t test P = 0.807). These collective findings suggest that persistent clones are enriched for features of antigen experience pre-RTX but do not acquire further antigen experience between pre-RTX and post-RTX time points.

Some persistent clones are disease relevant and bind MuSK. We then sought to investigate whether persistent B cell clones were autoantigen specific. In 2 previous studies, using the same 3 patients described here, we identified B cell clones during post-RTX relapse that were specific for autoantigen **(Supplemental Table 3)**. In the first study, 43 unique B cell clones were used to generate recombinant monoclonal antibodies, all of which were derived from circulating plasmablasts because this cell type was demonstrated to produce MuSK-specific antibodies when cultured in vitro (15). In the second, a fluorescent MuSK antigen bait was used to both identify and isolate MuSK-specific B cell clones, from which an additional 38 recombinant monoclonal antibodies were produced (16). In total, 11 members of these collective 81 clones bound surface-expressed MuSK across a

range of binding strengths when tested as monoclonal antibodies with a cell-based assay (15, 16). The BCR sequences of these clones were compared with the sequences in high-depth bulk repertoires to identify clonal relatives present both before and after treatment. Of these 81 clones, 27 were members of clones found in the bulk post-RTX BCR repertoires. This finding demonstrates that these clones were expanded because they were found in unique, independent sample aliquots. We tested whether members of these 81 clones were present in pre-RTX repertoires; members belonging to 74 clones were not observed. However, we observed that 7 clones could be found in pre-RTX repertoires **(Figure 3 and Supplemental Figures 3-5)**. One of these clones was among the 11 previously demonstrated to specifically bind MuSK **(Figure 3)** (15). Thus, disease-relevant and MuSK autoantigen-specific B cells present during relapse can derive from the failed depletion of B cell clones that existed before therapy.
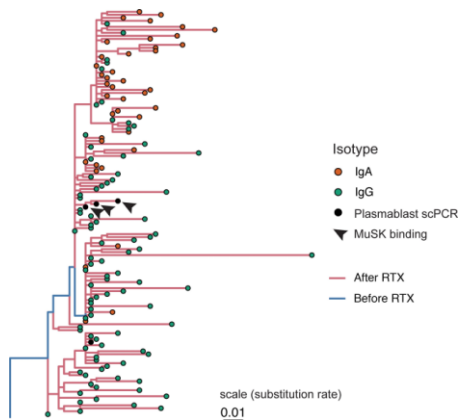
Figure 3. Example lineage tree of a disease-relevant B cell clone spanning both the pre- and post-RTX repertoire. Sequences isolated from plasmablasts using single-cell PCR (scPCR) sequencing-based approaches and tested as monoclonal antibodies are denoted as "Plasmablast scPCR" (black dots); 3 of these bind MuSK and are denoted as "MuSK binding" (black arrowheads). Lineage tree topology and branch lengths were estimated using maximum parsimony, with edge lengths representing the expected number of nucleotide substitutions per site (see scale) as estimated using dnapars v3.967 (89). Tips are colored by antibody isotype, and each internal branch is colored by whether its descendant node was determined to have occurred in the pre- or post-RTX repertoire using a constrained maximum parsimony algorithm (see Methods).

ASC-like B cells are more persistent than memory B cells. We next sought to characterize the transcriptional state of persistent B cells to determine their phenotype in an unbiased manner and quantify how different B cell subsets are represented among persistent populations. To accomplish this, we carried out single-cell transcriptome and paired BCR repertoire profiling of circulating post-RTX B cells. Owing to the high frequency of transitional B cells during post-RTX reconstitution, IgD^lo B cells were selected by sorting before single-cell analysis **(Supplemental Figure 6)**. Further, the analysis was limited to the switched IgG and IgA repertoire by computationally filtering out cells with V(D)Js paired with an IgD or IgM constant region. Clones were identified in the single-cell data sets that were related to clones present in pre-RTX high-depth bulk BCR repertoires. This allowed for direct interrogation of the transcriptomes of persistent B cells. That is, we leveraged the resolution offered by high-throughput single-cell transcriptomes and high-depth offered by bulk BCR analysis to perform STAIR. From single-cell sequencing, a total of 18,133 cells associated with 14,671 IGH V(D)J sequences were identified **(Supplemental Table 4)** from the same 3 patients with post-RTX relapse and an additional asymptomatic AChR MG patient used as a control. Gene expression pattern and repertoire characteristics were used to partition the cells into 11 distinct clusters **(Supplemental Figure 7, A-G, and Supplemental Table 5)**. Clusters of antibody-secreting cells (ASCs), memory B cells, mature naive B cells, and transitional B cells were assigned by analysis of the gene expression of these clusters **(Figure 4A)**. Because B cells from the single-cell expression analysis could not be experimentally isolated to assess for antibody secretion or

other functional features associated with plasmablasts/plasma cells, we chose to label the cluster most associated with a plasmablast/plasma cell signature as ASCs. By combining single-cell repertoires with high-depth bulk pre-RTX BCR repertoires, 820 persistent clones with members in the single-cell profiling data were identified. Persistent clones could be identified in both the ASC as well as memory B cell clusters. The ASC cluster had a higher frequency (27.9%) of persistent clones in comparison with the memory cluster (14.6%) **(Figure 4, B and C)** (t test P = 0.045). As further confirmation that some ASC and memory B cell clones were persistent, IGH sequences were also identified from single cells in the ASC and memory B cell cluster with identical V(D)J sequences as pre-RTX members **(Figure 4B)**. Thus, these data suggest that while both ASCs and memory B cells can persist, members of the ASC subset are more likely than memory B cells to persist after RTX.
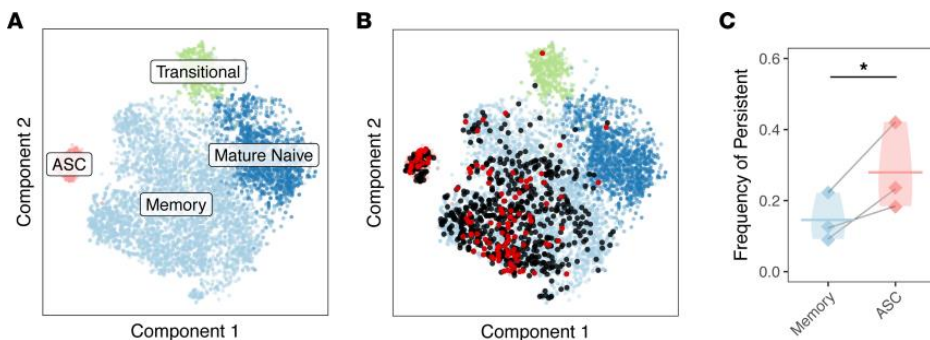
Figure 4. Persistent B cell clones are disproportionately represented by the ASC phenotype.
(A) Unbiased clustering of single-cell transcriptomes from all study subjects is visualized by t-distributed stochastic neighbor embedding (t-SNE) and colored based on B cell subset assignment. **(B)** V(D)J sequences associated with persistent B cell clones are visualized over the t-SNE plot labeled in **A**. B cells are colored black or red if the heavy chain V(D)J sequence paired with the cell is part of a persistent B cell clone. B cells are colored red if the heavy chain V(D)J sequence paired with the cell has the same V(D)J sequence as one present in a pre-RTX bulk repertoire and black if the clonal relative differs by 1 or more SHM. **(C)** The relative fractions of persistent compared with nonpersistent B cells for the memory B cell cluster compared with ASC cluster. A 1-tailed t test was used to assess the significance of the null hypothesis that ASCs would not be enriched compared with memory B cells. Horizontal bars show the average frequency of a given B cell subset across patients. Frequencies belonging to the same patient are paired with a gray line. Data for the same n = 3 patients are shown for all panels. Violin plots are used in place of error bars to show the full range of values. Statistical differences are shown only when significant (***$P < 0.001$; **$P < 0.01$; *$P < 0.05$).

ASCs have persistence-associated features compared with memory B cells. We next sought to investigate phenotypic characteristics of ASCs compared with memory B cells during post-RTX relapse to further understand their mechanism of persistence and identify possible subsets of persistent ASCs. The expression of CD20, the target of rituximab, was first investigated. To test the association between the expression of CD20 and persistence of ASCs, CD20 expression was examined among B cell subsets. The ASC cluster was observed to express lower CD20 levels when compared with memory B cells (t test $P = 0.021$) **(Figure 5A)**. However, when we examined the expression of CD20 on persistent ASCs

compared with nonpersistent ASCs, a decrease was observed, but this trend did not reach significance (t test P = 0.15) **(Figure 5B)**.

BAFF (also known as B cell activating factor, B lymphocyte stimulator, or BlyS) is a TNF superfamily member produced almost exclusively by myeloid cells (24, 25). BAFF (and another TNF superfamily ligand, APRIL) can bind a family of B cell-specific receptors to promote B cell survival. Given that APRIL/ BAFF receptor genes have been observed to play a role in mediating B cell survival after RTX depletion, we investigated the differential expression of APRIL/BAFF receptor genes (26–28). Persistent ASCs were not observed to differentially express APRIL/BAFF receptor genes (TACI, BAFF-R, and BCMA) (P = 0.085, 0.555, and 0.288 for TACI, BAFF-R, and BCMA, respectively) **(Figure 5B)**.

To investigate other features that might distinguish persistent and nonpersistent ASCs, the relative usage of different isotypes and average SHM frequencies were examined. Persistent ASCs were also not observed to differ in terms of isotype usage (ANOVA P = 0.194) or frequency of SHM (ANOVA P = 0.101) compared with their nonpersistent counterparts **(Supplemental Figure 8, A and B)**. The clonal diversity (more clonal expansions) of the ASC cluster was lower compared with memory B cells (t test P = 0.011) **(Figure 5C)**. However, when we examined clonal diversity within the ASC cluster, a consistent difference between persistent ASCs compared with nonpersistent ASCs was not observed (t test P = 0.079) **(Figure 5D)**. Finally, the fraction of cells in the ASC cluster was 10.0% of the total B cell repertoire in the post-RTX cohort **(Figure 5E)**. This was significantly elevated

compared with the 0.5% observed in the control asymptomatic AChR MG sample (1-sample t test P = 0.044). However, when we examined whether clonal expansion of persistent B cells between the pre-RTX and post-RTX time points could explain the abundance of ASC B cells that we observed post-RTX relapse, ASC B cell clones were not consistently found to expand (or acquire SHM); between pre-RTX and post-RTX time points, approximately half expanded and the other half shrunk. The average change in clonal size was therefore not consistent across patients (t test P = 0.099) **(Supplemental Figure 9, A-F)**. To summarize, persistent ASC cluster members were not observed to differ from nonpersistent members in terms of their expression of CD20 and receptors for BAFF/APRIL, clonal diversity, isotype usage, or SHM frequency. However, ASC cluster members expressed lower CD20 and were more clonally expanded than memory B cells overall; these data identify features of the ASC cluster as a whole that may explain their higher frequency among persistent clones.

Persistent memory B cell clones are expanded and express low levels of CD20. While ASC clones were observed to be more persistent than memory cells, ASC members of the MuSK-specific clone identified previously **(Figure 3)** were also observed to be related to 2 members of the memory B cell cluster. Moreover, given the high frequency of persistent memory B cells observed overall, we next sought to explore whether persistent memory B cells had distinct features compared with nonpersistent memory B cells. We tested CD20 expression, expression of APRIL/BAFF receptors, SHM, isotype usage, and clonal diversity **(Figure 6)**. Persistent memory B cells were observed to have significantly lower CD20

105

expression (t test P = 0.022). To investigate whether this difference in CD20 mRNA would be expected to correlate with surface CD20 expression, we examined B cells from a published data set generated using CITE-Seq (29, 30). CD20 surface expression was found to be significantly elevated in cells with higher CD20 mRNA expression across subjects **(t test P = 5.1e-5, Supplemental Figure 10)**. Other features of persistent memory B cells included higher expression of TACI (t test P = 0.037) but lower expression of BAFF-R (t test P = 0.037) **(Figure 6A)**. Analysis of SHM and isotype usage revealed that persistent memory B cells also had higher frequencies of SHM across isotypes (ANOVA P = 0.037) **(Figure 6B)**; the fraction of persistent memory B cells expressing IgG1 (t test P = 0.022) and IgG3 (t test P = 0.025) (ANOVA P = 0.007) was less than that of their nonpersistent counterparts **(Figure 6C)**. We next examined whether persistent memory B cells were clonally expanded compared with their nonpersistent counterparts. They were observed to have lower clonal diversity post-RTX, suggesting that they were clonally expanded (t test P = 0.030) **(Figure 6D)**. Initial clustering of cells based on single-cell gene expression identified 6 distinct sub-clusters of memory B cells. To better characterize the gene expression features of persistent memory B cells, we examined the most abundant subcluster among persistent memory B cells. This cluster (cluster 3) **(Figure 7, A and B)** represented 36.7% of all persistent memory B cells but only 25.0% of all memory B cells (not the most prevalent overall, which was cluster 2) **(Figure 7, B and C)**. Analysis of gene expression showed that cluster 3 was specifically characterized by lower CD20 expression (t test P = 0.005), higher TACI expression (t test P = 0.008), and lower BAFF-R expression (t test P = 0.014)

compared with other memory B cell subclusters **(Figure 7D and Supplemental Figure 11A)**. This cluster also displayed a higher frequency of SHM across all isotypes (ANOVA P = 1.46e-6) **(Supplemental Figure 11B)** and demonstrated increased usage of IgA compared with IgG isotypes (ANOVA P = 0.0103) **(Supplemental Figure 11C)** but was not more clonally expanded compared with other memory B cells (t test P = 0.169) **(Supplemental Figure 11D)**.

Unbiased differential gene expression identified 1282 differentially expressed genes between memory cluster 3 (enriched for persistent clones) and all other memory B cell subclusters **(Supplemental Figure 12 and Supplemental Data)** (FDR < 0.05). The upregulated subset of these genes was enriched for a MYC signature (or c-Myc, a transcription factor that enhances B cell survival) and BRCA1/TP53 signature (transcription factors that regulate cell senescence and cell cycle) **(Supplemental Figures 13 and 14)** (31–33). The expression of 2 tissue homing genes that are the targets of the immunotherapy agents natalizumab and fingolimod (ITGA4 and S1PR1, respectively) was also observed as upregulated among cluster 3 memory B cells (P = 0.049 for ITGA4, and P = 0.039 for S1PR1) **(Supplemental Data)** (34). Thus, persistent memory B cells are clonally expanded and are characterized by a subset of B cells with elevated SHM, less IgG1 and IgG3 usage, high expression of TACI, low expression of CD20, and a gene expression pattern associated with transcription factors that control cell survival, proliferation, and senescence.
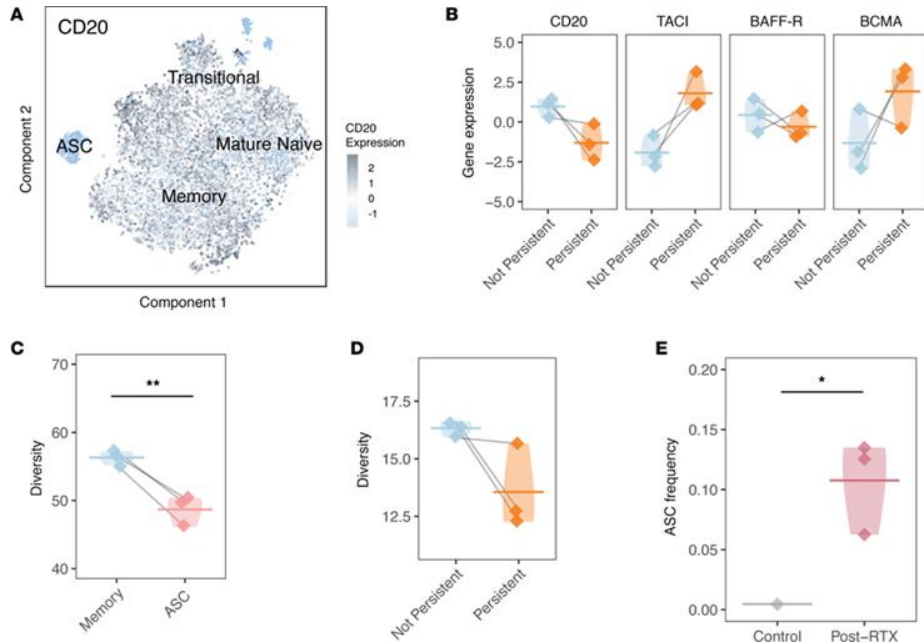
Figure 5. Unique characteristics of persistent ASCs. (A) Expression of log-normalized CD20 expression (Z score) visualized by intensity over t-SNE plot. **(B)** The expression of CD20 (the receptor target of RTX, gene symbol MS4A1) and BAFF or APRIL receptors (TACI or TNFRSF13B, BAFF-R or TNFRSF13C, BCMA or TNFRSF17) for persistent and nonpersistent members of the ASC cluster. Normalized gene expression values are computed from counts of gene expression transcripts. Paired 2-tailed t tests were used to test for the significant differential expression of each gene. Horizontal bars show the average expression of ASC cluster members for each patient for cells of a given status. **(C)** Clonal expansion expressed as Simpson's diversity for ASC and memory B cell clusters. A 1-tailed t test was used to assess the significance of the null hypothesis that ASCs would not be less diverse than memory B cell clones. Horizontal bars show the average diversity of cluster members for each patient of memory B cells or ASCs. **(D)** Simpson's diversity for persistent and nonpersistent members of the ASC cluster. A 1-tailed t test was used to assess the significance of the null hypothesis that persistent clones would not be less diverse than nonpersistent clones. Horizontal bars show the average diversity of ASC cluster members for each patient for cells of a given status. **(E)** The frequency of ASCs in post-RTX MuSK MG patients and a control AChR MG patient. The fraction of ASC cluster members is quantified as a ratio of the number of cells in the ASC cluster divided by the number of total B cells for each patient. A 1-sample t test was used to assess the significance of the null hypothesis that ASCs would not be more abundant in post-RTX samples compared with the asymptomatic AChR MG patient sample. Horizontal bars show the average frequency of ASC cluster members for each patient of a given status. Values belonging to the same patient are paired with a gray line for all graphs. Data for the same n = 3 patients are shown for all panels except panel E, which includes an asymptomatic patient sample (n = 4). Violin plots are used in place of error bars to show the full range of values. Statistical differences are shown only when significant (***P < 0.001; **P < 0.01; *P < 0.05).

108
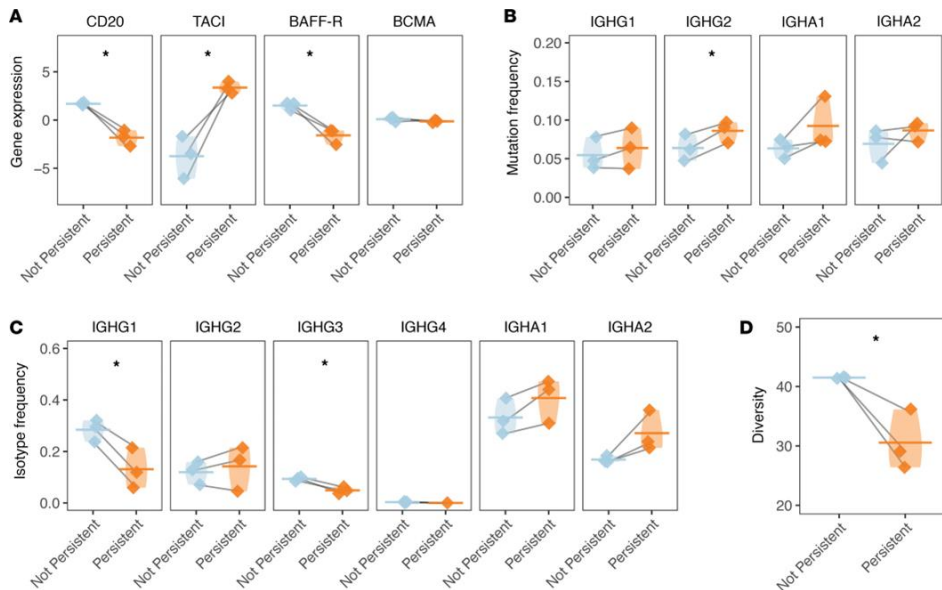
Figure 6. Memory B cells have distinct transcriptional and repertoire features associated with persistence. (A) The normalized gene expression of CD20 (the receptor target of RTX, gene symbol MS4A1) and BAFF or APRIL receptors (TACI or TNFRSF13B, BAFF-R or TNFRSF13C, BCMA or TNFRSF17) is presented for persistent and nonpersistent members of the memory B cell cluster for each patient for cells of a given status. Normalized gene expression values are computed from counts of gene expression transcripts. Paired 2-tailed t tests were used to test for the significant differential expression of each gene. **(B)** Individual SHM frequencies for persistent compared with nonpersistent cells are presented for memory B cell cluster members. Only mean SHM frequencies are computed for isotypes with more than 3 V(D)J sequences. Horizontal bars show the average SHM frequency for a given cluster. Paired 2-tailed t tests were used to assess the significance of differences in mutation frequency. **(C)** Overall constant region usage frequencies are quantified for persistent compared with nonpersistent memory B cell cluster members per patient. Horizontal bars show the average frequency of constant region usage across patients. Two-way ANOVA was performed to assess significance for an overall isotype usage difference between nonpersistent compared with persistent clones across isotype. Paired 2-tailed t tests were used to assess the significance for the differential usage of each constant region. **(D)** Clonal expansion expressed as Simpson's diversity of persistent compared with nonpersistent memory B cell cluster members. A 1-tailed t test was used to assess the significance of the null hypothesis that persistent clones would not be less diverse than nonpersistent clones. Horizontal bars show the aver- age diversity of memory B cell cluster members for each patient of a given status. Values belonging to the same patient are paired with a gray line for all graphs in this panel. Data for the same n = 3 patients are shown for all panels. Violin plots are used in place of error bars to show the full range of values. Statistical differences are shown only when significant (***$P < 0.001$; **$P < 0.01$; *$P < 0.05$).
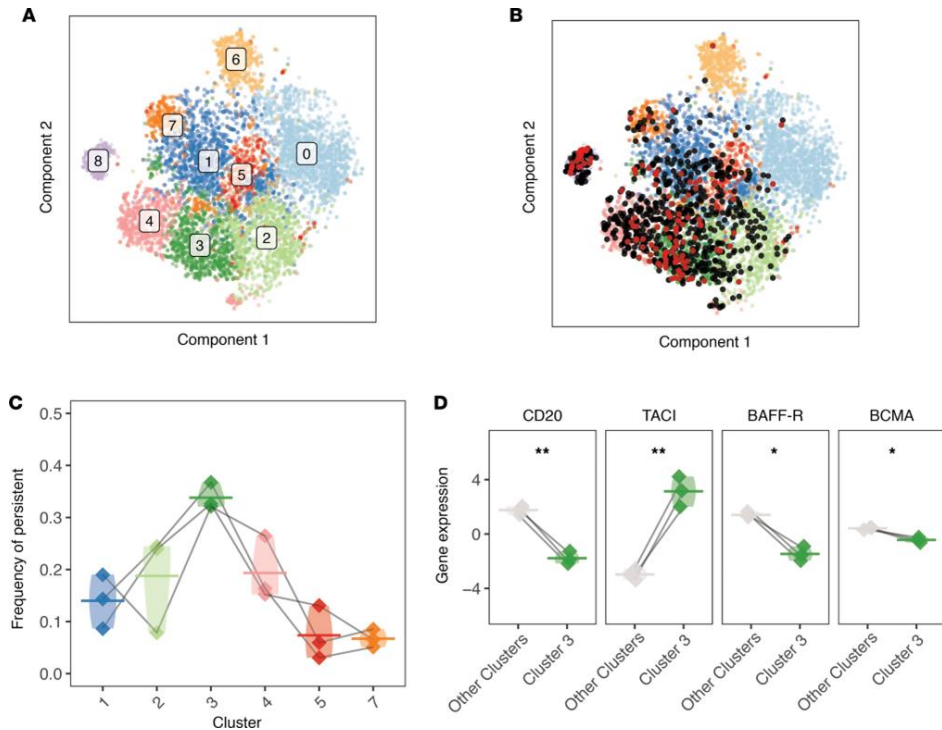
Figure 7. Identification of B cell clusters associated with resistance to RTX depletion (cluster 3). (A) Visualization of initial shared nearest-neighbor clustering of circulating B cells post-RTX by t-SNE with labels over clusters. **(B)** B cells that were clonally related to cells in the pre-RTX repertoire are indicated (red dot if the pre- and post-RTX V(D)J sequence is identical at the nucleotide level, and black dot otherwise). **(C)** The frequency of each cluster (by cell) among the set of persistent B cells is shown. **(D)** The expression of the receptor target of RTX, CD20 (MS4A1), is presented for members of cluster 3 and members of other memory B cell clusters. The expression of known receptors for BAFF and APRIL (TACI or TNFRSF13B, BAFF-R or TNFRSF13C, BCMA or TNFRSF17) is also presented. Differential expression of each gene was assessed using paired 2-tailed t tests. Horizontal bars show averages, with values belonging to the same patient paired with a gray line. Data for the same n = 3 patients are shown for all panels. Violin plots are used in place of error bars to show the full range of values. Statistical differences are shown in D (**P < 0.01; *P < 0.05).

Discussion

Recent studies have demonstrated the remarkable benefits of RTX-mediated BCDT in MuSK MG; however, relapses have been observed in some patients and are associated with the presence of circulating plasmablasts that express MuSK-specific autoantibodies (9, 10, 15, 16, 35, 36). Through investigating the characteristics of B cells that emerge post-RTX, we sought to determine whether these disease-relevant B cells derive either from the failed depletion of preexisting B cell clones or from de novo generation.

We show that B cell clones, including MuSK-specific autoantibody-secreting B cells, emerge from the failed depletion of preexisting clones and that memory B cells serve as a reservoir for these cells, including antigen-specific members **(Supplemental Figure 15)**. A potentially novel approach was used that combined multiple methods of sequencing the BCR repertoire with single-cell gene expression (STAIR) to demonstrate that persistent B cell clones are composed of expanded ASCs and memory B cell populations expressing low levels of CD20 associated with a unique gene expression profile. Although the persistence of B cell clones after RTX is not specific to MuSK MG relapse (37–39), MuSK-specific ASCs are found during MuSK MG relapse; we show here that these ASCs and their memory B cell precursors are incompletely depleted by RTX in a subset of patients with MG who experienced post-RTX relapses.

That many ASCs present after BCDT are related to preexisting populations is consistent with a large body of evidence showing that ASCs resist depletion owing

111

to their low levels of CD20 expression and tissue localization (17, 19, 20, 40); their frequency predicts poor treatment response in patients with systemic lupus erythematosus (SLE) and rheumatoid arthritis (RA) (41–44). The finding that circulating memory B cell clones are also persistent is consistent with data showing that the frequency of memory B cells also predicts poor responses to RTX in SLE and RA (21, 22, 45). While these previous studies were important for identifying predictors of outcome, they were not designed to highly resolve B cell subsets because of limitations inherent with flow cytometry. By comparison, here, the definition of memory using single-cell transcriptomes does not rely on flow cytometry markers, but rather hundreds of markers that allow for accurate identification of common gene expression patterns associated with memory B cells. Furthermore, by applying STAIR, we were able to profile persistent memory B cell subsets in detail. A recent study using bulk AIRR-Seq to investigate the use of RTX for treating ANCA-associated vasculitis demonstrated that persistent clonotypes are isotype switched, which we also observed in our study (38). Here, persistence also correlated with a specific gene expression signature, that is, lower CD20 expression and differences in APRIL/BAFF receptor expression relative to other memory B cells.

Studies of RTX responses in IgM anti-myelin-associated glycoprotein peripheral neuropathy and pemphigus vulgaris (45–47) demonstrated that poor responses to RTX are associated with increased repertoire clonality post-RTX. Our results show that persistent memory B cells are more clonally expanded than non-persistent memory B cells and suggest that the association between increased repertoire

clonality and poor responses to RTX may result from the persistence of clonally expanded memory B cells.

Our work is congruent with studies that have shown that BAFF and the differential expression of receptors for APRIL/BAFF (TACI, BAFF-R, BCMA) on antigen-experienced B cells may lead to poor outcomes after BCDT (26–28, 48). BAFF (also known as B cell activating factor, B lymphocyte stimulator, or BlyS) is a TNF superfamily member produced almost exclusively by myeloid cells (24, 25). BAFF (and APRIL) can bind a family of B cell–specific receptors to promote B cell survival. A higher frequency of memory B cells expressing lower BAFF-R can be detected in patients with RA relapsing after RTX (28) as well as in patients with graft-versus-host disease who respond poorly to RTX (27). This is consistent with our observation that persistent memory B cells express lower BAFF-R levels. Further, BAFF levels have been shown to negatively correlate with BAFF-R expression after RTX therapy in primary Sjögren's syndrome and SLE (48), and exposure of B cells to soluble BAFF decreases BAFF-R in vitro. By comparison, exposure to anti-BAFF increases the expression of BAFF-R on B cells (49). By directly characterizing B cell clones that resist RTX depletion, we are able to show that memory B cell subsets that persist after RTX express surface markers associated with poor responses to RTX during relapse.

Our analysis showed that ASCs and cluster 3 memory B cells during relapse were predominantly IgA switched. We speculate that the abundance of IgA-switched B cells could be related to BAFF expression given the known role of BAFF in class

113

switch recombination, particularly in the gut (50–52). The presence of IgA-switched circulating ASCs has been shown to depend on BAFF (53). Moreover, IgA-secreting plasma cells reduce disease severity in an experimental autoimmune encephalomyelitis model, owing to their production of IL-10 (54). Thus, further characterization of how the induction of IgA-producing B cell subsets by RTX occurs is needed to investigate alternative mechanisms of BCDT-mediated therapeutic benefit. The conclusions of this study offer insights into therapeutic and diagnostic avenues for patients who experience relapses after RTX. Our findings regarding the BAFF/APRIL system suggest that combining RTX with BAFF pathway inhibitors (e.g., belimumab) could offer ways to deplete B cells that persist after RTX, including autoantibody producers. Combination strategies involving both belimumab and RTX were successful in a phase IIa randomized clinical trial in SLE, now followed by an ongoing phase III trial (55, 56). A combination approach using belimumab and RTX has also shown promise for treating Sjögren's syndrome (57). This study by no means validates the use of combination therapy targeting BAFF as standard of care, nor do we argue that this is the only approach to combination therapy; further investigations are warranted to better understand such strategies. Mechanisms underlying RTX resistance are complex and may not be limited to B cell persistence. For example, a suggested role for variable complement activity could alter RTX effectiveness (58). Furthermore, concomitant statin treatment may introduce conformational changes in the CD20 receptor that impair RTX binding or disturb the integrity of RTX-induced translocation of CD20 into lipid rafts, both of which are important for cytotoxicity (59, 60).

We also observed that upregulated genes associated with the subset of memory B cells most resistant to depletion (cluster 3) included those involved in tissue homing (ITGA4, S1PR1). S1P receptor is upregulated in lymphocytes localized to lymph nodes and inflamed tissues and a target of the immunotherapeutic fingolimod. ITGA4 is a component of VLA-4, an integrin dimer also responsible for the localization of leukocytes to inflamed tissue, and target of natalizumab (34). We speculate this could reflect the tissue-associated origin for this subset. This is consistent with evidence showing that lymph nodes, spleen, bone marrow, and tonsils harbor RTX-resistant memory B cells (21, 61–63). Therapies such as engineered T cell technology, including chimeric-antigen receptor or chimeric-autoantibody receptor T cell therapy (64, 65), and other methods for eliminating tissue-localized subsets may be well suited for preventing and treating relapses.

Existing AIRR-Seq approaches for generating immune repertoires commonly begin with genomic DNA or mRNA and produce high-depth bulk repertoires of unpaired immunoglobulin or T cell receptor V(D)J sequences (66–68). More recent approaches use single-cell isolation techniques with high-throughput sequencing to construct repertoires, sometimes with paired gene expression (69–72). The use of these single-cell-based approaches was included in studies on tumor-infiltrating lymphocytes from cancer biopsies, infiltrates from the brains of mice, and B cells from the spleens of mice after vaccination in mice (70–72). No single-cell repertoire studies have investigated the B cell repertoire in autoimmune disease thus far to our knowledge. Our ability to extract biologically meaningful results from STAIR analysis suggests that tracing individual BCR sequences associated with relapse

115

could provide a powerful tool for monitoring patient responses to immunotherapies that deplete B and T cells. Moreover, in comparison with techniques that use bulk BCR repertoire sequencing to monitor therapy progress, this approach allows for the individual characterization of lymphocytes that resist therapy based on gene expression, which may suggest alternative avenues for treatment (73).

Several limitations of this study should be considered. First, the single-cell gene expression of B cells was characterized only after RTX depletion. Determining the phenotype of B cells that resist RTX depletion before therapy may be of interest to identify resistant subsets for targeting before relapse. A recent study demonstrated that not only do B cell clones move between peripheral blood and cerebrospinal fluid over the course of immunotherapy in some patients with multiple sclerosis (MS), but also many have both memory and plasma cell members (74). Similar studies using single-cell transcriptomics could identify memory B cell subsets that give rise to autoantibody-producing plasmablasts during relapse. Second, our results rely on tracing B cell clones by analyzing their IGH V(D)J sequences alone. While we (and others) have demonstrated that clonal relationships can be reliably inferred given the diversity of IGH V(D)J sequences, false positives may occur (23, 75, 76). Third, owing to the abundance of transitional B cells that repopulate the repertoire during RTX relapse and our interest in studying antigen-experienced B cell subsets, we excluded IgD$^+$ B cells from our single-cell analysis. Nevertheless, a small fraction of BCRs paired with an IGHD constant region (3.2%–11.4%) was found in our single-cell data. This is likely because flow-based sorting is not absolute in eliminating gated populations. Fourth, the expressed mRNA

transcriptome may not always reflect the expression of surface markers used for sorting. Nevertheless, in the specific case of CD20, we showed a consistent correlation between CD20 mRNA expression and CD20 surface expression; low expression of surface CD20 has been associated with resistance to RTX depletion in murine models (17, 20). Fifth, we were limited to a cohort of 3 patients owing to the rarity of MuSK MG relapse after RTX. This limitation was weighed against the benefits of studying a disease directly caused by antigen-specific antibodies, permitting more definitive statements about the contribution of persistent antigen-specific B cells to clinical relapse. Nevertheless, because of the small cohort size, caution should be taken when generalizing the results of this study to patients with MuSK MG. Finally, although we previously generated human recombinant MuSK-specific monoclonal antibodies from B cells present during post-RTX relapse, these monoclonal antibodies recognized MuSK with different binding capacities ranging from weak to very strong (15, 16). The one we were successful in tracing to the pre-RTX repertoire in the present study was among those showing weaker binding capacity. Accordingly, we can only speculate on its pathogenic capacity *in vivo*. That it was a member of a large expanded clone with multiple clonal variants may suggest that this particular clonal member represented an intermediate step toward a higher binding disease-causing relative.

The reported results motivate future investigations. By combining the depth offered by bulk repertoire sequencing with the resolution of single-cell repertoire and gene expression, STAIR analysis allows for the characterization of B cells present at multiple time points in detail. Extending these observations to studies where anti-

CD20 therapy has strong evidence for efficacy, such as MS, may be particularly worthwhile. Applying STAIR analysis to the simultaneous investigation of other therapies, such as anti-CD19 therapy (inebilizumab) - recently shown to be efficacious for the treatment of neuromyelitis optica - could allow for the optimal selection of B cell–depleting agents for preventing disease relapse (77). While RTX is a reliable treatment modality for MuSK MG, data for AChR MG has been mixed and patient relapses do occur (12). An investigation of factors that contribute to relapse after RTX in the context of AChR MG using similar approaches could lead to the development of improved therapeutics for diagnosing and treating patients with MG regardless of disease subtype.

Methods

Patient-derived specimens. Peripheral blood was collected from subjects with MG (Yale Myasthenia Gravis Clinic, New Haven, Connecticut, USA). A MuSK MG cohort (n = 3) was identified for investigation of post-RTX relapses with these characteristics that we have described previously: (a) an RTX-induced complete stable remission, minimal manifestation (CSR/MM) clinical status (>1 year); (b) repopulation of the B cell compartment after RTX; and (c) disease relapse following sustained CSR/MM after RTX (15, 16). Selected patients may have been treated with RTX before study entry. All pre-RTX sample collection time points precede post-RTX time points by at least 1 infusion of RTX. An additional asymptomatic (by Myasthenia Gravis Foundation of America classification score) AChR MG control subject was also included.

Bulk library preparation. RNA was prepared from frozen PBMCs using the RNeasy Mini Kit (QIA- GEN) per the manufacturer's instructions. Cells were pelleted and lysed in freezing medium without washing to preserve cell populations sensitive to cryopreservation. RNA libraries were made using reagents supplied by New England BioLabs (a gift from Eileen Dimalanta and Chen Song, Ipswich, Massachusetts, USA) as part of the NEBNext Immune Sequencing Kit. IGH library preparation and sequencing were performed in the same manner as previously published using only primers targeting IGHA, IGHD, IGHE, IGHG, and IGHM regions (78).

Raw read quality control and assembly for bulk libraries. Bulk repertoire data processing and analysis was carried out using tools in the Immcantation framework

(http://immcantation.org). Preprocessing was carried out using pRESTO v0.5.10 (79) as follows: (a) Reads with a mean Phred quality score below 20 were removed. (b) Reads were aligned against constant region primer and template switch sequences, with a maximum mismatch rate of 0.2 and 0.5, respectively. Reads failing to match both a constant region primer and template switch sequence were removed. (c) Remaining reads were grouped based on unique molecular identifier (UMI) sequences determined by the 17 nucleotides preceding the template switch site. (d) Separate consensus sequences for the forward and reverse reads within each UMI group were constructed with a maximum error score of 0.1 and minimum constant region primer frequency of 0.6. If multiple constant region primers were associated with a particular UMI group, the majority primer was used. (e) Forward and reverse consensus sequence pairs were aligned to each other with a minimum overlap of 8 nucleotides and a maximum mismatch rate of 0.3 and assembled into full-length sequences. Sequence pairs that failed to align to each other were assembled by alignment against the ImMunoGeneTics (IMGT) human germline IGHV reference database (IMGT/GENE-DB v3.1.19; retrieved June 21, 2018; http://www.imgt.org/genedb/) with a minimum overlap of 0.5 and an E value threshold of 1×10^5. (f) Isotypes were assigned by local alignment of the 3′ end of each consensus sequence to isotype-specific constant region sequences with a maximum mismatch rate of 0.4. (g) Duplicate sequences were removed, except those spanning multiple biological samples or with different isotype assignments. Constant region primers, isotype-specific internal constant region sequences, and

template switch sequences used are available at https://bitbucket.org/kleinstein/immcantation.

Single-cell library preparation and gene expression analysis. B cells were isolated from PBMCs by Easy-Sep Human Pan-B cell Enrichment Kit (immunomagnetic negative selection kit, STEMCELL Technologies) per the manufacturer's instructions. Additional fluorescence-activated cell sorting was then performed using a FACSAria flow cytometer (Becton Dickinson, Mountain View, California, USA) and visualized using the python package FlowCytometryTools v0.5.0; B cells labeled with 7AAD Viability Staining Solution (BioLegend) and FITC-labeled anti-IgD antibody (mouse anti-human monoclonal antibody, BioLegend clone IA6-2) were removed to exclude nonviable cells and all naive B cell populations. Sorted B cells were then loaded into the Chromium Controller (10x Genomics). Single-cell gene expression libraries were prepared using the Chromium Single-cell 5′ Reagent Kit (10x Genomics) for version 1 chemistry per the manufacturer's protocol. Samples were sequenced on the NovaSeq 6000 Sequencing System (Illumina) with 100×100 or 150×150 paired-end reads for gene expression and BCR libraries, respectively. Base calls were converted to FASTQ sequences, demultiplexed using the cellranger mkfastq function from 10x Genomics 2.2.0, and aligned to the GCRhg38 genome supplied by 10x Genomics. Sparse count matrices, bar code assignments, and feature calls were prepared using the cellranger count function. Seurat v.2.3.4 was used for gene expression analysis. Cells with fewer than 50 genes detected, with mitochondrial content above 0.2 of all transcripts, or expressing detectable CST3, CD3E, KLRB1, NKG7, and GATA2

transcripts (to remove non-B cell populations like T cells and myeloid cells) were excluded. Single-cell gene expression values were computed from log-normalized count values (80). A total of 12,534 cells were identified after filtering. t-SNE was computed after identifying highly variable genes using FindVariableGenes and correcting for batch effects using the first 20 dimensions from canonical correlation analysis after visualization of components with MetageneBicor-Plot. The first 10 dimensions were used for principal components analysis based on the location of the inflection point from PCElbowPlot. FindClusters was then used to identify clusters in Seurat v.2, which uses shared nearest-neighbor clustering (80).

Cell subsets were identified using a "basis set" of published marker genes called immunoStates (81). The mean expression of each gene was computed for each cluster from the scaled log-normalized expression values; each cluster was then assigned to the immunoStates subset with the highest Pearson correlation coefficient. The absence of transitional B cells in the immunoStates data set meant this cluster was identified manually using marker genes alone. Small clusters with elevated expression of mitochondria-associated genes were also excluded from further analysis. We confirmed our assignments by visualizing the expression of known gene expression markers, for instance, CD27 (for memory B cells), MS4A1 (CD20, for B cells in general except plasma cells), MME (CD10, for transitional B cells), and PRDM1 (BLIMP1 for plasma cells) **(Supplemental Figure 7, A–C)**. Overall marker expression was also visualized based on the percentage of cells in each cluster expressing the gene and the overall mean level of gene expression in each cluster **(Supplemental Figure 7, D and E)**. To further confirm the identities

of these single-cell clusters, we assessed their paired IGH repertoire features for mean SHM frequency and isotype usage, which were consistent with expected values **(Supplemental Figure 7, F and G)**.

Bulk BCR repertoire V(D)J gene annotation, additional sequence filtering, clonal assignment, and germline reconstruction for STAIR. Reconstructed V(D)J sequences from single-cell sequencing were extracted using the cellranger vdj function from FASTQ reads. Single-cell V(D)J BCR repertoires as well as previously published scPCR-derived V(D)J sequences were pooled with bulk V(D)J BCR repertoires (15, 16). V(D) J germline assignments were made with IgBLAST v1.7.0 (82) using the June 21, 2018, IMGT reference gene database from all repertoires. Cells with multiple IGH V(D)J sequences were assigned to the most abundant IGH V(D)J sequence by UMI count. Only functional V(D)J sequences were assigned into clonal groups using Change-O v0.3.4 (23). Sequences were first partitioned based on common IGHV and IGHJ gene annotations and junction lengths. Within groups, sequences differing by a length-normalized Hamming distance of 0.126 were defined as clones by single-linkage clustering. This distance threshold was determined based on the average local minima between the 2 modes of the within-sample bimodal distance-to-nearest histogram for the 3 patients across multiple time points; thresholds were determined using a kernel density estimate in the same manner described previously (23). Germline sequences were then reconstructed for each clonal cluster (VH) with D segment and N/P regions masked (replaced with Ns) using the CreateGermlines.py function within Change-O v0.3.4.

Differential gene expression analysis. Single-cell expression values were imputed using the ALRA algorithm to account for dropping out (83). Any gene with a mean expression value less than 0.1 across all cells after imputation was excluded. The gene expression of each gene per cell was subtracted by the mean expression of the gene for that sample; the average expression of each gene was then calculated for all cells of a given status (e.g., persistent vs. nonpersistent) to generate a matrix of pseudobulk expression values. This matrix was further Z score normalized by status. Paired 2-tailed t tests were performed to assign P values. FDR correction was performed using Storey's method implemented within the qvalue package v2.10.0 in R from Bioconductor (for 12,066 P values from cluster 3–associated genes) (84). The enrichr package v1.0 in R was used for gene ontology analysis, which implements Wilcoxon's signed rank test for significance (85). A q value (corrected P value) threshold of 0.05 was used for assigning significance.

CITE-Seq data used to investigate the association between CD20 mRNA (MS4A1) and surface protein expression levels were downloaded from the source publication (patients were healthy, between 18 and 45, and derived from a study on influenza vaccination, and samples were collected as frozen PBMCs; 10 patient samples were examined) (30). A cluster corresponding to non-ASC B cells (cluster K1) was extracted from the data object (cells from cluster C3); mRNA was normalized for each sample by Z score (as above). Cells were identified as CD20 mRNA high or low based on whether they fell above or below the 50th percentile in terms of CD20 mRNA expression, respectively.

Analysis of SHM, diversity, and clonal overlap from BCR repertoires. Mutations relative to the germline sequence were quantified using ShazaM v0.1.8 in R v3.4.2 (86). Diversity analysis was performed using Alakazam v0.2.11 and assessed using the generalized Hill index, with uniform downsampling to the number of V(D)J from the sample with the fewest sequences [to account for different sequencing depth] and 2000 replicates of bootstrapping from the inferred complete clonal abundance (87). Clonal overlap was computed using a Bray-Curtis metric implemented by the function scipy.spatial.distance.braycurtis in scipy v1.1.0 (88). Inference of B cell lineage trees and prediction of intermediate time points. B cell lineage tree topologies and branch lengths were estimated using the dnapars program distributed as part of PHYLIP (v3.697) (89). A maximum parsimony algorithm was used to label the internal nodes of each lineage tree as either pre-RTX or post-RTX, given the date of sampling of each sequence at the tree's tips. This was accomplished using an implementation of the Sankoff parsimony algorithm (90) in which switches from post-RTX to pre-RTX are forbidden using a cost matrix that weights post-RTX to pre-RTX switches as 1000 times more costly than switches in the opposite direction. Clusters of internal nodes separated by 0-length branches (polytomies) were reordered using nearest-neighbor interchange moves to minimize the number of label switches along the tree. These analyses were performed using IgPhyML v1.1.1 (91). Trees were visualized using the R packages ape v5.3 (92) and ggtree v2.0.4 (93).

Data availability. Gene expression and repertoire data in this study are available in the National Center for Biotechnology Information's Gene Expression Omnibus (GEO) database through GEO series accession number GSE149133.

Statistics. R v3.4.2 (86) and Python 3.5.4 were used for all statistical analysis (whereas phylogenetic analysis was performed using R v3.6.3). Venn diagram plotting was performed using the R package VennDiagram v1.6.20. Data frame handling and plotting were performed using functions from the tidyverse 1.2.1 in R and pandas 0.24.2, scipy 1.1.0, and matplotlib 2.2.2 in Python. All parametric statistical testing aside from that used for differential gene expression analysis (described previously) was performed in R using the aov function for 2-way ANOVA or t.test functions for paired 2-tailed t tests (or 1-tailed when appropriate). A significance threshold of $P < 0.05$ was shown on plots with a single asterisk; double asterisks correspond to $P < 0.01$, and triple asterisks correspond to $P < 0.001$. P values less than 0.05 were considered significant. Error bars are not presented in our analysis; violin plots are shown to highlight the full range of the distribution for all figures instead.

Study approval. This study was approved by Yale University's Institutional Review Board. Written informed consent was received from all participating patients before inclusion in this study.

Author contributions

Acknowledgments

Conflict of interest

Supplemental material

Contents:

Figure S13. Cluster 3 memory B cells have a MYC and p53/BRCA1 signature.

Figure S14. Cluster 3 memory B cells have a MYC and p53/BRCA1 signature.

Figure S15. Visual model outlining the likely source of antigen-specific B cells during post-RTX relapse.

Patient	Age	Sex	Collection	Event Type	Antibody Titer	MGFA Class
1	37 F		6	Pre-RTX	1:2560	I[1]
			2	Pre-RTX	1:2560	IIa
			7	Pre-RTX	1:5120	IIIb
			10	Post-RTX	5.70 nmol/L[4]	IIb
2	63 F		3	Pre-RTX	1:2560	IIb
			8	Pre-RTX	1:2560	Asymptomatic[2]
			9	Post-RTX	1:5120	IIb[3]
3	53 F		1	Pre-RTX	1:160	IIa
			5	Pre-RTX	<1:10	IIa
			12	Pre-RTX	<1:10	IIa
			4	Post-RTX	0.89 nmol/L[4]	IIa

Table S1. Clinical characteristics of MuSK MG study subjects at each collection time point. The Myasthenia Gravis Foundation of America (MGFA) clinial classification divides MG into five classes (I-V) based on signs and symptoms of disease severity. Reported age is at time of "Post- RTX" relapse.[1]Patient reported mild intermittent fatigable limb weakness prior but none on day of exam/collection, except for mild non-fatigable unilateral ptosis. [2]Complete Stable Remission (CSR); patient with clinical relapses 2 months later.[3]Patient with clinical relapse/exacerbation. [4]MuSK Antibody Level (reference range: positive > 0.02 nmol/L || Mayo Clinical Laboratory, USA). MuSK Antibody Titer (reference range: positive ≥ 1:20 || Athena Diagnostics, USA) is reported for all others as this was the only or preferred commercial lab available at the time of collection.

Patient	Collection	Relapse	Reads	Unique IgM	Unique IgG	Unique IgA	Clones
1	6	Pre-RTX	321622	19552	25596	26067	20084
	2	Pre-RTX	339025	11995	40274	33127	15015
	7	Pre-RTX	518947	29872	23544	26715	31820
	10	Post-RTX	810822	30492	12343	14239	31902
2	3	Pre-RTX	391364	4274	971	2617	5290
	8	Pre-RTX	108953	9477	1513	4154	10088
	9	Post-RTX	460288	13823	2475	7788	14630
3	1	Pre-RTX	364381	752	5785	2392	2427
	5	Pre-RTX	508120	29	669	1288	239
	12	Pre-RTX	188934	154	2321	4016	860
	4	Post-RTX	477305	7366	12952	10060	7999

Table S2. Counts of reconstructed V(D)J sequences by isotype and clones from sequencing of pre-RTX and post-RTX bulk BCR repertoires.

A

Patient 1

B

Patient 2

C

Patient 3
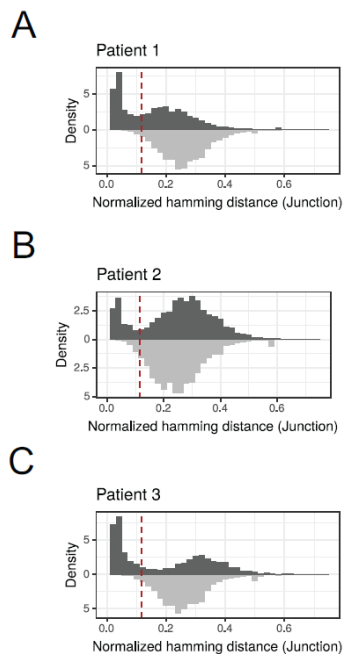
Figure S1. Distance-to-nearest plots used to identify a common threshold to use for hierarchical clustering-based grouping of V(D)J sequences from high throughout sequencing of BCR repertoires. Red dashed lines correspond to the threshold used for assigning clonal clusters. Dark grey bars represent the distribution of intra-subject distance-to-nearest distances while light grey bars represent the distribution of inter-subject distance-to-nearest distances.
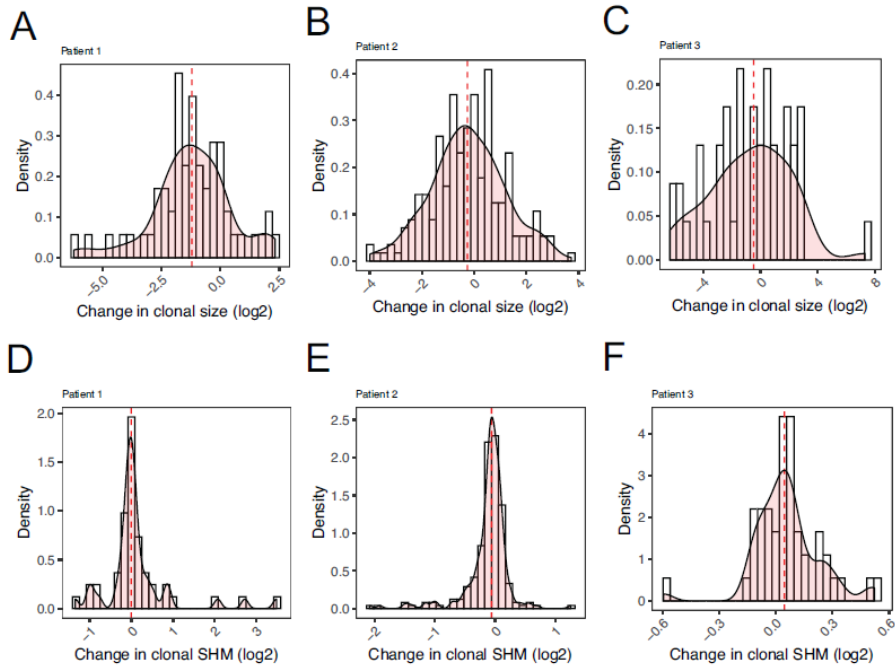
Figure S2. Persistent B cell clones do not show evidence of significant clonal expansion or accumulation of somatic hypermutations when comparing pre-RTX and post-RTX members. The presence of increases in overall somatic hypermutation for individual clones is quantified by comparing the average SHM frequency of each clone in the pre-RTX vs. post-RTX repertoire **(A-C)**. Ratios are visualized as a histogram of the log2-fold changes in somatic hypermutation frequency values for these clones for each patient. Red dashed lines correspond to the median of each distribution. The presence of clonal expansions is evaluated by comparing the overall frequency of individual persistent clones at the post-RTX time point vs. the pre-rituximab time point **(D-F)**. Frequencies are computed as a fraction of total unique V(D)J sequences and visualized in terms of a histogram of the log2 changes in total frequency for these clones. Red dashed lines correspond to the median of each distribution for each patient.

Stathopoulos et al. 2017, BCR sequences from scPCR of circulating plasmablasts			
Patient	Clones	Traceable clones	Pre-RTX clones
1	4	3	1
2	0	0	0
3	39	19	5*
Takata et al. 2019, BCR sequences from scPCR of tetramer binding B cells			
Patient	Clones	Traceable clones	Pre-RTX clones
1	22	3	1
2	4	0	0
3	12	2	0

Table S3. Count of plasmablast derived or tetramer-binding V(D)J sequences clonally related to members of the pre-RTX or post-RTX bulk BCR repertoire (Traceable clones) or to members of the pre-RTX and post-RTX bulk BCR repertoire (Pre-RTX clones). *One clone was observed to also correspond to a clone previously published to have specificity for MuSK autoantigen. The strongest binding member of this clone was annotated as "3-29" in the previous publication.
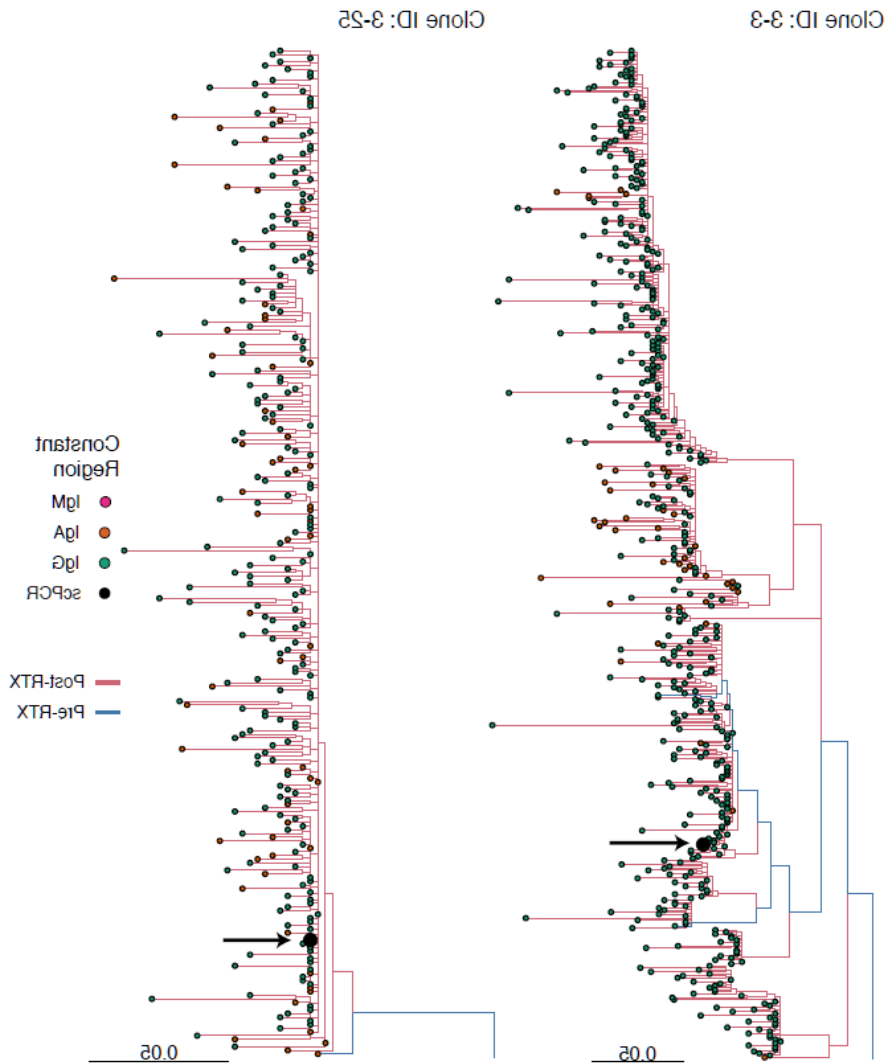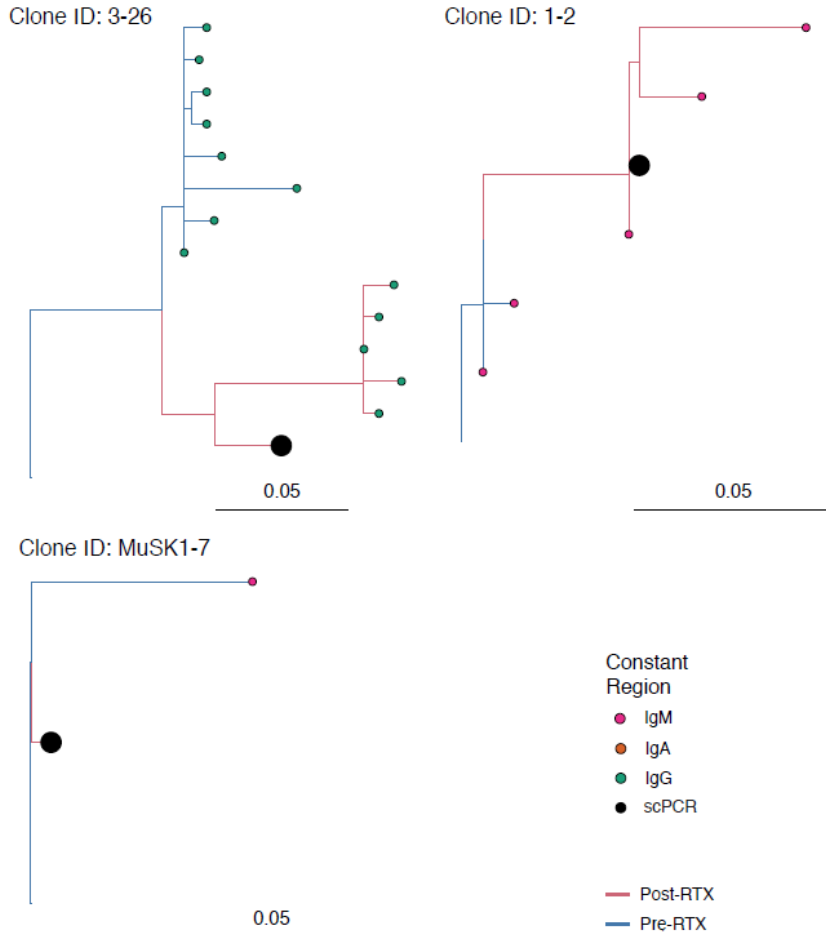
Figure S3. Clonal lineages containing scPCR-derived antibodies from Sanger sequencing identified in post-RTX repertoires. Maximum parsimony trees corresponding to clones that contain scPCR derived V(D)J sequences, and that have clonal variants present pre-RTX and post-RTX are presented. Sequences isolated using scPCR-based approaches from plasmablasts are denoted as "scPCR" using a large black dot and arrow along with the corresponding identity of the antibody from Stathopoulos et al. 2017 (ref. 15 in main manuscript). Edge lengths are quantified based on number of intervening somatic hypermutations per site between observed V(D)J sequences per the scale. Colors correspond to whether each V(D)J sequence was collected from a pre-RTX or post-RTX time point (or both) and also the associated constant region.

Clone ID: 3-31
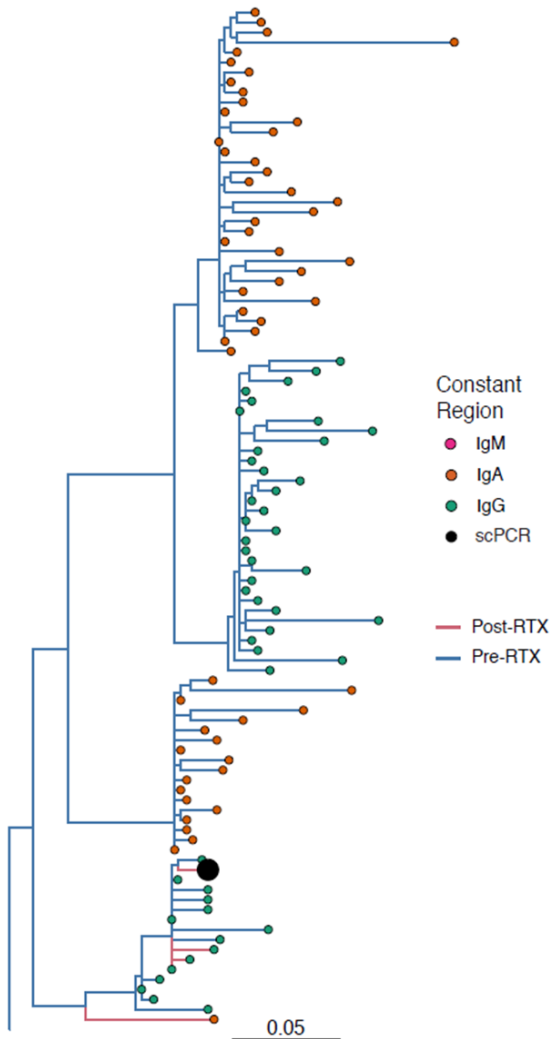
Figure S4. Clonal lineages containing scPCR-derived antibodies from Sanger sequencing identified in post-RTX repertoires. A maximum parsimony tree corresponding to a clone that contains scPCR derived V(D)J sequences, and that have clonal variants present pre-RTX and post-RTX is presented. Sequences isolated using scPCR-based approaches from plasmablasts are denoted as "scPCR" using a large black dot along with the corresponding identity of the antibody from Stathopoulos et al. 2017 (ref. 15 in main manuscript). Edge lengths are quantified based on number of intervening somatic hypermutations per site between observed V(D)J sequences per the scale. Colors correspond to whether each V(D)J sequence was collected from a pre-RTX or post-RTX time point (or both) and also the associated constant region.

Figure S5. Clonal lineages containing scPCR-derived antibodies from Sanger sequencing identified in post-RTX repertoires. Maximum parsimony trees corresponding to clones that contain scPCR derived V(D)J sequences, and that have clonal variants present pre-RTX and post-RTX are presented. Sequences isolated using scPCR-based approaches from plasmablasts are denoted as "scPCR" using a large black dot along with the corresponding identity of the antibody from Stathopoulos et al. 2017 (ref. 15 in main manuscript). Of note, the sequence associated with clone "MuSK1-7" was published in Takata et al. 2019 (ref. 16 in main manuscript) and was isolated using an antigen-specific tetramer. Edge lengths are quantified based on number of intervening somatic hypermutations per site between observed V(D)J sequences per the scale. Colors correspond to whether each V(D)J sequence was collected from a pre-RTX or post-RTX time point (or both) and also the associated constant region.

Patient	Collection	Status	Read Count	Cell Count	Mean Reads per Cell	Median Genes per Cell	VDJ Count
Control	A	AChR MG Asymptomatic	708747323	3580	197974	1499	3810
1	10	MuSK MG Post-RTX	303494244	3550	85491	1189	2859
2	9	MuSK MG Post-RTX	130365803	8502	15333	1130	6827
3	4	MuSK MG Post-RTX	112260566	2501	44886	1790	1175

Table S4. Quality control from paired single-cell transcriptome and repertoire sequencing.
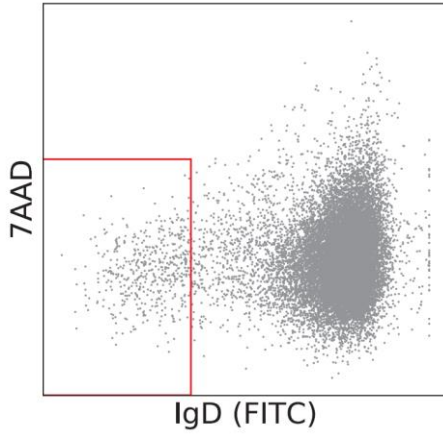
Figure S6. Example fluorescence activated cell sorting (FACS) gates for IgD^{low} B cells used as input for single-cell transcriptomics and BCR repertoire analysis. Example is shown for collection 10.

Cluster	Immunostates Assignment	Pearson Correlation	Final Assignment
0	naive_B_cell	0.234	Mature Naive
1	memory_B_cell	0.125	Memory
2	memory_B_cell	0.122	Memory
3	memory_B_cell	0.166	Memory
4	memory_B_cell	0.251	Memory
5	memory_B_cell	0.351	Memory
6	naive_B_cell	0.136	Transitional
7	not_assigned	-0.230	Not Assigned
8	plasma_cell	0.644	ASC
9	memory_B_cell	0.212	Memory
10	not_b_cell	0.063	Not B cell
11	not_assigned	-0.135	Not Assigned

Table S5. Table of cluster assignments using the immunoStates basis set. Clusters were assigned to the B cell immunostate with the maximum Pearson correlation coefficient when compared with the mean expression value of genes associated with each cluster. One naive B cell cluster was assigned to a transitional B cell subset based on marker expression (cluster 6) and another cluster (cluster 10) was excluded owing to elevated expression of mitochondrial genes.
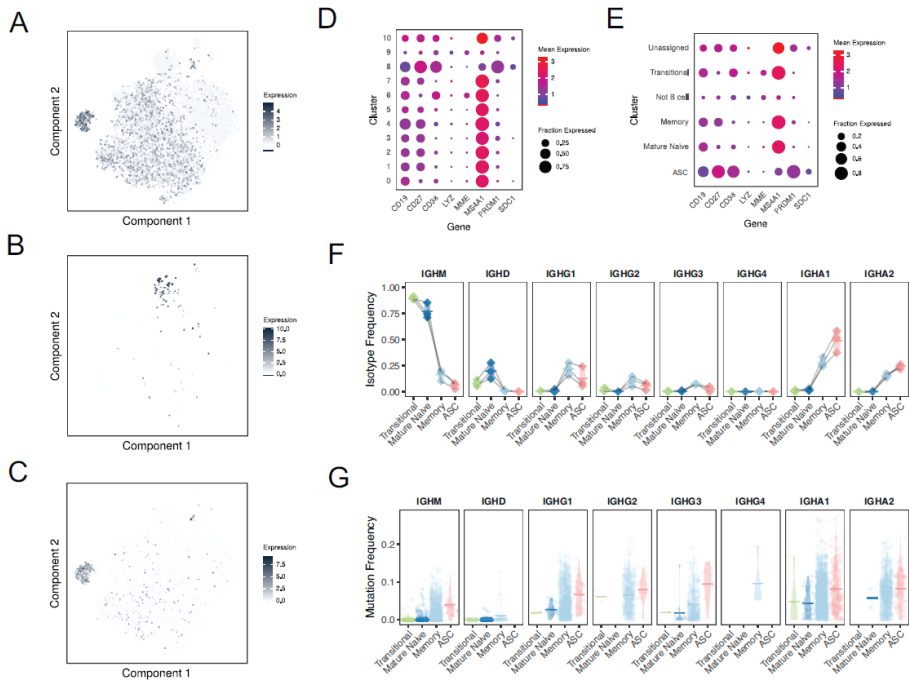
Figure S7. Assignment of B cell clusters based on single-cell transcriptome and repertoire according to known B cell subsets. Plotting of gene expression of key marker genes over t-SNE plot with intensity of shading correlated with amount of scaled log normalized expression for **(A)** CD27 **(B)** CD10 (MME) and **(C)** BLIMP1 (PRDM1). Dot plot of average log normalized expression (color) and fraction of cells expressing a set of marker genes (size) presented for B cell subsets derived from unbiased clustering **(D)** and when grouped into known B cell subset clusters **(E)**. **(F)** Overall usage of different constant regions by B cell subset as a fraction of all V(D)J sequences associated with each B cell subset cluster per sample. Horizontal bars show the average frequency of constant region usage across patients. Frequencies belonging to the same patient are paired with a gray line. **(G)** Distribution of somatic hypermutation frequencies among all V(D)J sequences assigned to each B cell subset cluster. Horizontal bars show the average somatic hypermutation frequency for a given B cell subset cluster.
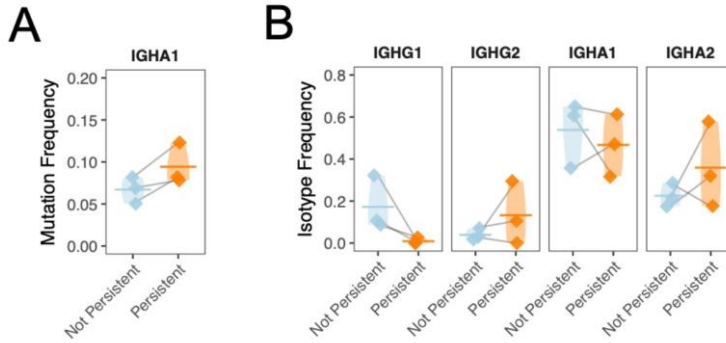
Figure S8. **Persistent and non-persistent ASCs are associated with similar V(D)J repertoire features.** Overall constant region usage frequencies are quantified for persistent compared to non-persistent cells for the **(A)** ASC cluster per patient. Horizontal bars show the average frequency of constant region usage across patients. Frequencies belonging to the same patient are paired with a gray line. Individual SHM frequencies for persistent compared to non-persistent cells are presented for ASC cluster members **(B)**. Only mean SHM frequencies are computed for isotypes with more than 3 V(D)J sequences. Horizontal bars show the average somatic hypermutation frequency for a given cluster. Frequencies belonging to the same patient are paired with a gray line. Statistical differences are shown only when significant (****P < 0.0001; ***P < 0.001; **P < 0.01; *P<0.05).
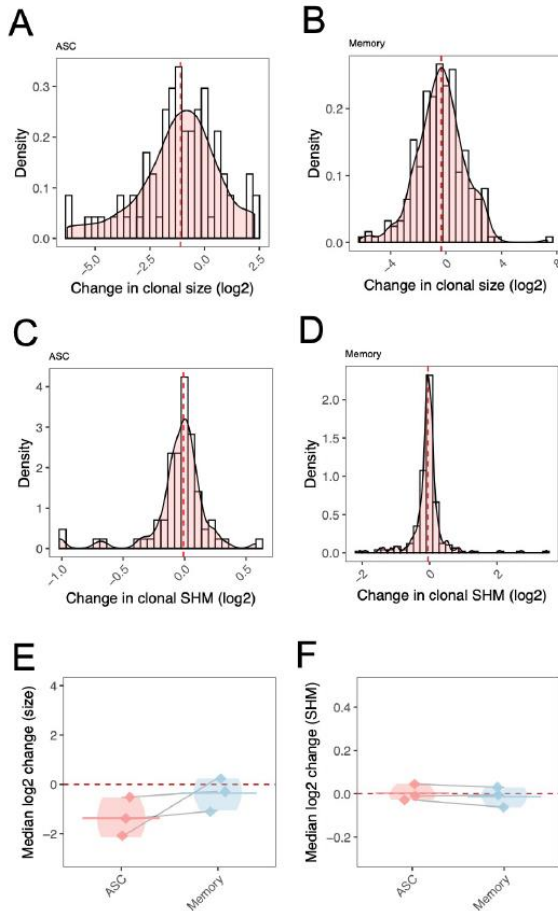
Figure S9. Persistent ASC and memory B cell clones do not show evidence of significant clonal expansion or accumulation of somatic hypermutations when comparing pre-RTX and post-RTX members. The presence of increases in overall SHM for individual clones is quantified by comparing the SHM frequencies averaged for each clone in the pre-RTX repertoire compared with post-RTX and visualized in terms of a histogram of the natural log change in somatic hypermutation frequency for each clone for each patient. Red dashed lines correspond to the median of each distribution for each patient. The set of clones examined is filtered for clones associated with ASCs **(A)** or memory B cells **(B)**. The presence of clonal expansions is evaluated by comparing the overall frequency of individual persistent clones at the post-RTX time point compared to the pre-RTX time point from bulk IGH repertoires as a fraction of total unique V(D)J sequences and visualized in terms of a histogram of the natural log change in total frequency for these clones. Red dashed lines correspond to the median of each distribution for each patient. The set of clones examined is filtered for clones associated with ASCs **(C)** or memory B cells **(D)**. The median of either the change **(E)** in clonal somatic hypermutation frequencies or clonal size distribution **(F)** associated with each patient is presented for each filtering strategy ("Total" for no filtering, "ASC" for filtering of ASC associated clones or "Memory" for filtering of Memory B cell associated clones. Horizontal bars show the median natural log change in clonal size or clonal somatic hypermutation frequency across patients. Values belonging to the same patient are paired with a gray line.
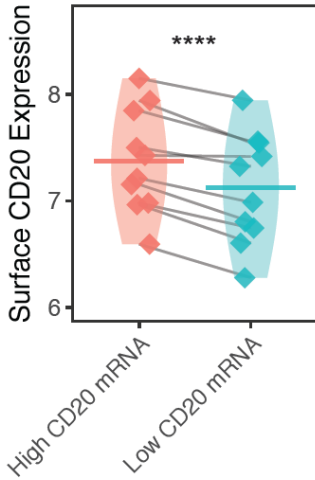
Figure S10. Elevated expression of surface CD20 for B cells with high CD20 mRNA expression. **Single** cells in the B cell cluster (excluding plasma cells) for each of six subjects in the dataset from Tsang et al. (ref. 30 in main manuscript) were split into high (top 50th percentile) and low (bottom 50th percentile) groups based on CD20 mRNA expression. The mean expression of surface CD20 is presented for each of these groups in each individual sample. Normalized gene expression values are computed from scaled log normalized counts of barcoded transcripts aligned to the CD20 gene. Horizontal bars show the average normalized gene expression across subjects. Expression values belonging to the same subject are paired with a gray line. Statistical differences are shown only when significant (****$P < 0.0001$; ***$P < 0.001$; **$P < 0.01$; *$P<0.05$).
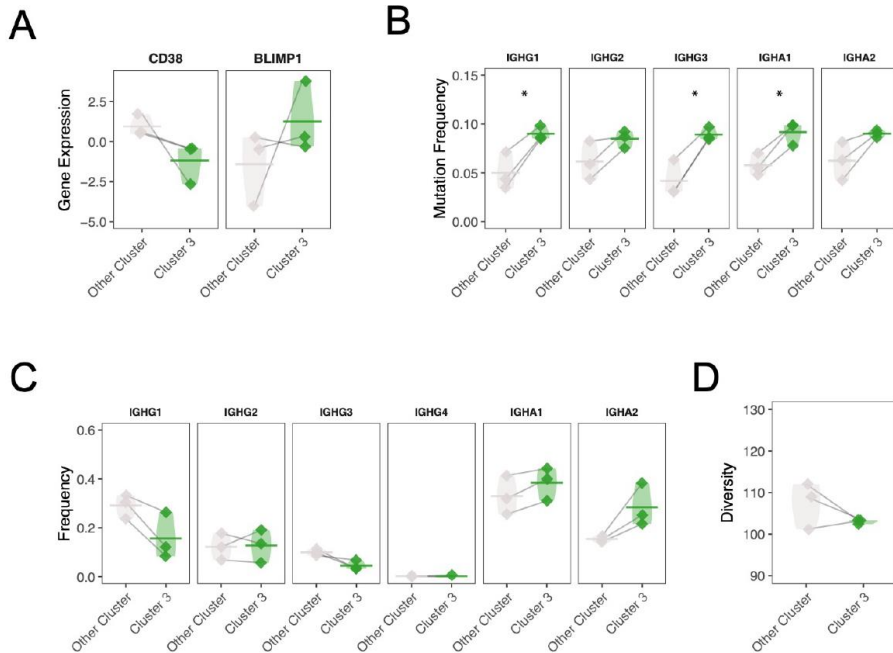
Figure S11. Cluster 3 has distinct transcriptional and V(D)J repertoire features. (A) The expression of plasma cell associated genes (CD38; BLIMP1 or PRDM1) is also presented for members of cluster 3 and members of other memory B cell clusters. Normalized gene expression values are computed from scaled log normalized counts of barcoded transcripts aligned to each gene. Horizontal bars show the average normalized gene expression across patients. Expression values belonging to the same patient are paired with a gray line. **(B)** Mean somatic hypermutation frequencies for cluster 3 compared to other memory B cells is quantified per patient. Horizontal bars show the average somatic hypermutation frequency for a given set of cells. Frequencies belonging to the same patient are paired with a gray line. **(C)** Overall constant region usage frequencies are quantified for cluster 3 compared to other memory B cells per patient. Horizontal bars show the average frequency of constant region usage across patients. Frequencies belonging to the same patient are paired with a gray line. **(D)** Simpson's diversity of cluster 3 members compared to other memory B cell cluster members. Statistical differences are shown only when significant (****$P < 0.0001$; ***$P < 0.001$; **$P < 0.01$; *$P<0.05$).

Data file S1. List of differentially expressed genes for cluster 3 compared to all other memory B cell clusters. Only differentially expressed genes with an adjusted p-value less than 0.05 with FDR correction by Storey's method are presented.
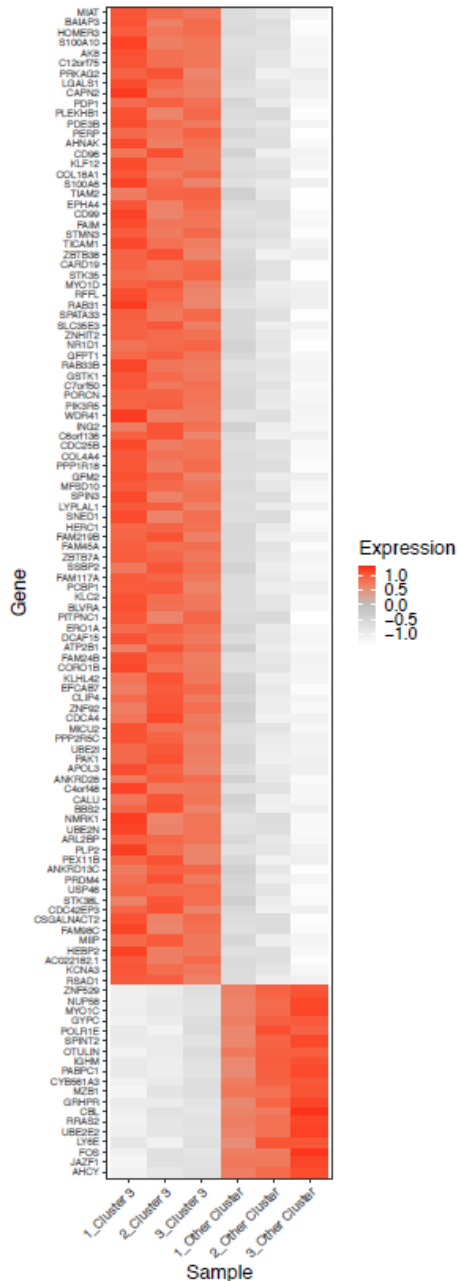
See attached cluster3.xlsx: https://insight.jci.org/articles/view/136471/sd/2

Figure S12. Cluster 3 memory B cells have a distinct gene signature. Heatmap of significantly differentially expressed genes for cluster 3 compared to other memory B cells, with a greater than >0.4 z-score difference between persistent and non-persistent labels.
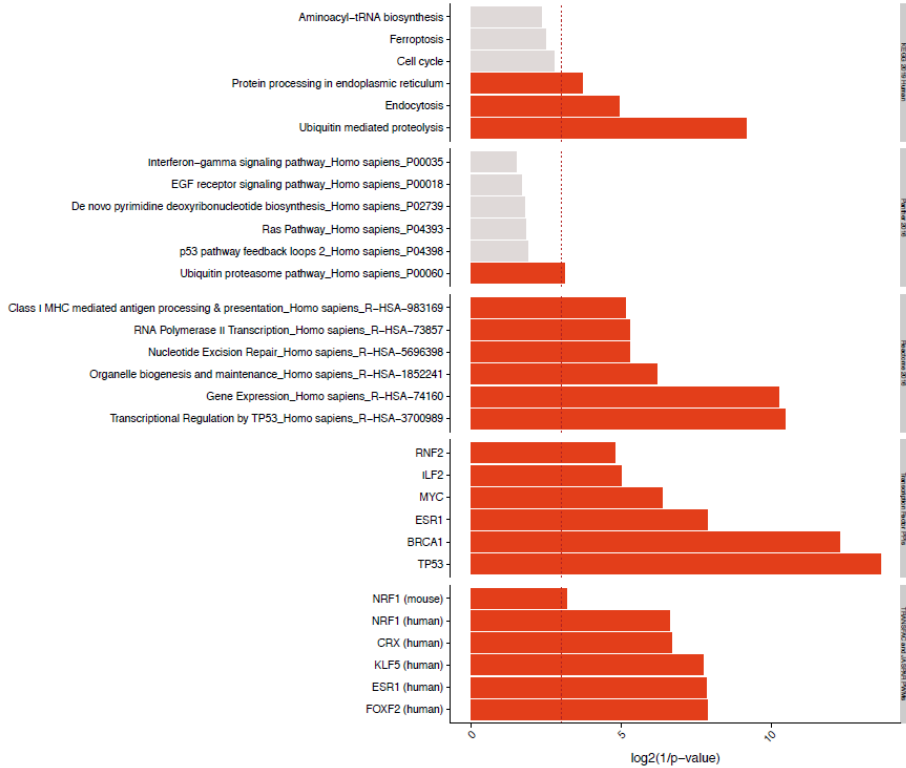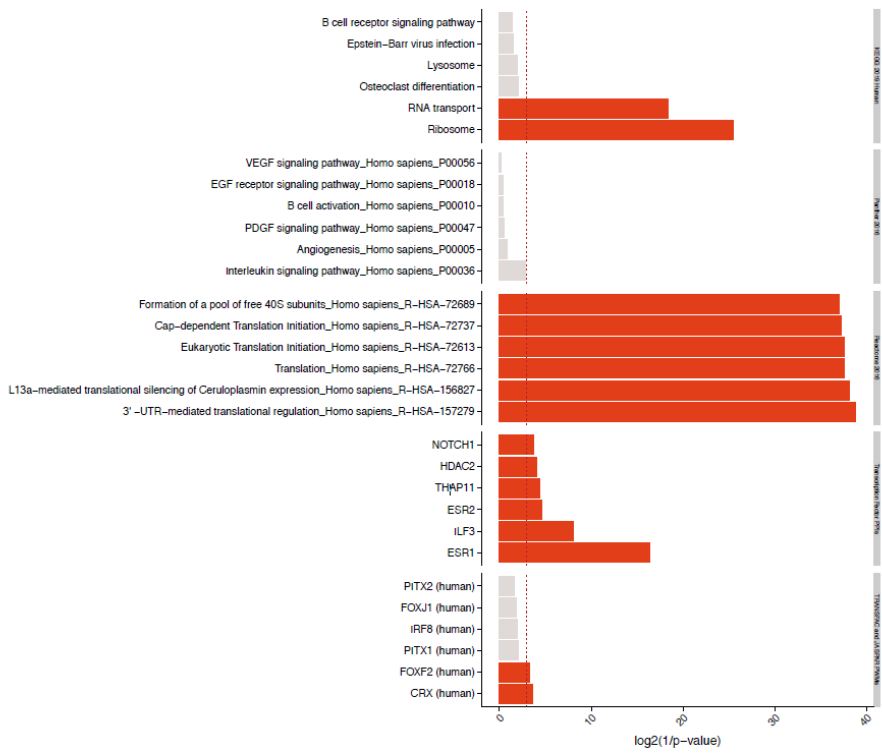
Figure S13. Cluster 3 memory B cells have a MYC and p53/BRCA1 signature. enrichR gene ontology analysis of either genes up-regulated among cluster 3 memory B cells compared to other memory B cells. Only differentially expressed genes with an adjusted p-value less than 0.05 with FDR correction by Storey's method were evaluated. Red bars correspond to significantly associated gene ontology assignments ($p < 0.05$ by wilcoxon signed rank test).

Figure S14. Cluster 3 memory B cells have a MYC and p53/BRCA1 signature. enrichR gene ontology analysis of either genes down-regulated among cluster 3 memory B cells compared to other memory B cells. Only differentially expressed genes with an adjusted p-value less than 0.05 with FDR correction by Storey's method were evaluated. Red bars correspond to significantly associated gene ontology assignments (p < 0.05 by wilcoxon signed rank test).
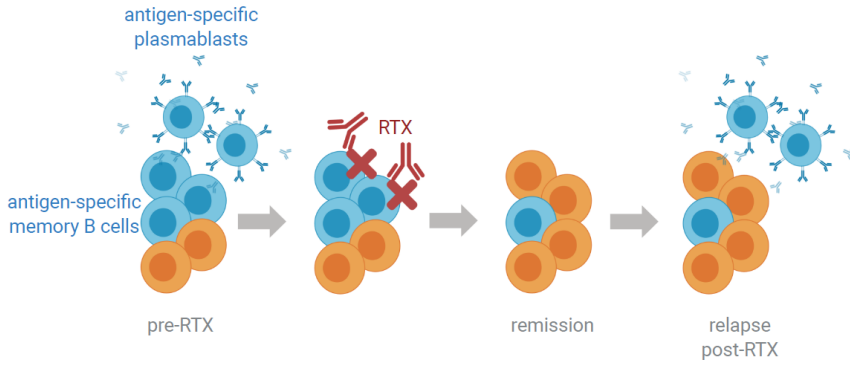
Figure S15. Visual model outlining the likely source of antigen-specific B cells during post-RTX relapse as shown in our study. Blue cells represent antigen-specific B cells whereas orange cells represent non-antigen specific B cells.

References

1. Gilhus NE, Skeie GO, Romi F, Lazaridis K, Zisimopoulou P, Tzartos S. Myasthenia gravis - autoantibody characteristics and their implications for therapy. Nat Rev Neurol. 2016;12(5):259–268.

2. McConville J, et al. Detection and characterization of MuSK antibodies in seronegative myasthenia gravis. Ann Neurol. 2004;55(4):580–584.

3. Hoch W, McConville J, Helms S, Newsom-Davis J, Melms A, Vincent A. Autoantibodies to the receptor tyrosine kinase MuSK in patients with myasthenia gravis without acetylcholine receptor antibodies. Nat Med. 2001;7(3):365–368.

4. DeChiara TM, et al. The receptor tyrosine kinase MuSK is required for neuromuscular junction formation in vivo. Cell. 1996;85(4):501–512.

5. Koneczny I, Cossins J, Waters P, Beeson D, Vincent A. MuSK myasthenia gravis IgG4 disrupts the interaction of LRP4 with MuSK but both IgG4 and IgG1-3 can disperse preformed agrin-independent AChR clusters. PLoS One. 2013;8(11):e80695.

6. Emery P, et al. The efficacy and safety of rituximab in patients with active rheumatoid arthritis despite methotrexate treatment: results of a phase IIB randomized, double-blind, placebo-controlled, dose-ranging trial. Arthritis Rheum. 2006;54(5):1390–1400.

7. Hauser SL, et al. B-cell depletion with rituximab in relapsing-remitting multiple sclerosis. N Engl J Med. 2008;358(7):676–688.

8. Jones RB, et al. Rituximab versus cyclophosphamide in ANCA-associated renal vasculitis. N Engl J Med. 2010;363(3):211–220.

9. Nowak RJ, Dicapua DB, Zebardast N, Goldstein JM. Response of patients with refractory myasthenia gravis to rituximab: a retrospective study. Ther Adv Neurol Disord. 2011;4(5):259–266.

10. Illa I, et al. Sustained response to Rituximab in anti-AChR and anti-MuSK positive Myasthenia Gravis patients. J Neuroimmunol. 2008;201-202:90–94.

11. Keung B, et al. Long-term benefit of rituximab in MuSK autoantibody myasthenia gravis patients. J Neurol Neurosurg Psychiatry. 2013;84(12):1407–1409.

12. Robeson KR, et al. Durability of the rituximab response in acetylcholine receptor autoantibody-positive myasthenia gravis. JAMA Neurol. 2017;74(1):60–66.

13. Blum S, et al. Use and monitoring of low dose rituximab in myasthenia gravis. J Neurol Neurosurg Psychiatry. 2011;82(6):659–663.

14. Guptill JT, Sanders DB, Evoli A. Anti-MuSK antibody myasthenia gravis: clinical findings and response to treatment in two large cohorts. Muscle Nerve. 2011;44(1):36–40.

15. Stathopoulos P, Kumar A, Nowak RJ, O'Connor KC. Autoantibody-producing plasmablasts after B cell depletion identified in muscle-specific kinase myasthenia gravis. JCI Insight. 2017;2(17):94263.

16. Takata K, et al. Characterization of pathogenic monoclonal autoantibodies derived from muscle-specific kinase myasthenia gravis patients. JCI Insight. 2019;4(12):127167.

17. Huang H, Benoist C, Mathis D. Rituximab specifically depletes short-lived autoreactive plasma cells in a mouse model of inflammatory arthritis. Proc Natl Acad Sci U S A. 2010;107(10):4658–4663.

18. Cho A, et al. Robust memory responses against influenza vaccination in pemphigus patients previously treated with rituximab. JCI Insight. 2017;2(12):93222.

19. Medina F, Segundo C, Campos-Caro A, González-García I, Brieva JA. The heterogeneity shown by human plasma cells from tonsil, blood, and bone marrow reveals graded stages of increasing maturity, but local profiles of adhesion molecule expression. Blood. 2002;99(6):2154–2161.

20. Withers DR, Fiorini C, Fischer RT, Ettinger R, Lipsky PE, Grammer AC. T cell-dependent survival of CD20+ and CD20- plasma cells in human secondary lymphoid tissue. Blood. 2007;109(11):4856–4864.

21. Anolik JH, et al. Delayed memory B cell recovery in peripheral blood and lymphoid tissue in systemic lupus erythematosus after B cell depletion therapy. Arthritis Rheum. 2007;56(9):3044–3056.

22. Adlowitz DG, et al. Expansion of activated peripheral blood memory B cells in rheumatoid arthritis, impact of B cell depletion therapy, and biomarkers of response. PLoS One. 2015;10(6):e0128269.

23. Gupta NT, Adams KD, Briggs AW, Timberlake SC, Vigneault F, Kleinstein SH. Hierarchical clustering can identify B cell clones with high confidence in Ig repertoire sequencing data. J Immunol. 2017;198(6):2489–2499.

24. Nardelli B, et al. Synthesis and release of B-lymphocyte stimulator from myeloid cells. Blood. 2001;97(1):198–204.

25. Schneider P, et al. BAFF, a novel ligand of the tumor necrosis factor family, stimulates B cell growth. J Exp Med. 1999;189(11):1747–1756.

26.   Pers JO, et al. BAFF-modulated repopulation of B lymphocytes in the blood and salivary glands of rituximab-treated patients with Sjögren's syndrome. Arthritis Rheum. 2007;56(5):1464–1477.

27.   Sarantopoulos S, et al. Recovery of B-cell homeostasis after rituximab in chronic graft-versus-host disease. Blood. 2011;117(7):2275–2283.

28.   Becerra E, De La Torre I, Leandro MJ, Cambridge G. B cell phenotypes in patients with rheumatoid arthritis relapsing after rituximab: expression of B cell-activating factor-binding receptors on B cell subsets. Clin Exp Immunol. 2017;190(3):372–383.

29.   Tsang JS, et al. Global analyses of human immune variation reveal baseline predictors of postvaccination responses. Cell. 2014;157(2):499–513.

30.   Kotliarov Y, et al. Broad immune activation underlies shared set point signatures for vaccine responsiveness in healthy individuals and disease activity in patients with lupus. Nat Med. 2020;26(4):618–629.

31.   Vaux DL, Cory S, Adams JM. Bcl-2 gene promotes haemopoietic cell survival and cooperates with c-myc to immortalize pre-B cells. Nature. 1988;335(6189):440–442.

32.   Serrano M, Lin AW, McCurrach ME, Beach D, Lowe SW. Oncogenic ras provokes premature cell senescence associated with accumulation of p53 and p16INK4a. Cell. 1997;88(5):593–602.

33.   Deng CX. BRCA1: cell cycle checkpoint, genetic instability, DNA damage response and cancer evolution. Nucleic Acids Res. 2006;34(5):1416–1426.

34.   Tintore M, Vidal-Jordana A, Sastre-Garriga J. Treatment of multiple sclerosis - success from bench to bedside. Nat Rev Neurol. 2019;15(1):53–58.

35.   Stathopoulos P, Kumar A, Heiden JAV, Pascual-Goñi E, Nowak RJ, O'Connor KC. Mechanisms underlying B cell immune dysregulation and autoantibody production in MuSK myasthenia gravis. Ann N Y Acad Sci. 2018;1412(1):154–165.

36.   Díaz-Manera J, et al. Long-lasting treatment effect of rituximab in MuSK myasthenia. Neurology. 2012;78(3):189–193.

37.   Hershberg U, et al. Persistence and selection of an expanded B-cell clone in the setting of rituximab therapy for Sjögren's syndrome. Arthritis Res Ther. 2014;16(1):R51.

38.   Bashford-Rogers RJM, et al. Analysis of the B cell receptor repertoire in six immune-mediated diseases. Nature. 2019;574(7776):122–126.

39. de Bourcy CFA, Dekker CL, Davis MM, Nicolls MR, Quake SR. Dynamics of the human antibody repertoire after B cell depletion in systemic sclerosis. Sci Immunol. 2017;2(15):eaan8289.

40. Hammarlund E, et al. Plasma cell survival in the absence of B cell memory. Nat Commun. 2017;8(1):1781.

41. Md Yusof MY, et al. Predicting and managing primary and secondary non-response to rituximab using B-cell biomarkers in systemic lupus erythematosus. Ann Rheum Dis. 2017;76(11):1829–1836.

42. Stradner MH, Dejaco C, Brickmann K, Graninger WB, Brezinschek HP. A combination of cellular biomarkers predicts failure to respond to rituximab in rheumatoid arthritis: a 24-week observational study. Arthritis Res Ther. 2016;18:190.

43. Thurlings RM, Vos K, Wijbrandts CA, Zwinderman AH, Gerlag DM, Tak PP. Synovial tissue response to rituximab: mechanism of action and identification of biomarkers of response. Ann Rheum Dis. 2008;67(7):917–925.

44. Vital EM, et al. B cell biomarkers of rituximab responses in systemic lupus erythematosus. Arthritis Rheum. 2011;63(10):3038–3047.

45. Nakou M, et al. Rituximab therapy reduces activated B cells in both the peripheral blood and bone marrow of patients with rheumatoid arthritis: depletion of memory B cells correlates with clinical response. Arthritis Res Ther. 2009;11(4):R131.

46. Colliou N, et al. Long-term remissions of severe pemphigus after rituximab therapy are associated with prolonged failure of desmoglein B cell response. Sci Transl Med. 2013;5(175):175ra30.

47. Maurer MA, et al. Rituximab induces clonal expansion of IgG memory B-cells in patients with inflammatory central nervous system demyelination. J Neuroimmunol. 2016;290:49–53.

48. Sellam J, et al. Decreased B cell activating factor receptor expression on peripheral lymphocytes associated with increased disease activity in primary Sjögren's syndrome and systemic lupus erythematosus. Ann Rheum Dis. 2007;66(6):790–797.

49. Pontarini E, et al. Treatment with belimumab restores B cell subsets and their expression of B cell activating factor receptor in patients with primary Sjogren's syndrome. Rheumatology (Oxford). 2015;54(8):1429–1434.

50. Litinskiy MB, et al. DCs induce CD40-independent immunoglobulin class switching through BLyS and APRIL. Nat Immunol. 2002;3(9):822–829.

51. Xu W, et al. Epithelial cells trigger frontline immunoglobulin class switching through a pathway regulated by the inhibitor SLPI. Nat Immunol. 2007;8(3):294–303.

52. Castigli E, et al. TACI and BAFF-R mediate isotype switching in B cells. J Exp Med. 2005;201(1):35–39.

53. Rojas OL, et al. Recirculating intestinal IgA-producing cells regulate neuroinflammation via IL-10. Cell. 2019;176(3):610–624.e18.

54. Suárez-Calvet X, et al. Altered RIG-I/DDX58-mediated innate immunity in dermatomyositis. J Pathol. 2014;233(3):258–268.

55. Teng YKO, et al. Phase III, multicentre, randomised, double-blind, placebo-controlled, 104-week study of subcutaneous belimumab administered in combination with rituximab in adults with systemic lupus erythematosus (SLE): BLISS-BELIEVE study protocol. BMJ Open. 2019;9(3):e025687.

56. Kraaij T, et al. The NET-effect of combining rituximab with belimumab in severe systemic lupus erythematosus. J Autoimmun. 2018;91:45–54.

57. De Vita S, et al. Sequential therapy with belimumab followed by rituximab in Sjögren's syndrome associated with B-cell lymphoproliferation and overexpression of BAFF: evidence for long-term efficacy. Clin Exp Rheumatol. 2014;32(4):490–494.

58. Bordron A, et al. Resistance to complement activation, cell membrane hypersialylation and relapses in chronic lymphocytic leukemia patients treated with rituximab and chemotherapy. Oncotarget. 2018;9(60):31590–31605.

59. Winiarska M, et al. Statins impair antitumor effects of rituximab by inducing conformational changes of CD20. PLoS Med. 2008;5(3):e64.

60. Lehane PB, Lacey S, Hessey EW, Jahreis A. Effect of concomitant statins on rituximab efficacy in patients with rheumatoid arthritis. Ann Rheum Dis. 2014;73(10):1906–1908.

61. Ramwadhdoebe TH, et al. Effect of rituximab treatment on T and B cell subsets in lymph node biopsies of patients with rheumatoid arthritis. Rheumatology (Oxford). 2019;58(6):1075–1085.

62. Leandro MJ, Cambridge G, Ehrenstein MR, Edwards JC. Reconstitution of peripheral blood B cells after depletion with rituximab in patients with rheumatoid arthritis. Arthritis Rheum. 2006;54(2):613–620.

63. Mamani-Matsuda M, et al. The human spleen is a major reservoir for long-lived vaccinia virus-specific memory B cells. Blood. 2008;111(9):4653–4659.

64. Ellebrecht CT, et al. Reengineering chimeric antigen receptor T cells for targeted therapy of autoimmune disease. Science. 2016;353(6295):179–184.

65. Kansal R, et al. Sustained B cell depletion by CD19-targeted CAR T cells is a highly effective treatment for murine lupus. Sci Transl Med. 2019;11(482):eaav1648.

66. Boyd SD, et al. Measurement and clinical monitoring of human lymphocyte clonality by massively parallel VDJ pyrosequencing. Sci Transl Med. 2009;1(12):12ra23.

67. Laserson U, et al. High-resolution antibody dynamics of vaccine-induced immune responses. Proc Natl Acad Sci U S A. 2014;111(13):4928–4933.

68. Hershberg U, Luning Prak ET. The analysis of clonal expansions in normal and autoimmune B cell repertoires. Philos Trans R Soc Lond, B, Biol Sci. 2015;370(1676):20140239.

69. DeKosky BJ, et al. Large-scale sequence and structural comparisons of human naive and antigen-experienced antibody repertoires. Proc Natl Acad Sci U S A. 2016;113(19):E2636–E2645.

70. Singh M, et al. High-throughput targeted long-read single cell sequencing reveals the clonal and transcriptional landscape of lymphocytes. Nat Commun. 2019;10(1):3120.

71. Dulken BW, et al. Single-cell analysis reveals T cell infiltration in old neurogenic niches. Nature. 2019;571(7764):205–210.

72. Oh JE, et al. Migrant memory B cells secrete luminal antibody in the vagina. Nature. 2019;571(7763):122–126.

73. Wu D, et al. Detection of minimal residual disease in B lymphoblastic leukemia by high-throughput sequencing of IGH. Clin Cancer Res. 2014;20(17):4540–4548.

74. Greenfield AL, et al. Longitudinally persistent cerebrospinal fluid B cells can resist treatment in multiple sclerosis. JCI Insight. 2019;4(6):126599.

75. Nouri N, Kleinstein SH. A spectral clustering-based method for identifying clones from high-throughput B cell repertoire sequencing data. Bioinformatics. 2018;34(13):i341–i349.

76. Zhou JQ, Kleinstein SH. Cutting edge: Ig H chains are sufficient to determine most B cell clonal relationships. J Immunol. 2019;203(7):1687–1692.

77. Cree BAC, et al. Inebilizumab for the treatment of neuromyelitis optica spectrum disorder (N-MOmentum): a double-blind, randomised placebo-controlled phase 2/3 trial. Lancet. 2019;394(10206):1352–1363.

78. Vander Heiden JA, et al. Dysregulation of B cell repertoire formation in myasthenia gravis patients revealed through deep sequencing. J Immunol. 2017;198(4):1460–1473.

79. Vander Heiden JA, et al. pRESTO: a toolkit for processing high-throughput sequencing raw reads of lymphocyte receptor repertoires. Bioinformatics. 2014;30(13):1930–1932.

80. Butler A, Hoffman P, Smibert P, Papalexi E, Satija R. Integrating single-cell transcriptomic data across different conditions, technologies, and species. Nat Biotechnol. 2018;36(5):411–420.

81. Vallania F, et al. Leveraging heterogeneity across multiple datasets increases cell-mixture deconvolution accuracy and reduces biological and technical biases. Nat Commun. 2018;9(1):4735.

82. Ye J, Ma N, Madden TL, Ostell JM. IgBLAST: an immunoglobulin variable domain sequence analysis tool. Nucleic Acids Res. 2013;41(Web Server issue):W34–W40.

83. Linderman GC, Zhao J, Kluger Y. Zero-preserving imputation of scRNA-seq data using low-rank approximation. bioRxiv. https://doi.org/10.1101/397588. Published August 22, 2018. Accessed June 18, 2020.

84. Storey JD, Tibshirani R. Statistical significance for genomewide studies. Proc Natl Acad Sci U S A. 2003;100(16):9440–9445.

85. Kuleshov MV, et al. Enrichr: a comprehensive gene set enrichment analysis web server 2016 update. Nucleic Acids Res. 2016;44(W1):W90–W97.

86. R Core Team. R: a language and environment for statistical computing. R Foundation for Statistical Computing, Vienna, Austria. http://www.R-project.org/. Accessed June 18, 2020.

87. Hill MO. Diversity and evenness: a unifying notation and its consequences. Ecology. 1973;54(2):427–432.

88. Virtanen P, et al. SciPy 1.0--fundamental algorithms for scientific computing in Python. Nat Med. 2020;17:261–272.

89. Felsenstein JP. PHYLIP - Phylogeny Inference Package (Version 3.2). Cladistics. 2004; 5:164–166.

90.   Sankoff D. Minimal mutation trees of sequences. SIAM J Appl Math. 1975;28(1):35–42.

91.   Hoehn KB, Vander Heiden JA, Zhou JQ, Lunter G, Pybus OG, Kleinstein SH. Repertoire-wide phylogenetic models of B cell molecular evolution reveal evolutionary signatures of aging and vaccination. Proc Natl Acad Sci U S A. 2019;116(45):22664–22672.

92.   Paradis E, Schliep K. ape 5.0: an environment for modern phylogenetics and evolutionary analyses in R. Bioinformatics. 2019;35(3):526–528.

93.   Yu G, Smith DK, Zhu H, Guan Y, Lam TTY. ggtree: an R package for visualization and annotation of phylogenetic trees with their covariates and other associated data. Methods Ecol Evol. 2017;8(1):28–36.

3.3. PUBLICATION III: REEMERGENCE OF PATHOGENIC, AUTOANTIBODY-PRODUCING B CELL CLONES IN MYASTHENIA GRAVIS FOLLOWING B CELL DEPLETION THERAPY

Acta Neuropathologica Communications

Reemergence of pathogenic, autoantibody-producing B cell clones in myasthenia gravis following B cell depletion therapy

Miriam L. Fichtner[1, 2], Kenneth B. Hoehn[3], Easton E. Ford[5], Marina Mane-Damas[6], Sangwook Oh[7], Patrick Waters[9], Aimee S. Payne[7], Melissa L. Smith[5,8], Corey T. Watson[5, 8], Mario Losen[6], Pilar Martinez-Martinez[6], Richard J. Nowak[1], Steven H. Kleinstein[2, 3, 4] and Kevin C. O'Connor[1, 2].

[1]Department of Neurology, Yale University School of Medicine, New Haven, CT 06511, USA; [2]Department of Immunobiology, Yale University School of Medicine, New Haven, CT 06511, USA; [3]Department of Pathology, Yale School of Medicine, New Haven, Connecticut, USA; [4]Program in Computational Biology & Bioinformatics, Yale University, New Haven, Connecticut, USA; [5]Department of Microbiology and Immunology, University of Louisville School of Medicine, Louisville, KY, USA; [6]Department of Psychiatry and Neuropsychology, School for Mental Health and Neuroscience, Maastricht University, Maastricht, The Netherlands; [7]Department of Dermatology, Perelman School of Medicine, University of Pennsylvania, Philadelphia, PA, USA; [8]Department of Biochemistry and Molecular Genetics, University of Louisville School of Medicine, Louisville, KY, USA; [9]Oxford Autoimmune Neurology Group, Nuffield Department of Clinical Neurosciences, University of Oxford, Oxford, UK.

Correspondence: kevin.oconnor@yale.edu

Abstract

Myasthenia gravis (MG) is an autoantibody-mediated autoimmune disorder of the neuromuscular junction. A small subset of patients (<10%) with MG, have autoantibodies targeting muscle-specific tyrosine kinase (MuSK). MuSK MG patients respond well to CD20-mediated B cell depletion therapy (BCDT); most achieve complete stable remission. However, relapse often occurs. To further understand the immunomechanisms underlying relapse, we studied autoantibody-producing B cells over the course of BCDT. We developed a fluorescently labeled antigen to enrich for MuSK-specific B cells, which was validated with a novel Nalm6 cell line engineered to express a human MuSK-specific B cell receptor. B cells ($\cong$ 2.6 million) from 12 different samples collected from nine MuSK MG patients were screened for MuSK specificity. We successfully isolated two MuSK-specific IgG4 subclass-expressing plasmablasts from two of these patients, who were experiencing a relapse after a BCDT-induced remission. Human recombinant MuSK mAbs were then generated to validate binding specificity and characterize their molecular properties. Both mAbs were strong MuSK binders, they recognized the Ig1-like domain of MuSK, and showed pathogenic capacity when tested in an acetylcholine receptor (AChR) clustering assay. The presence of persistent clonal relatives of these MuSK-specific B cell clones was investigated through B cell receptor repertoire tracing of 63,977 unique clones derived from longitudinal samples collected from these two patients. Clonal variants were detected at multiple timepoints spanning more than five years and reemerged after BCDT-mediated remission, predating disease relapse by several months. These findings

demonstrate that a reservoir of rare pathogenic MuSK autoantibody-expressing B cell clones survive BCDT and reemerge into circulation prior to manifestation of clinical relapse. Overall, this study provides both a mechanistic understanding of MuSK MG relapse and a valuable candidate biomarker for relapse prediction.

Introduction

Autoimmune myasthenia gravis (MG) is a prototypical autoantibody-mediated disease. Pathogenic autoantibodies in MG target proteins within the neuromuscular junction (NMJ), which interrupts neuromuscular transmission [16, 74]. The largest subset (≈ 85%) of MG patients have autoantibodies that target the acetylcholine receptor (AChR), but a small subset of patients, who are negative for AChR autoantibodies, harbor autoantibodies that bind to muscle-specific tyrosine kinase (MuSK) [26], low-density lipoprotein receptor-related protein 4 (LRP4) [25, 50, 83] or agrin [83].

The MG subtypes that are defined by the autoantibody specificity appear clinically similar, but the underlying immunopathology is remarkably distinct [13]. This is well highlighted by comparing the AChR and MuSK subtypes. While AChR MG is driven by the IgG1 and IgG3 subclass [56], MuSK MG is largely governed by the IgG4 subclass that mediates pathology by inhibiting the interaction between MuSK and LRP4 [30], which is essential for MuSK phosphorylation and subsequent effective AChR clustering and signaling. The phenotype of the B cells that produce pathogenic autoantibodies in AChR and MuSK MG also appear divergent. It is currently thought that short-lived plasmablasts are key autoantibody producers in MuSK MG [63, 64], while plasma cells mostly account for the production of AChR

autoantibodies [59, 77, 81]. These differences are highlighted by the outcomes reached through the use of biological therapeutics in clinical trials. Specifically, this is evident by the poor response to CD20-mediated (rituximab) B cell depletion therapy (BCDT) in AChR MG [47], in contrast to the significant response in MuSK MG [10, 33]. In clinical practice, most MuSK MG patients achieve complete stable remission following BCDT [10, 44, 48], which often includes reduction of autoantibody titer to undetectable levels. This fits well with an emerging pattern of BCDT efficacy in patients with other diseases mediated by pathogenic IgG4 autoantibodies, such as pemphigus with autoantibodies directed against the desmoglein adhesion molecules [32] and chronic inflammatory demyelinating polyneuropathy with paranodal protein-specific autoantibodies [52]. The clinically proven efficacy of BCDT notwithstanding, after an initial remission some MuSK MG patients experience relapse [4, 22, 48, 55], which can associate with an increased frequency of plasmablasts and memory B cells, including populations that express MuSK-specific autoantibodies [64, 67]. Not all of these B cells develop de novo after BCDT, as a proportion of B cell clones persist through treatment [31]. However, it is not clear how pathogenic MuSK autoantibody-expressing B cell clones behave during a given clinical course, as it includes phases of relapse and periods of remission induced by repeated BCDT treatment cycles.

To that end, we sought to isolate MuSK-specific autoantibody-producing B cells, validate their specificity, and determine whether these B cells are present in BCDT-treated patients over a period of time. We developed a monomeric fluorescently labeled MuSK antigen to enrich for MuSK-specific B cells and authenticated this

antigen bait using a novel B cell line (Nalm6 cells) that expressed a human MuSK-specific B cell receptor (BCR). We found that MuSK-specific B cells are exceptionally rare in the circulation, yet we were able to isolate two distinct clones from two different patients, the specificity of which was validated through testing of human recombinant monoclonal autoantibodies (mAbs). We collected upwards of 149,000 B cell receptor sequences from serial samples of these two patients to search for clonal variants. We found that MuSK-specific B cell clones persisted through repeated rounds of BCDT and reemerged prior to clinical relapse in association with increased autoantibody titers.

Material and methods

Human specimens

This study was approved by the Human Investigation Committee at the Yale School of Medicine (clinicaltrials.gov || NCT03792659). Informed written consent was obtained from all patients. All MuSK MG patients met definitive diagnostic criteria for MG, including positive serology for MuSK autoantibodies.

Fluorescently labeled MuSK, Nalm6 cells, and cell sorting

Recombinant human MuSK and the negative control protein recombinant human growth hormone (hGH) (BioLegend; 778006) were fluorescently labeled using the Alexa Fluor™ 647 Microscale Protein Labeling Kit (Invitrogen; A30009). Nalm6 cells (CRL-3273™) and Nalm6 cells containing the MuSK-specific MuSK3-28 B cell receptor (Nalm6_3-28) were cultured in RPMI 1640 media containing 10% FBS, 1% P/S and 1% HEPES. On the day of the CBA for the validation of the MuSK

reagent, the fluorescently labeled MuSK was added at a final concentration of 10, 1, 0.1 or 0.01 µg/ml. For sorting MuSK-reactive B cells, B cells were enriched from cryopreserved PBMCs using negative selection beads (Stemcell Technologies; 19554). They were incubated with live/dead stain, then stained for 30 minutes on ice with 1 µg/ml of fluorescently labeled MuSK antigen together with fluorescently labeled antibodies against CD3 (BD Biosciences, V500; UCTH1), CD14 (Invitrogen, Pacific orange; TUK4), CD19 (BioLegend, PE Cy7; SJ25C1), CD27 (BD Biosciences, PE; M-T271), IgD (BD Biosciences, FITC; IA6-2), IgM (BioLegend, PerCP/Cyanine5.5; MHM-88) and CD38 (BioLegend, BV421; HB-7) using manufacturer's recommended dilutions. The cells were sorted on an FACSAria (BD Biosciences) instrument. For general B cell immunophenotyping, B cells were defined as live CD3⁻CD14⁻CD19⁺ cells, memory B cells as live CD3⁻CD14⁻CD19⁺CD27⁺CD38⁻ cells, and antibody-secreting cells (plasmablast phenotype) as CD3⁻CD14⁻CD19⁺CD27⁺CD38hi. We sorted for CD3⁻CD14⁻CD19⁺IgD⁻CD27⁺IgM⁻MuSK⁺ cells for the single cell B cell culture experiments.

B cell culture, molecular cloning, and IgG subclass determination

MS40L^lo cells (kindly provided by Drs. Garnett Kelsoe and Dongmei Liao of Duke University; [40]) were maintained in IMDM media (Invitrogen, 12440-053) supplemented with 10% FCS (Thermo Scientific, SH30070.03), 1% Pen/Strep (Invitrogen, 15140-122) and 55 µM 2-ME (Invitrogen, 21985). For B cell culture the cells were suspended in B cell media (RPMI, 10% FBS, 1% Pen/Strep, 1% HEPES, 1% Sodium pyruvate, 1% MEM NEAA and 55 µM of 2-ME) and plated at a concentration of 3 x 103 cells per well into 96 well plates. The B cell media was

changed the following day to contain additionally 50 ng/ml IL-2 (Peprotech 100-02), 10 ng/ml IL-4 (Peprotech 200-04), 10 ng/ml IL-21 (Peprotech 200-21) and 10 ng/ml BAFF (Peprotech 310-13) and single B cells were sorted into each well. The culture was maintained for 20-30 days, then the supernatant was harvested and screened for MuSK-reactivity using a MuSK-specific cell-based assay (CBA). The RNA of cells in MuSK antibody positive wells was purified using the RNeasy Plus Mini Kit (Qiagen), followed by cDNA synthesis, single-cell PCR, IgG subclass determination and molecular cloning into the corresponding heavy, kappa or lambda vectors as previously described [67, 75]}.

Recombinant expression of MuSK and human mAbs and Fabs

The extracellular domain of MuSK (AA 22-452) was produced in stably transfected Drosophila S2 cells kindly provided by Dr. Patrick Waters (University of Oxford) as previously described [67]. The 2E6 and 6C6 mAbs and were expressed as IgG1 subclass whole antibodies as previously described [67]. The negative control mAb D12 was generated from patient MuSK MG-3. It was derived from single cell sorting and subsequent single cell PCR. The sort enriched for IgG4-specific memory B cells/plasmablasts (CD3^{neg}, CD14^{neg}, CD19^{+}, IgD^{neg}, CD27^{+}, IgG4^{+} (biotinylated IgG4-specific clone MH164-1, with APC streptavidin (Biolegend #405207) used for detection). The antibody subclass usage of this clone was verified as IgG4 through subclass PCR. The D12 mAb was expressed as an IgG4 subclass whole antibody, and then used as a negative control as no binding to MuSK via CBA was observed. The antigen binding fragments (Fabs) of 2E6 and 6C6 were expressed in a human Fab expression vector (see below for heavy chain plasmid description) using the

167

same expression system as described for the mAbs. Protein G Sepharose® 4 Fast Flow beads were used for mAb purification and the 6XHis-tagged Fabs and MuSK were affinity purified using HisPurTM Cobalt Resin according to manufacturer's protocol.

Immunofluorescence of mouse muscle sections

The binding of the mAb 2E6 and 6C6 to mouse MuSK was performed as previously described [67]. Briefly, positive control AChR-specific mAb 637 [18], 6C6 and 2E6 mAbs were added at a concentration of 4 µg/mL each combined with Alexa Fluor 647-conjugated α-bungarotoxin (1:300, B35450, Thermo Fischer Scientific). Human Fc-γ-specific Alexa Fluor 488-conjugated goat F(ab')2 (3 µg/mL, 109-546-170, Jackson ImmunoResearch) was subsequently added. Endplates were identified using the immunofluorescence of the α-bungarotoxin staining. Triple-fluorescent photomicrographs of the endplate regions were acquired using µManager software ver2.0 [69] on an Olympus BX51WI spinning-disk confocal fluorescence microscope with a Hamamatsu EM-CCD C9100 digital camera. Endplates were analyzed using ImageJ software (NIH) as described [17, 69].

Autoantibody binding cell-based assay

HEK293T cells were transfected with either full-length MuSK-GFP (kindly provided by Drs. David Beeson, Angela Vincent and Patrick Waters, Neurosciences Group at the Weatherall Institute of Molecular Medicine, University of Oxford) or different ectodomain variants of MuSK-GFP (previously described in [67]). The cell-based assay (CBA) was performed as previously decribed [14]. The autoantibody titer of

human sera was measured using 10 two-fold dilutions ranging from 1:20 to 1:10240. The binding of each mAb was detected with Alexa Fluor®-conjugated AffiniPure Rabbit Anti-Human IgG, Fcγ (309-605-008, Jackson ImmunoResearch) on a BD LSRFortessa® (BD Biosciences). FlowJo software (FlowJo, LLC) was used for analysis.

Human Fab expression vector construction

A human Fab expression vector was engineered from our human IgG1 heavy chain expression vector [49], following a human Fab VH vector design demonstrated to work with mammalian antibody expression [72]. The region coding for the IgG1 constant region was modified to terminate near the junction of the CH1 region and the upper hinge (TKVDKKV - EPKSC). At this region a linker sequence (GS) was added followed by a 6XHis-tag, then a stop codon (TKVDKKV - EPKSC - GS - HHHHHH - stop). A synthetic DNA fragment (gBlock™, Integrated DNA Technologies) coding for the modified constant region was amplified by PCR (GoTaq® DNA Polymerase; Promega (M3001)) and cloned into the original human IgG1 heavy chain expression vector at the Apa I site-located at the beginning of the CH1- and a Bam HI site, which is located at the end of CH3 immediately downstream of the stop codon. The sequence integrity of this new human Fab heavy chain expression vector was confirmed by both Sanger sequencing of the insert and sequencing of the entire plasmid with the Oxford Nanopore platform (Plasmidsaurus). The variable regions coding for the heavy chains of the mAbs 2E6, 6C6, MuSK1A and IgG4 D12 were then subcloned into the Fab expression vector at the Afe I and Apa I sites following standard procedures. The plasmids

were transformed into NEB® 5-alpha Competent E. coli (New England BioLabs, Inc.). Plasmid DNA was then isolated with the QIAprep Spin Miniprep Kit (Qiagen) and sequenced by Sanger sequencing to confirm the presence of each specific variable region.

Polyreactivity, HEp-2 ELISA and AChR clustering assay

Recombinant human mAbs were tested for polyreactivity on microplates coated with 20 µg/ml double-stranded DNA (dsDNA), 10 µg/ml lipopolysaccharide (LPS), or 15 µg/ml recombinant human insulin (all purchased from SIGMA-Aldrich) using a previously described approach [75]. Highly polyreactive antibody ED38 was used as positive control [62]. Purified recombinant IgGs were tested for autoreactivity on a commercially available human epithelial type 2 (HEp-2) cell lysate ELISA kit (INOVA) according to the manufacturer's instructions with minor modifications that have been described previously [84]. The ELISA plates were read using a PowerWave XS (BIO-TEK). The C2C12 AChR clustering assay was performed as previously reported [14, 67].

Bulk library preparation

RNA was isolated from frozen PBMCs using the RNeasy Mini Kit (Qiagen, 74104) according to manufacturer's instructions. BCR libraries were either generated using the NEBNext Immune Sequencing Kit (NEB) as previously published [31] or the SMARTer® Human BCR IgG IgM H/K/L Profiling Kit (Takara Bio USA, Inc.) using the primers targeting IgA, IgG and IgG-subclasses. Four libraries were pooled in equimolar amounts and prepared for sequencing on the Pacific Biosciences

(PacBio) Sequel II machine by B Cell Receptor Repertoire SMRTbell® Library (PacBio) preparation.

Single-cell library preparation

B cells were enriched from cryopreserved PBMCs using negative selection beads (Stemcell Technologies; 19554). They were incubated with live/dead stain, then stained for 30 minutes on ice with fluorescently labeled antibodies against CD3 (BD Biosciences, V500; UCTH1), CD14 (Invitrogen, Pacific orange; TUK4), CD19 (BioLegend, PE Cy7; SJ25C1), CD27 (BD Biosciences, PE; M-T271), IgD (BD Biosciences, FITC; IA6-2), IgM (BioLegend, PerCP/Cyanine5.5; MHM-88) and CD38 (BioLegend, BV421; HB-7) using manufacturer's recommended dilutions. The cells were sorted on an FACSAria (BD Biosciences) instrument and the population of $CD3^-CD14^-CD19^+IgD^-CD27^+IgM^-CD38^+$ was collected for subsequent analysis by 10x Genomics. Sorted B cells were then loaded into the Chromium Controller (10x Genomics). Single-cell gene expression libraries were prepared using the Chromium Single-cell 5′ Reagent Kit (10x Genomics; V 2.0) according to manufacturer's instructions. Samples were sequenced on the NovaSeq 6000 Sequencing System (Illumina) with HiSeq paired-end 150bp reads for 10x Single cell BCR (BCR libraries) and 10x Single cell 5 Prime (gene expression).

Single B cell RNA-seq analysis

Single cell RNA-seq gene expression information from all subjects was processed using Seurat v4.1.1 [23] in R v4.1.0. To remove apoptotic or lysing cells, cells with a ≥ 10% of RNA transcripts from mitochondrial genes were excluded. To exclude

poor quality cells, only cells with reads from > 400 features were retained. Read counts were log-normalized using a scaling factor of 10^4. To account for variability in gene expression, log-normalized read counts were then scaled and centered for each feature. The top 2000 variable genes were then identified using Seurat's "vst" method. V, D, and J genes from the IGH, IGL, and IGK loci were removed so that the properties of the BCR expressed by the cell would remain independent of the cluster to which it was assigned. Seurat's IntegrateData function was then used to combine data from both sequencing runs. Integration was performed using the previously identified top variable genes of each run, and the first 20 dimensions. Following integration, variable gene expression values were re-scaled and centered. This data was then reduced to the first 20 principal components. To annotate B cell subtypes, cells were clustered by Seurat's shared nearest neighbor clustering algorithm with a resolution of 0.5. The B cell subtype of each cluster was then determined by gene expression correlations to cell types in the immunoStates database [5]. This resulted in 3 clusters identified as plasmablasts, 6 identified as memory B cells, and 2 identified as naïve B cells. These cell type annotations were verified using known marker genes for plasmablasts (PRDM1, XBP1), memory B cells (CD24, TNFRSF13B) and naïve B cells (IGHD, IL4R, TCL1A). One cluster of plasmablasts was further identified as "proliferating plasmablasts" due to high expression of MKI67.

B cell receptor sequence processing

Bulk and single cell B cell receptor sequences were obtained from four different data sources: 10X Genomics single cell RNAseq + BCR sequencing, bulk heavy-

chain only BCR from New England Biolabs NEBNext sequencing kits, Takaras SMARTer® Human BCR IgG IgM H/K/L Profiling Kit, and previously published, processed bulk BCR sequences from the same patients, which we previously reported [43]. All BCR repertoire sequence data were analyzed using the Immcantation (www.immcantation.org) framework. Heavy and light chain BCR sequence data from 10X Genomics scRNA-seq + BCR sequencing began with the filtered V(D)J contigs from Cell Ranger. To obtain V and J gene assignments, these contigs were aligned to the IMGT GENE-DB [19] (v3.1.23, obtained August 3, 2019) human germline reference database using IgBlast v1.13.0 [80]. Preprocessing of NEBNext BCR sequences was performed using pRESTO v0.6.2 [71]. Quality control was first performed by removing all reads with a Phred quality score < 20. Reads which did not match to a constant region primer (maximum error rate 0.2) or template switch sequence (maximum error rate 0.5) were discarded. A unique molecular identifier (UMI) was assigned to each read using the first 17 nucleotides following the template switch site. Sequences within each UMI group were then collapsed into consensus sequences. Clusters with error rates exceeding 0.1 or majority isotype found in less than 60% of sequences were discarded. Positions containing more than 50% gap sequences were removed from the consensus. Mate-pairs were assembled into sequences with a minimum overlap of 8 nucleotides and a maximum error of 0.3. Isotypes were then assigned by local alignment of the 3' end of the assembled sequences to known isotype-constant region sequences with a maximum error rate of 0.3. Duplicate sequences were collapsed except if assigned to different isotypes. Sequences represented by a

single reconstructed mate-pair were discarded. To obtain V and J gene assignments, remaining sequences were aligned to the IMGT GENE-DB human reference database (v3.1.23, obtained August 3, 2019) using IgBlast v1.13.0.

Pacific Biosciences B cell receptor sequence preprocessing

HiFi reads generated from single molecule, real-time (SMRT) sequencing data were first demultiplexed using the Lima tool (https://github.com/PacificBiosciences/pbbioconda) based on the Illumina indices integrated during library construction. Sample-level demultiplexed reads were then further processed using pRESTO [71], following a similar workflow to that used for the NEBNext-generated libraries. Briefly, reads with Phred quality scores < 20 were removed, followed by the identification of the universal primer on the 5' end of each read; reads with primer annotation error rates exceeding 0.3 were discarded. Sequences with the same UMIs were then clustered and aligned to generate collapsed consensus sequences representing each unique UMI. Consensus reads with < 2 representative sequences from the dataset were removed. The remaining reads for each sample were assigned to respective IGHV, IGHD, and IGHJ genes using IgBLAST with the IMGT database as the reference (downloaded February 21, 2022).

B cell clonal analysis

BCR sequences from all data sources were pooled together and grouped by subject. Nonproductive heavy chains were removed. Light chain sequences were excluded from clonal clustering analysis. To limit low-coverage sequences, all

sequences with fewer than 300 unambiguous nucleotide characters (ATCG) were discarded. Novel IGHV alleles and subject-specific IGHV genotypes were inferred using TIgGER v1.0.0 [15]. To identify B cell clones, sequences were first partitioned based on common V and J gene annotations, as well as junction length. Within these groups, sequences differing from one another by a Hamming distance threshold of 0.15 within the junction region were clustered into clones using single linkage hierarchical clustering [20, 21] implemented in Change-O v1.2.0 [21]. This Hamming distance threshold was determined by manual inspection of distance to the nearest sequence neighbor plot using shazam v1.1.0 [79]. Three clones containing both high-throughput BCR sequences and monoclonal antibody sequences were identified. Unmutated germline V and J gene sequences were then reconstructed for each of these clones using the createGermlines function within dowser v1.0.0 [27]. To infer lineage trees, tree topologies, branch lengths, and substitution model parameters were estimated first under the GY94 model [46] and then under the HLP19 model [28]. All lineage tree analysis used IgPhyML v1.1.4 [28] and dowser v1.0.0 [27]. Trees were visualized using dowser v1.0.0, ggtree v3.0.4 [82], and ggplot v3.3.6 [76]. All B cell clonal analyses were performed using R v4.1.0. Scripts for performing B cell receptor sequence processing and analyses are available at https://bitbucket.org/kleinstein/projects.

Statistics

Statistical significance was assessed with Prism Software (GraphPad; version 8.0) by multiple comparison ANOVA with Dunnett's correction for AChR clustering in the C2C12 assay.

Data Availability

Anonymized data will be shared on request from qualified investigators and completion of materials transfer agreements. The anonymized BCR sequencing data reported in this paper have been deposited in the National Center for Biotechnology Information Gene Expression Omnibus Archive, https://www.ncbi.nlm.nih.gov/geo (BioProject ID: PRJNA886711; GEO accession: GSE215237). Code used in this study is available in a publicly accessible repository at https://bitbucket.org/ kleinstein/projects.

Results

Validation of fluorescently labeled MuSK

We generated a fluorescently labeled human MuSK ectodomain to specifically identify and isolate MuSK-specific B cells from patient samples **(Supplement Fig. 1)**. We verified the utility of the labeled MuSK by testing it with a human B cell precursor line (Nalm6), which was modified to express a MuSK-specific human recombinant mAb (MuSK3-28) in the form of a BCR [11, 64, 67]. Fluorescently labeled recombinant human growth hormone (hGH) was used as a negative control antigen. The fluorescently labeled MuSK was tested over a broad range of concentrations (0.01, 0.1, 1.0 and 10 µg/mL), and showed strong binding to the Nalm6 cells, which expressed the MuSK3-28 BCR **(Supplement Fig. 1a, b)**. No binding of either antigen was observed with the unmodified Nalm6 cells **(Supplement Fig. 1c)** or with the hGH tested on the Nalm6 cells, expressing the MuSK3-28 BCR.

Generation of MuSK-specific human mAbs from circulating B cells

We developed a flow cytometry panel to isolate MuSK-specific B cells (CD3-CD14-CD19+IgD-CD27+IgM-MuSK+) using the fluorescently labeled MuSK antigen **(Supplement Fig. 2)**. We started with 107 PBMCs from each of twelve samples, derived from nine unique MuSK-MG patients **(Supplement Table 1)**, then after B cell enrichment, sorted single MuSK positive B cells. These single B cells (N = 672) were individually cultured using a well-established system that induces differentiation to antibody-secreting cells (ASC) such that the supernatant can be screened for antibody specificity [66]. Screening identified two different MuSK autoantibody-expressing cells isolated from patients MuSK MG-1 and MuSK MG-4 **(Fig. 1a; Table 1)**. Index sorting showed that both originated from plasmablasts **(Table 1)**, subclass PCRs showed that both expressed IgG4, and they had acquired somatic mutations including those coding for variable region glycosylation sites. Next, mAbs (referred to as 2E6 and 6E6) were generated from the BCRs of these two cells and their MuSK binding specificity was tested with three independent techniques. The mAbs bound MuSK over a broad range of concentrations (ranging from ≈ 0.03-10 µg/mL) in a live cell-based assay **(Fig. 1b; Supplement Fig. 3)**. This binding specificity was also verified by a clinical radioimmunoassay **(Supplement Table 2)** tested with both MuSK and AChR; both mAbs bound only to the former. Additionally, binding to MuSK expressed on muscle tissue was tested by immunofluorescent staining of murine neuromuscular junctions. Both mAbs bound to MuSK, closely associated with the AChR at the neuromuscular junction **(Supplement Fig. 4)**.

Name of IgG4 Clone (mAb)	MG Patient ID	B cell subset phenotype (by index sorting)	Isotype and IgG subclass	Variable region family and allele	Joining region family and allele	Diversity region family and allele	Amino acid replacements in variable region gene segment	Amino acid replacements in CDR3	CDR3 length (NT)	N-linked glycosylation site In variable region
2E6	MuSK MG-1	Plasmablast	IgG4	IGHV4-61*01,IGHV4-61*08	IGHJ6*03 F (b)	IGHD3-3*01 F	23 + 2 insertions	4	78	1 acquired in FR1
			2E6 CVA (IgG)	IGHV4-61*01,IGHV4-61*08	IGHJ6*03 F	IGHD3-10*01 F	17 + 2 insertions	3	78	1 acquired in FR1
			2E6 CVB (IgG4)	IGHV4-61*01,IGHV4-61*08	IGHJ6*03 F	IGHD3-3*01 F	17 + 2 insertions	5	78	1 acquired in FR1
			2E6 CVC (IgG4) and 2E6 CVC (IgG)	IGHV4-61*01,IGHV4-61*08	IGHJ6*03 F	IGHD3-3*01 F	24 + 2 insertions	4	78	1 acquired in FR1
			κ	IGKV3-20*01 F	IGKJ3*01 F (a)	-	9	1	33	-
6C6	MuSK MG-4	Plasmablast	IgG4	IGHV3-11*01 F	IGHJ4*02 F	IGHD3-10*01 F	14	3	39	-
			κ	IGKV3-11*01 F	IGKJ4*01 F	-	14	2	39	1 acquired CDR2/FR2

Table 1. Molecular characteristics of the human MuSK autoantibodies. The molecular characteristics of the human MuSK-specific mAbs 2E6, 6C6 and the clonal variants of 2E6. The replacement mutations in the variable region gene segment were counted from the beginning of framework 1 through the invariable cysteine at position 104. The mutations in the CDR3 were counted between cysteine 104 and the invariable tryptophan (W) or phenylalanine (F) at position 118 in both the heavy chain and the light chain, respectively. No FR4 mutations were observed. N-linked glycosylation motif (N-X-S/T; X is any AA except proline).
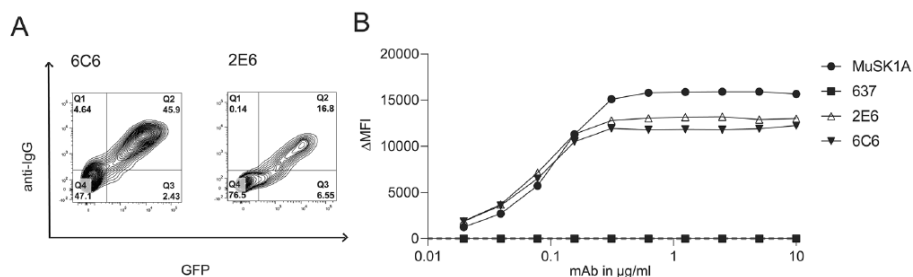
Fig.1: MuSK autoantibody binding. A live cell-based assay (CBA) was used to screen B cell culture media for MuSK IgG and to validate the binding of the human MuSK specific mAbs 2E6 and 6C6. **(a)** To generate MuSK mAbs, patient-derived B cells were sorted for single cell culture, after which the secreted IgG was tested for MuSK-specificity using a CBA. The contour plots from this screening show that MuSK-specific IgG are present in the supernatant of two culture wells from which the mAbs 2E6 and 6C6 were subsequently derived. The x-axis represents GFP fluorescence intensity and, consequently, the fraction of HEK cells transfected with MuSK. The y-axis represents Alexa Fluor 647 fluorescence intensity, which corresponds to secondary anti–human IgG Fc antibody binding and, consequently, primary antibody binding to MuSK. Hence, transfected cells are located in the right quadrants and cells with MuSK antibody binding in the upper quadrants. **(b)** Binding to MuSK by mAbs 2E6 and 6C6 was tested over a series of ten two-fold dilutions ranging from 10-0.02 µg/ml. The ΔMFI was calculated by subtracting the signal acquired from non-transfected cells from the signal of transfected cells. The MuSK-specific human mAb MuSK1A was used as a positive control and the AChR-specific human mAb 637 used as a negative control. Each data point represents the mean value from three independent experiments. Bars or symbols represent means and error bars SDs. Values greater than the mean + 4SD of the negative control mAb at 1.25 µg/ml (indicated by the horizontal dotted line) were considered positive.

Characterization of MuSK mAbs 2E6 and 6C6

The extracellular domain of MuSK is comprised of three Ig-like domains and a frizzled-like domain **(Fig. 2a)**. Most pathogenic MuSK autoantibodies recognize the Ig1-like domain [29, 30] while a smaller subset bind to the Ig2-like domain [67]. We found that both 2E6 and 6C6 bound to the Ig1-like domain of MuSK and showed no reactivity towards other domains **(Fig 2b, c)**. Valency plays an important role in the pathogenic capacity of MuSK autoantibodies. Monovalent antibodies or Fabs - emulating fab-arm exchanged IgG4- are more potent in disrupting the MuSK-LRP4 interaction which is necessary for the clustering and functionality of the AChR [14, 29, 73]. Therefore, we evaluated the pathogenic capacity of 2E6 and 6C6 as both

divalent mAbs and monovalent Fabs by using an established in vitro AChR clustering assay [67]. This assay specifically evaluates the capability of autoantibodies to interfere with AChR-clustering, which is dependent upon the MuSK-LRP4 pathway. The number of AChR clusters that formed in response to agrin alone was assigned a value of 100%, and the number that formed in the presence of the mAb or monovalent Fab (tested at equimolar concentrations) was expressed relative to this value. The mAb 2E6 reduced the number of clusters by 53% and mAb 6C6 by 71%. The monovalent Fab of 2E6 reduced the AChR clusters by 61%, while the monovalent Fab of 6C6 reduced the clusters by 96%, similar to the Fab of the positive control MuSK-specific human mAb MuSK1A **(Fig 2d)**.

Unmutated common ancestors (UCA) approximate germline encoded versions of mature antibodies. UCA versions of MuSK mAbs can bind to the cognate self-antigen with high affinity [14]. Therefore, we investigated whether the UCAs of 2E6 and 6C6 can bind to MuSK. We found that the UCA of 6C6 was able to bind to MuSK over a broad range of concentrations (10 - 0.3 µg/ml), while the UCA of 2E6 only showed binding at the highest concentration tested (10 µg/ml) **(Supplement Fig. 5)**. Next, we tested whether the binding of the mAbs and their UCA counterparts is a consequence of polyspecificity **(Supplement Fig. 6)**. We used a well-established approach to test binding to insulin, dsDNA, LPS and a HEp-2 cell lysate [75]. We found that 6C6, the UCA of 6C6 and 2E6 were neither polyreactive nor specific for the HEp-2 lysate, while the UCA of 2E6 was both polyreactive and specific for the HEp-2 lysate **(Supplement Fig. 6a, b)**.
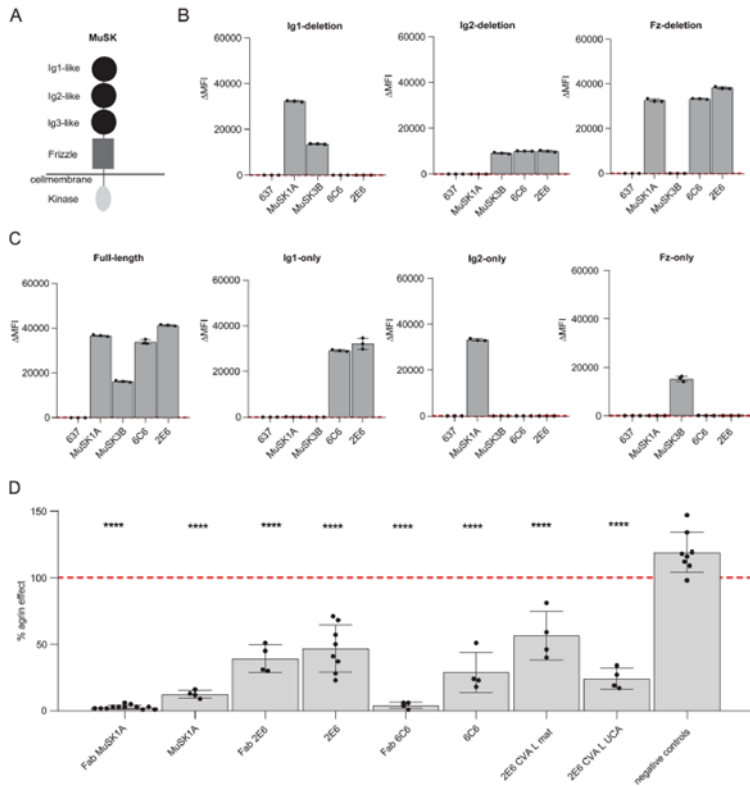
Fig. 2: Epitope specificity and pathogenic capacity of MuSK-specific mAbs 2E6 and 6C6. The mAbs 2E6 and 6C6 were tested for domain binding with a CBA expressing MuSK-GFP domain variants. **(a)** Illustration of the full-length MuSK domains. **(b, c)** The ectodomain of MuSK consists of several different Ig-like domains and a frizzled-like domain. Different mutations of the MuSK protein either consisting of a domain deletion or specific domain-only construct were tested for binding by the mAbs. MuSK-specific human mAbs MuSK1A and MuSK3B were used as positive controls (MuSK1A for the Ig2-like domain and MuSK3B for frizzled-like domain) and the AChR-specific human mAb 637 as the negative control. The mAbs were added at a concentration of 10 µg/ml. Results for each mAb are shown. The ΔMFI was calculated by subtracting the signal acquired from non-transfected cells from the signal of transfected cells. Each data point represents a separate replicate within the same experiment, which was measured in triplicate. Bars represent means and error bars SDs. Values greater than the mean + 4SD of the negative control mAb 637, indicated by horizontal dotted lines, were considered positive. **(d)** AChR-clustering assay in C2C12 mouse myotubes demonstrates pathogenic capacity of MuSK mAbs. The presence of agrin in C2C12 myotube cultures leads to dense clustering of AChRs that can be readily visualized with fluorescent α-bungarotoxin and then quantified. Pathogenic MuSK autoantibodies disrupt this clustering. The mAbs 2E6 and 6C6 were tested for their ability to disrupt the AChR clustering. They were tested as divalent mAbs (1 µg/mL) and monovalent Fabs (0.3 µg/mL). Clonal variant, CVA, of mAb 2E6 was tested with either the mature (mutated) or an unmutated common ancestor (UCA) of the light chain from mAb 2E6, given that the clonal variants were identified with heavy chain-only sequencing. Quantitative measurements of the C2C12 clustering were normalized to the agrin-only effect of each individual experiment. Each data point represents the mean value from 2-8 individual values from a total of 4-10 independent experiments. Bars represent the mean of means and error bars SDs. Multiple comparisons ANOVA (against the pooled results for the three human non- MuSK-specific mAbs), Dunnett's test; * $p<0.05$, ** $p<0.01$, *** $p<0.001$, **** $p<0.0001$, only shown when significant.

Phenotype of plasmablasts in MuSK MG at time of relapse after BCDT

The 2E6 and 6C6 mAbs were both isolated from IgG4-expressing plasmablasts during post-BCDT relapse, as were several human MuSK mAbs that we previously produced [64, 67]. Given the increased frequency of plasmablasts in MuSK MG patients during relapse and that these cells can express pathogenic autoantibodies, we sought to explore whether their gene expression profile displayed any unique characteristics, such as expression of pro-survival genes that have been associated with BCDT resistance [9].

To that end, we used single cell gene expression profiling to investigate the phenotype of the plasmablasts at the time of relapse. Single-cell BCR sequencing was performed at the same time to search for clones related to 2E6 and 6C6, and also to explore the MuSK specificity of the IgG4-expressing plasmablast compartment. We used the specific samples from which 2E6 and 6C6 were obtained; MG-1 timepoint 70 months and MG-4 timepoint 25 months respectively (Supplement Tables 1 and 3). B cells were sorted to enrich for plasmablasts (CD3⁻CD14⁻CD19⁺IgD⁻CD27⁺IgM⁻CD38⁺), but with gating that did not entirely exclude other B cell phenotypes. By clustering cells based on gene expression information, we identified 11 distinct clusters, annotated as naïve, memory and plasmablast populations **(Fig. 3 a, b; Supplement Fig. 7)**. We found IgG4 enriched among specific populations in the plasmablast and memory B cell clusters **(Supplement Fig. 7b, 8c)**. Plasmablasts were defined by expression of XBP1, IRF4, PRDM1 and high levels of somatic hypermutations **(Cluster 2,8 and 10; Fig. 3 c, Supplement Fig. 7)**. One plasmablast cluster (number 10) expressed high levels of MKI67,

which is associated with proliferation **(Fig. 3 a, b, c)**. We found that CD20 (MS4A1) was expressed at low levels in 25% of the cells within the plasmablast subpopulations, while low level expression of CD19 was found in 25-50% of the population **(Fig. 3 b)**. The expression of high levels of TACI (TNFRSF13B) and BCMA (TNFRSF17) ranged between 25-100% in all three plasmablast subpopulations, while the expression levels of BAFF-R (TNFRSF13C) were low (0-10%) **(Fig. 3 b)**. Using the single-cell BCR sequencing data, we did not identify clonal relatives of 2E6 or 6C6 indicating that MuSK-specific clones comprise only a small fraction of circulating plasmablasts in these patients.
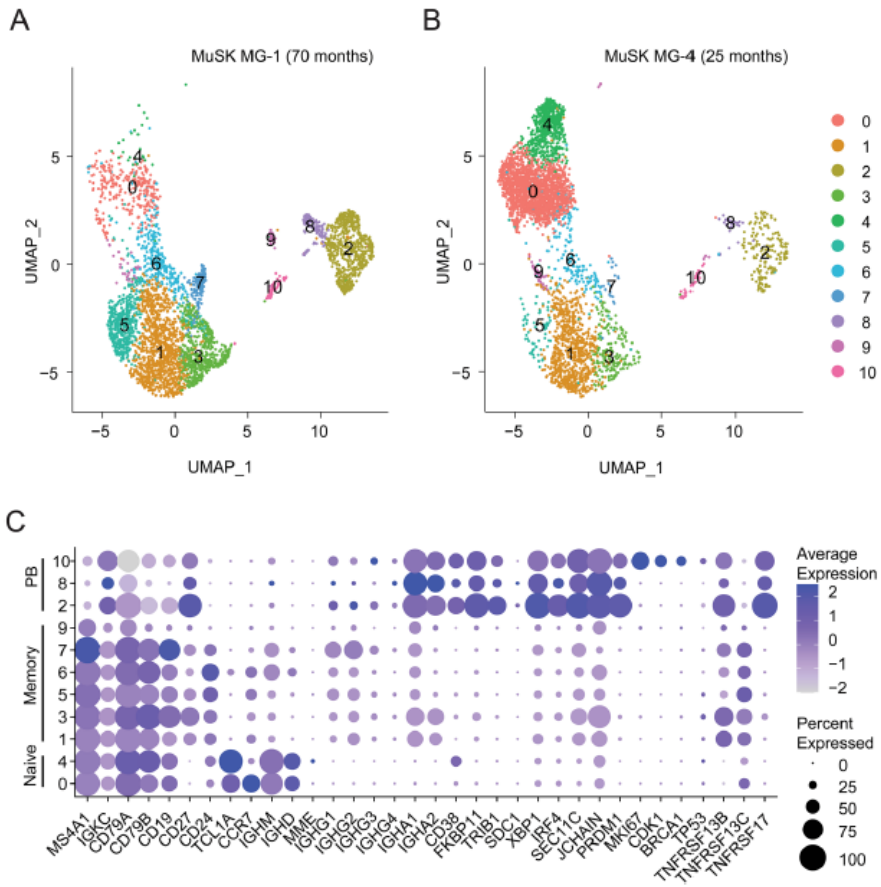
Fig. 3: Single cell RNAseq characterization of MuSK MG patient B cells at the time of relapse. Single cell transcriptional profiling was used to characterize B cell samples from patients MG-1 and MG-4 taken at timepoint 70 and 25 months respectively, when MuSK-specific mAbs 2E6 and 6C6 were isolated. Both patients were experiencing a relapse at the time of sample collection. **(a, b)** Uniform Manifold Approximation and Projection (UMAP) of B cells showing 10 populations. Each point represents a single cell. **(c)** Dot plots showing expression of selected B cell marker genes for naive, memory, and plasmablast B cell subsets for the clusters identified in **(a, b)**.

MuSK-specific B cell clones persist through BCDT and reemerge during relapses

We next investigated whether we could detect historic clonal variants of the pathogenic mAbs 2E6 and 6C6. We had collected serial samples from patient MG-1 (from whom mAb 2E6 was cloned) that made it possible to follow the clinical and treatment course for 79 months, and from patient MG-4 (from whom mAb 6C6 was cloned) for 25 months **(Supplement Table 3)**. We produced BCR repertoire libraries using bulk heavy chain only RNA sequencing and single-cell BCR sequencing to collectively obtain 50,948 unique clones for patient MG-1 and 13,029 clones for patient MG-4 **(Supplement Table 4)**. We identified B cell clones - cells that descend from a common V(D)J rearrangement - by clustering BCR heavy chain sequences by sequence similarity **(Methods, Supplement Fig. 9)**. No historic clones or clonal variants (CV) of mAb 6C6 were found. However, we identified three clonal variants of 2E6, two of which (CVA and CVB) were identified in samples collected prior to that which harbored the plasmablast that produced mAb 2E6, and one (CVC) was identified in the sample that produced mAb 2E6 **(Fig. 4 a; Supplement Table 3)**.

We next tested whether the other members of the 2E6 clone had pathogenic capacity. Given that bulk-RNA sequencing provided only the heavy chain of each clonal variant, we confirmed the specificity of the variants for MuSK by pairing the heavy chain with either the mature or UCA light chain of 2E6 to approximate the range of light chain sequence variation within the clone. We found that all clonal variants of 2E6 bound to MuSK over a wide range of concentrations when paired

185

with either the mature or UCA light chain of 2E6 (10-0.02 µg/ml) **(Fig. 4 b)**. The mAb of 2E6 originated from a polyspecific germline-encoded UCA antibody that gained specificity towards MuSK over time through affinity maturation **(Supplement Fig. 6)**. Thus, we tested whether the earliest-sampled clonal variant of 2E6 (2E6 CVA) showed pathogenic capacity and specific binding to MuSK. We found that 2E6 CVA showed pathogenic capacity in vitro **(Fig. 2 d)**. 2E6 CVA paired with the mature light chain reduced the AChR clusters by 43% and 2E6 CVA paired with the UCA light chain by 76% **(Fig. 2 d)**. Neither recombinant variants of 2E6 CVA (VL mature and VL UCA) were polyreactive, nor did they react to HEp-2 **(Supplement Fig. 6 a, b)**. Both variants bound to MuSK over a wide range of concentrations (10-0.02 µg/ml) **(Fig. 4 b)**. The MuSK MG patient harboring this clone had received rituximab-mediated BCDT 28 months before the patient presented with relapse at the first collection timepoint **(Supplement Table 3)**. The patient received BCDT six additional times over the course of 79 months (6.6 years) and received two cycles of BCDT between the identification of the first clonal variant 2E6 CVA and 2E6 CVB which was 31 months apart **(Fig. 4 c; Supplement Table 3)**. Thus, 2E6 persisted through BCDT and reemerged over time.

MuSK autoantibody titer may be a biomarker for detecting relapse after BCDT-induced remission [68]. In agreement with this finding, we observed that the MuSK autoantibody titer started to increase several months prior to relapse (range: 7-9 months), while the patient was still free of symptoms **(Fig. 4 c; Supplement Table 3)**. The titer remained at the same level during the subsequent relapse and decreased after BCDT **(Fig. 4 c; Supplement Table 3)**. The clonal variants 2E6

CVA and 2E6 CVB were identified at timepoints that preceded relapse by two months **(Fig. 4 c)**. In summary, we found three unique clonal variants of 2E6, which persisted through BCDT. Two of these clonal variants were found during the time at which MuSK autoantibody titer increased and importantly, two months prior to relapse. Together, these results demonstrate the existence of pathogenic B cell clones that survive BCDT and emerge before clinically-detected relapse in MuSK MG.
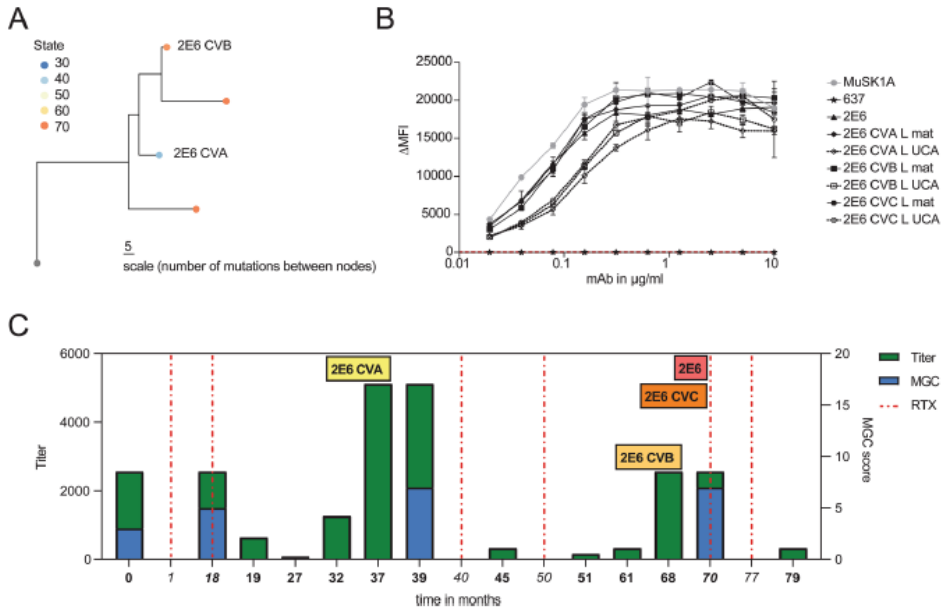
Fig. 4: Characteristics of a persistent MuSK-specific B cell clone. Clonal variants of the MuSK-specific mAb 2E6 were identified in longitudinally collected samples from patient MuSK MG-1. **(a)** Clonal lineage containing BCR sequences from bulk RNA sequencing of serial samples collected from patient MuSK MG-1 from whom mAb 2E6 was cloned. A maximum likelihood tree of the 2E6 clone, with clonal variants CVA, CVB, and CVC is shown. Edge lengths represent the expected number of intervening somatic mutations between nodes (see scale bar). Colors correspond to the collection time point (months) at which each clone (sequence) was identified in relation to the first available collection time point. **(b)** Binding to MuSK by mAb 2E6 and clonal variants was tested in a CBA over a series of ten two-fold dilutions of each mAb ranging from 10-0.02 µg/ml. Clonal variants, CVA, CVB and CVC were each tested with either the mature (mutated) or an unmutated common ancestor (UCA) of the light chain from mAb 2E6, given that the clonal variants were identified with heavy chain-only sequencing. The MuSK-specific human mAb MuSK1A was used as the positive control and AChR-specific human mAb 637 as the negative control. The ΔMFI was calculated by subtracting the signal acquired with the non-transfected cells from the signal of transfected cells. Each data point represents the mean value from three independent experiments. Bars or symbols represent means and error bars SDs. Values greater than the mean + 4SD of the negative control mAb at 1.25 µg/ml (indicated by the horizontal dotted line) were considered positive. **(c)** The x-axis depicts the time in months representing the clinical course of patient MuSK MG-1 from whom the mAb 2E6 was isolated. The bold timepoints indicate longitudinal sample collection and clinical assessment; the italicized timepoints indicate BCDT administration. The left y-axis indicates the MuSK autoantibody titer at each timepoint. The autoantibody titer was measured by CBA using 10 two-fold dilutions ranging from 1:20 to 1:10240. The right y-axis shows the MGC score at each timepoint. Dotted vertical lines indicate the timepoints where the patient received rituximab mediated BCDT. Colored boxes indicate the timepoints at which both clonal variants and the original 2E6 mAb were identified. The blue bars show the MGC score, while the green bars show the autoantibody titer.

188

Discussion

Most MuSK MG patients respond very well to rituximab-mediated BCDT with a rate of remission approaching 100% [10, 33]. However, these patients often experience relapse after approximately 1-3.5 years depending on the rituximab treatment regime [7], and a minority of patients do not respond to BCDT therapy [44]. Plasmablast and memory B cell populations are increased at the time of relapse [64, 67] and a subpopulation of these B cells produce MuSK-reactive antibodies [64]. These B cells can, in part, be traced back to clones that existed before BCDT [31].

The isolation of the two mAbs, 6C6 and 2E6, was achieved through enriching PBMCs for IgG-expressing memory B cells and plasmablasts that bound to a soluble MuSK antigen. This process required screening of 2.6 x 106 B cells from 12 patient samples; 672 of which were MuSK positive and sorted into plates. Of these 672 sorted cells, two clones were validated and 10 showed high MuSK reactivity, as measured by flow cytometry during the sorting procedure. Although the technical approach is not without limitations, it appears that B cells producing MuSK autoantibodies are exceptionally rare, and that their frequency varies through the course of disease. These findings are consistent with other studies; our own and from other groups who have isolated MuSK mAbs [29, 64, 67]. Furthermore, the number of unique clones in an individual patient appears to be low. In this study we isolated only one clone from each patient and in our other studies we isolated as few as one or two clones from single patients. Although the plasmablast compartment frequency -relative to the B cell population - increases at

disease exacerbation, it appears that MuSK-specific plasmablasts make up a very minor population of this expanded compartment. This observation contrasts with findings from studies of acute responses to environmental antigens, where expanded plasmablast clones producing antibodies to COVID or influenza antigens are predominantly antigen-specific and include a diverse clonal repertoire [70, 78]. MuSK autoimmunity may differ in this regard in that only few clones -or even a single clone- could contribute to the production of circulating pathogenic autoantibody, and the expanded plasmablast compartment appears to include many specificities, few of which are MuSK-specific.

The characterization of the MuSK mAbs 2E6 and 6C6 showed that MuSK autoantibodies are heterogenous. Although both MuSK mAbs are not polyreactive, their pathogenic development is quite different. Previously, we had found that the UCA of MuSK mAbs recognize their cognate self-antigen without being polyreactive and that these antibodies develop exceptionally high affinities through the process of affinity maturation necessary to reach their pathogenic potential [14]. These self-reactive antibodies within the naïve B cell repertoire are most likely the consequence of impaired elimination of self-/poly-reactive clones during central and peripheral tolerance checkpoints during B cell development [37, 45, 75]. The approximated naïve precursor (UCA) of 6C6 does recognize MuSK and it was not polyreactive - consistent with our previous findings [14]. However, 2E6 developed from a polyreactive precursor gaining specificity for MuSK through affinity maturation. Furthermore, 2E6 and 6C6 differ in terms of how valency effects their pathogenic capacity. The pathogenic capacity of 6C6 increases as a monovalent

Fab, while 2E6 shows similar pathogenic capacity when expressed as a monovalent Fab and divalent mAb. Although it was shown that monovalency increases the pathogenic effect of MuSK antibodies [14, 29, 35, 73], it was also found that an autoantibody requires high affinity towards MuSK to be pathogenic [14]. Therefore, possible explanations for the differing results might be different affinities and binding kinetics of mAbs 2E6 and 6C6, or that heteroligation may be relevant for mAb 2E6.

We demonstrated that the pathogenic 2E6 clone persists through BCDT. The long-term survival of this clone could be the consequence of tissue-based homing, as rituximab is not highly effective in depleting B cells localized in tissues as it is at targeting those in the circulation [2, 36, 42, 54]. Although plasmablasts can express CD20 [31, 51, 64], we found that 25% of plasmablasts in these patients express low levels of CD20 at the time of relapse. Therefore, clone 2E6 might originate from a plasmablast with low expression of CD20 affording it survival through BCDT. Thus, it might be beneficial to use therapies targeting other surface molecules to improve targeting of disease relevant B cell subsets. Recently, new therapies have been developed that deplete B cells, including therapies targeting CD19 [1, 6, 8, 60]. Inebilizumab (anti-CD19) has been approved for the treatment of neuromyelitis optica spectrum disorder (NMOSD) [8], and a clinical trial on the efficacy of inebilizumab in MG (MINT; ClinicalTrials.gov Identifier: NCT04524273) is currently ongoing. We additionally detected high levels of the receptors TACI and BCMA within the plasmablast subpopulations, but low levels of BAFF-R. TACI and BCMA are part of the BAFF/APRIL-system that regulates the survival of B cells [41, 57].

BAFF-R is the third receptor of the system and the detection of low levels of BAFF-R fits well with previous studies and is indicative of poor response to treatment with rituximab [3, 31, 58]. The low expression of BAFF-R negatively correlates with BAFF levels [61] and high levels of BAFF are associated with autoimmune diseases, including MG [34, 39, 41]. Hence, the BAFF/APRIL axis has been considered as a valuable therapeutic target in the context of autoimmunity and B cell malignancies [38, 65]. Belimumab (anti-BAFF) was already investigated as an add-on therapy in generalized MG patients and showed a subtle positive effect [24]. More recently, chimeric antigen receptor (CAR)-T cells targeting BCMA and/or TACI and anti-BCMA mAbs show promising effects in the treatment of multiple myeloma [38, 53], and autoimmune disease [12], including an ongoing clinical trial in generalized MG (ClinicalTrials.gov Identifier: NCT04146051).

In summary, we generated two new MuSK mAbs that bind to the Ig1-like domain of MuSK and show pathogenic capacity in vitro. These autoantibodies were isolated from a sample collected at the time of relapse after BCDT and originated from plasmablasts. The phenotype of the expanded plasmablast population at time of relapse showed variable expression levels of CD20 and CD19, identifying these cells as potential candidates for BCDT, but highlighting that a subpopulation may escape deletion. Clonal variants of a pathogenic, MuSK-specific B cell were identified prior to relapse together with increased MuSK autoantibody levels, both of which may serve as valuable prognostic biomarkers for predicting post-BCDT relapse [68].

Author contributions

This study was originally conceived, initiated, and directed by KCO and MLF. MLF led the laboratory work at Yale, designing, executing, and interpreting experiments associated with the B cell isolation, mAb expression, functional and binding assays, BCR sequencing, and 10x sample preparation. KBH and SHK performed the computational biology for the 10x and BCR sequencing analysis from the NEB data sets and PacBio sets transformed into the Change-O format. EEF, MLS and CTW performed the computational biology for the BCR sequencing analysis from the PacBio data sets. MMD, PMM, and ML performed and interpreted the mAb tissue staining on mouse muscle. SO and ASP engineered and generated the NALM cells expressing MuSK specific BCRs. PW performed the RIA binding studies and interpreted the data. RJN provided the clinical specimens from which the mAbs were derived and provided insight on the clinical and therapeutic relevance of the findings. The manuscript was initially drafted by MLF and KCO. All authors contributed substantially to the intellectual content of the work, and all discussed results, and made key contributions to editing and revising the manuscript. All authors read and approved the final manuscript.
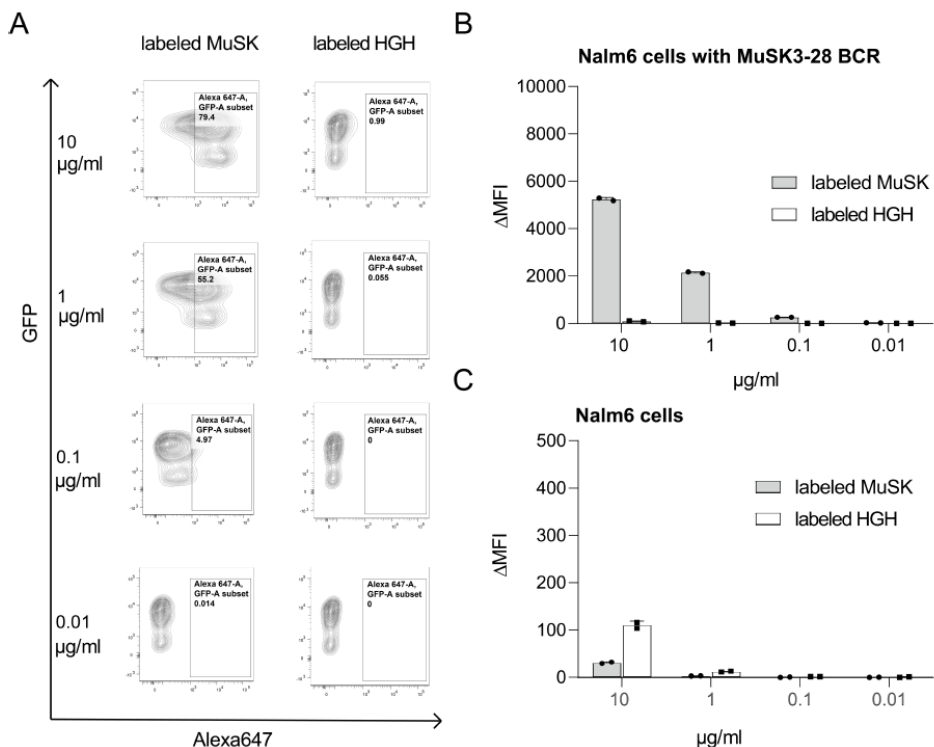
Competing Interests

KCO has received research support from Alexion, now part of AstraZeneca, and Viela Bio, now part of Horizon Therapeutics, and Cabaletta Bio. KCO is a consultant and equity shareholder of Cabaletta Bio. During the last two years, KCO has served as consultant/advisor for Alexion Pharmaceuticals, now part of AstraZeneca, and

Supplemental Material

196

Supplement Figure 1. Validation of a fluorescently labeled MuSK ectodomain reagent to identify MuSK autoantibody-expressing cells. A monomeric fluorescently labeled (Alexa Fluor 647) MuSK ectodomain was tested for use in labeling Nalm6-GFP cells, which were engineered to express a B cell receptor (BCR) derived from a MuSK autoantibody (human recombinant mAb MuSK 3-28). Labeled human growth hormone (hGH) was used as negative control. **(a)** Representative flow cytometry contour plots are shown for MuSK and hGH binding to Nalm6-GFP cells expressing a MuSK3-28 BCR. The y-axis represents GFP fluorescence intensity. The x-axis represents Alexa Fluor 647 fluorescence intensity, which corresponds to antigen bound by the BCR. Hence, cells binding to antigen labeled with Alexa Fluor 647 are in the right quadrants. The plots show testing with an antigen (MuSK or hGH) concentration of 10, 1, 0.1 and 0.01 µg/ml. **(b, c)** Binding to antigen was tested with Nalm6-GFP cells expressing the MuSK 3-28 BCR **(b)** or unmodified Nalm6-GFP cells **(c)**. Antigen binding was tested at 10, 1, 0.1 and 0.01 µg/ml. The ΔMFI was calculated by subtracting the signal acquired from testing cells with antigen added from the signal acquired from cells with no antigen added. Each data point represents the mean of value from two independent experiments. Bars or symbols represent means and error bars SDs.
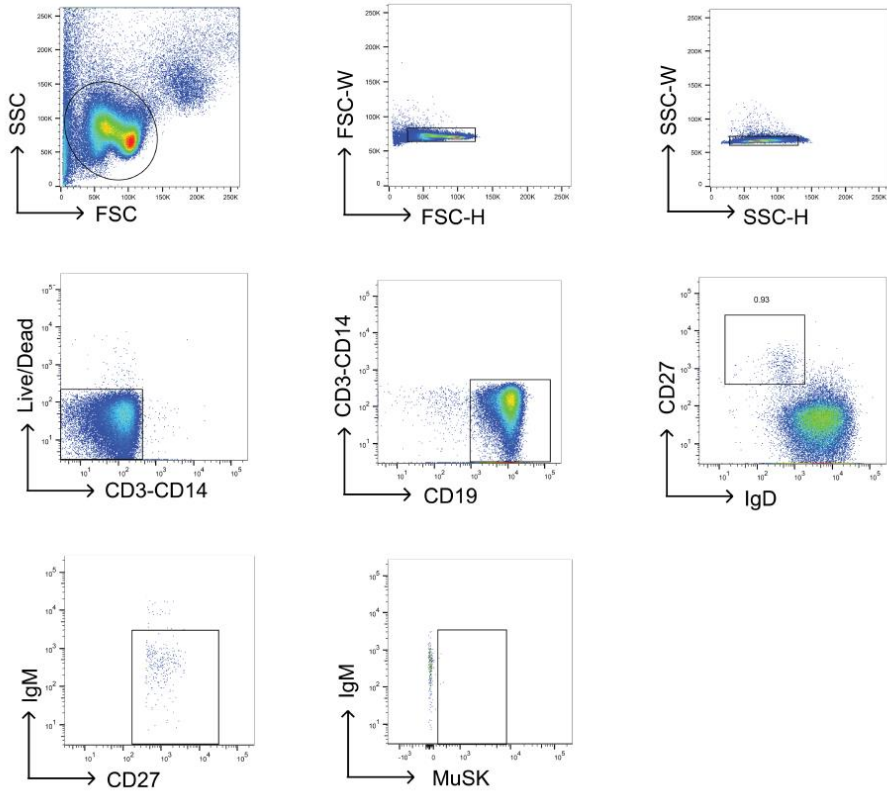
Supplement Figure 2. Flow cytometry gating strategy for isolation of MuSK-specific B cells. A representative example of the gating strategy featuring the fluorescently labeled MuSK ectodomain reagent is shown. After B cell enrichment using negative selection beads, single cells were gated using the forward (FSC) and side (SSC) scatter. Dead cells were excluded, then CD3^{neg} CD14^{neg} CD19^{+} IgD^{neg} CD27^{+} IgM^{neg} MuSK-reagent^{+} cells were single cell sorted for subsequent B cell culture and expansion.
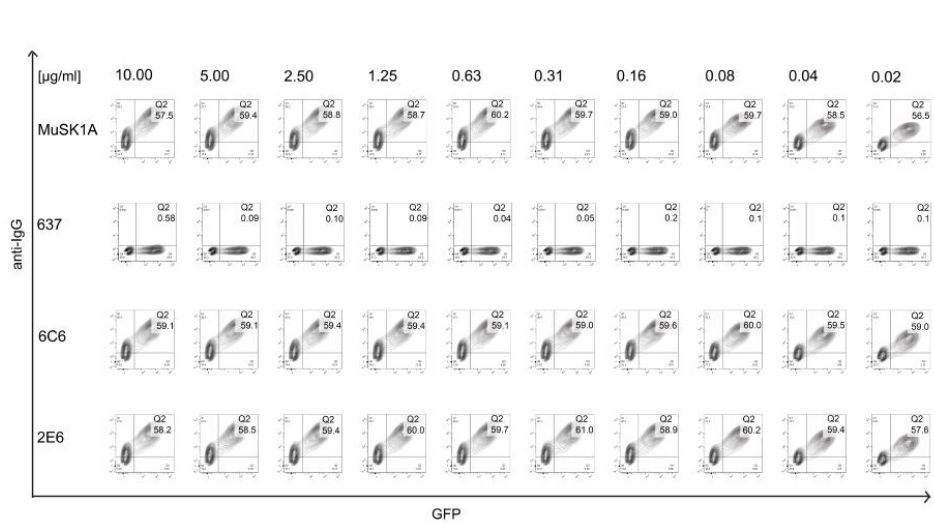
Supplement Figure 3. Cell-based assay contour plots showing dilution series of mAbs 2E6 and 6C6. Binding to MuSK was tested over a series of ten two-fold dilutions of each mAb ranging from 10-0.02 µg/ml. The x-axis represents GFP fluorescence intensity and, consequently, the fraction of HEK cells transfected with MuSK. The y-axis represents Alexa Fluor 647 fluorescence intensity, which corresponds to the secondary anti–human IgG Fc antibody binding and, consequently, primary antibody binding to MuSK. Hence, transfected cells are located in the right quadrants and cells with MuSK antibody binding in the upper quadrants. The MuSK-specific human mAb MuSK1A was used as a positive control and the AChR-specific human mAb 637 used as a negative control.
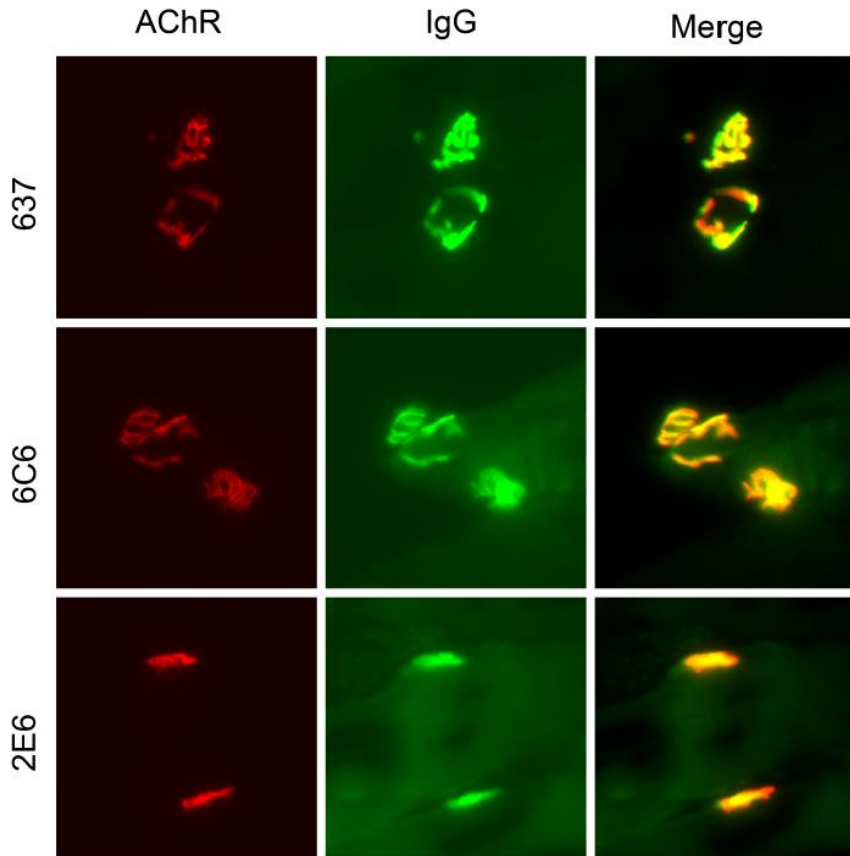
Supplement Figure 4. Staining murine neuromuscular junctions with MuSK mAbs 2E6 and 6C6. Immunofluorescent staining of mouse neuromuscular junctions (NMJ). Tibialis anterior muscles were cut longitudinally in cryosections and fixed with PFA. AChRs were stained with Alexa Fluor 648 α-bungarotoxin (shown in red). The mAb 637 was used a positive control, to identify the location of the AChR. Binding of mAbs was detected with goat anti–human IgG Alexa Fluor 488 (IgG, shown in green).
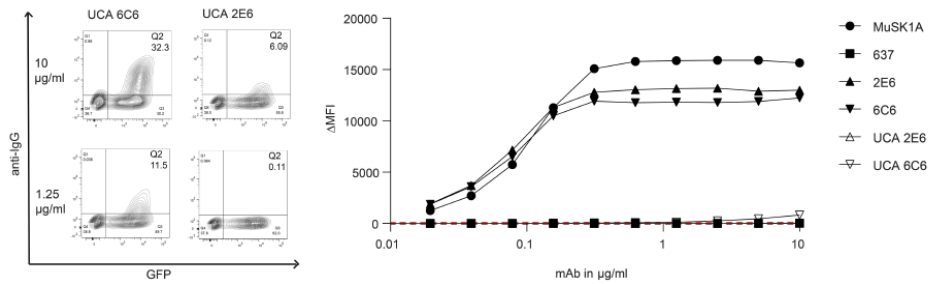
Supplement Figure 5. Binding properties of unmutated common ancestors from MuSK mAbs 2E6 and 6C6. Representative cell-based assay (CBA) contour plots are shown **(left)** for the unmutated common ancestors (UCA) of 2E6 and 6C6. The x-axis represents GFP fluorescence intensity and, consequently, the fraction of HEK cells transfected with MuSK. The y-axis represents Alexa Fluor 647 fluorescence intensity, which corresponds to secondary anti–human IgG Fc antibody binding and, consequently, primary antibody binding to MuSK. Hence, transfected cells are located in the right quadrants and cells with MuSK antibody binding in the upper quadrants. The plots show testing with a mAb concentrations of 10 and 1.25 µg/ml. Binding to MuSK was tested over a series of ten two-fold dilutions of each mAb ranging from 10-0.02 µg/ml **(right)**. The MuSK1A mAb was used as the positive control and AChR-specific mAb 637 as the negative control. The ΔMFI was calculated by subtracting the signal acquired by testing non-transfected cells from the signal acquired by testing transfected cells. Each data point represents the mean value from three independent experiments. Symbols represent means and error bars SDs. Values greater than the mean + 4SD of the negative control mAb at 1.25 µg/ml (indicated by the horizontal dotted line) were considered positive.
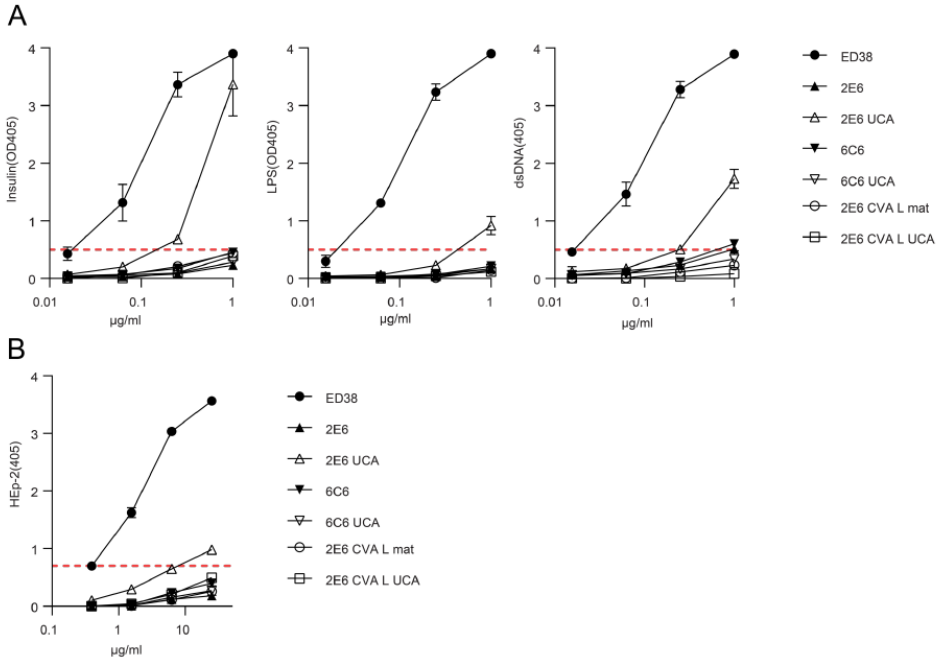
Supplement Figure 6. Polyreactivity and self-reactivity of MuSK mAbs. Polyreactivity and HEp-2 reactivity of MuSK specific mAbs 2E6, 6C6 and their corresponding unmutated common ancestors (UCA). **(a)** The reactivity of the mAbs against LPS, dsDNA and insulin was tested by ELISA. Each data point represents the mean value of two independent experiments and the error bars represent SDs. Dotted horizontal red lines mark the positive reactivity cut-off (0.5) at OD405. **(b)** Purified antibodies were tested for autoreactivity on a solid-phase ELISA against human epithelial type 2 (HEp-2) cell lysate. Antibody reactivity to HEp-2 lysate is illustrated by the binding curves. Each data point represents the mean value of two independent experiments and the error bars represent SDs. Dotted horizontal red lines mark the positive reactivity cut-off (0.7) at OD405. ED38, a monoclonal antibody cloned from a VpreB+L+ peripheral B cell, was used as a positive control for both assays.
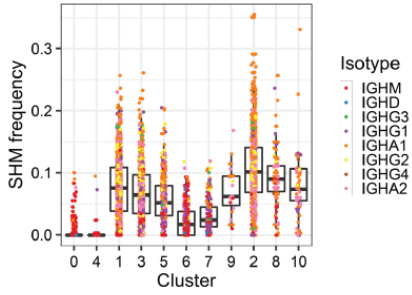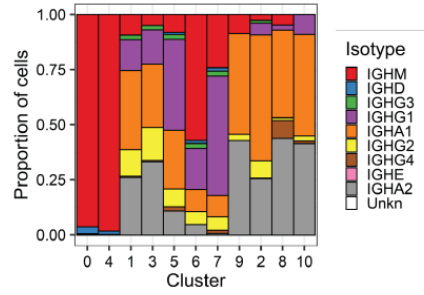
Supplement Figure 7. Somatic mutation frequency and isotype distribution of B cells examined with single cell transcriptional profiling. The frequency of somatic mutations **(a)** and isotype frequency **(b)** of the B cell subset clusters shown in Figure 3 a, b.
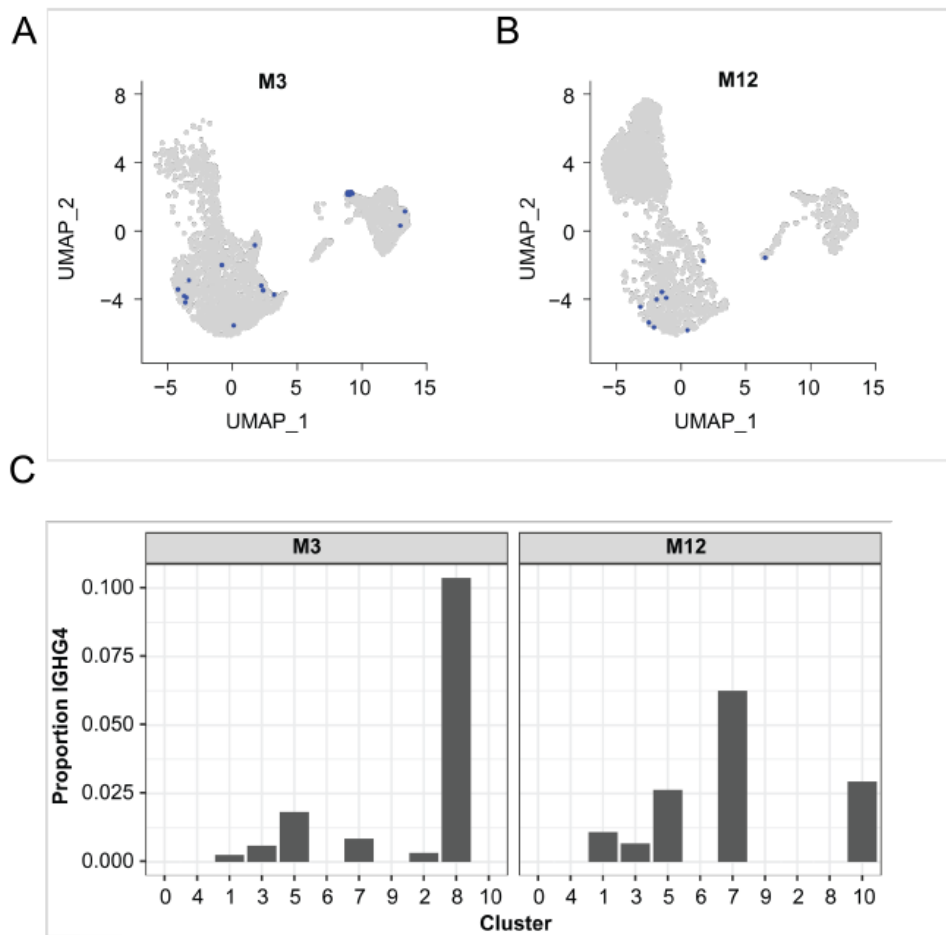
Supplement Figure 8. Distribution of IgG4 expression among B cells clusters identified by single cell transcriptional profiling. (a, b) Manifold Approximation and Projection (UMAP) of B cells obtained at the timepoint 2E6 (**a** (= MuSK MG1 (70 months))) and 6C6 (**b** (= MuSK MG-4 (25 months))) were produced. Each point represents a single cell. B cells expressing IgG4 subclass are indicated with a blue dot. **(c)** Proportion of B cells in each cluster shown in Figure 3 a, b with IgG4 constant regions.
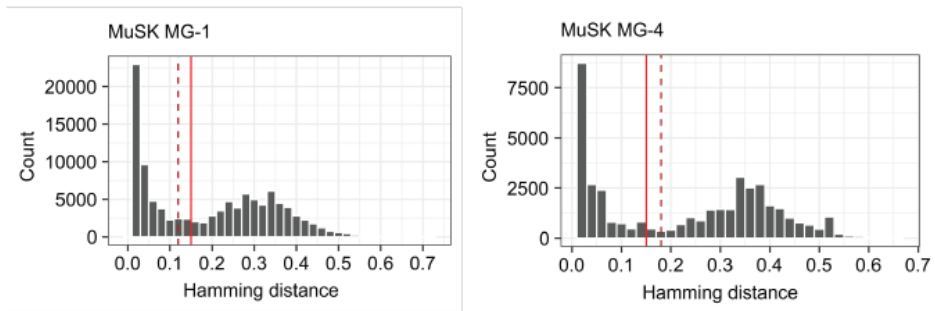
Supplement Figure 9. Distance-to-nearest plots used to identify the threshold required for assigning clonal members in the BCR sequencing data. Distance-to-nearest plots used to identify a common threshold to use for hierarchical clustering-based grouping of V(D)J sequences from high throughout sequencing of BCR repertoires. Red dashed lines correspond to the threshold used for assigning clonal clusters. Grey bars represent the distribution of intra-subject distance-to-nearest distances.

Patient ID	Time (months) since first collection	Sex	Age	Diagnosis	Antibody status	MGFA, MGC class at TOC	Time since last rituximab (years)	Other therapy	Serum MuSK antibody titer
MuSK MG-1	70	F	65	Generalized MuSK MG	MuSK	IIb; 7	1.8	Pred 5 mg/day	56.0
MuSK MG-2	105	F	40	Generalized MuSK MG	MuSK	IIb; 2	1.5	None	12.7
MuSK MG-3	47	F	55	Generalized MuSK MG	MuSK	IIb; 4	0.2	Pred 10 mg/day	0.15
MuSK MG-4	0	F	41	Generalized MuSK MG	MuSK	IIIb; 16	-	Pred 35 mg/day; IVIg 1g/kg q3wks	27.3
MuSK MG-4	25	F	43	Generalized MuSK MG	MuSK	IIIb; 13	1.5	None	16.5
MuSK MG-5	3	F	31	Generalized MuSK MG	MuSK	IIB; 7	-	None	2.01
MuSK MG-5	7	F	31	Generalized MuSK MG	MuSK	IIb; 6	-	PLEX	8.54
MuSK MG-6	0	M	68	Generalized MuSK MG	MuSK	IIIa; 15	-	Pred 60 mg/day; AZA 150 mg/day; Mestinon 60 mg TID; Plex last in Oct 2014	1:320*
MuSK MG-6	16	M	70	Generalized MuSK MG	MuSK	IIb; 8	0.8	Pred 10 mg/day; AZA 150 mg/day	0.03
MuSK MG-7	35	F	36	Generalized MuSK MG	MuSK	IIb; 4	0.9	MMF 1000 mg BD	0.89
MuSK MG-8	94	M	76	Generalized MuSK MG	MuSK	I; 1	7.8	None	0.0
MuSK MG-9	0	F	32	Generalized MuSK MG	MuSK	IIb; 5	-	Pred 40 mg qd	1.75

Supplement Table 1. Study subject clinical, laboratory, and demographic data. MuSK MG patients (n=9 unique patients, n=12 different sample collections) from whom samples were used for isolation of MuSK-specific B cells through single cell sorting followed by B cell culturing. Antibody titer was either measured by Athena Diagnostics (unit = fold dilution) or at the Mayo Clinic Laboratory (unit = nmol/L). Samples measured at Athena Diagnostics are indicated by an (*). The reference range for positivity varies according to the measuring facility. For samples measured by Athena Diagnostics the titer range is negative for <1:10, borderline for 1:10 and positive for >1:20. The cut off for negativity for samples measured at Mayo Clinic Laboratory is ≤ 0.02 nmol/L. TOC = time of collection; Pred = Prednisone; PLEX = plasma exchange; AZA = azathioprine; MMF = Mycophenolate mofetil.

mAb	AChR (CPM)	AChR (∆CPM)	MuSK (CPM)	MuSK (∆CPM)	Result
HC1	916	153	51	-6	neg
HC2	494	-269	62	5	neg
HC3	878	115	59	2	neg
AChR PC1	15908	15145	81	24	AChR+
AChR PC2	18913	18150	73	16	AChR+
MuSK PC1	967	204	8916	8859	MuSK +
MuSK PC2	994	231	8712	8655	MuSK +
mAb 2E6	667	-96	8268	8211	MuSK +
mAb 6C6	710	-53	7211	7154	MuSK +

Supplement Table 2. Radioimmunoassay-based testing of the 2E6 and 6C6 mAbs. The radioimmunoassay RIAs were carried out as per manufacturer's instructions. Serum (5 μl) or 5 μl mAb (1 μg/μl) was incubated with 50 μl ^{125}I-MuSK overnight at 4°C. Carrier was added to mAb tubes followed by 50 μL of anti-human IgG to all tubes for 1 hr. The complex was precipitated by centrifugation, washed, and counted for 1 min on a gamma counter. CPM=counts per minute, ∆CPM=CPM-background, HC=healthy control, PC=positive control.

Patient ID	Time Point in Months	Diagnosis	Antibody status	MGF, MGC at TOC	Time since last Rituximab in months	Other therapy	Serum MuSK antibody titer	Sequencing Data available	Origin of Clone or clonal variant
MuSK MG-1	0	Generalized MuSK MG	MuSK	IIb; 3	28	-	1:2560	+	-
MuSK MG-1	18	Generalized MuSK MG	MuSK	IIb; 5	17	-	1:2560	-	-
MuSK MG-1	19	Generalized MuSK MG	MuSK	0; 0	1	-	1:640	-	-
MuSK MG-1	27	Generalized MuSK MG	MuSK	0; 0	9	-	1:80	-	-
MuSK MG-1	32	Generalized MuSK MG	MuSK	0; 0	14	-	1:1260	+	-
MuSK MG-1	37	Generalized MuSK MG	MuSK	0; 0	19	-	1:5120	+	2E6_CVA
MuSK MG-1	39	Generalized MuSK MG	MuSK	IIb; 7	21	-	1:5120	+	-
MuSK MG-1	45	Generalized MuSK MG	MuSK	0; 0	5	-	1:320	-	-
MuSK MG-1	51	Generalized MuSK MG	MuSK	0; 0	1	-	1:160	-	-
MuSK MG-1	61	Generalized MuSK MG	MuSK	0; 0	11	-	1:320	+	-
MuSK MG-1	68	Generalized MuSK MG	MuSK	0; 0	18	-	1:2560	+	2E6_CVB
MuSK MG-1	70	Generalized MuSK MG	MuSK	IIb; 7	20	Pred 5 mg/day	1:2560	+	2E6 2E6_CVC
MuSK MG-1	79	Generalized MuSK MG	MuSK	0; 0	2	-	1:320	-	-
MuSK MG-4	0	Generalized MuSK MG	MuSK	IIIb; 16	Pre-rituximab	Pred 35 mg/day; IVIg	27.3*	+	-
MuSK MG-4	4	Generalized MuSK MG	MuSK	IIb; 5	2	Pred 15 mg/day	25.0*	-	-
MuSK MG-4	25	Generalized MuSK MG	MuSK	IIIb; 13	18	-	16.5*	+	6C6

Supplement Table 3. Characteristics and analysis status of serial samples from patient MuSK MG-1 and MuSK MG-4. These longitudinally collected samples were used for investigating whether clones or clonal variants of mAbs 6C6 and 2E6 were present. Antibody titer was either measured by CBA in our laboratory or at the Mayo Clinic Laboratory. Samples of MuSK MG-4 measured at Mayo Clinic Laboratory are indicated by an (*); the unit is nmol/L. The cut off for negativity for samples measured at Mayo Clinic Laboratory is ≤ 0.02 nmol/L. The autoantibody titers of MuSK MG-1 measured by our CBA was performed using 10 two-fold dilutions ranging from 1:20 to 1:10240. TOC = time of collection; Pred = Prednisone.

Patient ID	Time Point in Months	Source	Reads	IGHA	IGHD	IGHE	IGHG	IGHM	Clones
MuSK MG-1	0	Mandel-Brehm et al. 2021	7666	1514	498	1	529	3707	5319
MuSK MG-1	32	Mandel-Brehm et al. 2021	16117	5559	1811	2	1416	2697	5612
MuSK MG-1	37	Mandel-Brehm et al. 2021	15117	2102	930	0	699	8459	10235
MuSK MG-1	39	Mandel-Brehm et al. 2021	24834	3770	2675	0	1080	11571	15822
MuSK MG-1	61	PacBio	9912	2878	0	0	1111	0	2150
MuSK MG-1	68	NEB	3362	1687	91	0	486	544	1537
MuSK MG-1	68	PacBio	10659	3086	0	0	1106	0	2736
MuSK MG-1	70	10x	3581	1575	11	0	711	446	2218
MuSK MG-1	70	NEB	5476	2697	134	1	694	744	2247
MuSK MG-1	70	PacBio	10526	2815	0	0	1801	0	3072
MuSK MG-4	0	NEB	997	379	19	3	311	125	632
MuSK MG-4	0	PacBio	17059	2955	0	0	1808	0	3995
MuSK MG-4	25	10x	3669	499	78	0	329	2576	3434
MuSK MG-4	25	NEB	4994	1188	353	1	992	1448	2711
MuSK MG-4	25	PacBio	15162	1924	0	0	1345	0	2257

Supplement Table 4. Counts of reconstructed V(D)J sequences by isotype and clones from sequencing of bulk BCR repertoires and single cell transcriptional profiling.

References

1.   Agius MA, Klodowska-Duda G, Maciejowski M, Potemkowski A, Li J, Patra K, Wesley J, Madani S, Barron G, Katz E et al (2019) Safety and tolerability of inebilizumab (MEDI-551), an anti-CD19 monoclonal antibody, in patients with relapsing forms of multiple sclerosis: Results from a phase 1 randomised, placebo-controlled, escalating intravenous and subcutaneous dose study. Multiple Sclerosis Journal 25: 235-245 Doi 10.1177/1352458517740641

2.   Anolik JH, Barnard J, Owen T, Zheng B, Kemshetti S, Looney RJ, Sanz I (2007) Delayed memory B cell recovery in peripheral blood and lymphoid tissue in systemic lupus erythematosus after B cell depletion therapy. Arthritis Rheum 56: 3044-3056 Doi 10.1002/art.22810

3.   Becerra E, De La Torre I, Leandro MJ, Cambridge G (2017) B cell phenotypes in patients with rheumatoid arthritis relapsing after rituximab: expression of B cell-activating factor-binding receptors on B cell subsets. Clinical and experimental immunology 190: 372-383 Doi 10.1111/cei.13024

4.   Blum S, Gillis D, Brown H, Boyle R, Henderson R, Heyworth-Smith D, Hogan P, Kubler P, Lander C, Limberg N et al (2011) Use and monitoring of low dose rituximab in myasthenia gravis. Journal of neurology, neurosurgery, and psychiatry 82: 659-663 Doi 10.1136/jnnp.2010.220475

5.   Butler A, Hoffman P, Smibert P, Papalexi E, Satija R (2018) Integrating single-cell transcriptomic data across different conditions, technologies, and species. Nature biotechnology 36: 411-420 Doi 10.1038/nbt.4096

6.   Chen D, Blazek M, Ireland S, Ortega S, Kong X, Meeuwissen A, Stowe A, Carter L, Wang Y, Herbst R et al (2014) Single Dose of Glycoengineered Anti-CD19 Antibody (MEDI551) Disrupts Experimental Autoimmune Encephalomyelitis by Inhibiting Pathogenic Adaptive Immune Responses in the Bone Marrow and Spinal Cord while Preserving Peripheral Regulatory Mechanisms. The Journal of Immunology 193: 4823-4832 Doi 10.4049/jimmunol.1401478

7.   Cortés-Vicente E, Rojas-Garcia R, Díaz-Manera J, Querol L, Casasnovas C, Guerrero-Sola A, Muñoz-Blanco JL, Bárcena-Llona JE, Márquez-Infante C, Pardo J et al (2018) The impact of rituximab infusion protocol on the long-term outcome in anti-MuSK myasthenia gravis. Annals of Clinical and Translational Neurology 5: 710-716 Doi https://doi.org/10.1002/acn3.564

8. Cree BAC, Bennett JL, Kim HJ, Weinshenker BG, Pittock SJ, Wingerchuk DM, Fujihara K, Paul F, Cutter GR, Marignier R et al (2019) Inebilizumab for the treatment of neuromyelitis optica spectrum disorder (N-MOmentum): a double-blind, randomised placebo-controlled phase 2/3 trial. Lancet (London, England): Doi 10.1016/S0140-6736(19)31817-3

9. Crickx E, Chappert P, Sokal A, Weller S, Azzaoui I, Vandenberghe A, Bonnard G, Rossi G, Fadeev T, Storck S et al (2021) Rituximab-resistant splenic memory B cells and newly engaged naive B cells fuel relapses in patients with immune thrombocytopenia. Sci Transl Med 13: eabc3961 Doi 10.1126/scitranslmed.abc3961

10. Diaz-Manera J, Martinez-Hernandez E, Querol L, Klooster R, Rojas-Garcia R, Suarez-Calvet X, Munoz-Blanco JL, Mazia C, Straasheijm KR, Gallardo E et al (2012) Long-lasting treatment effect of rituximab in MuSK myasthenia. Neurology 78: 189-193 Doi 10.1212/WNL.0b013e3182407982

11. Ellebrecht CT, Bhoj VG, Nace A, Choi EJ, Mao X, Cho MJ, Di Zenzo G, Lanzavecchia A, Seykora JT, Cotsarelis G et al (2016) Reengineering chimeric antigen receptor T cells for targeted therapy of autoimmune disease. Science (New York, NY) 353: 179-184 Doi 10.1126/science.aaf6756

12. Feng J, Xu H, Cinquina A, Wu Z, Chen Q, Zhang P, Wang X, Shan H, Xu L, Zhang Q et al (2021) Treatment of Aggressive T Cell Lymphoblastic Lymphoma/leukemia Using Anti-CD5 CAR T Cells. Stem cell reviews and reports 17: 652-661 Doi 10.1007/s12015-020-10092-9

13. Fichtner ML, Jiang R, Bourke A, Nowak RJ, O'Connor KC (2020) Autoimmune Pathology in Myasthenia Gravis Disease Subtypes Is Governed by Divergent Mechanisms of Immunopathology. Front Immunol 11: 776 Doi 10.3389/fimmu.2020.00776

14. Fichtner ML, Vieni C, Redler RL, Kolich L, Jiang R, Takata K, Stathopoulos P, Suarez PA, Nowak RJ, Burden SJ et al (2020) Affinity maturation is required for pathogenic monovalent IgG4 autoantibody development in myasthenia gravis. Journal of Experimental Medicine 217: Doi 10.1084/jem.20200513

15. Gadala-Maria D, Yaari G, Uduman M, Kleinstein SH (2015) Automated analysis of high-throughput B-cell sequencing data reveals a high frequency of novel immunoglobulin V gene segment alleles. Proceedings of the National Academy of Sciences of the United States of America: Doi 10.1073/pnas.1417683112

16. Gilhus NE (2016) Myasthenia Gravis. The New England journal of medicine 375: 2570-2581 Doi 10.1056/NEJMra1602678

17. Gomez AM, Stevens JA, Mane-Damas M, Molenaar P, Duimel H, Verheyen F, Cossins J, Beeson D, De Baets MH, Losen M et al (2016) Silencing of Dok-7 in Adult Rat Muscle Increases Susceptibility to Passive Transfer Myasthenia Gravis. The American journal of pathology 186: 2559-2568 Doi 10.1016/j.ajpath.2016.05.025

18. Graus YF, de Baets MH, Parren PW, Berrih-Aknin S, Wokke J, van Breda Vriesman PJ, Burton DR (1997) Human anti-nicotinic acetylcholine receptor recombinant Fab fragments isolated from thymus-derived phage display libraries from myasthenia gravis patients reflect predominant specificities in serum and block the action of pathogenic serum antibodies. J Immunol 158: 1919-1929

19. Guidicelli V, Chaume D, Bodmer J, Müller W, Busin C, Mash S, Bontrop R, Marc L, Malik A, Lefranc MP (1997) IMGT, The International ImMunoGeneTics database. 25: 206-211. Doi: 10.1093/nar/25.1.206.

20. Gupta NT, Adams KD, Briggs AW, Timberlake SC, Vigneault F, Kleinstein SH (2017) Hierarchical Clustering Can Identify B Cell Clones with High Confidence in Ig Repertoire Sequencing Data. J Immunol 198: 2489-2499 Doi 10.4049/jimmunol.1601850

21. Gupta NT, Vander Heiden JA, Uduman M, Gadala-Maria D, Yaari G, Kleinstein SH (2015) Change-O: a toolkit for analyzing large-scale B cell immunoglobulin repertoire sequencing data. Bioinformatics (Oxford, England) 31: 3356-3358 Doi 10.1093/bioinformatics/btv359

22. Guptill JT, Sanders DB, Evoli A (2011) Anti-MuSK antibody myasthenia gravis: clinical findings and response to treatment in two large cohorts. Muscle & nerve 44: 36-40 Doi 10.1002/mus.22006

23. Hao Y, Hao S, Andersen-Nissen E, Mauck WM, 3rd, Zheng S, Butler A, Lee MJ, Wilk AJ, Darby C, Zager M et al (2021) Integrated analysis of multimodal single-cell data. Cell 184: 3573-3587.e3529 Doi 10.1016/j.cell.2021.04.048

24. Hewett K, Sanders DB, Grove RA, Broderick CL, Rudo TJ, Bassiri A, Zvartau-Hind M, Bril V (2018) Randomized study of adjunctive belimumab in participants with generalized myasthenia gravis. Neurology 90: e1425-e1434 Doi 10.1212/wnl.0000000000005323

25. Higuchi O, Hamuro J, Motomura M, Yamanashi Y (2011) Autoantibodies to low-density lipoprotein receptor-related protein 4 in myasthenia gravis. Annals of neurology 69: 418-422 Doi 10.1002/ana.22312

26. Hoch W, McConville J, Helms S, Newsom-Davis J, Melms A, Vincent A (2001) Auto-antibodies to the receptor tyrosine kinase MuSK in patients with myasthenia gravis without acetylcholine receptor antibodies. Nature medicine 7: 365-368. Doi 10.1038/85520

27. Hoehn KB, Pybus OG, Kleinstein SH (2022) Phylogenetic analysis of migration, differentiation, and class switching in B cells. PLoS computational biology 18: e1009885 Doi 10.1371/journal.pcbi.1009885

28. Hoehn KB, Vander Heiden JA, Zhou JQ, Lunter G, Pybus OG, Kleinstein SH (2019) Repertoire-wide phylogenetic models of B cell molecular evolution reveal evolutionary signatures of aging and vaccination. Proceedings of the National Academy of Sciences of the United States of America 116: 22664-22672 Doi 10.1073/pnas.1906020116

29. Huijbers MG, Vergoossen DL, Fillie-Grijpma YE, van Es IE, Koning MT, Slot LM, Veelken H, Plomp JJ, van der Maarel SM, Verschuuren JJ (2019) MuSK myasthenia gravis monoclonal antibodies: Valency dictates pathogenicity. Neurology(R) neuroimmunology & neuroinflammation 6: e547 Doi 10.1212/NXI.0000000000000547

30. Huijbers MG, Zhang W, Klooster R, Niks EH, Friese MB, Straasheijm KR, Thijssen PE, Vrolijk H, Plomp JJ, Vogels P et al (2013) MuSK IgG4 autoantibodies cause myasthenia gravis by inhibiting binding between MuSK and Lrp4. Proceedings of the National Academy of Sciences of the United States of America 110: 20783-20788 Doi 10.1073/pnas.1313944110

31. Jiang R, Fichtner ML, Hoehn KB, Pham MC, Stathopoulos P, Nowak RJ, Kleinstein SH, O'Connor KC (2020) Single-cell repertoire tracing identifies rituximab-resistant B cells during myasthenia gravis relapses. JCI Insight: Doi 10.1172/jci.insight.136471

32. Joly P, Maho-Vaillant M, Prost-Squarcioni C, Hebert V, Houivet E, Calbo S, Caillot F, Golinski ML, Labeille B, Picard-Dahan C et al (2017) First-line rituximab combined with short-term prednisone versus prednisone alone for the treatment of pemphigus (Ritux 3): a prospective, multicentre, parallel-group, open-label randomised trial. Lancet (London, England) 389: 2031-2040 Doi 10.1016/s0140-6736(17)30070-3

33. Keung B, Robeson KR, DiCapua DB, Rosen JB, O'Connor KC, Goldstein JM, Nowak RJ (2013) Long-term benefit of rituximab in MuSK autoantibody myasthenia gravis patients. Journal of neurology, neurosurgery, and psychiatry 84: 1407-1409 Doi 10.1136/jnnp-2012-303664

34. Kim JY, Yang Y, Moon JS, Lee EY, So SH, Lee HS, Park KD, Choi YC (2008) Serum BAFF expression in patients with myasthenia gravis. Journal of neuroimmunology 199: 151-154 Doi 10.1016/j.jneuroim.2008.05.010

35. Koneczny I, Stevens JA, De Rosa A, Huda S, Huijbers MG, Saxena A, Maestri M, Lazaridis K, Zisimopoulou P, Tzartos S et al (2017) IgG4 autoantibodies against muscle-specific kinase undergo Fab-arm exchange in myasthenia gravis patients. Journal of autoimmunity 77: 104-115 Doi 10.1016/j.jaut.2016.11.005

36. Leandro MJ, Cambridge G, Ehrenstein MR, Edwards JCW (2006) Reconstitution of peripheral blood B cells after depletion with rituximab in patients with rheumatoid arthritis. Arthritis & Rheumatism 54: 613-620 Doi https://doi.org/10.1002/art.21617

37. Lee JY, Stathopoulos P, Gupta S, Bannock JM, Barohn RJ, Cotzomi E, Dimachkie MM, Jacobson L, Lee CS, Morbach H et al (2016) Compromised fidelity of B-cell tolerance checkpoints in AChR and MuSK myasthenia gravis. Ann Clin Transl Neurol 3: 443-454 Doi 10.1002/acn3.311

38. Lee L, Draper B, Chaplin N, Philip B, Chin M, Galas-Filipowicz D, Onuoha S, Thomas S, Baldan V, Bughda R et al (2018) An APRIL-based chimeric antigen receptor for dual targeting of BCMA and TACI in multiple myeloma. Blood 131: 746-758 Doi 10.1182/blood-2017-05-781351

39. Lisak RP, Ragheb S (2012) The role of B cell-activating factor in autoimmune myasthenia gravis. Annals of the New York Academy of Sciences 1274: 60-67 Doi 10.1111/j.1749-6632.2012.06842.x

40. Luo XM, Maarschalk E, O'Connell RM, Wang P, Yang L, Baltimore D (2009) Engineering human hematopoietic stem/progenitor cells to produce a broadly neutralizing anti-HIV antibody after in vitro maturation to human B lymphocytes. Blood 113: 1422-1431 Doi 10.1182/blood-2008-09-177139

41. Mackay F, Schneider P (2009) Cracking the BAFF code. Nature reviews Immunology 9: 491-502 Doi 10.1038/nri2572

42. Mamani-Matsuda M, Cosma A, Weller S, Faili A, Staib C, Garçon L, Hermine O, Beyne-Rauzy O, Fieschi C, Pers JO et al (2008) The human spleen is a major reservoir for long-lived vaccinia virus–specific memory B cells. Blood 111: 4653-4659 Doi 10.1182/blood-2007-11-123844

43. Mandel-Brehm C, Fichtner ML, Jiang R, Winton VJ, Vazquez SE, Pham MC, Hoehn KB, Kelleher NL, Nowak RJ, Kleinstein SH et al (2021) Elevated N-Linked Glycosylation of IgG V Regions in Myasthenia Gravis Disease Subtypes. The Journal of Immunology: ji2100225 Doi 10.4049/jimmunol.2100225

44. Marino M, Basile U, Spagni G, Napodano C, Iorio R, Gulli F, Todi L, Provenzano C, Bartoccioni E, Evoli aA (2020) Long lasting rituximab-induced reduction of specific - but not of total- IgG4 in MuSK-positive myasthenia gravis. Frontiers in Immunology doi: 10.3389/fimmu.2020.00613

45. Meffre E, O'Connor KC (2019) Impaired B-cell tolerance checkpoints promote the development of autoimmune diseases and pathogenic autoantibodies. Immunol Rev 292: 90-101 Doi 10.1111/imr.12821

46.   Nielsen R, Yang Z (1998) Likelihood models for detecting positively selected amino acid sites and applications to the HIV-1 envelope gene. Genetics 148: 929-936 Doi 10.1093/genetics/148.3.929

47.   Nowak RJ, Coffey CS, Goldstein JM, Dimachkie MM, Benatar M, Kissel JT, Wolfe GI, Burns TM, Freimer ML, Nations S et al (2021) Phase 2 Trial of Rituximab in Acetylcholine Receptor Antibody-Positive Generalized Myasthenia Gravis: The BeatMG Study. Neurology 98: e376-389 Doi 10.1212/wnl.0000000000013121

48.   Nowak RJ, Dicapua DB, Zebardast N, Goldstein JM (2011) Response of patients with refractory myasthenia gravis to rituximab: a retrospective study. Therapeutic advances in neurological disorders 4: 259-266 Doi 10.1177/1756285611411503

49.   Owens GP, Bennett JL, Lassmann H, O'Connor KC, Ritchie AM, Shearer A, Lam C, Yu X, Birlea M, Dupree C et al (2009) Antibodies produced by clonally expanded plasma cells in multiple sclerosis cerebrospinal fluid. Annals of neurology 65: 639-649 Doi 10.1002/ana.21641

50.   Pevzner A, Schoser B, Peters K, Cosma NC, Karakatsani A, Schalke B, Melms A, Kroger S (2012) Anti-LRP4 autoantibodies in AChR- and MuSK-antibody-negative myasthenia gravis. Journal of neurology 259: 427-435 Doi 10.1007/s00415-011-6194-7

51.   Quach TD, Rodriguez-Zhurbenko N, Hopkins TJ, Guo X, Hernandez AM, Li W, Rothstein TL (2016) Distinctions among Circulating Antibody-Secreting Cell Populations, Including B-1 Cells, in Human Adult Peripheral Blood. J Immunol 196: 1060-1069 Doi 10.4049/jimmunol.1501843

52.   Querol L, Rojas-García R, Diaz-Manera J, Barcena J, Pardo J, Ortega-Moreno A, Sedano MJ, Seró-Ballesteros L, Carvajal A, Ortiz N et al (2015) Rituximab in treatment-resistant CIDP with antibodies against paranodal proteins. Neurology(R) neuroimmunology & neuroinflammation 2: e149 Doi 10.1212/nxi.0000000000000149

53.   Raje N, Berdeja J, Lin Y, Siegel D, Jagannath S, Madduri D, Liedtke M, Rosenblatt J, Maus MV, Turka A et al (2019) Anti-BCMA CAR T-Cell Therapy bb2121 in Relapsed or Refractory Multiple Myeloma. The New England journal of medicine 380: 1726-1737 Doi 10.1056/NEJMoa1817226

54.   Ramwadhdoebe TH, van Baarsen LGM, Boumans MJH, Bruijnen STG, Safy M, Berger FH, Semmelink JF, van der Laken CJ, Gerlag DM, Thurlings RM et al (2019) Effect of rituximab treatment on T and B cell subsets in lymph node biopsies of patients with rheumatoid arthritis. Rheumatology 58: 1075-1085 Doi 10.1093/rheumatology/key428

55. Robeson KR, Kumar A, Keung B, DiCapua DB, Grodinsky E, Patwa HS, Stathopoulos PA, Goldstein JM, O'Connor KC, Nowak RJ (2016) Durability of the Rituximab Response in Acetylcholine Receptor Autoantibody-Positive Myasthenia Gravis. JAMA Neurol: Doi 10.1001/jamaneurol.2016.4190

56. Rodgaard A, Nielsen FC, Djurup R, Somnier F, Gammeltoft S (1987) Acetylcholine receptor antibody in myasthenia gravis: predominance of IgG subclasses 1 and 3. Clinical and experimental immunology 67: 82-88

57. Samy E, Wax S, Huard B, Hess H, Schneider P (2017) Targeting BAFF and APRIL in systemic lupus erythematosus and other antibody-associated diseases. Int Rev Immunol 36: 3-19 Doi 10.1080/08830185.2016.1276903

58. Sarantopoulos S, Stevenson KE, Kim HT, Washel WS, Bhuiya NS, Cutler CS, Alyea EP, Ho VT, Soiffer RJ, Antin JH et al (2011) Recovery of B-cell homeostasis after rituximab in chronic graft-versus-host disease. Blood 117: 2275-2283 Doi 10.1182/blood-2010-10-307819

59. Scadding GK, Vincent A, Newsom-Davis J, Henry K (1981) Acetylcholine receptor antibody synthesis by thymic lymphocytes: correlation with thymic histology. Neurology 31: 935-943

60. Schiopu E, Chatterjee S, Hsu V, Flor A, Cimbora D, Patra K, Yao W, Li J, Streicher K, McKeever K et al (2016) Safety and tolerability of an anti-CD19 monoclonal antibody, MEDI-551, in subjects with systemic sclerosis: a phase I, randomized, placebo-controlled, escalating single-dose study. Arthritis Research & Therapy 18: 131 Doi 10.1186/s13075-016-1021-2

61. Sellam J, Miceli-Richard C, Gottenberg JE, Ittah M, Lavie F, Lacabaratz C, Gestermann N, Proust A, Lambotte O, Mariette X (2007) Decreased B cell activating factor receptor expression on peripheral lymphocytes associated with increased disease activity in primary Sjögren's syndrome and systemic lupus erythematosus. Annals of the rheumatic diseases 66: 790-797 Doi 10.1136/ard.2006.065656

62. Sng J, Ayoglu B, Chen JW, Schickel J-N, Ferre EMN, Glauzy S, Romberg N, Hoenig M, Cunningham-Rundles C, Utz PJ et al (2019) AIRE expression controls the peripheral selection of autoreactive B cells. Sci Immunol 4: eaav6778 Doi 10.1126/sciimmunol.aav6778

63. Stathopoulos P, Kumar A, Heiden JAV, Pascual-Goni E, Nowak RJ, O'Connor KC (2018) Mechanisms underlying B cell immune dysregulation and autoantibody production in MuSK myasthenia gravis. Annals of the New York Academy of Sciences 1412: 154-165 Doi 10.1111/nyas.13535

64.   Stathopoulos P, Kumar A, Nowak RJ, O'Connor KC (2017) Autoantibody-producing plasmablasts after B cell depletion identified in muscle-specific kinase myasthenia gravis. JCI Insight 2: e94263-e94275 Doi 10.1172/jci.insight.94263

65.   Stohl W, Scholz JL, Cancro MP (2011) Targeting BLyS in rheumatic disease: the sometimes-bumpy road from bench to bedside. Curr Opin Rheumatol 23: 305-310 Doi 10.1097/BOR.0b013e328344c15e

66.   Su K-Y, Watanabe A, Yeh C-H, Kelsoe G, Kuraoka M (2016) Efficient Culture of Human Naive and Memory B Cells for Use as APCs. J Immunol 197: 4163-4176 Doi 10.4049/jimmunol.1502193

67.   Takata K, Stathopoulos P, Cao M, Mane-Damas M, Fichtner ML, Benotti ES, Jacobson L, Waters P, Irani SR, Martinez-Martinez P et al (2019) Characterization of pathogenic monoclonal autoantibodies derived from muscle-specific kinase myasthenia gravis patients. JCI Insight 4: Doi 10.1172/jci.insight.127167

68.   Triplett JD, Hardy TA, Riminton DS, Chu SYK, Reddel SW (2019) Association between musk antibody concentrations and the myasthenia gravis composite score in 3 patients: A marker of relapse? Muscle & nerve 60: 307-311Doi 10.1002/mus.26609

69.   Tse N, Morsch M, Ghazanfari N, Cole L, Visvanathan A, Leamey C, Phillips WD (2014) The neuromuscular junction: measuring synapse size, fragmentation and changes in synaptic protein density using confocal fluorescence microscopy. J Vis Exp: Doi 10.3791/52220

70.   Turner JS, O'Halloran JA, Kalaidina E, Kim W, Schmitz AJ, Zhou JQ, Lei T, Thapa M, Chen RE, Case JB et al (2021) SARS-CoV-2 mRNA vaccines induce persistent human germinal centre responses. Nature 596: 109-113 Doi 10.1038/s41586-021-03738-2

71.   Vander Heiden JA, Yaari G, Uduman M, Stern JN, O'Connor KC, Hafler DA, Vigneault F, Kleinstein SH (2014) pRESTO: a toolkit for processing high-throughput sequencing raw reads of lymphocyte receptor repertoires. Bioinformatics (Oxford, England) 30: 1930-1932 Doi 10.1093/bioinformatics/btu138

72.   Vazquez-Lombardi R, Nevoltris D, Luthra A, Schofield P, Zimmermann C, Christ D (2018) Transient expression of human antibodies in mammalian cells. Nature Protocols 13: 99-117 Doi 10.1038/nprot.2017.126

73.   Vergoossen DLE, Plomp JJ, Gstöttner C, Fillié-Grijpma YE, Augustinus R, Verpalen R, Wuhrer M, Parren P, Dominguez-Vega E, van der Maarel SM et al (2021) Functional monovalency amplifies the pathogenicity of anti-MuSK IgG4 in myasthenia gravis. Proceedings of the National Academy of

Sciences of the United States of America 118: Doi 10.1073/pnas.2020635118

74. Vincent A (2002) Unravelling the pathogenesis of myasthenia gravis. Nature reviews Immunology 2: 797-804 Doi 10.1038/nri916

75. Wardemann H, Yurasov S, Schaefer A, Young JW, Meffre E, Nussenzweig MC (2003) Predominant autoantibody production by early human B cell precursors. Science (New York, NY) 301: 1374-1377 Doi 10.1126/science.1086907

76. Wickham H (2016) ggplot2: Elegant Graphics for Data Analysis Springer-Verlag New York, City

77. Willcox HN, Newsom-Davis J, Calder LR (1984) Cell types required for anti-acetylcholine receptor antibody synthesis by cultured thymocytes and blood lymphocytes in myasthenia gravis. Clinical and experimental immunology 58: 97-106

78. Wrammert J, Smith K, Miller J, Langley WA, Kokko K, Larsen C, Zheng NY, Mays I, Garman L, Helms C et al (2008) Rapid cloning of high-affinity human monoclonal antibodies against influenza virus. Nature 453: 667-671 Doi: 10.1038/nature06890.

79. Yaari G, Vander Heiden JA, Uduman M, Gadala-Maria D, Gupta N, Stern JN, O'Connor KC, Hafler DA, Laserson U, Vigneault F et al (2013) Models of somatic hypermutation targeting and substitution based on synonymous mutations from high-throughput immunoglobulin sequencing data. Front Immunol 4: 358 Doi 10.3389/fimmu.2013.00358

80. Ye J, Ma N, Madden TL, Ostell JM (2013) IgBLAST: an immunoglobulin variable domain sequence analysis tool. Nucleic acids research 41: W34-40 Doi 10.1093/nar/gkt382

81. Yi JS, Guptill JT, Stathopoulos P, Nowak RJ, O'Connor KC (2018) B cells in the pathophysiology of myasthenia gravis. Muscle & nerve 57: 172-184 Doi 10.1002/mus.25973

82. Yu G, Lam TT, Zhu H, Guan Y (2018) Two Methods for Mapping and Visualizing Associated Data on Phylogeny Using Ggtree. Molecular biology and evolution 35: 3041-3043 Doi 10.1093/molbev/msy194

83. Yu Z, Zhang M, Jing H, Chen P, Cao R, Pan J, Luo B, Yu Y, Quarles BM, Xiong W et al (2021) Characterization of LRP4/Agrin Antibodies From a Patient with Myasthenia Gravis. Neurology: Doi 10.1212/wnl.0000000000012463

84.   Yurasov S, Wardemann H, Hammersen J, Tsuiji M, Meffre E, Pascual V, Nussenzweig MC (2005) Defective B cell tolerance checkpoints in systemic lupus erythematosus. The Journal of experimental medicine 201: 703-711 Doi 10.1084/jem.20042251

4. GENERAL DISCUSSION, LIMITATIONS, CONCLUSION AND OUTLOOK

4.1. GENERAL DISCUSSION

In this thesis, we aimed to investigate how individual autoantibodies contribute to disease pathology and the immunomechanisms of relapse after anti-CD20-mediated BCDT in MuSK MG. We had previously identified a population of circulating B cells (plasmablasts) that produce MuSK autoantibodies [143]. Having demonstrated that circulating plasmablasts contributed to MuSK autoantibody production, we next sought a means of more directly isolating these important cells. We produced a fluorescently labelled bait antigens (a tetramer and a monomer) that could identify and direct the sorting of rare autoantibody-expressing B cells from patient-derived blood samples [135, 178]. We used these rare cells to produce six recombinant human MuSK MG mAbs so that we could more deeply understand the mechanisms of disease pathology. These mAbs have been instrumental in uncovering novel aspects of MG immunopathology. MG autoantibodies can recognize unique epitopes on the MuSK receptor and affect neuromuscular transmission by inhibiting AChR clustering. We further investigated the B cell repertoire in MuSK MG patients pre- and post-anti-CD20-mediated BCDT and we traced disease-relevant B cell clones in longitudinal samples demonstrating that anti-CD20-mediated BCDT is not fully effective at eliminating disease-relevant B cells [177, 178]. The titer of MuSK was observed to increase before clinically detectable relapse [173]. We found that pathogenic B cell clones were present in patients through anti-CD20-mediated BCDT and reemerged months prior clinical

relapse together with the MuSK titer making both a potential biomarker for relapse prediction.

4.1.1. HUMAN MUSK MONOCLONAL AUTOANTIBODIES

We developed bait antigens to enrich for MuSK-specific B cells in the circulation. We were able to isolate six MuSK-specific B cells using this approach. We found that all six antibodies could bind to MuSK over a wide range of concentrations, and we used an array of assays including cell-based assay, ELISA, radioimmunoassay, and mouse muscle staining to validate the specificity of our antibodies. It is important to note that we also isolated many other antibodies that showed reactivity towards MuSK. These autoantibodies had some common features. First, these mAbs only detected MuSK at the highest concentration of 10 µg/ml and showed no reactivity at lower concentrations in contrast to the six MuSK-specific mAbs. Thus, we set our cut-off for the determination of antigen-specificity and biological relevance at 1 µg/ml. Second, these mAbs had variable regions that contained no or negligible levels of mutations indicating that these mAbs did not go through antigen-driven affinity maturation. These germline-encoded mAb are probably derived from B cells within the naïve repertoire that show a broader reactivity against a variety of antigens including MuSK. Indeed, we tested some of these antibodies for polyreactivity (data not shown) and found that these mAbs are polyspecifc and able to detect other antigens as well. Thirdly, several of these autoantibodies where of the IgM subclass. It was previously shown that IgM subclass antibodies increase the rate of false-positive signals in CBAs detecting MOG and MuSK and that the usage of IgG-specific secondaries for detection

reduced these unspecific signals [179, 180]. Five of our six mAbs originated from IgG subclass antibodies with accumulated SHM in their variable regions which is consistent with the characteristics of pathogenic autoantibodies isolated in other autoimmune diseases including neuromyelitis optica (NMO), pemphigus vulgaris (PV), and AChR MG [106, 181, 182]. The MuSK-specific mAb MuSK3B, however, was originally of the IgM subclass with germline-encoded variable regions. MuSK3B did not show any pathogenic capacity in contrast to the other five MuSK mAbs. The functional relevance of non-pathogenic mAbs in the immunopathology of MuSK MG remains unknown.

In a study not included in this thesis, we found that the germline-encoded precursor mAbs of MuSK1A, MuSK1B and MuSK3-28 recognized the autoantigen MuSK indicating that B cells from the naïve B cell repertoire are self-reactive in these patients [149]. We found that the germline precursor of 6C6 similarly recognized MuSK, while the precursor of 2E6 showed polyspecific properties that disappeared after the process of affinity maturation and the acquisition of SHM. MuSK mAbs are mainly of the IgG4 subclass which can undergo a process termed Fab-arm exchange resulting in functionally monovalent antibodies [140, 144, 146-148]. We had previously found that the acquisition of SHM through the process of affinity maturation enabled the mature mAbs MuSK1A and MuSK1B to reach a high affinity threshold thought to be indispensable for pathogenic capacity in the context of Fab-arm exchange [149]. Here we found that the mature 6C6 showed strong pathogenic capacities as a Fab, while we could not see any increase of pathogenic capacity for 2E6 as a Fab. Although MuSK autoantibodies are mostly of the IgG4 subclass

222

[140, 144, 146], we found that 2 out of the 6 MuSK mAbs were originally IgG3 or IgM. This is in concordance with other findings were MuSK mAbs were produced that were originally of IgG1 subclass [136]. Thus, complement may potentially contribute to the immunopathology in a subcohort of MuSK MG patients. Our cumulative findings indicate that the characteristics of individual MuSK mAbs are heterogenous.

This heterogeneity can also be observed in the different epitopes these mAbs recognize on the MuSK receptor. The MuSK receptor contains three Ig-like domains (1-3) and a frizzled domain on the extracellular domain [183, 184]. We found two mAbs that recognized the Ig-like domain 1 and three mAbs that recognized the Ig-like domain 2 which is consistent with previous findings that most MuSK mAbs detect the Ig-like domain 1 and Ig-like domain 2 [9, 146]. Autoantibodies targeting the Ig-like domain 1 interfere directly with the interaction of MuSK with LRP4 and inhibit subsequently the clustering of the AChR [139, 185]. The mechanism of how antibodies directed at the Ig-like domain 2 interfere with the MuSK/LRP4 pathway is currently not known and leaves room for future investigations. The antibody that detected the frizzled domain on the MuSK receptor did not show any pathogenic properties (MuSK3B). Although the MuSK titer correlates generally well with clinical disease severity [144, 186], it is interesting to note that some non-pathogenic MuSK-binding autoantibodies are present in the circulation of MuSK patients with no known function other than receptor recognition.

We noticed that MuSK-reactive B cells were extremely rare within the circulation, even at the time of relapse. Plasmablasts are an important source of autoantibodies in MuSK MG [143] and most of our mAbs originated from plasmablasts. These mAbs were isolated from patients that experienced relapse after BCDT which is associated with expanded plasmablast and memory B cell populations within the circulation [143, 174, 175]. MuSK-reactive plasmablasts seem, however, to be only a minor subset within the expanded post-anti-CD20-mediated BCDT relapse plasmablast repertoire. The scarcity of MuSK-reactive B cells was further observed by other groups [136] and is not specific for the patients in our biorepository. Quite the reverse can be observed in infectious diseases like COVID and influenza where the immune system reacts to foreign antigens [187, 188]. Although autoantibody-producing plasmablasts are increased similarly to MuSK MG, these plasmablast repertoires consist of several different expanded clones specific for and directed toward the corresponding viral antigen [187, 188]. The antigen-specificity and function of the majority of expanded plasmablast clones at the time of post-anti-CD20-mediated BCDT relapse in MuSK MG is at this time not understood and the subject of future investigations.

4.1.2. B CELL DEPLETION THERAPY

We used two approaches to investigate the immunomechanisms of relapse after anti-CD20-mediated BCDT in MuSK MG. First, we compared the B cell repertoire of intrapatient samples pre- and post-relapse and found that some B cell clones survive anti-CD20-mediated BCDT. We found that these persistent clones were

mainly memory B cells and antibody-secreting cells (ASCs) with unique features in comparison to non-persistent clones. Second, we traced pathogenic B cell clones of our MuSK mAbs in longitudinal samples and found that some pathogenic B cell clones persevere in patients over several years through BCDT.

We found several features that were characteristic for persistent B cell clones. The surface expression level of CD20 is important for the efficiency of anti-CD20-mediated BCDT [189]. ASCs have low expression levels of CD20 [151, 190]. We found in our study that persistent memory B cells and ASCs express low levels of CD20. We found additionally that plasmablast populations at the time of relapse express varying levels of CD20. Thus, subsets of plasmablasts are potential targets for anti-CD20-mediated BCDT at the time of relapse. Indeed, recurring anti-CD20-mediated BCDT in our patient led to remission and almost non-detectable antibody levels suggesting that pathogenic clones do express CD20 at the time of remission and are successfully targeted with anti-CD20-mediated BCDT. Furthermore, BCDT-resistant memory B cell subsets were shown to reside in tissue [174, 191-193]. We also noticed that persistent B cell clones upregulated genes associated with tissue homing indicating an origin from tissue-resident B cells. One of these tissue homing genes (ITGA4) was upregulated in plasmablasts at the time of relapse (data not shown) as well. We further detected a pathogenic clone and its clonal variants that reemerged over several years though BCDT. We noticed that the clonal variants accumulated SHM in their variable regions indicating continuous affinity maturation in tissue-based germinal centers. Nevertheless, anti-CD20-mediated BCDT was demonstrated to be effective in eliminating antigen-specific B

225

cells and antibodies from lymph nodes in neuromyelitis optica spectrum disorder [194]. Thus, tissue-based location seems not to be a prerequisite for BCDT evasion. We further found that persistent memory B cell clones were more expanded than non-persistent clones. Increased clonal expansion was shown to be associated with a worse response to anti-CD20-mediated BCDT in PV and IgM anti-myelin-associated glycoprotein peripheral neuropathy [195-197]. These clonally expanded B cell subsets might on the one hand be easier to detect within the circulation in the blood and on the other hand be harder to eliminate due to distribution in different compartments and to various phenotypes present at the time of treatment. The BAFF/APRIL system is associated with B cell survival [198]. It consists of the three receptors BAFF-R, BCMA and TACI and the two ligands BAFF and APRIL [199]. The expression of these receptors differs during the development of B cells [151]. BAFF-R is expressed on B cells from the stage of immature B cells to plasmablasts, while TACI and BCMA are mainly expressed on plasmablasts and plasma cells [151]. High levels of BAFF are associated with autoimmunity [200, 201] and reduced BAFF-R expression is found in patients relapsing from anti-CD20-mediated BCDT in RA [202]. Low BAFF-R expression is also associated with poor response to anti-CD20-mediated BCDT in graft-versus-host disease [203]. We, indeed, found reduced expression levels of BAFF-R in persistent clones and the plasmablast repertoire at the time of relapse and further observed high levels of TACI and BCMA. The BAFF/APRIL-system is involved in IgG and IgA class switch recombination [204-206]. IgA is predominantly secreted in the gut and IgA subclass switched B cells are the main B cell population within the gut [207, 208].

We found that ASCs, plasmablasts and subsets of memory B cells were mainly of the IgA subclass at the time of relapse. This is on the one hand indicative of a gut-based origin and might on the other hand be the consequence of the overexpression of BAFF/APRIL-receptors. Thus, we found that persistent clones are more clonally expanded, express proteins associated with prior tissue homing and B cell survival and express less CD20 on their cell surface.

The persistence of B cell clones through BCDT is not a unique feature of MuSK MG; B cell clones were shown to persist through BCDT in several autoimmune disorders including Sjögren's syndrome, systemic lupus erythematosus, systemic sclerosis, and ANCA-associated vasculitis (AAV) [209-211]. Furthermore, anti-CD20-mediated BCDT is not solely affecting B cells, subsets of T cells express CD20 on their surface [212-214] and these CD20-expressing T cells were shown to be depleted with anti-CD20-mediated therapy in MS [214, 215]. In addition, therapies affect the B cell repertoire differently highlighting the potential beneficial impact of combination therapy. Persistent B cells have different phenotypes after mycophenolate mofetil and anti-CD20-mediated BCDT in SLE and AAV patients [210]. Moreover, alternative approaches of BCDT show promising effects and are currently investigated in the context of malignant B cell pathologies and autoimmune therapies. These therapies target CD19 [216-219], the BAFF/APRIL-system [220, 221], proteins associated with the cell-cycle and apoptosis (proteasome inhibitors) [222-224], B cell receptor signaling (Bruton Tyrosine Kinase (BTK) Inhibitors) [225-227] or use chimeric antigen (CAR) or chimeric autoantibody (CAAR) receptor T cell therapies [228-232] including anti-BCMA [228-230] which is

also investigated in the context of MG (ClinicalTrials.gov identifier: NCT04146051), anti-CD19 [232] (ClinicalTrials.gov identifier: NCT03030976) and most recently anti-MuSK which showed first beneficial effects in mouse model for MG [231]. Future investigations into the phenotype of persistent clones and the effect of these therapies on the B cell repertoire will help to make informed decisions on the application of combination therapies.

4.2. LIMITATIONS

The work of this thesis is, of course, not without limitations. First, the number of patients used in these studies is limited. The six mAbs generated for these studies are derived from four different patients. Therefore, the results derived from these studies might only present a small sub-cohort of MuSK MG patients and extrapolation of these results to all MuSK MG patients' needs to be done with caution. Furthermore, all four of these patients were women. The immune system and immune response of men and women differs [233, 234]. Thus, one needs to be careful when generalizing these results. Nevertheless, our cohort is representative for MuSK MG as women are predominantly affected by this debilitating disease [16-19]. Second, we analyzed the gene expression of B cell subsets only after anti-CD20-mediated BCDT. Therefore, we cannot identify markers and expression signatures that predispose B cell subsets for survival of BCDT. Additionally, we do not know whether the B cell signatures that we identified are the consequence of BCDT or if they show the phenotype of an inherent B cell population with better resistance to BCDT. Third, the mRNA transcriptome does not always correlate well with surface expression of proteins. We could, however, show that the surface and mRNA expression of CD20 correlate well. Fourth, B cell repertoire tracing is based on analyzing the IGH V(D)J sequence. Although the diversity of the IGH V(D)J sequence generally enables the identification of clonal relationships, one needs to take under consideration that false positives are possible [235-237]. Fifth, we identified the clonal variants of the MuSK mAb 2E6 using the IGH V(D)J sequence and can therefore not make any assumptions on

the corresponding light-chain of these clonal variants. To make sure that our results are a good estimation of the corresponding light-chain we expressed the mAbs of the clonal variants with both the mature light-chain of 2E6 and the germline-encoded unmutated common ancestor light-chain. Sixth, we tested the pathogenicity of all six MuSK mAbs using an *in vitro* AChR clustering assay. Future studies will show how these autoantibodies behave *in vivo* using mouse models.

4.3. CONCLUSION AND OUTLOOK

We developed bait antigens to isolate MuSK-specific B cell and generated six MuSK-specific mAbs. These mAbs have been instrumental in uncovering novel aspects of MG immunopathology. We found that MG autoantibodies can recognize unique epitopes of MuSK (Ig-like domain 2) and disrupt the neuromuscular transmission by inhibiting clustering of the AChR. We were further able to trace MuSK mAbs in patients over years through anti-CD20-mediated BCDT and we studied B cells that persisted through anti-CD20-mediated BCDT and found unique phenotypic features of these cells. Thus, we were able to gain more insight into the immunopathology of MuSK MG and into the immunomechanism of relapse after anti-CD20-mediated BCDT.

We additionally want to further understand the molecular and pathogenic properties of human-derived MuSK mAbs. It will be interesting to investigate the molecular mechanism of how Ig-like domain2-specific MuSK mAbs interrupt the clustering of the AChR. We evaluated the pathogenic properties of our MuSK mAbs using *in vitro* approaches and plan to test their pathogenicity *in vivo* in mouse models. Many new therapies with direct effects on B cells are currently being tested in MG patient trials and other autoimmune diseases or B cell malignancies. Future studies focusing on how these therapies effect the B cell repertoire will give valuable insight into the efficacy of therapies and possible candidates for combination therapy.

5. REFERENCES

1. Vincent, A., Unravelling the pathogenesis of myasthenia gravis. Nat Rev Immunol, 2002. 2(10): p. 797-804.

2. Gilhus, N.E., Myasthenia Gravis. N Engl J Med, 2016. 375(26): p. 2570-2581.

3. Bubuioc, A.M., et al., The epidemiology of myasthenia gravis. J Med Life, 2021. 14(1): p. 7-16.

4. Phillips, L.H., The epidemiology of myasthenia gravis. Semin Neurol, 2004. 24(1): p. 17-20.

5. Nel, M. and J. Heckmann, Myasthenia Gravis and Related Disorders. Myasthenia Gravis Relat Disord, 2018.

6. Meriggioli, M.N. and D.B. Sanders, Autoimmune myasthenia gravis: emerging clinical and biological heterogeneity. Lancet Neurol, 2009. 8(5): p. 475-90.

7. Zhang, J., et al., Effects of thymectomy on late-onset non-thymomatous myasthenia gravis: systematic review and meta-analysis. Orphanet J Rare Dis, 2021. 16(1): p. 232.

8. Vincent, A., D. Beeson, and B. Lang, Molecular targets for autoimmune and genetic disorders of neuromuscular transmission. Eur J Biochem, 2000. 267(23): p. 6717-28.

9. Hoch, W., et al., Auto-antibodies to the receptor tyrosine kinase MuSK in patients with myasthenia gravis without acetylcholine receptor antibodies. Nat Med, 2001. 7(3): p. 365-8.

10. Lehnerer, S., et al., Burden of disease in myasthenia gravis: taking the patient's perspective. J Neurol, 2022. 269(6): p. 3050-3063.

11. Higuchi, O., et al., Autoantibodies to low-density lipoprotein receptor-related protein 4 in myasthenia gravis. Ann Neurol, 2011. 69(2): p. 418-22.

12. Yu, Z., et al., Characterization of LRP4/Agrin Antibodies From a Patient with Myasthenia Gravis. Neurology, 2021.

13. Pevzner, A., et al., Anti-LRP4 autoantibodies in AChR- and MuSK-antibody-negative myasthenia gravis. J Neurol, 2012. 259(3): p. 427-35.

14.   Simpson, J.F., Myasthenia gravis. An analysis of 295 cases. Acta Neurol Scand, 1996. 42: p. 1-27.

15.   Schwab, R.S. and C.C. Leland, SEX AND AGE IN MYASTHENIA GRAVIS AS CRITICAL FACTORS IN INCIDENCE AND REMISSION. Journal of the American Medical Association, 1953. 153(14): p. 1270-1273.

16.   Guptill, J.T., D.B. Sanders, and A. Evoli, Anti-MuSK antibody myasthenia gravis: clinical findings and response to treatment in two large cohorts. Muscle Nerve, 2011. 44(1): p. 36-40.

17.   Rodolico, C., et al., MuSK-Associated Myasthenia Gravis: Clinical Features and Management. Front Neurol, 2020. 11: p. 660.

18.   Evoli, A. and J. Lindstrom, Myasthenia gravis with antibodies to MuSK: another step toward solving mystery? Neurology, 2011. 77(20): p. 1783-4.

19.   Evoli, A., et al., Myasthenia gravis with antibodies to MuSK: an update. Ann N Y Acad Sci, 2018. 1412(1): p. 82-89.

20.   Grob, D., et al., Lifetime course of myasthenia gravis. Muscle Nerve, 2008. 37(2): p. 141-9.

21.   Wendell, L.C. and J.M. Levine, Myasthenic crisis. The Neurohospitalist, 2011. 1(1): p. 16-22.

22.   Schroeter, M., G. Thayssen, and J. Kaiser, Myasthenia Gravis – Exacerbation and Crisis. Neurology International Open, 2018. 02: p. E10-E15.

23.   Dendrou, C.A., L. Fugger, and M.A. Friese, Immunopathology of multiple sclerosis. Nat Rev Immunol, 2015. 15(9): p. 545-58.

24.   Mok, C.C. and C.S. Lau, Pathogenesis of systemic lupus erythematosus. J Clin Pathol, 2003. 56(7): p. 481-90.

25.   Yi, J.S., et al., B cells in the pathophysiology of myasthenia gravis. Muscle Nerve, 2018. 57(2): p. 172-184.

26.   Paschou, S.A., et al., On type 1 diabetes mellitus pathogenesis. Endocr Connect, 2018. 7(1): p. R38-r46.

27.   Phillips, W.D. and A. Vincent, Pathogenesis of myasthenia gravis: update on disease types, models, and mechanisms. F1000Res, 2016. 5.

28.   Chia, R., et al., Identification of genetic risk loci and prioritization of genes and pathways for myasthenia gravis: a genome-wide association study. Proc Natl Acad Sci U S A, 2022. 119(5).

29.   Gregersen, P.K., et al., Risk for myasthenia gravis maps to a (151) Pro-->Ala change in TNIP1 and to human leukocyte antigen-B*08. Ann Neurol, 2012. 72(6): p. 927-35.

30.   Renton, A.E., et al., A genome-wide association study of myasthenia gravis. JAMA Neurol, 2015. 72(4): p. 396-404.

31.   Waterhouse, P., et al., Lymphoproliferative disorders with early lethality in mice deficient in Ctla-4. Science, 1995. 270(5238): p. 985-8.

32.   Tivol, E.A., et al., Loss of CTLA-4 leads to massive lymphoproliferation and fatal multiorgan tissue destruction, revealing a critical negative regulatory role of CTLA-4. Immunity, 1995. 3(5): p. 541-7.

33.   Cheng, S., et al., Expression and function of HLA-DQ8 (DQA1*0301/DQB1*0302) genes in transgenic mice. Eur J Immunogenet, 1996. 23(1): p. 15-20.

34.   Regueiro, C., et al., HLA-B*08 Identified as the Most Prominently Associated Major Histocompatibility Complex Locus for Anti-Carbamylated Protein Antibody-Positive/Anti-Cyclic Citrullinated Peptide-Negative Rheumatoid Arthritis. Arthritis Rheumatol, 2021. 73(6): p. 963-969.

35.   Shamilov, R. and B.J. Aneskievich, TNIP1 in Autoimmune Diseases: Regulation of Toll-like Receptor Signaling. J Immunol Res, 2018. 2018: p. 3491269.

36.   Stanford, S.M. and N. Bottini, PTPN22: the archetypal non-HLA autoimmunity gene. Nat Rev Rheumatol, 2014. 10(10): p. 602-11.

37.   Ramanujam, R., et al., Utilizing twins concordance rates to infer the predisposition to myasthenia gravis. Twin Res Hum Genet, 2011. 14(2): p. 129-36.

38.   Glass, D.J., et al., Agrin acts via a MuSK receptor complex. Cell, 1996. 85(4): p. 513-23.

39.   Ohkawara, B., M. Ito, and K. Ohno, Secreted Signaling Molecules at the Neuromuscular Junction in Physiology and Pathology. Int J Mol Sci, 2021. 22(5).

40.   Hoffmann, S., et al., Complement deposition at the neuromuscular junction in seronegative myasthenia gravis. Acta Neuropathol, 2020. 139(6): p. 1119-1122.

41.   Masi, G., et al., The clinical need for clustered AChR cell-based assay testing of seronegative MG. J Neuroimmunol, 2022. 367: p. 577850.

42.   Devic, P., et al., Antibodies to clustered acetylcholine receptor: expanding the phenotype. Eur J Neurol, 2014. 21(1): p. 130-4.

43.   Vincent, A., et al., Antibodies identified by cell-based assays in myasthenia gravis and associated diseases. Ann N Y Acad Sci, 2012. 1274: p. 92-8.

44.   Sheng, J.R., K. Rezania, and B. Soliven, Impaired regulatory B cells in myasthenia gravis. J Neuroimmunol, 2016. 297: p. 38-45.

45.   Zhang, X., et al., The Presence of Survivin on B Cells from Myasthenia Gravis Patients and the Potential of an Antibody to a Modified Survivin Peptide to Alleviate Weakness in an Animal Model. J Immunol, 2020. 205(7): p. 1743-1751.

46.   Pillai, S., H. Mattoo, and A. Cariappa, B cells and autoimmunity. Curr Opin Immunol, 2011. 23(6): p. 721-31.

47.   Meffre, E. and K.C. O'Connor, Impaired B-cell tolerance checkpoints promote the development of autoimmune diseases and pathogenic autoantibodies. Immunol Rev, 2019. 292(1): p. 90-101.

48.   Nemazee, D., Mechanisms of central tolerance for B cells. Nat Rev Immunol, 2017. 17(5): p. 281-294.

49.   Tonegawa, S., et al., Evidence for somatic generation of antibody diversity. Proc Natl Acad Sci U S A, 1974. 71(10): p. 4027-31.

50.   Tonegawa, S., Somatic generation of antibody diversity. Nature, 1983. 302(5909): p. 575-81.

51.   Halverson, R., R.M. Torres, and R. Pelanda, Receptor editing is the main mechanism of B cell tolerance toward membrane antigens. Nature Immunology, 2004. 5(6): p. 645-650.

52.   Tiegs, S.L., D.M. Russell, and D. Nemazee, Receptor editing in self-reactive bone marrow B cells. J Exp Med, 1993. 177(4): p. 1009-20.

53.   Goodnow, C.C., et al., Altered immunoglobulin expression and functional silencing of self- reactive B lymphocytes in transgenic mice. Nature, 1988. 334(6184): p. 676-682.

54.   Hippen, K.L., et al., In vivo assessment of the relative contributions of deletion, anergy, and editing to B cell self-tolerance. J Immunol, 2005. 175(2): p. 909-16.

55.   Chan, T.D., et al., Elimination of germinal-center-derived self-reactive B cells is governed by the location and concentration of self-antigen. Immunity, 2012. 37(5): p. 893-904.

56.   Young, C., A.W.Y. Lau, and D.L. Burnett, B cells in the balance: Offsetting self-reactivity avoidance with protection against foreign. Frontiers in Immunology, 2022. 13.

57.   Yurasov, S., et al., Defective B cell tolerance checkpoints in systemic lupus erythematosus. J Exp Med, 2005. 201(5): p. 703-11.

58.   Samuels, J., et al., Impaired early B cell tolerance in patients with rheumatoid arthritis. J Exp Med, 2005. 201(10): p. 1659-67.

59.   Glauzy, S., et al., Defective Early B Cell Tolerance Checkpoints in Sjogren's Syndrome Patients. Arthritis Rheumatol, 2017. 69(11): p. 2203-2208.

60.   Cotzomi, E., et al., Early B cell tolerance defects in neuromyelitis optica favour anti-AQP4 autoantibody production. Brain, 2019. 142(6): p. 1598-1615.

61.   Kinnunen, T., et al., Specific peripheral B cell tolerance defects in patients with multiple sclerosis. J Clin Invest, 2013. 123(6): p. 2737-41.

62.   Lee, J.Y., et al., Compromised fidelity of B-cell tolerance checkpoints in AChR and MuSK myasthenia gravis. Ann Clin Transl Neurol, 2016. 3(6): p. 443-54.

63.   Keller, C.W., et al., Impaired B cell Expression of the Inhibitory Fcγ Receptor IIB in Myasthenia Gravis. Ann Neurol, 2022.

64.   Vander Heiden, J.A., et al., Dysregulation of B Cell Repertoire Formation in Myasthenia Gravis Patients Revealed through Deep Sequencing. J Immunol, 2017. 198(4): p. 1460-1473.

65. Lisak, R.P., et al., In vitro synthesis of antibodies to acetylcholine receptor by peripheral blood mononuclear cells of patients with myasthenia gravis. Neurology, 1983. 33(5): p. 604-8.

66. Lisak, R.P., et al., In vitro synthesis of antibodies to acetylcholine receptor by peripheral blood cells: role of suppressor T cells in normal subjects. Neurology, 1984. 34(6): p. 802-5.

67. Authier, F.J., et al., Transient myasthenia gravis during HIV infection. Muscle Nerve, 1995. 18(8): p. 914-6.

68. Nath, A., et al., Immune studies in human immunodeficiency virus infection with myasthenia gravis: a case report. Neurology, 1990. 40(4): p. 581-3.

69. Cao, Y., et al., Autoreactive T Cells from Patients with Myasthenia Gravis Are Characterized by Elevated IL-17, IFN-gamma, and GM-CSF and Diminished IL-10 Production. J Immunol, 2016.

70. Wang, Z.Y., et al., T-cell recognition of muscle acetylcholine receptor subunits in generalized and ocular myasthenia gravis. Neurology, 1998. 50(4): p. 1045-54.

71. Schaffert, H., et al., IL-17-producing CD4 T cells contribute to the loss of B-cell tolerance in experimental autoimmune myasthenia gravis. Eur J Immunol, 2015.

72. Vignali, D.A.A., L.W. Collison, and C.J. Workman, How regulatory T cells work. Nature Reviews Immunology, 2008. 8(7): p. 523-532.

73. Balandina, A., et al., Functional defect of regulatory CD4(+)CD25+ T cells in the thymus of patients with autoimmune myasthenia gravis. Blood, 2005. 105(2): p. 735-41.

74. Thiruppathi, M., et al., Impaired regulatory function in circulating CD4(+)CD25(high)CD127(low/-) T cells in patients with myasthenia gravis. Clin Immunol, 2012. 145(3): p. 209-23.

75. Zhu, Y., L. Zou, and Y.C. Liu, T follicular helper cells, T follicular regulatory cells and autoimmunity. Int Immunol, 2016. 28(4): p. 173-9.

76. Ma, C.S. and E.K. Deenick, Human T follicular helper (Tfh) cells and disease. Immunol Cell Biol, 2014. 92(1): p. 64-71.

77. Wollenberg, I., et al., Regulation of the germinal center reaction by Foxp3+ follicular regulatory T cells. J Immunol, 2011. 187(9): p. 4553-60.

78.   Linterman, M.A., et al., Foxp3+ follicular regulatory T cells control the germinal center response. Nat Med, 2011. 17(8): p. 975-82.

79.   Chung, Y., et al., Follicular regulatory T cells expressing Foxp3 and Bcl-6 suppress germinal center reactions. Nat Med, 2011. 17(8): p. 983-8.

80.   Luo, C., et al., Expansion of circulating counterparts of follicular helper T cells in patients with myasthenia gravis. J Neuroimmunol, 2013. 256(1-2): p. 55-61.

81.   Saito, R., et al., Altered expression of chemokine receptor CXCR5 on T cells of myasthenia gravis patients. J Neuroimmunol, 2005. 170(1-2): p. 172-8.

82.   Wen, Y., et al., Imbalance of circulating CD4(+)CXCR5(+)FOXP3(+) Tfr-like cells and CD4(+)CXCR5(+)FOXP3(-) Tfh-like cells in myasthenia gravis. Neurosci Lett, 2016. 630: p. 176-182.

83.   Ingelfinger, F., et al., Single-cell profiling of myasthenia gravis identifies a pathogenic T cell signature. Acta Neuropathol, 2021. 141(6): p. 901-915.

84.   Newsom-Davis, J., N. Willcox, and L. Calder, Thymus cells in myasthenia gravis selectively enhance production of anti-acetylcholine-receptor antibody by autologous blood lymphocytes. N Engl J Med, 1981. 305(22): p. 1313-8.

85.   Leprince, C., et al., Thymic B cells from myasthenia gravis patients are activated B cells. Phenotypic and functional analysis. J Immunol, 1990. 145(7): p. 2115-22.

86.   Gradolatto, A., et al., Both Treg cells and Tconv cells are defective in the Myasthenia gravis thymus: roles of IL-17 and TNF-alpha. J Autoimmun, 2014. 52: p. 53-63.

87.   Mittag, T., et al., Detection of anti-acetylcholine receptor factors in serum and thymus from patients with myasthenia gravis. N Engl J Med, 1976. 294(13): p. 691-4.

88.   Vincent, A., et al., In-vitro synthesis of anti-acetylcholine-receptor antibody by thymic lymphocytes in myasthenia gravis. Lancet, 1978. 1(8059): p. 305-7.

89.   Levinson, A.I. and L.M. Wheatley, The thymus and the pathogenesis of myasthenia gravis. Clin Immunol Immunopathol, 1996. 78(1): p. 1-5.

90.   Khan, M.A. and F. Anjum, Thymic Hyperplasia, in StatPearls. 2022, StatPearls Publishing. Copyright © 2022, StatPearls Publishing LLC.: Treasure Island (FL).

91.   Cron, M.A., et al., Thymus involvement in early-onset myasthenia gravis. Ann N Y Acad Sci, 2018. 1412(1): p. 137-145.

92.   Wakkach, A., et al., Expression of acetylcholine receptor genes in human thymic epithelial cells: implications for myasthenia gravis. J Immunol, 1996. 157(8): p. 3752-60.

93.   Matsumoto, Y., et al., Primary cultures of human myasthenia gravis thymus and normal thymus. Studies of cell morphology, cell proliferative pattern and localization of alpha-bungarotoxin binding sites on cultured thymic cells. J Neurol Sci, 1986. 75(2): p. 121-33.

94.   Romi, F., Thymoma in myasthenia gravis: from diagnosis to treatment. Autoimmune Dis, 2011. 2011: p. 474512.

95.   Kirchner, T., et al., Pathogenesis of myasthenia gravis. Acetylcholine receptor-related antigenic determinants in tumor-free thymuses and thymic epithelial tumors. Am J Pathol, 1988. 130(2): p. 268-80.

96.   Wolfe, G.I., et al., Long-term effect of thymectomy plus prednisone versus prednisone alone in patients with non-thymomatous myasthenia gravis: 2-year extension of the MGTX randomised trial. Lancet Neurol, 2019. 18(3): p. 259-268.

97.   Yu, S., et al., Eight-year follow-up of patients with myasthenia gravis after thymectomy. Acta Neurol Scand, 2015. 131(2): p. 94-101.

98.   Kaufman, A.J., et al., Thymectomy for Myasthenia Gravis : Complete Stable Remission and Associated Prognostic Factors in Over 1000 Cases. Seminars in Thoracic and Cardiovascular Surgery, 2016. 28(2): p. 561-568.

99.   Jiang, R., et al., Thymus-derived B cell clones persist in the circulation after thymectomy in myasthenia gravis. Proc Natl Acad Sci U S A, 2020. 117(48): p. 30649-30660.

100.   Clifford, K.M., et al., Thymectomy may not be associated with clinical improvement in MuSK myasthenia gravis. Muscle Nerve, 2019. 59(4): p. 404-410.

101.   Leite, M.I., et al., Fewer thymic changes in MuSK antibody-positive than in MuSK antibody-negative MG. Ann Neurol, 2005. 57(3): p. 444-8.

102.   Aoki, S., et al., Anti-LRP4 Antibody-associated Myasthenia Gravis with a Rare Complication of Thymoma Successfully Treated by Thymectomy. Intern Med, 2020. 59(9): p. 1219-1222.

103.   Koneczny, I., et al., Characterization of the thymus in Lrp4 myasthenia gravis: Four cases. Autoimmunity Reviews, 2019. 18(1): p. 50-55.

104.   Willcox, H.N., J. Newsom-Davis, and L.R. Calder, Cell types required for anti-acetylcholine receptor antibody synthesis by cultured thymocytes and blood lymphocytes in myasthenia gravis. Clin Exp Immunol, 1984. 58(1): p. 97-106.

105.   Scadding, G.K., et al., Acetylcholine receptor antibody synthesis by thymic lymphocytes: correlation with thymic histology. Neurology, 1981. 31(8): p. 935-43.

106.   Graus, Y.F., et al., Human anti-nicotinic acetylcholine receptor recombinant Fab fragments isolated from thymus-derived phage display libraries from myasthenia gravis patients reflect predominant specificities in serum and block the action of pathogenic serum antibodies. J Immunol, 1997. 158(4): p. 1919-29.

107.   Saxena, A., et al., Characterization of an anti-fetal AChR monoclonal antibody isolated from a myasthenia gravis patient. Sci Rep, 2017. 7(1): p. 14426.

108.   Makino, T., et al., Analysis of peripheral B cells and autoantibodies against the anti-nicotinic acetylcholine receptor derived from patients with myasthenia gravis using single-cell manipulation tools. PLoS One, 2017. 12(10): p. e0185976.

109.   Rose, N., et al., Receptor clustering and pathogenic complement activation in myasthenia gravis depend on synergy between antibodies with multiple subunit specificities. Acta Neuropathol, 2022.

110.   Toyka, K.V., et al., Myasthenia gravis: passive transfer from man to mouse. Science, 1975. 190(4212): p. 397-9.

111.   Melber, D., Maternal-fetal transmission of myasthenia gravis with acetylcholine-receptor antibody. N Engl J Med, 1988. 318(15): p. 996.

112.   Vernet-der Garabedian, B., et al., Association of neonatal myasthenia gravis with antibodies against the fetal acetylcholine receptor. J Clin Invest, 1994. 94(2): p. 555-9.

113.   Donaldson, J.O., et al., Antiacetylcholine receptor antibody in neonatal myasthenia gravis. Am J Dis Child, 1981. 135(3): p. 222-6.

114.   Rodgaard, A., et al., Acetylcholine receptor antibody in myasthenia gravis: predominance of IgG subclasses 1 and 3. Clin Exp Immunol, 1987. 67(1): p. 82-8.

115.   Nakano, S. and A.G. Engel, Myasthenia gravis: quantitative immunocytochemical analysis of inflammatory cells and detection of complement membrane attack complex at the end-plate in 30 patients. Neurology, 1993. 43(6): p. 1167-72.

116.   Lefvert, A.K., S. Cuenoud, and B.W. Fulpius, Binding properties and subclass distribution of anti-acetylcholine receptor antibodies in myasthenia gravis. J Neuroimmunol, 1981. 1(1): p. 125-35.

117.   Engel, A.G., E.H. Lambert, and F.M. Howard, Immune complexes (IgG and C3) at the motor end-plate in myasthenia gravis: ultrastructural and light microscopic localization and electrophysiologic correlations. Mayo Clin Proc, 1977. 52(5): p. 267-80.

118.   Engel, A.G., et al., Passively transferred experimental autoimmune myasthenia gravis. Sequential and quantitative study of the motor end-plate fine structure and ultrastructural localization of immune complexes (IgG and C3), and of the acetylcholine receptor. Neurology, 1979. 29(2): p. 179-88.

119.   Howard, J.F., Jr., et al., Safety and efficacy of eculizumab in anti-acetylcholine receptor antibody-positive refractory generalised myasthenia gravis (REGAIN): a phase 3, randomised, double-blind, placebo-controlled, multicentre study. Lancet Neurol, 2017. 16(12): p. 976-986.

120.   Muppidi, S., et al., Long-term safety and efficacy of eculizumab in generalized myasthenia gravis. Muscle Nerve, 2019. 60(1): p. 14-24.

121.   Howard, J.F., Jr., et al., Clinical Effects of the Self-administered Subcutaneous Complement Inhibitor Zilucoplan in Patients With Moderate to Severe Generalized Myasthenia Gravis: Results of a Phase 2 Randomized, Double-Blind, Placebo-Controlled, Multicenter Clinical Trial. JAMA neurology, 2020. 77(5): p. 582-592.

122.   Hara, H., et al., Detection and characterization of blocking-type anti-acetylcholine receptor antibodies in sera from patients with myasthenia gravis. Clin Chem, 1993. 39(10): p. 2053-7.

123. Whiting, P., A. Vincent, and J. Newsom-Davis, Monoclonal antibodies to Torpedo acetylcholine receptor. Characterisation of antigenic determinants within the cholinergic binding site. Eur J Biochem, 1985. 150(3): p. 533-9.

124. Almon, R.R., C.G. Andrew, and S.H. Appel, Serum globulin in myasthenia gravis: inhibition of alpha-bungarotoxin binding to acetylcholine receptors. Science, 1974. 186(4158): p. 55-7.

125. Drachman, D.B., et al., Myasthenic antibodies cross-link acetylcholine receptors to accelerate degradation. N Engl J Med, 1978. 298(20): p. 1116-22.

126. Loutrari, H., A. Kokla, and S.J. Tzartos, Passive transfer of experimental myasthenia gravis via antigenic modulation of acetylcholine receptor. European Journal of Immunology, 1992. 22(9): p. 2449-2452.

127. Lefvert, A.K., et al., Determination of acetylcholine receptor antibody in myasthenia gravis: clinical usefulness and pathogenetic implications. J Neurol Neurosurg Psychiatry, 1978. 41(5): p. 394-403.

128. Lindstrom, J.M., et al., Antibody to acetylcholine receptor in myasthenia gravis. Prevalence, clinical correlates, and diagnostic value. Neurology, 1976. 26(11): p. 1054-9.

129. Tindall, R.S., Humoral immunity in myasthenia gravis: clinical correlations of anti-receptor antibody avidity and titer. Ann N Y Acad Sci, 1981. 377: p. 316-31.

130. Vincent, A. and J. Newsom Davis, Anti-acetylcholine receptor antibodies. J Neurol Neurosurg Psychiatry, 1980. 43(7): p. 590-600.

131. Aurangzeb, S., et al., Relationship between anti-acetylcholine receptor antibody titres and severity of myasthenia gravis. J Pak Med Assoc, 2009. 59(5): p. 289-92.

132. Kaminski, H.J. and J. Denk, Corticosteroid Treatment-Resistance in Myasthenia Gravis. Frontiers in Neurology, 2022. 13.

133. Kojima, Y., et al., Rate of change in acetylcholine receptor antibody levels predicts myasthenia gravis outcome. J Neurol Neurosurg Psychiatry, 2021. 92(9): p. 963-968.

134. Vincent, A., Using AChR antibody titres to predict treatment responses in myasthenia gravis. J Neurol Neurosurg Psychiatry, 2021. 92(9): p. 915.

135.   Takata, K., et al., Characterization of pathogenic monoclonal autoantibodies derived from muscle-specific kinase myasthenia gravis patients. JCI insight, 2019. 4(12): p. e127167.

136.   Huijbers, M.G., et al., MuSK myasthenia gravis monoclonal antibodies: Valency dictates pathogenicity. Neurol Neuroimmunol Neuroinflamm, 2019. 6(3): p. e547.

137.   Jennings, C.G., S.M. Dyer, and S.J. Burden, Muscle-specific trk-related receptor with a kringle domain defines a distinct class of receptor tyrosine kinases. Proceedings of the National Academy of Sciences of the United States of America, 1993. 90(7): p. 2895-2899.

138.   Otsuka, K., et al., Collagen Q and anti-MuSK autoantibody competitively suppress agrin/LRP4/MuSK signaling. Sci Rep, 2015. 5: p. 13928.

139.   Huijbers, M.G., et al., MuSK IgG4 autoantibodies cause myasthenia gravis by inhibiting binding between MuSK and Lrp4. Proc Natl Acad Sci U S A, 2013. 110(51): p. 20783-8.

140.   Klooster, R., et al., Muscle-specific kinase myasthenia gravis IgG4 autoantibodies cause severe neuromuscular junction dysfunction in mice. Brain, 2012. 135(Pt 4): p. 1081-101.

141.   Plomp, J.J., et al., Pathogenic IgG4 subclass autoantibodies in MuSK myasthenia gravis. Ann N Y Acad Sci, 2012. 1275: p. 114-22.

142.   Cole, R.N., et al., Anti-MuSK patient antibodies disrupt the mouse neuromuscular junction. Ann Neurol, 2008. 63(6): p. 782-9.

143.   Stathopoulos, P., et al., Autoantibody-producing plasmablasts after B cell depletion identified in muscle-specific kinase myasthenia gravis. JCI Insight, 2017. 2(17): p. e94263-e94275.

144.   Niks, E.H., et al., Clinical fluctuations in MuSK myasthenia gravis are related to antigen-specific IgG4 instead of IgG1. J Neuroimmunol, 2008. 195(1-2): p. 151-6.

145.   Ohta, K., et al., Clinical and experimental features of MuSK antibody positive MG in Japan. Eur J Neurol, 2007. 14(9): p. 1029-34.

146.   McConville, J., et al., Detection and characterization of MuSK antibodies in seronegative myasthenia gravis. Ann Neurol, 2004. 55(4): p. 580-4.

147. van der Neut Kolfschoten, M., et al., Anti-inflammatory activity of human IgG4 antibodies by dynamic Fab arm exchange. Science, 2007. 317(5844): p. 1554-7.

148. Koneczny, I., et al., IgG4 autoantibodies against muscle-specific kinase undergo Fab-arm exchange in myasthenia gravis patients. J Autoimmun, 2017. 77: p. 104-115.

149. Fichtner, M.L., et al., Affinity maturation is required for pathogenic monovalent IgG4 autoantibody development in myasthenia gravis. Journal of Experimental Medicine, 2020. 217(12).

150. Vergoossen, D.L.E., et al., Functional monovalency amplifies the pathogenicity of anti-MuSK IgG4 in myasthenia gravis. Proc Natl Acad Sci U S A, 2021. 118(13).

151. Krumholz, M., et al., B cells and antibodies in multiple sclerosis pathogenesis and therapy. Nat Rev Neurol, 2012. 8(11): p. 613-23.

152. Maloney, D.G., et al., Phase I clinical trial using escalating single-dose infusion of chimeric anti-CD20 monoclonal antibody (IDEC-C2B8) in patients with recurrent B-cell lymphoma. Blood, 1994. 84(8): p. 2457-66.

153. Nadler, L.M., et al., Serotherapy of a Patient with a Monoclonal Antibody Directed against a Human Lymphoma-associated Antigen1. Cancer Research, 1980. 40(9): p. 3147-3154.

154. McLaughlin, P., et al., Rituximab chimeric anti-CD20 monoclonal antibody therapy for relapsed indolent lymphoma: half of patients respond to a four-dose treatment program. Journal of Clinical Oncology, 1998. 16(8): p. 2825-2833.

155. Hauser, S.L., et al., B-cell depletion with rituximab in relapsing-remitting multiple sclerosis. N Engl J Med, 2008. 358(7): p. 676-88.

156. Edwards, J.C., et al., Efficacy of B-cell-targeted therapy with rituximab in patients with rheumatoid arthritis. N Engl J Med, 2004. 350(25): p. 2572-81.

157. Joly, P., et al., First-line rituximab combined with short-term prednisone versus prednisone alone for the treatment of pemphigus (Ritux 3): a prospective, multicentre, parallel-group, open-label randomised trial. Lancet, 2017. 389(10083): p. 2031-2040.

158. Diaz-Manera, J., et al., Long-lasting treatment effect of rituximab in MuSK myasthenia. Neurology, 2012. 78(3): p. 189-93.

159.   Querol, L., et al., Antibodies to contactin-1 in chronic inflammatory demyelinating polyneuropathy. Ann Neurol, 2012.

160.   Nowak, R.J., et al., Phase 2 Trial of Rituximab in Acetylcholine Receptor Antibody-Positive Generalized Myasthenia Gravis: The BeatMG Study. Neurology, 2021. 98(4): p. e376-89.

161.   Landon-Cardinal, O., et al., Efficacy of Rituximab in Refractory Generalized anti-AChR Myasthenia Gravis. J Neuromuscul Dis, 2018. 5(2): p. 241-249.

162.   Bastakoti, S., et al., Rituximab in the Management of Refractory Myasthenia Gravis and Variability of Its Efficacy in Anti-MuSK Positive and Anti-AChR Positive Myasthenia Gravis. Cureus, 2021. 13(11): p. e19416.

163.   Piehl, F., et al., Efficacy and Safety of Rituximab for New-Onset Generalized Myasthenia Gravis: The RINOMAX Randomized Clinical Trial. JAMA Neurol, 2022. 79(11): p. 1105-1112.

164.   Fichtner, M.L., et al., Autoimmune Pathology in Myasthenia Gravis Disease Subtypes Is Governed by Divergent Mechanisms of Immunopathology. Front Immunol, 2020. 11: p. 776.

165.   Obaid, A.H., et al., Heterogeneity of Acetylcholine Receptor Autoantibody-Mediated Complement Activity in Patients With Myasthenia Gravis. Neurol Neuroimmunol Neuroinflamm, 2022. 9(4).

166.   Sieb, J.P., Myasthenia gravis: an update for the clinician. Clin Exp Immunol, 2014. 175(3): p. 408-18.

167.   Evoli, A., et al., Heterogeneity in myasthenia gravis: considerations for disease management. Expert Rev Clin Immunol, 2021. 17(7): p. 761-771.

168.   Querol, L., et al., Rituximab in treatment-resistant CIDP with antibodies against paranodal proteins. Neurol Neuroimmunol Neuroinflamm, 2015. 2(5): p. e149.

169.   Marino, M., et al., Long lasting rituximab-induced reduction of specific - but not of total- IgG4 in MuSK-positive myasthenia gravis. Frontiers in Immunology, 2020. doi: 10.3389/fimmu.2020.00613

170.   Nowak, R.J., et al., Response of patients with refractory myasthenia gravis to rituximab: a retrospective study. Therapeutic Advances in Neurological Disorders, 2011. 4(5): p. 259-266.

171. Robeson, K.R., et al., Durability of the Rituximab Response in Acetylcholine Receptor Autoantibody-Positive Myasthenia Gravis. JAMA Neurol, 2016.

172. Blum, S., et al., Use and monitoring of low dose rituximab in myasthenia gravis. J Neurol Neurosurg Psychiatry, 2011. 82(6): p. 659-63.

173. Triplett, J.D., et al., Association between musk antibody concentrations and the myasthenia gravis composite score in 3 patients: A marker of relapse? Muscle Nerve, 2019. 60(3): p. 307-311.

174. Anolik, J.H., et al., Delayed memory B cell recovery in peripheral blood and lymphoid tissue in systemic lupus erythematosus after B cell depletion therapy. Arthritis Rheum, 2007. 56(9): p. 3044-56.

175. Adlowitz, D.G., et al., Expansion of Activated Peripheral Blood Memory B Cells in Rheumatoid Arthritis, Impact of B Cell Depletion Therapy, and Biomarkers of Response. PLoS One, 2015. 10(6): p. e0128269.

176. Koul, R., A. Al Futaisi, and R. Abdwani, Rituximab in severe seronegative juvenile myasthenia gravis: review of the literature. Pediatr Neurol, 2012. 47(3): p. 209-12.

177. Jiang, R., et al., Single-cell repertoire tracing identifies rituximab-resistant B cells during myasthenia gravis relapses. JCI Insight, 2020.

178. Fichtner, M.L., et al., Reemergence of pathogenic, autoantibody-producing B cell clones in myasthenia gravis following B cell depletion therapy. Acta Neuropathologica Communications, 2022. 10(1): p. 154.

179. Huda, S., et al., IgG-specific cell-based assay detects potentially pathogenic MuSK-Abs in seronegative MG. Neurol Neuroimmunol Neuroinflamm, 2017. 4(4): p. e357.

180. Waters, P., et al., MOG cell-based assay detects non-MS patients with inflammatory neurologic disease. Neurol Neuroimmunol Neuroinflamm, 2015. 2(3): p. e89.

181. Bennett, J.L., et al., Intrathecal pathogenic anti-aquaporin-4 antibodies in early neuromyelitis optica. Ann Neurol, 2009. 66(5): p. 617-29.

182. Di Zenzo, G., et al., Pemphigus autoantibodies generated through somatic mutations target the desmoglein-3 cis-interface. J Clin Invest, 2012. 122(10): p. 3781-90.

183. Stiegler, A.L., S.J. Burden, and S.R. Hubbard, Crystal structure of the agrin-responsive immunoglobulin-like domains 1 and 2 of the receptor tyrosine kinase MuSK. J Mol Biol, 2006. 364(3): p. 424-33.

184. Stiegler, A.L., S.J. Burden, and S.R. Hubbard, Crystal structure of the frizzled-like cysteine-rich domain of the receptor tyrosine kinase MuSK. J Mol Biol, 2009. 393(1): p. 1-9.

185. Huijbers, M.G., et al., Longitudinal epitope mapping in MuSK myasthenia gravis: implications for disease severity. J Neuroimmunol, 2016. 291: p. 82-8.

186. Bartoccioni, E., et al., Anti-MuSK antibodies: correlation with myasthenia gravis severity. Neurology, 2006. 67(3): p. 505-7.

187. Turner, J.S., et al., SARS-CoV-2 mRNA vaccines induce persistent human germinal centre responses. Nature, 2021. 596(7870): p. 109-113.

188. Wrammert, J., et al., Rapid cloning of high-affinity human monoclonal antibodies against influenza virus. Nature, 2008. 453(7195): p. 667-71.

189. Singh, V., et al., Surface levels of CD20 determine anti-CD20 antibodies mediated cell death in vitro. PLoS One, 2014. 9(11): p. e111113.

190. Pavlasova, G. and M. Mraz, The regulation and function of CD20: an "enigma" of B-cell biology and targeted therapy. Haematologica, 2020. 105(6): p. 1494-1506.

191. Ramwadhdoebe, T.H., et al., Effect of rituximab treatment on T and B cell subsets in lymph node biopsies of patients with rheumatoid arthritis. Rheumatology, 2019. 58(6): p. 1075-1085.

192. Leandro, M.J., et al., Reconstitution of peripheral blood B cells after depletion with rituximab in patients with rheumatoid arthritis. Arthritis & Rheumatism, 2006. 54(2): p. 613-620.

193. Mamani-Matsuda, M., et al., The human spleen is a major reservoir for long-lived vaccinia virus–specific memory B cells. Blood, 2008. 111(9): p. 4653-4659.

194. Damato, V., et al., Rituximab abrogates aquaporin-4–specific germinal center activity in patients with neuromyelitis optica spectrum disorders. Proceedings of the National Academy of Sciences, 2022. 119(24): p. e2121804119.

195. Nakou, M., et al., Rituximab therapy reduces activated B cells in both the peripheral blood and bone marrow of patients with rheumatoid arthritis: depletion of memory B cells correlates with clinical response. Arthritis Research & Therapy, 2009. 11(4): p. R131.

196. Colliou, N., et al., Long-term remissions of severe pemphigus after rituximab therapy are associated with prolonged failure of desmoglein B cell response. Sci Transl Med, 2013. 5(175): p. 175ra30.

197. Maurer, M.A., et al., Rituximab induces clonal expansion of IgG memory B-cells in patients with inflammatory central nervous system demyelination. J Neuroimmunol, 2016. 290: p. 49-53.

198. Mackay, F., et al., BAFF AND APRIL: a tutorial on B cell survival. Annu Rev Immunol, 2003. 21: p. 231-64.

199. Samy, E., et al., Targeting BAFF and APRIL in systemic lupus erythematosus and other antibody-associated diseases. Int Rev Immunol, 2017. 36(1): p. 3-19.

200. Mackay, F. and P. Schneider, Cracking the BAFF code. Nat Rev Immunol, 2009. 9(7): p. 491-502.

201. Steri, M., et al., Overexpression of the Cytokine BAFF and Autoimmunity Risk. N Engl J Med, 2017. 376(17): p. 1615-1626.

202. Becerra, E., et al., B cell phenotypes in patients with rheumatoid arthritis relapsing after rituximab: expression of B cell-activating factor-binding receptors on B cell subsets. Clin Exp Immunol, 2017. 190(3): p. 372-383.

203. Sarantopoulos, S., et al., Recovery of B-cell homeostasis after rituximab in chronic graft-versus-host disease. Blood, 2011. 117(7): p. 2275-83.

204. Castigli, E., et al., TACI and BAFF-R mediate isotype switching in B cells. The Journal of experimental medicine, 2005. 201(1): p. 35-39.

205. Cerutti, A., The regulation of IgA class switching. Nature Reviews Immunology, 2008. 8(6): p. 421-434.

206. He, B., et al., The transmembrane activator TACI triggers immunoglobulin class switching by activating B cells through the adaptor MyD88. Nat Immunol, 2010. 11(9): p. 836-45.

207. Pabst, O. and E. Slack, IgA and the intestinal microbiota: the importance of being specific. Mucosal Immunology, 2020. 13(1): p. 12-21.

208. Mora, J.R. and U.H. von Andrian, Differentiation and homing of IgA-secreting cells. Mucosal Immunol, 2008. 1(2): p. 96-109.

209. Hershberg, U., et al., Persistence and selection of an expanded B-cell clone in the setting of rituximab therapy for Sjögren's syndrome. Arthritis Research & Therapy, 2014. 16(1): p. R51.

210. Bashford-Rogers, R.J.M., et al., Analysis of the B cell receptor repertoire in six immune-mediated diseases. Nature, 2019. 574(7776): p. 122-126.

211. de Bourcy, C.F.A., et al., Dynamics of the human antibody repertoire after B cell depletion in systemic sclerosis. Sci Immunol, 2017. 2(15).

212. Vlaming, M., et al., CD20 positive CD8 T cells are a unique and transcriptionally-distinct subset of T cells with distinct transmigration properties. Scientific Reports, 2021. 11(1): p. 20499.

213. Lee, A.Y.S., CD20(+) T cells: an emerging T cell subset in human pathology. Inflamm Res, 2022. 71(10-11): p. 1181-1189.

214. Schuh, E., et al., Features of Human CD3+CD20+ T Cells. J Immunol, 2016. 197(4): p. 1111-7.

215. Palanichamy, A., et al., Rituximab efficiently depletes increased CD20-expressing T cells in multiple sclerosis patients. J Immunol, 2014. 193(2): p. 580-586.

216. Chen, D., et al., Single Dose of Glycoengineered Anti-CD19 Antibody (MEDI551) Disrupts Experimental Autoimmune Encephalomyelitis by Inhibiting Pathogenic Adaptive Immune Responses in the Bone Marrow and Spinal Cord while Preserving Peripheral Regulatory Mechanisms. The Journal of Immunology, 2014. 193(10): p. 4823-4832.

217. Agius, M.A., et al., Safety and tolerability of inebilizumab (MEDI-551), an anti-CD19 monoclonal antibody, in patients with relapsing forms of multiple sclerosis: Results from a phase 1 randomised, placebo-controlled, escalating intravenous and subcutaneous dose study. Multiple Sclerosis Journal, 2019. 25(2): p. 235-245.

218. Cree, B.A.C., et al., Inebilizumab for the treatment of neuromyelitis optica spectrum disorder (N-MOmentum): a double-blind, randomised placebo-controlled phase 2/3 trial. Lancet, 2019.

219. Schiopu, E., et al., Safety and tolerability of an anti-CD19 monoclonal antibody, MEDI-551, in subjects with systemic sclerosis: a phase I,

randomized, placebo-controlled, escalating single-dose study. Arthritis Research & Therapy, 2016. 18(1): p. 131.

220. Stohl, W., J.L. Scholz, and M.P. Cancro, Targeting BLyS in rheumatic disease: the sometimes-bumpy road from bench to bedside. Curr Opin Rheumatol, 2011. 23(3): p. 305-10.

221. Merrill, J.T., et al., Efficacy and Safety of Atacicept in Patients With Systemic Lupus Erythematosus: Results of a Twenty-Four-Week, Multicenter, Randomized, Double-Blind, Placebo-Controlled, Parallel-Arm, Phase IIb Study. Arthritis Rheumatol, 2018. 70(2): p. 266-276.

222. Alexander, T., et al., The proteasome inhibitior bortezomib depletes plasma cells and ameliorates clinical manifestations of refractory systemic lupus erythematosus. Ann Rheum Dis, 2015. 74(7): p. 1474-8.

223. Gomez, A.M., et al., Proteasome inhibition with bortezomib depletes plasma cells and specific autoantibody production in primary thymic cell cultures from early-onset myasthenia gravis patients. J Immunol, 2014. 193(3): p. 1055-63.

224. Teicher, B.A., et al., The proteasome inhibitor PS-341 in cancer therapy. Clin Cancer Res, 1999. 5(9): p. 2638-45.

225. Herman, S.E., et al., Bruton tyrosine kinase represents a promising therapeutic target for treatment of chronic lymphocytic leukemia and is effectively targeted by PCI-32765. Blood, 2011. 117(23): p. 6287-96.

226. Pal Singh, S., F. Dammeijer, and R.W. Hendriks, Role of Bruton's tyrosine kinase in B cells and malignancies. Mol Cancer, 2018. 17(1): p. 57.

227. Ringheim, G.E., M. Wampole, and K. Oberoi, Bruton's Tyrosine Kinase (BTK) Inhibitors and Autoimmune Diseases: Making Sense of BTK Inhibitor Specificity Profiles and Recent Clinical Trial Successes and Failures. Front Immunol, 2021. 12: p. 662223.

228. Lee, L., et al., An APRIL-based chimeric antigen receptor for dual targeting of BCMA and TACI in multiple myeloma. Blood, 2018. 131(7): p. 746-758.

229. Raje, N., et al., Anti-BCMA CAR T-Cell Therapy bb2121 in Relapsed or Refractory Multiple Myeloma. N Engl J Med, 2019. 380(18): p. 1726-1737.

230. Zhang, W., et al., Treatment of Systemic Lupus Erythematosus using BCMA-CD19 Compound CAR. Stem Cell Rev Rep, 2021. 17(6): p. 2120-2123.

231. Oh, S., et al., Precision targeting of autoantigen-specific B cells in muscle-specific tyrosine kinase myasthenia gravis with chimeric autoantibody receptor T cells. Nature Biotechnology, 2023.

232. Ying, Z., et al., A safe and potent anti-CD19 CAR T cell therapy. Nat Med, 2019. 25(6): p. 947-953.

233. Klein, S.L. and K.L. Flanagan, Sex differences in immune responses. Nat Rev Immunol, 2016. 16(10): p. 626-38.

234. Ghazeeri, G., L. Abdullah, and O. Abbas, Immunological differences in women compared with men: overview and contributing factors. Am J Reprod Immunol, 2011. 66(3): p. 163-9.

235. Gupta, N.T., et al., Hierarchical Clustering Can Identify B Cell Clones with High Confidence in Ig Repertoire Sequencing Data. J Immunol, 2017. 198(6): p. 2489-2499.

236. Nouri, N. and S.H. Kleinstein, A spectral clustering-based method for identifying clones from high-throughput B cell repertoire sequencing data. Bioinformatics, 2018. 34(13): p. i341-i349.

237. Zhou, J.Q. and S.H. Kleinstein, Cutting Edge: Ig H Chains Are Sufficient to Determine Most B Cell Clonal Relationships. The Journal of Immunology, 2019. 203(7): p. 1687.

6.   IMPACT

Society and patients. The number of MG patients in Europe is estimated at 56.000 to 123.000 [1] and at around 60.000 patients in the United States [2]. The incidence and prevalence of MG have risen over the last century [3, 4]. Patients present clinically with skeletal muscle weakness and fatigability due to interrupted signaling from the nerves to the muscles [5]; ~ 30% of patients report that they do not achieve an acceptable disease status [6]. Around 20% of patients experience at least one MG crisis in their lifetime and require hospitalization and mechanical ventilation [7]; around 12 % of these patients die [8]. The burden of disease is high both individually and socially [9], despite the orphan disease status as a rare disease and fundamental treatability. The high burden of disease is the consequence of MG being a chronic disease that usually has to be treated for life; this is important as MG can affect young patients between 20-30 years of age and children [3]. The standard therapies are mostly insufficiently effective, slow and have a lot of side effects. Over the last couple of years progress has been made by the introduction of new therapies that either aim to prevent effector functions, reduce the amount of circulating Abs or directly target B cells (see summary in review [10, 11]). Modern therapies are very expensive and most of them have to be used regularly which has a huge economic impact. Most MG patients have an estimated annual treatment related cost of 1-20,000 $ [12] and these new expensive therapies will most likely increase these annual costs. More effective treatments will reduce the burden of disease which will directly reduce the economic impact of MG and increase the number of patients that can work who before were not able to go to

work because of a high burden of disease. **Therefore, our study of the immunomechanism of relapse after anti-CD20 mediated BCDT for this doctoral thesis aims to ensure the well-being of patients. We found a possible mechanism of relapse and hope that this knowledge will help to develop new and more (cost-) effective therapies.**

Scientists and Physicians. MG presents a unique and rich opportunity for studying autoimmunity, not only because of the anticipated benefits for patients, but also because B cells and autoantibodies (Abs) play a direct role in the disease pathology [13]. **Thus, MG may serve as a prototypic disorder for studying immunopathological mechanisms of other autoantibody-mediated diseases including pemphigus vulgaris, NMOSD, and CIDP.** The studies of chapter I-III in this thesis address an intractable problem in this neuromuscular autoimmune disease; that is, defining the mechanisms of cellular immune-mediated pathology for a debilitating disease for which many disease mechanisms remain poorly understood. We produced six unique MuSK monoclonals and found that MuSK mAbs recognizing the Ig-like domain 2 on the MuSK receptor can interrupt the MuSK/LRP4 pathway. These mAbs have provided unprecedented insight into the details of MG autoimmune mechanisms. We were further able to provide new insights into the immunomechanisms of relapse after BCDT. We found that some B cells persist through BCDT indicating that a subset of B cells at the time of relapse re-populate the circulation from a pre-existing pool of B cells. Variable expression levels of CD20 and CD19 were found in the plasmablast population at time of relapse along with the expression of receptors associated with B cell survival

253

(BCMA, TACI). Therefore, in addition to anti-CD20-mediated BCDT, which is currently used, new therapies targeting CD19, or these survival receptors might be potential candidate therapies for relapse. We found that clonal variants of pathogenic clones are present in the circulation before relapse becomes clinically visible and that MuSK titer increases simultaneously. **Thus, both the titer as well as the presence of circulating MuSK-specific B cells could be used as biomarkers for relapse prediction after BCDT.**

Summary. **Overall, the work in this thesis (i) elucidated new properties of human MuSK mAbs, (ii) gave new insights into the immunomechanisms of relapse after BCDT, which will support the development of new therapies and personalized tailoring of existing therapies for MuSK MG, and (iii) it will provide important therapy-relevant insights into the immunopathology of other autoimmune disorders, as MG is a prototypical B cell mediated autoimmune disease.**

References

1. Nel, M. and J. Heckmann, Myasthenia Gravis and Related Disorders. Myasthenia Gravis Relat Disord, 2018.

2. Phillips, L.H., The epidemiology of myasthenia gravis. Semin Neurol, 2004. 24(1): p. 17-20.

3. Dresser, L., et al., Myasthenia Gravis: Epidemiology, Pathophysiology and Clinical Manifestations. Journal of clinical medicine, 2021. 10(11): p. 2235.

4. Yi, J.S., et al., B cells in the pathophysiology of myasthenia gravis. Muscle Nerve, 2018. 57(2): p. 172-184.

5. Querol, L. and I. Illa, Myasthenia gravis and the neuromuscular junction. Curr Opin Neurol, 2013. 26(5): p. 459-65.

6.   Mendoza, M., et al., Patient-acceptable symptom states in myasthenia gravis. Neurology, 2020. 95(12): p. e1617-e1628.

7.   Wendell, L.C. and J.M. Levine, Myasthenic crisis. The Neurohospitalist, 2011. 1(1): p. 16-22.

8.   Neumann, B., et al., Myasthenic crisis demanding mechanical ventilation: A multicenter analysis of 250 cases. Neurology, 2020. 94(3): p. e299-e313.

9.   Lehnerer, S., et al., Burden of disease in myasthenia gravis: taking the patient's perspective. J Neurol, 2022. 269(6): p. 3050-3063.

10.   Fichtner, M.L., et al., Autoimmune Pathology in Myasthenia Gravis Disease Subtypes Is Governed by Divergent Mechanisms of Immunopathology. Front Immunol, 2020. 11: p. 776.

11.   Schneider-Gold, C. and N.E. Gilhus, Advances and challenges in the treatment of myasthenia gravis. Ther Adv Neurol Disord, 2021. 14: p. 17562864211065406.

12.   Guptill, J.T., et al., Cost analysis of myasthenia gravis from a large U.S. insurance database. Muscle Nerve, 2011. 44(6): p. 907-11.

13.   Vincent, A., Unravelling the pathogenesis of myasthenia gravis. Nat Rev Immunol, 2002. 2(10): p. 797-804.

7.   CURRICULUM VITAE

Miriam Franziska Laura Fichtner was born on January 4th 1990 in Augsburg, Germany. She graduated from the Deutschherren-Gymnasium as valedictorian in 2009 and got accepted into the medical school of the Ludwig Maximilian University (LMU) in Munich (Germany) which she finished as a state certified physician at the end of 2017. During her medical studies Dr. Fichtner developed a keen interested on immunology and neurology and received her medical dorctorate in the lab of Professor Edgar Meinl at the Institute of Clinical Neuroimmunology at the end of 2018. During her thesis she worked on the receptor transmembrane activator and CAML interactor (TACI) and characterized the long and short isoform of the receptor.

For further scientific training in the context of B cells Dr. Fichtner joined the laboratory of Professor Kevin C. O'Connor at Yale University in the departments of neurology and immunobiology at the beginning of 2018 and simultaneously began her PhD together with Professor Pilar Martinez and Dr. Mario Losen at University of Maastricht in the fall of 2018. Over the 4.5 years at Yale, Dr. Fichtner has worked on several projects to further the understanding of the immunopathology that underlies the prototypical B cell mediated autoimmune disorder myasthenia gravis. She investigated pathogenic autoantibodies, B cells, the complement system and the immunopathology of relapse after initial positive response to B cell depleting therapy in MG patients with autoantibodies targeting the muscle specific tyrosine kinase (MuSK). She is currently building up her own Junior Group at Charité in Berlin.

8.   LIST OF PUBLICATIONS

PEER-REVIEWED JOURNAL PUBLICATIONS:

- **M.L Fichtner**, H. Rübsamen, M. Smolle, J. Schaller, R. Feederle, A. Bültmann, T. Kümpfel, P. Schneider, F.S. Thaler, E. Meinl. 2023. Features of Isoforms of Human Soluble TACI. Journal of Immunology 211: 199-208.

- **M. L. Fichtner**, K. B. Hoehn, E. E. Ford, M. Mane-Damas, S. Oh, P. Waters, A. S. Payne, M. L. Smith, C. T. Watson, M. Losen, P. Martinez-Martinez, R. J. Nowak, S. H. Kleinstein, and K. C. O'Connor. 2022. Reemergence of pathogenic, autoantibody-producing B cell clones in myasthenia gravis following B cell depletion therapy. Acta Neuropathologica Communications 10: 154.

- A.H. Obaid, C. Zografou, D.D. Vadysirisack, B. Munro-Sheldon, **M.L. Fichtner**, B. Roy, W.M. Philbrick, J.L. Bennett, R.J. Nowak, K.C. O'Connor. 2022. Heterogeneity of Acetylcholine Receptor Autoantibody-Mediated Complement Activity in Patients With Myasthenia Gravis. Neurology(R) neuroimmunology & neuroinflammation 9: Doi 10.1212/nxi.0000000000001169

- **M. L. Fichtner**, MD Hoarty, DD Vadysirisack, B Munro-Sheldon, RJ Nowak, KC O'Connor. 2022. Myasthenia gravis complement activity is independent of autoantibody titer and disease severity. PloS one 17: e0264489 Doi 10.1371/journal.pone.0264489

- **C. Mandel-Brehm, M. L. Fichtner, R. Jiang**, V. J. Winton, S. E. Vazquez, M. C. Pham, K. B. Hoehn, N. L. Kelleher, R. J. Nowak, S. H. Kleinstein, M. R. Wilson, J. L. DeRisi, and K. C. O'Connor. 2021. 'Elevated N-Linked Glycosylation of IgG V Regions in Myasthenia Gravis Disease Subtypes', The Journal of Immunology: ji2100225. **(Co-First Author)**

- **M. L. Fichtner**, C. Vieni, R. L. Redler, L. Kolich, R. Jiang, K. Takata, P. Stathopoulos, P. A. Suarez, R. J. Nowak, S. J. Burden, D. C. Ekiert, K. C. O'Connor; Affinity maturation is required for pathogenic monovalent IgG4 autoantibody development in myasthenia gravis. Journal Experimental Medicine. 2020; 217 (12): e20200513.

- J. Ruoyi, **M. L. Fichtner**, K. B. Hoehn, M. C. Pham, P. Stathopoulos, R. J. Nowak, S. H. Kleinstein, and K. C. O'Connor. "Single-Cell Repertoire Tracing Identifies Rituximab-Resistant B Cells During Myasthenia Gravis Relapses." JCI Insight. 2020; 5(14): e136471.

- **M. L. Fichtner,** R. Jiang, A. Bourke, R. J. Nowak and K. C. O'Connor (2020). "Autoimmune Pathology in Myasthenia Gravis Disease Subtypes Is Governed by Divergent Mechanisms of Immunopathology." Frontiers in Immunology 11: 776.
- P. Stathopoulos, A. Chastre, P. Waters, S. Irani, **M.L. Fichtner**, E.S. Benotti, J.M. Guthridge, J. Seifert, R.J. Nowak, J.H. Buckner, V.M. Holers, J.A. James, D.A. Hafler, and K.C. O'Connor. 2019. Autoantibodies against Neurologic Antigens in Nonneurologic Autoimmunity. Journal of Immunology 202:2210-2219.
- K. Takata, P. Stathopoulos, M. Cao, M. Mane-Damas, **M.L. Fichtner**, E.S. Benotti, L. Jacobson, P. Waters, S.R. Irani, P. Martinez-Martinez, D. Beeson, M. Losen, A. Vincent, R.J. Nowak, and K.C. O'Connor. Characterization of pathogenic monoclonal autoantibodies derived from muscle-specific kinase myasthenia gravis patients. JCI Insight. 2019;4(12).

INVITED SHORT REVIEWS

1. **M.L. Fichtner.** Short review: Identifizierung von Risikogenorten für AChR Myasthenia Gravis. DMG Aktuell, 1-2022
2. **M.L. Fichtner**. Short review: Affinity maturation is required for pathogenic monovalent IgG4 autoantibody development in myasthenia gravis. Yearbook of the ‚Deutsche Gesellschaft für Muskelkranke e.V.' (DGM)2021
3. **M.L. Fichtner**. Pathogenität von LRP4/Agrin Antikörpern. DMG Aktuell (Journal of the German Society of Myasthenia Gravis), 3-2021
4. **M.L. Fichtner**. Eberhard Pfleiderer Myasthenie Forschungspreisträgerin. DMG Aktuell (Journal of the German Society of Myasthenia Gravis), 2-2021
5. **M.L. Fichtner**, and K.C. O'Connor. 2019. Fast-acting autoantibodies muscle in on encephalitis. Sci Immunol, Vol. 4, Issue 42, eaba3068.

9.   ACKNOWLEDGEMENTS

"Immigrants, we get the job done."

-from the song Yorktown in the Musical Hamilton (2015)

I want to thank Professor Dr. Kevin C. O'Connor, Professor Dr. Mario Losen and Professor Dr. Pilar Martinez-Martinez for giving me the opportunity to obtain my PhD at Maastricht University. I am grateful for your great mentorship, guidance, and support on this journey. Special thanks go to Kevin and his support of my development into an independent scientist during my postdoctoral training at Yale. I also want to thank all of the many professional collaborators that helped on these projects and gave valuable input and insights. I further want to thank Prof. Dr. Peter Molenaar for his help with the Dutch translation of the abstract of the summary of this thesis.

I could not have done all of this without the support of my friends and family. My experience would not have been the same without you. Special shoutouts to Natsuko, Elif, Christina, Delphine, Flo, Ana, Joyce, Dana, Diana, Caroline, and Antonella who I had the fortune to meet at work. I also was very lucky to meet Polina, Theresa and Sandy through the GAIN Stammtisch in New Haven. I will always cherish the wonderful times and fun we had together. My German friends Bea, Vroni, Netti, Tina, and Birgit remained close friends and supporters during my time abroad. Thanks to all of you for being such wonderful friends and I am happy that we can meet in person again. Additionally, I want to thank my parents and

sister for their continuous support of my career – even if it means that I worked very far from home. My work in the US gave me the opportunity to get closer to my family in Texas: Annamaria, Gerhard, Lena and Marie. Thank you for giving me a second home in the US.

"Best to take the moment present as a present for the moment"

- from the song 'Any moment' in the musical 'Into the Woods' (2002) by Stephen Sondheim, Hudson Talbott, James Lapine